On the elastic web crippling stiffness of thin-walled cold-formed steel members : an anlytical approach

Vaessen, M.J.

Award date:
1995

On the elastic web crippling stiffness of thin-walled cold-formed steel members

an analytical approach

M.J. Vaessen, June 1995

On the elastic web crippling stiffness of thin-walled cold-formed steel members

an analytical approach

Supervision:	Prof. Ir. H.H. Snijder Prof. Dr. Ir. J.G.M. Kerstens Mrs. Dr. Ir. M.C.M. Bakker
Period:	October 1994 - June 1995
In commission of:	Eindhoven University of Technology Department of Building Science
Author:	Maarten J. Vaessen
Identity number:	306880

Acknowledgements

Special acknowledgement is made to the members of the graduate commission: Prof. Ir. H.H. Snijder, Prof. Dr. Ir. J.G.M. Kerstens and Mrs. Dr. Ir. M.C.M. Bakker. Their permanent encouragement and enthusiasm was a source of inspiration. During the many sessions the cooperation was very constructive and contributed considerably to the development of this project.

Thanks are due to Ir. P. Hiemstra for his comments and coaching.

Gratitude is expressed to Ing. J.J. v. Ishoven and Ing. J.J.P. van den Oever for their assistance in the numerical research.

Finally, appreciation is recorded to all those, who have contributed in various ways to the completion of this graduate research project.

Summary

Thin-walled cold-formed steel members are frequently used as structural elements in buildings, for instance roof, floor and wall elements. When such a member is subjected to a concentrated load or reaction, its web may cripple due to the high local intensity of the load. This type of localized failure is denoted as web crippling. The current design formulae that predict the ultimate web crippling resistance are based on curve fitting of test results rather than on an analytical description of the failure mechanisms. These web crippling prediction formulae appear to give inconsistent and sometimes unsafe results *(Bakker and Pekőz, 1985)*.
An analytical model that describes the web crippling behaviour based on a physical understanding of the failure mechanisms has been developed by Bakker *(1992)*. According to this model the load-web crippling deformation behaviour at interior supports of continuous members is elastic until the development of a spatial plastic mechanism, where the web crippling deformation is defined to be the decrease in height of the web of the member. The load corresponding to this plastic mechanism is denoted as the mechanism initiation load. Although the mechanism initiation load may be lower than the ultimate web crippling resistance, Bakker argued that it might be a reasonable approach to develop design formulae based on the prediction of the mechanism initiation load. In Bakker's model the mechanism initiation load is determined as the point of intersection of the elastic curve and a rigid-plastic mechanism initiation curve containing all load-deformation combinations where the rigid-plastic mechanism is initiated.
The rigid-plastic mechanism initiation curve has been derived by Bakker *(1992)*, using generalized yield line theory. The subject of this study is the analytical determination of the elastic curve. Since it is assumed that thin-walled cold-formed steel members exhibit a linear elastic web crippling behaviour, the elastic curve can be fully described by its slope, the web crippling stiffness. The study is restricted to hat sections and first generation deck panels. Two different analytical web crippling stiffness models are developed, namely the beam on elastic foundation model and the energy model.

In the beam on elastic foundation model the loaded cross-section of an infinitely small slice of the member is schematized to a portal frame (the so-called two-dimensional portal frame model). The web crippling stiffness of this slice is determined using Castigliano's law. A first generation deck panel is thought of as a series of hat sections that are loaded similarly and connected together at the bottom flanges. The calculation of the web crippling deformation of a first generation deck panel may then be reduced to the calculation of one hat section, except for some additional boundary conditions due to compatibility requirements of the bottom flanges.
Web crippling results in local deformations. The variation of the web crippling deformations over the length of the member are taken into account by means of the theory of a beam on an elastic foundation. According to this theory the web of the member can be thought of as a continuous elastic support (foundation) of the top flange and a part of the web (beam). Within the application of the beam on elastic foundation theory two fundamental different approaches can be distinguished: the effective length approach and the full length approach.

In the effective length approach the web crippling deformations are assumed to stretch out within an effective length, whose magnitude is derived with the beam on elastic foundation theory. In the effective length area the web crippling deformations are described by a trilinear function. The maximum web crippling deformation is taken equal to the web crippling deformation of the two-dimensional portal frame model.
The full length approach asserts that the web crippling deformation variations over the length of the member can be described properly by the deflection curve of the beam on elastic foundation theory.
The beam on elastic foundation model requires the definition of a foundation and a beam stiffness. In both the full length and the effective length approach the foundation stiffness of the continuous elastic support is defined to be the two-dimensional web crippling stiffness of the portal frame model. The beam stiffness depends on a model factor α, determining the part of the web that, together with the top flange, constitutes the beam. In both approaches this factor α is treated as an empirical parameter with which the model can be fitted on experimental results and numerical simulations. In this study the full length approach is preferred to the effective length approach.

The energy model is based upon the principle of stationary total potential energy. The application of this extremum principle points the way towards establishing an energy functional. Substituting assumed deformation functions in the energy functional, involving adjustable parameters, the stationary conditions are determined with respect to these parameters. It is assumed that the geometrical configuration which the member takes up is identified by these stationary conditions. This principle provides a direct method for obtaining approximate solutions to the web crippling stiffness.
In the energy model, the member is idealized to be consist of a top flange and two web plates (the bottom flange plates are neglected in this idealization, as their deformation variations are negligibly small). These plates are connected to each other and hence their deformations need to be compatible. Two different compatibility assumptions are made within the energy model, leading to different web crippling stiffnesses. The so-called geometrical compatibility approach, is based upon the assumption that the plates are rigidly connected at their ends, whereas the hinge compatibility approach is based upon the assumption that the plates are connected by hinge-joints.
Over the cross-section the assumed deformation solution is described by a fourth degree polynomial for both the top flange and the web, with a maximum deformation at the centre of these plates. The quotient n of these maximum deformations is thought to be a function of the geometrical deformations of the cross-section only. The factor n is derived using the above mentioned portal frame idealization.
Over the length of the member three different deformation solutions are applied for all plates, namely a bilinear function, a trilinear function (which has constant deformations underneath the load bearing plate) and a fourth degree polynomial. It is assumed that these deformations stretch over an effective length, outside where the deformations are negligibly small.
The potential energy is minimized with respect to the effective length and the maximum deformation of the top flange and web plates, which are related to each other by the factor n.
Apparently, only the bilinear function enables a manageable solution in the application of the energy model for both the geometrical and the hinge compatibility approach. Both the trilinear function and the fourth

degree polynomial give tedious mathematical problems in determining the web crippling stiffness, due to the way the effective length is accounted for in the energy functional. Hereby, within the application of the trilinear function for both the geometrical and the hinge compatibility approach it is assumed that the effective length equals the span length, thus avoiding the above mentioned problems. In case of the fourth degree polynomial (for both the geometrical and the hinge compatibility approach), several energy contributions are left out of the energy functional because they are negligibly small compared to others. This results in a tractable energy functional.
Just as in the portal frame model, the calculation of the web crippling stiffness of a first generation deck panel in the energy model may be reduced to the calculation of a hat section, except that it has some extra boundary conditions. Hence, the resulting web crippling stiffness formulae for hat sections and first generation deck panels differ from each other only in the determination of the factor n.

Both the energy model (six combinations of deformation description functions and compatibility approaches) and the beam on elastic foundation model are validated in a parameter study against finite element simulations of web crippling tests using a finite element model in the finite element program ANSYS. In simulating several experimental tests, the finite element model appears to produce reliable results, except for members having small corner radii. This might be caused by the fact that the magnitude of the corner radii has a very large influence on the web crippling stiffness, especially in case of small corner radii, while it is difficult to determine the exact magnitude of small corner radii in experimental tests.
According to the parameter study, web crippling is a local phenomenon that is independent of the span length of the member. This justifies the introduction of an effective length. Furthermore, the web crippling stiffness turns out to be mainly dependent of the corner radii and the wall thickness. The web crippling stiffness is more or less inversely proportional to the top flange corner radius and proportional to the wall thickness raised to the 5/2 power.
For α having a constant value the beam on elastic foundation model treats the corner radii, the web and the web angle poorly. The poor treatment of the corner radii might be caused by the fact that the bottom flange corner radii are not taken into account. To improve this performance, the beam on elastic foundation model is adjusted by defining the factor α to be a function of the corner radii.
In the energy model (i.e. from now on this refers to the combination of the geometrical compatibility approach and the fourth degree polynomial, because this combination performs best on the other parameters) the corner radii, the load bearing plate the web angle and the wall thickness are poorly accounted for. In case of the load bearing plate this is caused by the chosen deformation description over the length of the member (fourth degree polynomial), which implies the neglect of some upward curling of the top flange underneath the load bearing plate. The wall thickness is poorly take into account, because of the neglect of axial deformations. Considering the corner radii and the wall thickness, the model has been adjusted by adding an empirically derived correction factor γ. Moreover the model has been made independent of the length of the load bearing plate, which corresponds to the results of the parameter study.
Both the adjusted models produce accurate results as far as the influence of the corner radii is concerned. In case of the beam on elastic foundation model, especially the poor treatment of the web can hardly be

adjusted, without affecting the basis of the model, namely the web continuously supporting a part of the web and the top flange.

The poor treatment of the web angle in the (adjusted) energy model might be caused by the fact that the maximum deformation of the web not exactly occurs at the centre of the web but somewhat higher. Hereby, a better performance can be established by using slightly different deformation descriptions over the cross-section, which are a function of the web.

It may be concluded that the energy model needs some further adjustments on the treatment of the web angle but it is assumed that this model is capable of producing the most reliable approximations of the web crippling stiffness, after these adjustments. So far, the adjusted energy model produces reliable web crippling stiffness predictions for members with vertical webs and having geometrical dimensions within certain ranges.

Table of contents

Notation

The most frequently used symbols are explained below. Other symbols are explained in the text where they occur.

Geometry

A	area
b_{bf}	width of the bottom flange, measured between the points of intersection of the web and flange midlines
b_{tf}	width of the top flange, measured between the points of intersection of the web and flange midlines
b_w	width of the web, measured between the points of intersection of the web and flange midlines
h_w	height of the web (=height of the section)
I	moment of inertia
L_{ef}	effective length
r_i	interior corner radius
$r_{i;bf}$	interior corner radius between the web and the bottom flange
$r_{i;tf}$	interior corner radius between the web and the top flange
t	wall thickness, plate thickness
θ_w	web angle
L_{lb}	length of the load bearing plate
L_{rb}	length of the reaction bearing plate
L_{span}	span length of the member

Displacements and deformations

Δh_w	web crippling deformation
$\Delta h_{w;2D}$	two-dimensional web crippling deformation
$\Delta h_{w;imec}$	web crippling deformation at the initiation of the plastic hinge mechanism
u_s	stretching actions in x direction
v_s	stretching actions in y direction
w	deflection
w_1	maximum deflection of the top flange
w_2	maximum deflection of the web
φ_{mec}	mechanism rotation
φ_i	rotation around i axis

Stresses, strains and forces

ϵ	strain
F	concentrated load, external force
F_{imec}	mechanism initiation load
F_u	ultimate load
M	bending moment
M_u	ultimate bending moment resistance (Eurocode 3)
N	axial force
σ	stress
T	torsion

Coefficients and factors

a_i	Rayleigh-Ritz coefficient
α	part of the web belonging to the beam in the beam in elastic foundation model
b_i	Rayleigh -Ritz coefficient
β	constant in beam on elastic foundation theory
c_i	Rayleigh-Ritz coefficient
γ	correction parameter in energy model
γ_i	Rayleigh-Ritz function
k	foundation stiffness
$k_{\Delta h_w}$	web crippling stiffness
$k_{\Delta h_w;2D}$	two-dimensional web crippling stiffness
ϕ_i	Rayleigh-Ritz function
ψ_i	Rayleigh-Ritz function

Material and structural properties

D	flexural rigidity of plate
E	modulus of elasticity
G	shear modulus of elasticity
μ	Poisson's ratio

Energy and work

U	strain energy
V	total potential energy
W_{int}	internal work
W_{ext}	external work
Ω	potential energy of external loads

Chapter 1: Introduction

This chapter gives a general introduction into thin-walled cold-formed steel members, the context in which this research project should be placed and the main objectives of the project.

1.1 General introduction

This report is the result of a research project on web crippling of thin-walled cold-formed steel members which are subjected to a concentrated load. These steel members are a relatively new product: they were not widely used until around 1940. In the USA, the first design code for cold-formed steel structural members was issued in the 1970s. Today these members are frequently used as structural elements in buildings, such as roof, floor and wall elements.

Cold-formed steel members are composed of cold-formed sections, which are formed by press braking, bending braking or roll-forming. Due to the production method they have typical features which distinguish them from the familiar hot-rolled shapes, such as the uniform wall-thickness, the curved transition between the web, flanges and stiffeners, and a relatively large width-to-thickness ratio of their webs and flanges.

The cold-forming process allows much freedom in forming the shape, often resulting in much more different shapes compared to the hot-rolled members. Sections may be formed with inclined webs and with various types of intermediate and edge stiffeners in the web and flange elements (figure 1.1).

Cold-formed steel members may be distinguished into beams, which have only a load carrying function, and panels, which have both a load carrying and a space enclosing function.

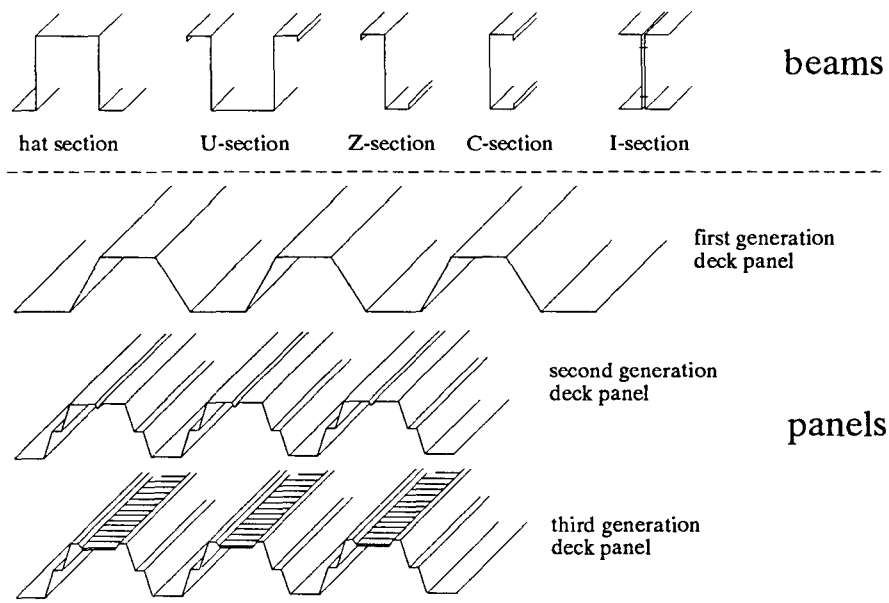

Figure 1.1: *Various types of cold formed steel sections*

Beams can be characterized as linear elements. Sometimes these beams are more expensive with respect to their weight than the hot-rolled shapes, but due to the larger freedom in forming the shapes, cold-formed members can be created with a better stiffness-to-weight ratio and a better resistance-to-weight ratio. Panels can be thought of as planar elements. They have a limited width but may be connected to form floors, roofs and walls. Based on the connection between the panels they can be classified as deck panels (connected by overlapping flange elements) or as standing seam panels (connected by overlapping web elements). The sheets are profiled to obtain sufficient stiffness and resistance. Note that, for the determination of their mechanical properties, panels are usually idealized to beams.

Cold-formed steel members consist of web and flange elements. To increase the load carrying capacity of the members these elements may be stiffened with various types of stiffeners that provide stiffness against buckling. Stiffened elements may be distinguished into longitudinally stiffened elements (with intermediate stiffeners parallel to the stress direction) and transversely stiffened elements (with intermediate stiffeners perpendicular to the stress direction). Based on the chronology in the first use of different types of stiffeners, Baehre *(1982)* classified deck panels as first, second and third generation decks. First generation decks have plane flange and web elements, second generation decks have elements with longitudinal intermediate stiffeners, while third generation decks have both longitudinal and transverse stiffeners. An overview of different types of beams and panels is given in figure 1.1.

When a thin-walled cold-formed steel member (a panel or a beam) is subjected to a concentrated load, its web may cripple due to the high local intensity of the load. This type of localized failure of flexural members is denoted as web crippling (figure 1.2).

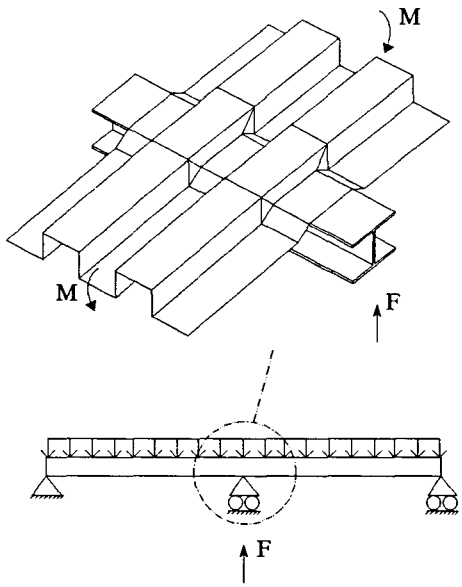

Figure 1.2: *Web crippling at the interior support of a continuous member (Reinsch, 1983)*

At interior supports of continuous members the concentrated load is accompanied by a bending moment, which reduces the resistance of the member against the concentrated load.

Web crippling is only one of the many failure modes which should be considered in the design of cold-formed steel structures. For many failure modes reliable design formulae have already been developed. These formulae, based on research findings and accumulated practical experience, have been compiled into cold-formed steel design codes, such as Eurocode 3 and AISI. The design formulae which predict the ultimate web crippling resistance (web crippling prediction formulae) are based on curve fitting of test results and not on an analytical or numerical description of the failure mechanisms. In the approach of the current web crippling prediction formulae the influence of the concentrated load is described separately from that of the bending moment. It is assumed that small bending moments have a negligible influence on the ultimate web crippling resistance. The influence of larger bending moments is taken into account by means of interaction formulae, whose format is given in figure 1.3.

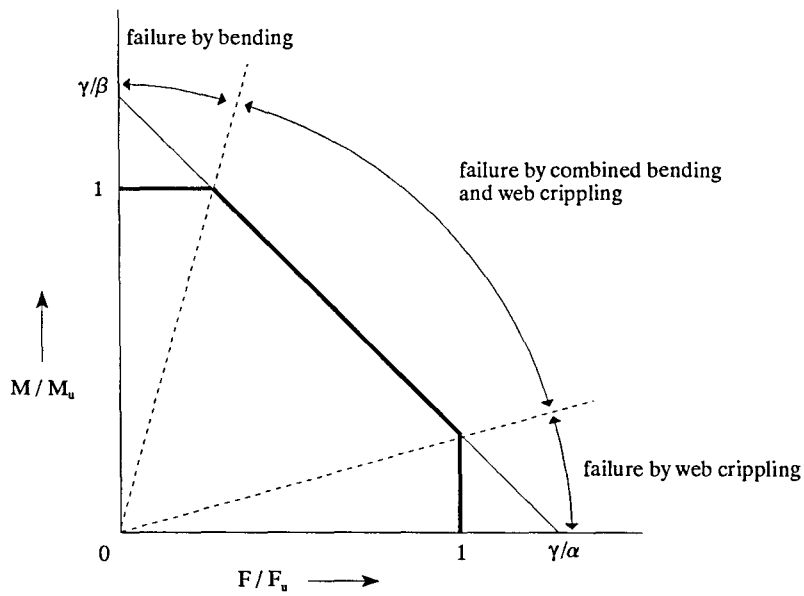

Figure 1.3: *Graphical presentation of the format of interaction formulae (Bakker, 1992)*

Here F and M represent the occurring concentrated load and bending moment, F_u represents the ultimate web crippling resistance of a member subjected to a concentrated load and a bending moment which is assumed to be negligibly small and M_u is the ultimate bending moment resistance of the member. The constants α, β and γ are determined from curve fitting of the results of combined bending and web crippling tests. An evaluation of these web crippling prediction formulae showed that the formulae for members having single unstiffened webs give inconsistent and sometimes unsafe results *(Bakker and Pekőz, 1985)*. Empirical formulae in general have a limited and often not well described range of applicability. Of course, each

formula correlates well with the test results of its population, but the correlation is worse for test results from other populations.

An analytical model which describes the web crippling behaviour based on a physical understanding of the failure mechanisms was developed by Bakker *(1992)*. According to this model the load-web crippling deformation behaviour at interior supports of continuous members is elastic until the development of a spatial plastic mechanism, where the web crippling deformation Δh_w is defined to be the decrease in the height of the web h_w underneath the load bearing plate (figure 1.4). Note that only a part of the loaded cross-section of a first generation deck panel is given in figure 1.4 because the deformation of the rest of the loaded cross-section is similar to this part.

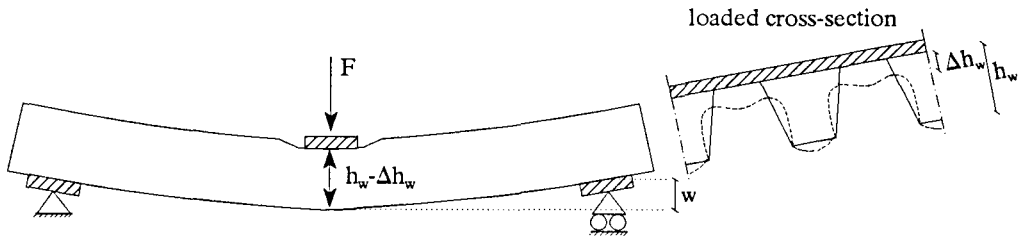

Figure 1.4: *Web crippling deformation*

The load corresponding to the initiation of the spatial plastic mechanism is denoted as the mechanism initiation load. This load is determined as the point of intersection of an elastic curve and a rigid-plastic mechanism initiation curve. This rigid-plastic mechanism initiation curve contains all load-deformation combinations where the rigid-plastic mechanism of each member might be initiated (the dotted line in figure 1.5). The load-web crippling deformation behaviour after the development of the mechanism is described by a rigid-plastic curve (the solid line in figure 1.5).

Although the ultimate web crippling resistance may be higher than the mechanism initiation load, Bakker argued that it might be a reasonable approach to develop design formulae based on the prediction of the mechanism initiation load.

Most of Bakker's thesis is dedicated to the derivation of the rigid-plastic mechanism initiation curve by using generalized yield line theory. The analytical determination of the elastic curve has not been treated. It is assumed that thin-walled cold-formed steel members exhibit a linear elastic web crippling behaviour upto the initiation of the rigid-plastic mechanism, so that the elastic curve can simply be taken as a straight line and is described by its slope. This slope is denoted as 'web crippling stiffness'.

The web crippling stiffness of a (cold-formed) thin-walled steel member can thus be defined as:

The required concentrated load on a thin-walled member that results in a decrease in the height of the web of the member under the concentrated load that equals unity.

In Bakker's model the determination of the web crippling stiffness is based upon test results.

According to Bakker the simplification of the elastic curve to a straight line is sufficiently accurate for the determination of the rigid-plastic mechanism initiation curve and hence, the mechanism initiation load. A description of the load-web crippling deformation behaviour in Bakker's model is given in figure 1.5.

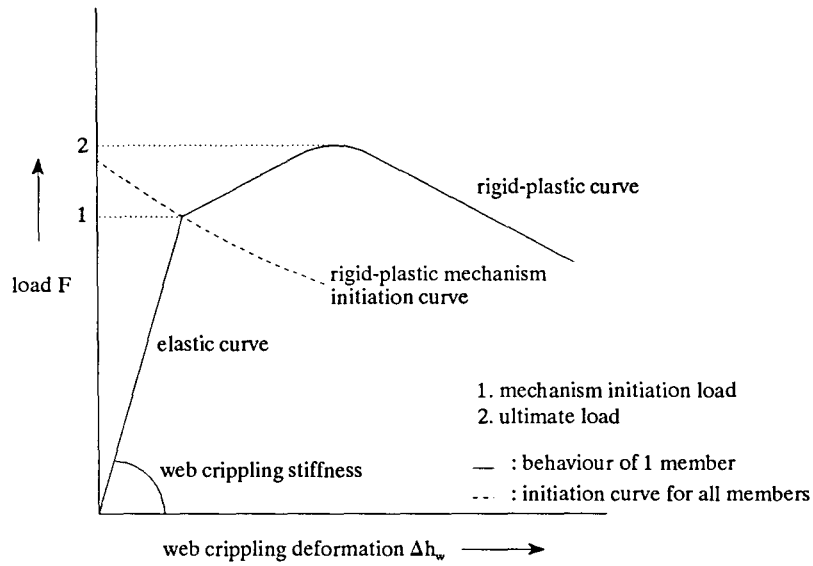

Figure 1.5: *Load-deformation behaviour according to Bakker's model*

The influence of the bending moment M is linked to the influence of the concentrated load F. Hence, there is no need for an interaction formula in this model. For a more detailed description of the model the reader is referred to section 2.4.

1.2 Objective

This research project was prompted by the lack of a reliable analytical description of the elastic curve in the model of Bakker. Furthermore, no analytical or numerical models exist which describes the elastic web crippling load-deformation behaviour of cold-formed steel members, subjected to a concentrated load. If both the rigid-plastic mechanism initiation curve and the elastic curve are described by an analytical model, then it is possible to predict the mechanism initiation load, without the need of test results. Future design formulae might be based upon this analytical prediction of the mechanism initiation load.

The primary object of the research is the development of an analytical model which describes the elastic web crippling load-deformation behaviour and thus the web crippling stiffness.

Two different analytical web crippling stiffness models are developed: The beam on elastic foundation model and the energy model. The latter is based upon the principle of stationary total potential energy, while the former is based upon the theory of a beam on an elastic foundation. The underlying reason for the develop-

ment of two different models is that the beam on elastic foundation model, which is developed first, turned out to be quite cumbersome in calculating the web crippling stiffness. For the eventual aim of this study being the prediction of the web crippling stiffness by means of an analytical model, the object of the study is already satisfied with the beam on elastic foundation model. However, the analytical web crippling stiffness model need to be as simple as possible in order to establish manageable prediction formulae. A completely different approach in the derivation of a web crippling stiffness model might result in a more simple model and is therefore thought to be worth trying.

The developed analytical models are validated in two different ways:

- Firstly, the models are compared with the results of numerical finite element simulations, which are carried out during this project. Basically, a numerical web crippling simulation gives the same kind of information as a web crippling test. Each parameter of the analytical model can be validated separately in a parameter study. A parameter study gives the opportunity to establish the incompleteness of a model with respect to each individual parameter and to optimize the model by adding (empirical) parameters, if necessary. For parameter studies numerical simulations are simpler than testing. The elastic web crippling behaviour is investigated numerically with a finite element model, using the general finite element program ANSYS [version 5.0 A].
- Secondly, the models are compared with test results of experimental studies *(Bakker, 1992)*.

1.3 Scope

Web crippling may occur under varying loading conditions. In the AISI specification (1986) the type of load application is divided in 'One Flange loadings', in which the force is applied to one flange and resisted by shear forces in the web (figure 1.6a), and 'Two Flange loadings', in which the force is applied to one flange and transferred through the web directly to the other flange, where the reaction occurs (figure 1.6b).

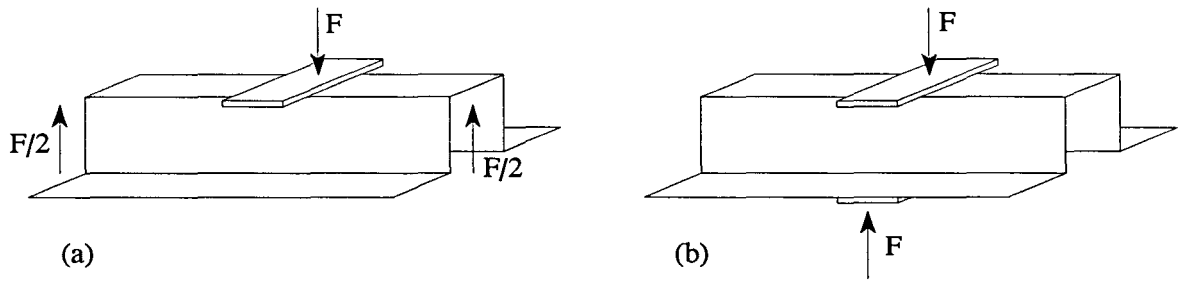

Figure 1.6: *Classification of loading conditions (Eurocode 3 & AISI)*

Furthermore, a distinction is made between 'Exterior loadings', in which the concentrated load is applied near the end of the member, and 'Interior loadings', in which the concentrated load is applied somewhere in the middle of the member. This results in four types of loading conditions: an Interior One flange (IOF) loading, an Interior Two Flange (ITF) loading, an Exterior One Flange (EOF) loading and an Exterior Two Flange (ETF) loading (figure 1.7). The current research is restricted to members subjected to an IOF loading because

the analytical model developed by Bakker is confined to this type of loading.

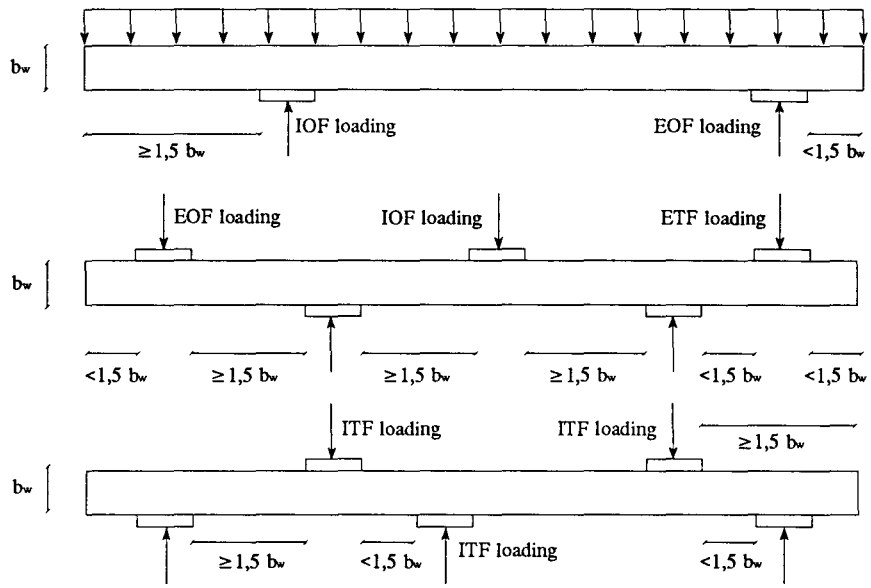

Figure 1.7: *Classification of loading condition occurring in practice (Yu, 1985)*

Due to the production method cold-formed steel members contain residual stresses. Residual stresses may decrease the ultimate web crippling resistance. However, the residual stresses do not influence the elastic web crippling behaviour. Therefore, they are not considered in this project.

From figure 1.1 it is clear that many different types of thin-walled cold-formed steel members are used in practice. This study is confined to members with unstiffened elements because the web crippling behaviour of this type of members can be described analytically much easier than that of members with stiffened elements. Once an analytical model describing the web crippling stiffness of members with unstiffened elements has been derived, it might be generalized for members with stiffened elements. It must be noted however that there are no experimental results of web crippling tests on members with intermediate stiffeners, with which an analytical model might be compared. Therefore, this study is restricted to cold-formed unstiffened hat sections (beams) and first generation deck panels (figure 1.8).

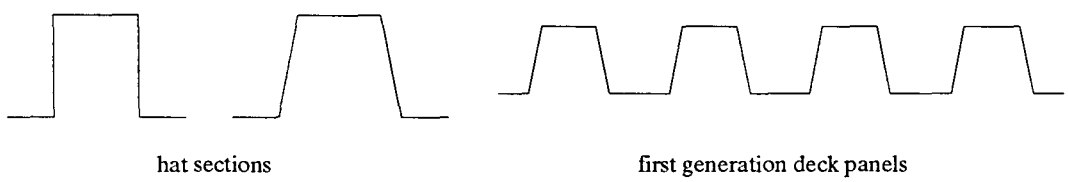

Figure 1.8: *Section types included in the research*

In the derivation of the analytical models describing the elastic web crippling deformation curve, a distinction is made between first generation deck panels and hat sections. In these models the first generation deck panels are geometrically idealized to hat sections, only with different boundary conditions (see for instance the sections 3.2 and 3.3).

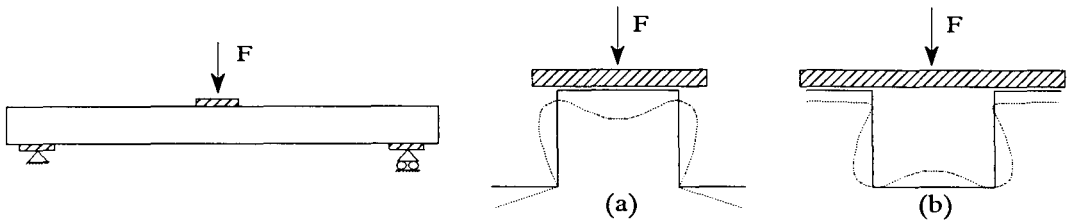

Figure 1.9: *Loading applications of hat sections and first generation deck panels*

The hat sections and the first generation deck panels are loaded with a doubly supported compression flange (figure 1.9a) and not with a singly supported compression flange (figure 1.9b).
Principally, both the beam on elastic foundation and the energy model are valid for all *M/F* ratios. However, the validation of the analytical models against finite element simulations is confined to *M/F* ratios from 130 upto 650. The members corresponding to these ratios tend to show a failure by combined bending and web crippling (figure 1.3).

1.4 Structure of the report

First, a qualitative description of the web crippling behaviour is given in chapter 2, as well as an overview of the existing empirical calculation models describing the web crippling stiffness. This chapter gives a general introduction into the phenomena affecting the web crippling behaviour. As mentioned in section 1.3 two different analytical models are developed within this study: the beam on elastic foundation model and the energy model. For sake of clarity these analytical models and their main validation possibilities (section 1.3) are shown graphically in figure 1.10.

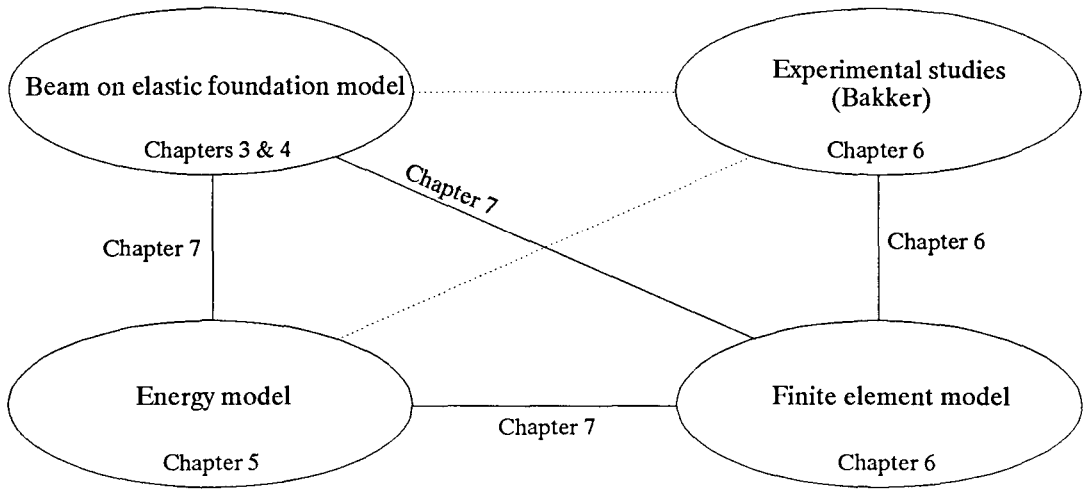

Figure 1.10: *Analytical models and their validation possibilities; structure of the report*

Both the beam on elastic foundation model and to a less extent the energy model are based upon a two-dimensional model: the portal frame model. Chapter 3 describes the derivation of the portal frame model. In chapter 4 the portal frame model is extended to the beam on elastic foundation model. The energy model, which is based upon a completely different, energy oriented, approach in the derivation of the web crippling stiffness, is treated in chapter 5. Chapter 6 describes the specifications of the finite element model. Furthermore, the experimental study of Bakker as well as a comparison between the experimental study and the finite element model is also treated in chapter 6. A comparison between the analytical models and the experimental study (the dotted lines in figure 1.10) is found to be rather useless, because of existing measuring-inaccuracies in the experimental study. The reader is referred to section 6.3 where a more detailed description is given of these measuring-inaccuracies. Chapter 7 describes the parameter study and summarizes the conclusions on the comparison between the results of the analytical models and the finite element results. Finally, the conclusions and recommendations for future research are given in chapter 8.

Chapter 2: Web crippling behaviour

This chapter gives a qualitative description of the web crippling behaviour as well as an overview of the existing calculation models describing this behaviour.

2.1 Introduction

The behaviour of cold-formed steel members subjected to a concentrated load and a bending moment is thought to be determined by three important phenomena: the web deformation mode, the formation of a plastic hinge mechanism in the member and local buckling.

The actual web crippling failure is caused by the formation of a plastic hinge mechanism. Since the deformations of the flange and web elements need to be compatible, this mechanism is characterized by both flange and web deformations. Based on the mode of web deformation, two different mechanisms can be distinguished, namely a yield arc mechanism and a rolling mechanism. These two mechanisms are described in section 2.2. Both in the yield arc and the rolling mechanism, the flange deformations result in the formation of a spatial plastic hinge mechanism (section 2.3). This hinge mechanism affects the global load-deformation behaviour of the member. The concentrated load acting on the member corresponding to the initiation of the hinge mechanism is defined to be the mechanism initiation load. The model of Bakker (section 2.4) distinguishes an elastic curve, a rigid-plastic mechanism curve and a rigid-plastic mechanism initiation curve. The mechanism initiation load is the point of intersection between of the elastic curve and the mechanism initiation curve. After the initiation of the mechanism the load-deformation behaviour is described by a rigid-plastic mechanism curve.

Bakker's model is directed to the rolling mechanism. The rigid-plastic mechanism initiation curve of the rolling mechanism was derived using generalized yield line theory. The elastic curve (and hence the web crippling stiffness) may be described by an analytical model which is valid for both the rolling mechanism and the yield arc mechanism. Such an analytical model does not exist today, but there do exist some empirical models. These models, which were developed within the last decade, will be treated in section 2.5.

Local buckling influences the stress distribution in the flange and web elements. Due to the post-buckling resistance of the member, the ultimate web crippling resistance (attained after the formation of the spatial plastic hinge mechanism) will be larger than the load corresponding to the initiation of local buckling. In Bakker's model the influence of local buckling on the elastic curve is thought to be negligible. The influence of local buckling on the rigid-plastic mechanism initiation curve is taken into account by means of an effective width approach, and will not further be treated here.

2.2 Web deformation modes

An important parameter in describing and modelling the web crippling behaviour is the web crippling

deformation Δh_w, which is defined as the decrease in the height of the web of the member underneath the load bearing plate (figure 1.4). The web crippling deformation is not a complete characterization of the web deformation, because it does not describe the out-of-plane deflections of the web.

Two different types of web crippling failure modes can be distinguished: the yield arc mechanism and the rolling mechanism. These failure mechanisms are characterized by different web deformation modes and seem to be determined primarily by the corner radius between the loaded flange and the web, the yield arc mechanism occurring in members with a small corner radius (around 1 mm), the rolling mechanism in members with a large corner radius (around 10 mm).

2.2.1 *Rolling mechanism*

In the rolling mechanism, the web crippling deformation is caused by a rolling process, in which the corner radius 'rolls down' through the web; a process which can be modelled with two moving yield lines (figure 2.1).

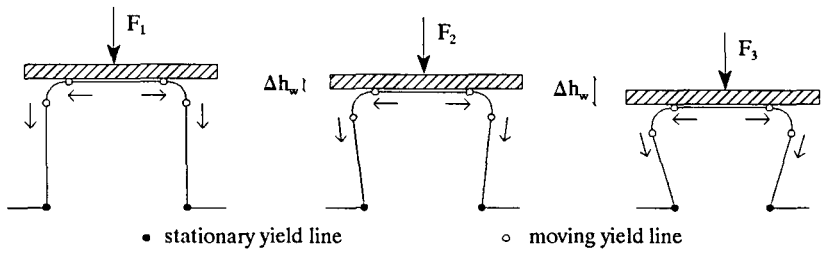

Figure 2.1: Rolling mechanism modeled with moving yield lines (Bakker, 1992)

The first yield line bends the (web) plate into curvature, the second straightens the (flange) plate again. The process of winding and rewinding of a metal strip is referred to as a rolling process in the literature *(Abramowicz and Wierzbicki, 1979)*. Hence the name rolling mechanism. The load-deformation behaviour of a member failing by the rolling mechanism is shown in figure 2.2.

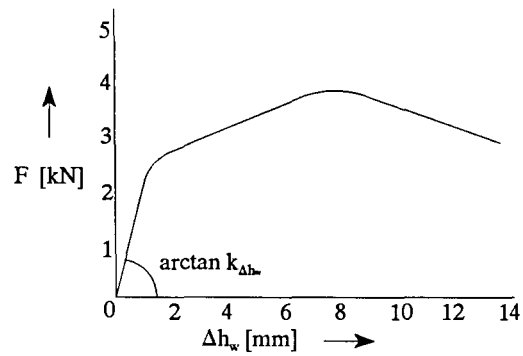

Figure 2.2: Load-deformation behaviour of a member failing by the rolling mechanism (Bakker, 1992)

After a rather sudden decrease in the web crippling stiffness $k_{\Delta h_w}$, the load steadily increases up to the ultimate load, whereafter it slowly decreases. Hereby, the rolling mechanism is characterized by a safe 'plastic' behaviour. The sudden decrease in the web crippling stiffness (marked by a bend in the load-web crippling diagram) corresponds to the formation of a hinge mechanism (section 2.3). Note that figure 2.2 represents the load-web crippling deformation behaviour occurring underneath the load bearing plate.

2.2.2 *Yield arc mechanism*

In the yield arc mechanism the web crippling deformation is caused by a yield arc (curved yield line) in the web underneath the load bearing plate (figure 2.3).

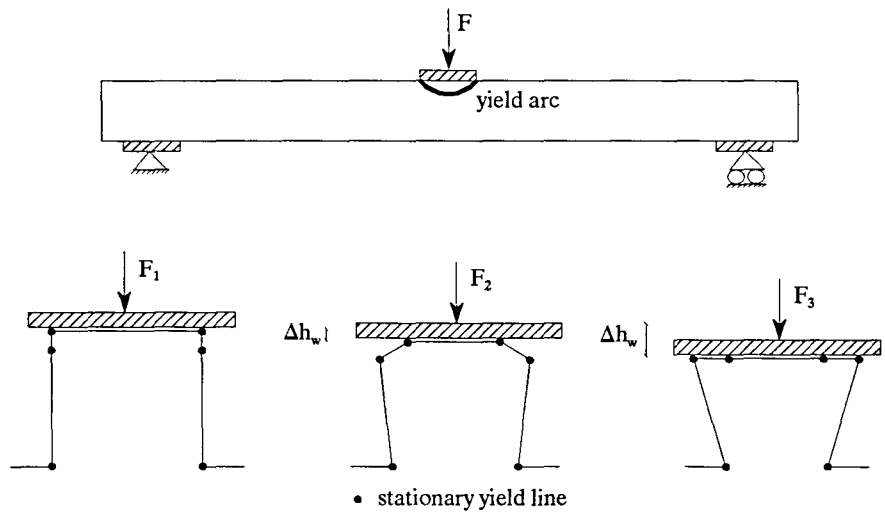

Figure 2.3: *Web deformations in the yield arc mechanism (Bakker, 1992)*

This failure mode may be initiated by web buckling but the ultimate web crippling load is not equal to the web buckling load *(Bakker, 1992)*. The load-deformation diagram of a member failing by the yield arc mechanism is shown in figure 2.4.

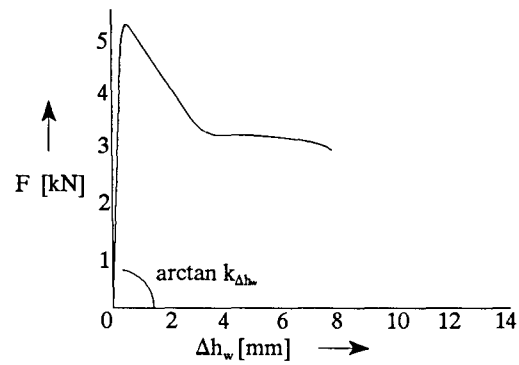

Figure 2.4: *Load-deformation behaviour of a member failing by the yield arc mechanism (Bakker, 1992)*

The ultimate resistance is attained for small web crippling deformations and flange deformations, after which the load suddenly drops. Hereby, the yield arc mechanism is characterized by an unsafe 'collapse' behaviour. For large web crippling deformations, when the web underneath the load bearing plate almost contacts this plate, the deformation process begins to resemble that of the rolling mechanism.

2.3 *Plastic hinge mechanism*

Web crippling at interior supports results in the formation of a plastic hinge mechanism, which influences the bending moment distribution in continuous members. However, in the current approach of the web crippling prediction formulae it is assumed that web crippling is a local phenomenon, not influencing the overall force distribution. The hinge mechanism results in a non-linear relation between the concentrated load F and the rotation of the member, denoted as the mechanism rotation φ_{mec} (figure 2.5).
The hinge mechanism should not be confused with the simple plastic hinge as known from the theory of plastic analysis of frames. In a simple plastic hinge the rotation is caused by in-plane yielding of the flange and web elements due to the bending moment while in a hinge mechanism the rotation is primarily caused by the web crippling deformation Δh_w.

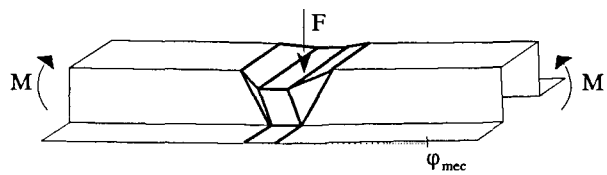

Figure 2.5: *Plastic hinge mechanism in a cold-formed hat section*

The hinge mechanism may even develop in members subjected to a concentrated load only with no bending moment at all *(Bakker, 1992)*. Furthermore, a simple plastic hinge can only partially develop in thin-walled cold-formed steel members because the flange and web elements become unstable before the yield stress is reached.
For members failing by the yield arc mechanism, the formation of the hinge mechanism more or less corresponds to the attainment of the ultimate resistance (figure 2.4). For members failing by the rolling mechanism the formation of the hinge mechanism merely results in a change in the load-deformation behaviour, the ultimate resistance being attained after some mechanism rotation (figure 2.2).

2.4 *Model of Bakker*

The web crippling model of Bakker is based on the idea that the web crippling behaviour can be described approximately by using two different models: a model describing the elastic behaviour for the first phase of loading (elastic curve), and a model describing the initiation of the rigid-plastic behaviour after the formation

of the hinge mechanism (rigid-plastic mechanism initiation curve). The mechanism initiation load F_{imec} is determined as the point of intersection of these two curves in a load-web crippling deformation diagram. The definition of the mechanism initiation load as the load corresponding to the initiation of the hinge mechanism suggests that there is a specific load at which this mechanism is formed. In reality there is a gradual progression from the elastic curve to the rigid-plastic mechanism curve. The actual load-deformation behaviour of the member will start to deviate from the elastic curve at first yield, and will coincide with the rigid-plastic mechanism curve only after the formation of the hinge mechanism (the dotted line in figure 2.6). Therefore a sharp intersection point between the two curves does not exist. In figure 2.6 a graphical representation of the model is given for both the yield arc mechanism (figure 2.6a) and the rolling mechanism (figure 2.6b).

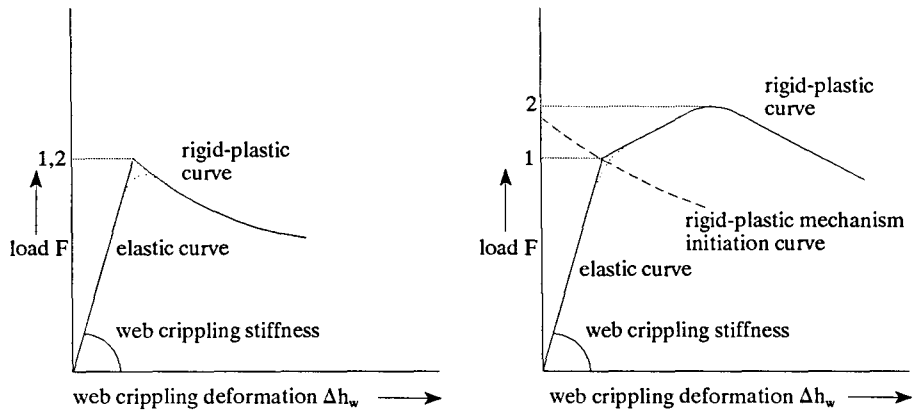

Figure 2.6: *Graphical presentation of Bakker's model*

It is assumed that web crippling deformations smaller than $\Delta h_{w;imec}$, corresponding to the initiation of the hinge mechanism, do not result in a mechanism rotation.

The rigid-plastic mechanism initiation curve contains all possible load-deformation combinations where the plastic mechanism might be initiated. An analytical model describing this rigid-plastic mechanism initiation curve for members failing by the rolling mechanism has been derived by using generalized yield line theory (a model for the yield arc mechanism was not developed). This model is based on a simplified work method. The work method means that the mechanism (initiation) load is calculated by equating the external incremental work by the applied loads to the internal incremental energy dissipation in the yield lines.

In Bakker's model it is assumed that the elastic load-web crippling deformations are linear up to the initiation of the rolling mechanism, and can therefore be characterized by the initial web crippling stiffness. However,

in reality the load-web crippling deformation becomes non-linear before the initiation of the mechanism, due to the gradual development of the hinge mechanism. It is not ruled out that this non-linear behaviour is also caused by local buckling. Since the mechanism initiation curve is a descending curve in case of the rolling mechanism (figure 2.6), it is to be expected that the neglect of the non-linear web crippling deformations results in an overestimation of the mechanism initiation load by the model. This overestimation appears to amount up to 7% but considering the non-linear web crippling deformations does not result in a consistently better prediction of the mechanism initiation load *(Bakker, 1992)*. Since the non-linear web crippling deformations at the initiation of the mechanism are expected to decrease with increasing span length, it is likely that the influence of these non-linear deformations may also be neglected in longer span tests. An analytical model describing this elastic curve is developed within this research project. Here, the non-linear web crippling deformations are not taken into account either.

2.5 *Empirical models describing the web crippling stiffness*

Besides Bakker's model, several other analytical web crippling models have been described in the literature. The treatment of these models is beyond the scope of this research project but two of these models include empirically derived predictions of the initial web crippling stiffness. Since it is assumed in Bakker's model that the elastic load-web crippling deformation is given by a straight line, these initial web crippling stiffnesses correspond to the web crippling stiffness in the model of Bakker.
In these models the web crippling stiffness is a function of several (geometrical) parameters. Geometrical parameters that might influence the web crippling stiffness are given in figure 2.7.

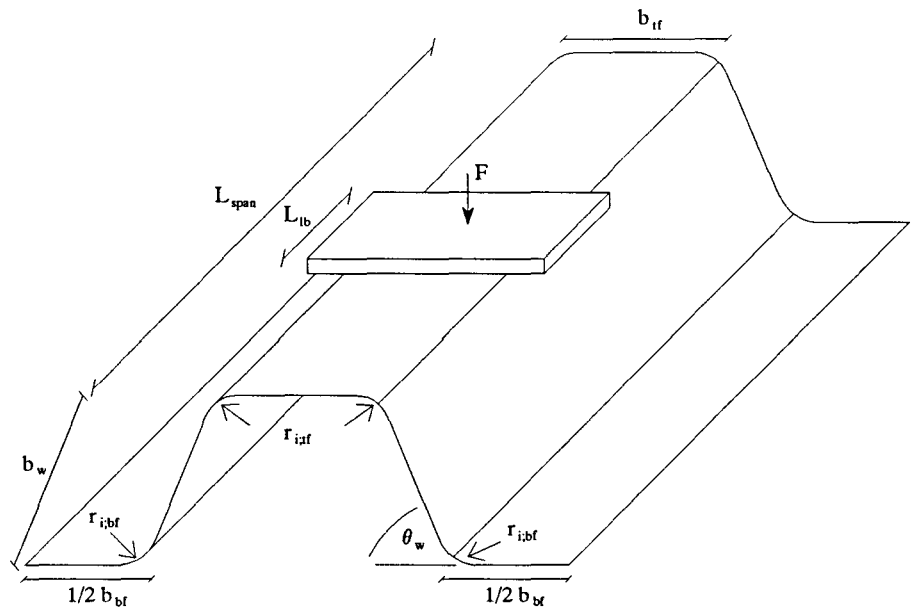

Figure 2.7: *Geometrical parameters determining the web crippling stiffness*

The two analytical models which include an empirically derived prediction of the web crippling stiffness are the models of Reinsch and Tsai.

2.5.1 *Model of Reinsch*

Reinsch *(1983)* developed an analytical model to determine the load carrying capacity of continuous multi-span cold-formed steel members. The model includes an empirical prediction of the (initial) web crippling stiffness of hat sections with two webs, which is given (in N/mm) by

$$k_{\Delta h_w} = \frac{1500000 \cdot t^3}{b_w} \tag{2.1}$$

where the values of the plate thickness t and the width of the web b_w should be entered in millimetres. According to Reinsch, the web crippling stiffness is independent of the corner radius between the web and the top flange $r_{i;tf}$ and the width of the top flange b_{tf}. The formula was derived for first generation decks, with a length of the load bearing plate L_{lb}=60 mm, a yield strength f_y=300 N/mm^2, and a web angle θ_w=90°. It is striking that in the tests carried out by Bakker the corner radius $r_{i;tf}$ appeared to be the most important parameter in determining the web crippling stiffness, while according to Reinsch the initial web crippling stiffness is independent of this corner radius.

2.5.2 *Model of Tsai*

Tsai (1987) developed an analytical model to determine the load-deformation behaviour of members subjected to the combined action of a concentrated load and a bending moment. The model is based on Reinsch's formulae and the idea to distinguish between elastic and rigid-plastic structural behaviour. The description of the elastic behaviour includes an empirical model from which the initial web crippling stiffness of first generation deck panels can be calculated (in N/mm) as:

$$k_{\Delta h_w} = 1500 \cdot k_t \cdot k_{r_i} \cdot k_{L_{lb}} \cdot k_{bw} \cdot k_{\theta_w} \tag{2.2}$$

where

$$k_t = 2.22 \cdot t^2 - 1.72 \cdot t + 0.5 \qquad (0.7 < t < 1.2) \tag{2.3}$$

$$k_{r_i} = 0.102 \cdot r_i^2 - 1.52 \cdot r_i + 6.28 \qquad (3.0 < r_i < 10.0) \tag{2.4}$$

$$k_{L_{lb}} = 0.563 \cdot \frac{L_{lb}}{100} + 0.437 \qquad (0 < L_{lb} < 180) \tag{2.5}$$

$$k_{b_w} = 0.74 \cdot (\frac{b_w}{100})^2 - 1.7 \cdot \frac{b_w}{100} + 1.91 \qquad (55 < b_w < 100) \tag{2.6}$$

$$k_{\theta_w} = 3.39 \cdot (\frac{\theta_w}{90^\circ})^2 - 8.01 \cdot (\frac{\theta_w}{90^\circ}) + 5.29 \qquad (50^\circ < \theta_w < 90^\circ) \tag{2.7}$$

In these formulae r_i, L_{lb} and b_w should be expressed in millimetres. It is assumed that the corner radius between the web and the top flange is equal to that between the web and the bottom flange; they are both represented by r_i. According to equations 2.2 to 2.7 Tsai's formula exclude any influence of the width of the top flange. The formula is based on curve fitting of finite element simulations.

The formula of Tsai does not give good results for the tests carried out by Bakker. This may be caused by the fact that for most of Bakker's tests the plate thickness was (slightly) smaller than 0.7 mm, and that in most of the tests the bottom flange corner radius was smaller than the top flange corner radius, while in Tsai's tests the bottom flange corner radius was equal to the top flange corner radius. Comparing the empirical formulae of Reinsch and Tsai, it is clear that they do not correspond very well. This is caused by basing them upon different tests which are carried out with different values of the parameters t, r_i, L_{lb} and b_w.

Chapter 3: Portal frame model, a 2D approach

The elastic web deformation behaviour may be analyzed by taking the loaded cross section of a member as a portal frame. The resulting two-dimensional model is described in this chapter.

3.1 Introduction

In section 2.5 it has become clear that the existing empirical web crippling stiffness prediction formulae do not give satisfactory results for tests from other populations than the ones they are based upon. Furthermore these prediction formulae are not based on a physical understanding of the elastic web crippling behaviour. Evidently, they cannot be used in the prediction of the web crippling stiffness of hat sections and deck sections in general, since they only give reasonable good approximations for members which have (geometrical) parameters with a magnitude which lies within certain limits.

In the model of Bakker however, the web crippling stiffness needs to be predicted in order to determine the point of intersection between the elastic curve and the rigid-plastic curve (and thus the mechanism initiation load). Hence, the need for an analytical model seems clear.

The approach in the analytical model is based upon the belief that relatively simple models may not be very accurate but do give a clear insight in the physical behaviour, from which more complicated models can be derived. Initially, a two-dimensional model is developed that offers a clear insight in the parameters of the cross section determining the web crippling stiffness. Hereafter, this two-dimensional model is extended to a three-dimensional model, taking the length of the member into account (chapter 4).

Probably the simplest approach to investigate the influence of several parameters of the cross section on the web crippling stiffness, is to idealize the cross section that is loaded by a concentrated load to a portal frame. Due to this idealization, a 'two-dimensional' web crippling stiffness can be calculated. This may be identified as a two-dimensional approach because only the cross section of a small slice of the member is taken into account while the length of the member is ignored. Web crippling results in local deformations that have maximum values under the concentrated load (figure 1.4). The portal frame model does not take these deformation variations over the length of the member into account. Eventually, the portal frame model is extended to a three-dimensional model, that does take these deformation variations over the length of the member into account, the so-called beam on elastic foundation model, which is treated in the chapter 4.

In the derivation of the portal frame model a distinction is made between hat sections and first generation deck panels. The assumptions that are made in the derivation of both portal frame models are described in section 3.2. Section 3.3 gives an overview of the derivation of the model describing the two-dimensional web crippling stiffness for hat sections, while in section 3.4 the derivation of the model for first generation deck panels is summarized. The influence of the schematisation of the rounding of the top flange corners within the portal frame model is discussed in section 3.5.

3.2 Assumptions

In the derivation of the portal frame model several assumptions are made. Some of these assumptions are made automatically by applying existing mechanical theories and will not be described here. For example, the hypothesis of Bernoulli is assumed to be valid in this model. Therefore, the applied laws of mechanics, which enable the calculation of the moment and stress distribution, may be used. The derivation of the model is based on these applied laws. The most important assumptions are summarized as follows:

- *Cross-section of the portal frame*

  In the (two-dimensional) portal frame model deformation variations over the length of the member are ignored. Only an infinitely small slice *dx* of the loaded part of the member is taken into account. The web crippling deformations are assumed to have a constant value over the length of this slice *dx*. The slice is idealized to a portal frame. The cross-section of this portal frame is characterized by its height and width. The height is taken equal to the wall thickness *t* of the member, while the width equals *dx*. An example of such a portal frame in case of hat sections is given in figure 3.1.

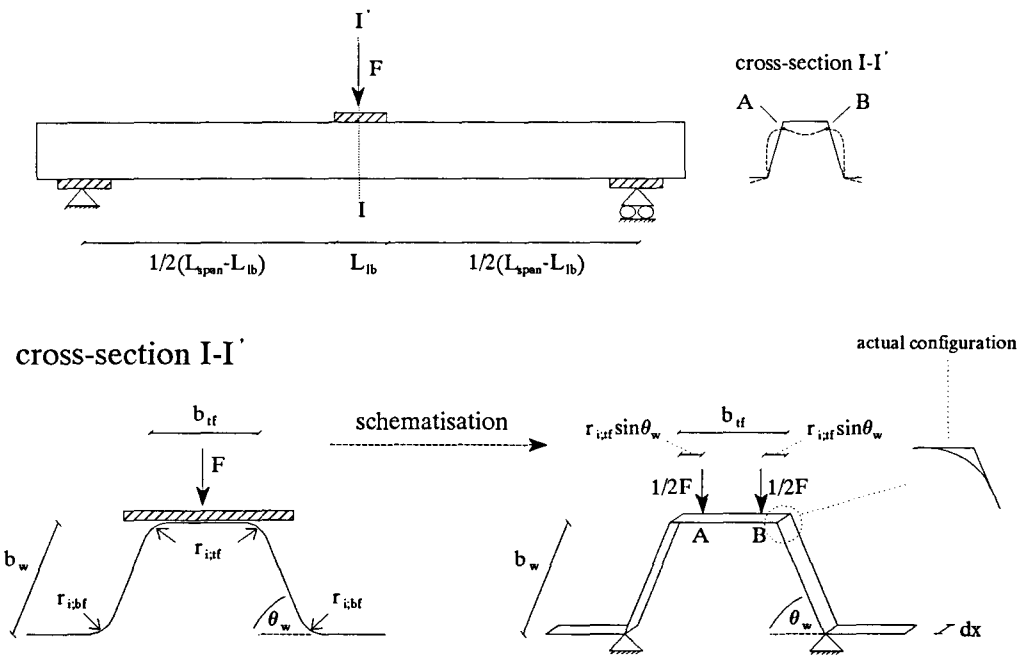

Figure 3.1: Schematisation of the cross-section to a portal frame

The schematisation of first generation deck panels to a portal frame differs slightly from the schematisation of figure 3.1, because they are thought of as a series of hat sections that are loaded uniformly and tied together at their unloaded flanges (section 3.4).

- *Supports*

  Since the objective of the model is to calculate the web crippling deformation (i.e. the decrease of the height of the web h_w underneath the load bearing plate), the vertical translation of the member itself is of no interest. The frame is modelled with hinged supports at the connection between the web and the unloaded flange (figure 3.1). Hence, the web crippling deformation in this model can be defined as the deflection at the concentrated loads (points A and B in figure 3.1). As a result from the schematisation the web crippling deformations in the portal frame model are composed of bending deformations of the top flange corner radius and axial deformations of the web. The horizontal reaction forces, that are required to establish equilibrium, are supplied by the unloaded flange. Since the unloaded flanges of hat sections can translate freely unlike the coupled unloaded flanges of deck panels, the horizontal reaction force is applied at different points for hat sections and deck panels (section 3.3 and 3.4).

- *Corner radii*

  In figure 3.1 it is shown that the loaded cross-section of the member is schematised to a portal frame composed of straight beam sections. In describing the geometry of the cross-section the rounding of the top flange corners is thus ignored, except that the eccentrical load application of F which is caused by the rounding of the corners is taken into account explicitly. The eccentrical load application is expected to have a large influence on the web crippling deformations due to the extra bending deformations. In section 3.5 it is shown that the geometrical simplification of not taking the rounding of the corners into account does not have a significant influence on the calculated web crippling deformation. The rounding of the bottom flange corners is not taken into account either. The transmission of the load F to the supports of the member occurs mainly by the transmission of shear stresses in the web. Although the supports are applied eccentrically with respect to the web, this is expected to have nearly no influence on the web crippling deformations of the loaded cross-section of the member and thus on the portal frame, because the resulting extra bending deformations due to the eccentrical application of the supports will only occur within a small region of the supports. This is confirmed by finite element simulations (chapter 7) which indicate that the web crippling deformations are only influenced by a small part of the member near the load bearing plate (the web crippling stiffness appears to be independent of the span length). Hence, the eccentrical application is not taken into account and the supports of the portal frame model are applied right underneath the web. Hereby, the web crippling stiffness will not be dependent on the bottom flange corner radii.

- *Application of the loads*

  In figure 3.1 it is shown that in the model the loading is applied by two concentrated loads, while in reality the load is applied by a load bearing plate which covers the whole width of the top flange.

However, the downward curling of the flange underneath the load bearing plate (the dotted line in figure 3.1) results in only two contact points (*A* and *B*) between flange and load bearing plate after initial loading. Therefore, the transmission of the load *F* is limited to these points and each point transmit *1/2F*. To model this eccentric load application with respect to the web, the contact points are located at a distance $r_{i;tf} \cdot \sin\theta_w$ from the point of intersection of the top flange and web.

- *Shear deformations*

  The portal frame deforms due to shear forces, axial forces and bending moments. In the model it is assumed that the shear deformations have a negligibly small influence on the overall deformation and are therefore not taken into account.

3.3 *Derivation of the portal frame model of hat sections*

In the following an overview is given of the derivation of the portal frame model of hat sections with inclined or vertical webs (web angle $\theta_w \leq 90°$). A more detailed derivation is given in appendix A.1. The web crippling deformation is given by the displacement of the points *A* and *B* with respect to the supports (figure 3.1). Note that in this model the top flange corner radius $r_{i;tf}$ is considered to belong to the web and hence contributes to the web crippling deformations. The displacement of *A* (which equals the displacement of *B* due to symmetry) can be calculated by using Castigliano's law. This law points out that the displacement of any point *j* in the direction of a concentrated force F_j at point *j* can be calculated by differentiating the external work (which equals the internal work) with respect to this force F_j. The general format of this law is given by

$$\frac{\partial W}{\partial F_j} = w_j \tag{3.1}$$

where the internal work of a beam with a length *l* equals

$$W = \frac{1}{2} \cdot \int_0^l \left(\frac{N^2}{EA} + \eta \cdot \frac{V^2}{GA} + \frac{T^2}{GI_{wr}} + \frac{M^2}{EI_y}\right) dx \tag{3.2}$$

In the portal frame model shear deformations are not taken into account and torsion does not to take place due to symmetry. Therefore, in equation 3.2 these terms may be omitted.

In a portal frame that is divided in *n* different beams with a certain length *l*, the displacement of *j* can thus be calculated as

$$w_j = \frac{\partial}{\partial F_j} \sum_{i=1}^{n} \frac{1}{2} \cdot \int_0^{l_i} \left(\frac{N^2}{EA} + \frac{M^2}{EI}\right) dx \tag{3.3}$$

The statical system of the portal frame in case of hat sections is given in figure 3.2.
The end of the unloaded flanges of a hat section can rotate and translate freely. In case of hat sections, the horizontal support (that is required for equilibrium) is applied at the connection between the web and the unloaded flange (at the same place as the vertical support). According to the model the unloaded flange does thus not influence the stress distribution in the frame. In reality, that is, in the three-dimensional situation, the unloaded flange of a hat section only resists the overall bending moment over the length of the member (together with the loaded flange). Hence this model seems to be an acceptable two-dimensional approach.

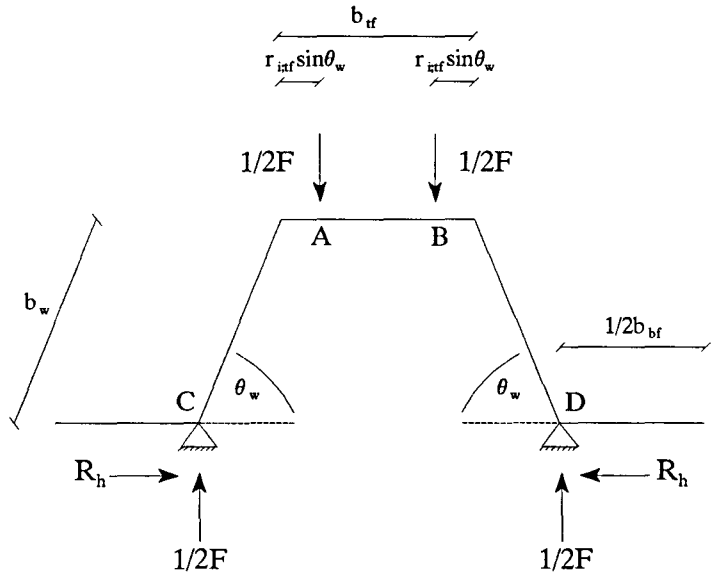

Figure 3.2: *Statical system of the portal frame model of hat sections*

To calculate the web crippling deformation Δh_w;*2D*, that is, the vertical displacement of point A, w_A, it is necessary to calculate the reaction forces at the supports first. Due to symmetry the vertical reaction forces at *C* and *D* equal *1/2F*. The portal frame is one-fold statically undetermined and the horizontal reaction forces at *C* and *D*, R_h, can be derived with Castigliano's law, using the condition

$$u_C = u_D = 0 \tag{3.4}$$

in which u_i represents the horizontal displacement of point *i*.
Using equation 3.2 the internal work of the portal frame can be specified as

$$W = \int_0^{b_w} \left[\frac{(R_h \cdot \cos\theta_w + 1/2 \cdot F \cdot \sin\theta_w)^2}{EA} + \frac{(R_h \cdot x \cdot \sin\theta_w - 1/2 \cdot F \cdot x \cdot \cos\theta_w)^2}{EI} \right] dx$$

$$+ \int_0^{r_{i;tf}\cdot\sin\theta_w} [\frac{R_h^2}{EA} + \frac{(1/2\cdot F\cdot x - R_h\cdot b_w\cdot\sin\theta_w + 1/2\cdot F\cdot b_w\cdot\cos\theta_w)^2}{EI}]\,dx$$

$$+ \int_0^{1/2\cdot b_{tf} - r_{i;tf}\cdot\sin\theta_w} [\frac{R_h^2}{EA} + \frac{(1/2\cdot F\cdot b_w\cdot\cos\theta_w - R_h\cdot b_w\cdot\sin\theta_w + 1/2\cdot F\cdot r_{i;tf}\cdot\sin\theta_w)^2}{EI}]\,dx \qquad (3.5)$$

in which

$A = dx\cdot t$

and

$I = \frac{dx\cdot t^3}{12}$

Combining equations 3.1 and 3.4, the reaction force R_h can be calculated by solving

$$\frac{\partial W}{\partial R_h} = u_D = 0 \qquad (3.6)$$

If the deformations due to axial forces are ignored (appendix A.1), R_h becomes

$$R_h = \frac{F}{4\cdot b_w\cdot\sin\theta_w}\cdot[\frac{2/3\cdot b_w^2\cdot\cos\theta_w + r_{i;tf}\cdot b_{tf}\cdot\sin\theta_w + b_{tf}\cdot b_w\cdot\cos\theta_w - r_{i;tf}^2\cdot\sin^2\theta_w}{1/2\cdot b_{tf} + 1/3\cdot b_w}] \qquad (3.7)$$

Strictly spoken, this approach is not reliable for members where θ_w has a magnitude around 0, but in that case the sections can't be thought of as hat sections anymore. Since it is defined that

$$\frac{\partial W}{\partial 1/2\cdot F} = w_A = \Delta h_w;2D$$

in which $\Delta h_w;2D$ represents the (two-dimensional) web crippling deformation of a slice dx, the web crippling deformation can be derived by differentiating equation 3.5 with respect to the applied force at A, which gives

$$\Delta h_w;2D = \frac{b_w\cdot\sin\theta_w}{EA}\cdot[2\cdot R_h\cdot\cos\theta_w + F\cdot\sin\theta_w] + \frac{F}{EI}\cdot[1/3\cdot b_w^3\cdot\cos\theta_w + 1/2\cdot b_{tf}\cdot b_w^2\cdot\cos^2\theta_w]$$

$$+ \frac{F}{EI}\cdot[r_{i;tf}\cdot\sin\theta_w\cdot(b_{tf}\cdot b_w\cdot\cos\theta_w - r_{i;tf}\cdot\sin\theta_w\cdot(b_w\cdot\cos\theta_w - 1/2\cdot b_{tf} + 2/3\cdot r_{i;tf}\cdot\sin\theta_w))]$$

$$-\frac{R_h \cdot b_w \cdot \sin\theta_w}{EI} \cdot [2/3 \cdot b_w^2 \cdot \cos\theta_w - r_{i;tf}^2 \cdot \sin^2\theta_w + b_{tf} \cdot r_{i;tf} \cdot \sin\theta_w + b_{tf} \cdot b_w \cdot \cos\theta_w] \tag{3.8}$$

The web crippling stiffness is defined to be

$$k_{\Delta h_w;2D} = \frac{F}{\Delta h_w;2D} \tag{3.9}$$

After substitution of equation 3.7 into equation 3.8 and applying equation 3.9, the reciproke two-dimensional web crippling stiffness can be specified as

$$\frac{1}{k_{\Delta h_w;2D}} = \frac{b_w \cdot \sin^2\theta_w}{EA} + \frac{\cos\theta_w}{EA} \cdot [\frac{b_w \cdot \cos\theta_w \cdot (2/3 \cdot b_w + b_{tf}) + r_{i;tf} \cdot b_{tf} \cdot \sin\theta_w - r_{i;tf}^2 \cdot \sin^2\theta_w}{b_{tf} + 2/3 \cdot b_w}]$$

$$+ r_{i;tf}^2 \cdot \sin^2\theta_w \cdot [\frac{b_w \cdot (b_{tf} - 4/3 \cdot r_{i;tf} \cdot \sin\theta_w) + r_{i;tf} \cdot \sin\theta_w \cdot (b_{tf} - 3/2 \cdot r_{i;tf} \cdot \sin\theta_w)}{EI \cdot (3 \cdot b_{tf} + 2 \cdot b_w)}] \tag{3.10}$$

For hat sections with vertical webs (θ_w=90°) equation 3.10 can be reduced to

$$\frac{1}{k_{\Delta h_w;2D}} = \frac{b_w}{EA} + r_{i;tf}^2 \cdot [\frac{b_w \cdot (b_{tf} - 4/3 \cdot r_{i;tf}) + r_{i;tf} \cdot (b_{tf} - 3/2 \cdot r_{i;tf})}{EI \cdot (3 \cdot b_{tf} + 2 \cdot b_w)}] \tag{3.11}$$

Equations 3.10 and 3.11 show that the web crippling stiffness is determined by bending deformations and deformations due to axial forces. Note that the bending deformations are independent of the magnitude of θ_w. The deformations due to axial forces in both equations 3.10 and 3.11 are relatively small compared to the bending deformations. In fact, they appear to be negligibly small, particularly in case of hat sections with rather large corner radii (about 10 mm). From an investigation of the influence of the web crippling deformations due to axial forces (appendix A.4) it becomes clear that this influence mainly depends on the magnitude of the corner radii and the wall thickness. Apparently, the web crippling deformations due to axial forces may be neglected if $r_{i:tf} > 2\ mm$ and $t < 2\ mm$.

3.4 *Derivation of the portal frame model of first generation deck panels*

First generation deck panels are assumed to be loaded by a concentrated load over the whole width of the panel and to have hinged supports over the whole width of the panel.

This corresponds with the schematisation of figure 1.4 in section 1.1. Since first generation deck panels are uniformly loaded over their width, they can be thought of as a composition of hat sections tied together at the unloaded flange (figure 3.3). This is an important assumption in the derivation of the web crippling stiffness for first generation deck panels.

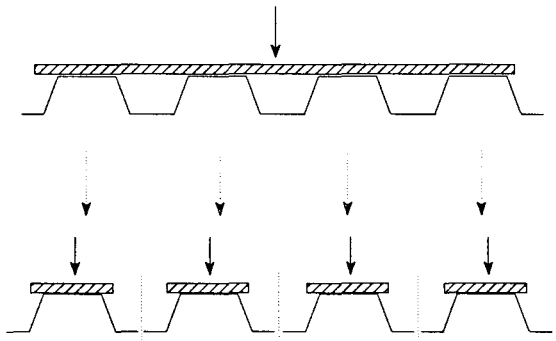

Figure 3.3: *Schematisation of a first generation deck panel as a series of hat sections*

Each of these hat sections will show the same physical web crippling behaviour, because they are loaded similarly. An exception has to be made for the two outer hat sections that are not tied together at their outer unloaded flange, resulting in a slightly different web crippling behaviour. However, this different behaviour is not expected to have a significant influence on the overall behaviour of the panel. Therefore, the calculation of the web crippling stiffness of a first generation deck panel can be reduced to the calculation of a hat section. Since the hat sections are tied together at the unloaded flanges, the rotations and displacements of the ends of the unloaded flanges have to be compatible. Due to the fact that each hat section deforms symmetrically, the ends of the unloaded flanges will show opposite rotations and horizontal displacements. Hence, the rotation φ_E and the horizontal displacement u_E of the end of the unloaded flange need to be zero. This may be schematized by a fixed end which can displace vertically (figure 3.4).

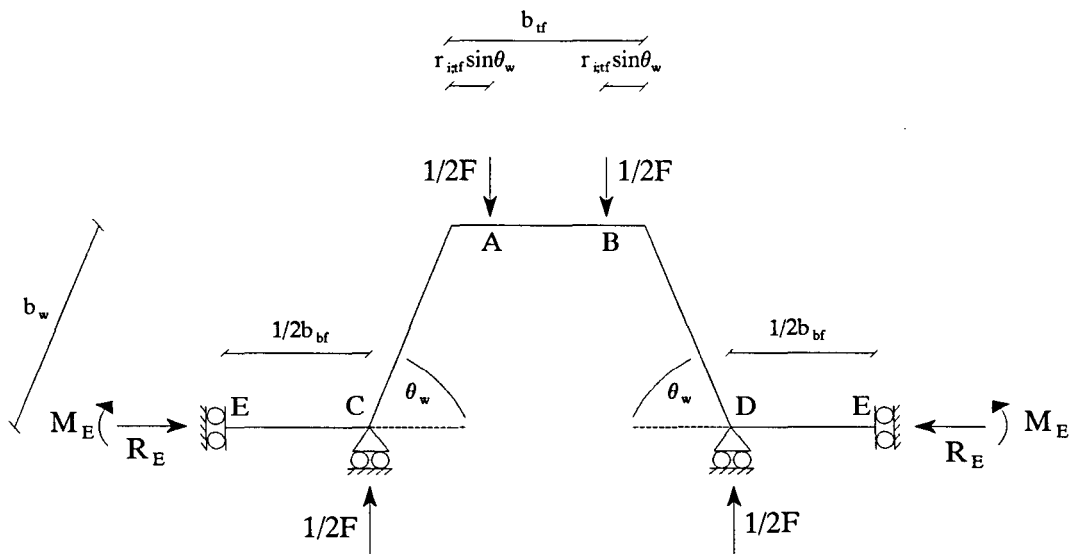

Figure 3.4: *Statical system of the portal frame model of first generation deck panels*

The bending moment M_E and the horizontal reaction force R_E maintain the continuity of the deck panel. Except the application of the supports in the statical system, the other assumptions which are made in the derivation of the model of hat sections remain valid.

The portal frame of figure 3.4 is twofold statically undetermined and the determination of R_E and M_E can be established by using Castigliano's law (equation 3.1), whereafter the web crippling deformation can be calculated with the same law.

In this model shear deformations are not taken into account and torsion does not take place due to symmetry. Using equation 3.2 the internal work of the portal frame of figure 3.4 can be specified as

$$W = \int_0^{1/2 \cdot b_{bf}} \left[\frac{R_E^2}{EA} + \frac{M_E^2}{EI}\right] dx + \int_0^{b_w} \left[\frac{(R_E \cdot \cos\theta_w + 1/2 \cdot F \cdot \sin\theta_w)^2}{EA} + \frac{(R_E \cdot x \cdot \sin\theta_w - 1/2 \cdot Fx\cos\theta_w - M_E)^2}{EI}\right] dx$$

$$+ \int_0^{r_{i;tf} \cdot \sin\theta_w} \left[\frac{R_E^2}{EA} + \frac{(1/2 \cdot F \cdot x - R_E \cdot b_w \cdot \sin\theta_w + 1/2 \cdot F \cdot b_w \cdot \cos\theta_w + M_E)^2}{EI}\right] dx$$

$$+ \int_0^{1/2 \cdot b_{tf} - r_{i;tf} \cdot \sin\theta_w} \left[\frac{R_E^2}{EA} + \frac{(1/2 \cdot F \cdot (b_w \cdot \cos\theta_w + r_{i;tf} \cdot \sin\theta_w) - R_E \cdot b_w \cdot \sin\theta_w + M_E)^2}{EI}\right] dx \qquad (3.12)$$

R_E and M_E can be found by solving the equations

$$\frac{\partial W}{\partial R_E} = u_E = 0 \qquad (3.13a)$$

and

$$\frac{\partial W}{\partial M_E} = \varphi_E = 0 \qquad (3.13b)$$

After proper substitutions (appendix A.2) it follows that

$$R_E = \frac{F \cdot (b_w \cdot \cos\theta_w \cdot (b_{bf} \cdot (3 \cdot b_{tf} + 2 \cdot b_w) + b_w \cdot (2 \cdot b_{tf} + b_w)) - 3 \cdot r_{i;tf} \cdot \sin\theta_w \cdot (b_{bf} + b_w) \cdot (r_{i;tf} \cdot \sin\theta_w - b_{tf}))}{2 \cdot b_w \cdot \sin\theta_w \cdot (b_{bf} \cdot (3 \cdot b_{tf} + 2 \cdot b_w) + b_w \cdot (2 \cdot b_{tf} + b_w))} \qquad (3.14a)$$

and

$$M_E = -\frac{F \cdot r_{i;tf} \cdot b_w \cdot \sin\theta_w \cdot (r_{i;tf} \cdot \sin\theta_w - b_{tf}))}{2 \cdot (b_{bf} \cdot (3 \cdot b_{tf} + 2 \cdot b_w) + b_w \cdot (2 \cdot b_{tf} + b_w))} \qquad (3.14b)$$

Now, the web crippling deformation (i.e. the displacement of point A with respect to the supports) can be calculated by differentiating equation 3.12 (the internal work) with respect to the applied force at A, which

results in

$$\Delta h_{w;2D} = \frac{b_w \cdot \sin\theta_w}{EA} \cdot (2 \cdot R_E \cdot \cos\theta_w + F \cdot \sin\theta_w) + \frac{F}{EI} \cdot (1/3 \cdot b_w^3 \cdot \cos^2\theta_w)$$

$$+ \frac{F}{EI} \cdot (1/2 \cdot b_{tf} \cdot b_w^2 \cdot \cos^2\theta_w + b_w \cdot r_{i;tf} \cdot \sin\theta_w \cdot \cos\theta_w \cdot (b_{tf} - r_{i;tf} \cdot \sin\theta_w) + 1/2 \cdot b_{tf} \cdot r_{i;tf}^2 \cdot \sin^2\theta_w - 2/3 \cdot r_{i;tf}^3 \cdot \sin^3\theta_w)$$

$$+ \frac{M_E}{EI} \cdot (b_w \cdot \cos\theta_w \cdot (b_w + 2 \cdot r_{i;tf} \cdot \sin\theta_w) + r_{i;tf}^2 \cdot \sin^2\theta_w + 2 \cdot (r_{i;tf} \cdot \sin\theta_w + b_w \cdot \cos\theta_w) \cdot (1/2 \cdot b_{tf} - r_{i;tf} \cdot \sin\theta_w))$$

$$- \frac{R_E \cdot b_w \cdot \sin\theta_w}{EI} \cdot (2/3 \cdot b_w^2 \cdot \cos\theta_w - r_{i;tf}^2 \cdot \sin^2\theta_w + b_{tf} \cdot (r_{i;tf} \cdot \sin\theta_w + b_w \cdot \cos\theta_w)) \qquad (3.15)$$

Using equation 3.10 and substituting equations 3.14a and 3.14b into equation 3.15 gives

$$\frac{1}{k_{\Delta h_w;2D}} = \frac{b_{bf} \cdot b_w \cdot (3 \cdot b_{tf} + 2 \cdot b_w) + 3 \cdot r_{i;tf} \cdot \sin\theta_w \cdot \cos\theta_w \cdot (b_{bf} + b_w) \cdot (b_{tf} - r_{i;tf} \cdot \sin\theta_w) + b_w^2 \cdot (2 \cdot b_{tf} + b_w)}{EA \cdot (b_{bf} \cdot (3 \cdot b_{tf} + 2 \cdot b_w) + b_w \cdot (2 \cdot b_{tf} + b_w))}$$

$$+ \frac{r_{i;tf}^2 \cdot \sin^2\theta_w \cdot b_{bf} \cdot (r_{i;tf} \cdot \sin\theta_w \cdot (6 \cdot b_{tf} - 9 \cdot r_{i;tf} \cdot \sin\theta_w) + b_w \cdot (6 \cdot b_{tf} - 8 \cdot r_{i;tf} \cdot \sin\theta_w))}{6 \cdot EI \cdot (b_{bf} \cdot (3 \cdot b_{tf} + 2 \cdot b_w) + b_w \cdot (2 \cdot b_{tf} + b_w))}$$

$$+ \frac{b_w \cdot r_{i;tf}^2 \cdot \sin^2\theta_w \cdot (4 \cdot r_{i;tf} \cdot \sin\theta_w \cdot (b_{tf} - b_w) + 3 \cdot b_{tf} \cdot b_w - 6 \cdot r_{i;tf}^2 \cdot \sin^2\theta_w)}{6 \cdot EI \cdot (b_{bf} \cdot (3 \cdot b_{tf} + 2 \cdot b_w) + b_w \cdot (2 \cdot b_{tf} + b_w))} \qquad (3.16)$$

Equation 3.16 shows that the web crippling stiffness is determined by bending deformations and deformations due to axial forces. Note that the bending deformations are independent of the magnitude of θ_w (as with hat sections).

The deformations due to axial forces in equation 3.16 are relatively small compared to the bending deformations. In fact, they appear to be negligibly small, particularly in case of hat sections with rather large corner radii (about 10 mm). From the investigation of the web crippling deformations due to axial forces (appendix A.5) it becomes clear that this influence mainly depends on the magnitude of the corner radii and the wall thickness. The deformations due to axial forces may be neglected if $r_{i;tf} > 2\ mm$ and $t < 2\ mm$.

3.5 *Influence of the rounding of the top flange corners*

In the derived model the top flange corner radii are taken into account by means of an eccentric application of the loads. However, in describing the geometry of the cross-section the rounding of the top flange corners is ignored, as can be seen in figure 3.1. In this section the influence of this geometrical simplification on the web crippling stiffness will be analyzed. Only hat sections will be considered, since it is assumed that the influence in first generation deck panels will not differ much from that in hat sections. If the rounding of the

top flange corners is taken into account a different and more complicate approximation of the web crippling stiffness will be obtained. This is caused by a different transmission of the concentrated load at the curved transitions compared to the linear schematisation of figure 3.1.

The influence of the rounding of the corners is only investigated for hat sections with vertical webs (θ_w=90°). For members having inclined webs the horizontal reaction force R_h will be larger, which may imply a larger influence of the rounding of the corners on the resulting web crippling stiffness. However, for rather regular . members ($\theta_w \geq 45°$) this influence is only slightly larger. Hence, if the influence appears to be negligibly small for members having vertical webs, this holds also approximately true for members having inclined webs.

According to the derived model, where the rounding of the corners is ignored, the web crippling stiffness of is given by

$$\frac{1}{k_{\Delta h_w;2D}} = \frac{b_w}{EA} + r_{i;tf}^2 \cdot \left[\frac{b_w \cdot (b_{tf} - 4/3 \cdot r_{i;tf}) + r_{i;tf} \cdot (b_{tf} - 3/2 \cdot r_{i;tf})}{EI \cdot (3 \cdot b_{tf} + 2 \cdot b_w)}\right] \tag{3.17}$$

If the curved transitions are taken into account, the statical system of hat sections with vertical webs can be specified as in figure 3.5.

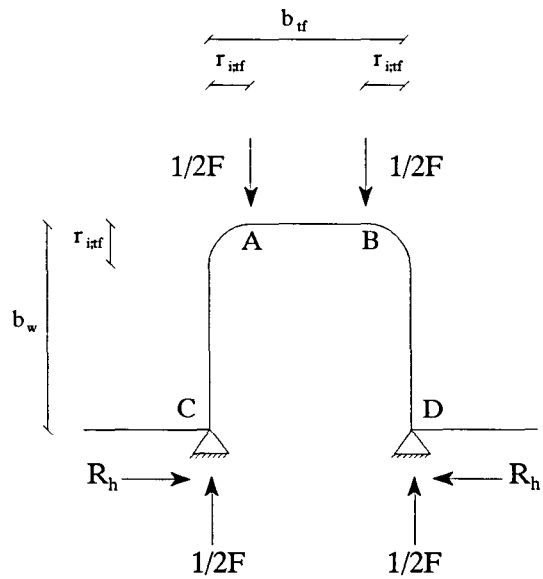

Figure 3.5: *Statical system of hat sections, taking the curved transitions into account*

Now, it can be derived (appendix A.3) that

$$\frac{1}{k_{\Delta h_w;2D}} = \frac{3 \cdot \pi \cdot r_{i;tf}^2}{4 \cdot b_w \cdot EA} \cdot \left[\frac{b_{tf} - r_{i;tf}}{3 \cdot b_{tf} + 2 \cdot b_w}\right] + \frac{(1/4 \cdot \pi - 1) \cdot r_{i;tf} + b_w}{EA} + \frac{3/2 \cdot (\pi - 3)}{b_w \cdot EI} \cdot \left[\frac{r_{i;tf}^4 \cdot (b_{tf} - r_{i;tf})}{3 \cdot b_{tf} + 2 \cdot b_w}\right]$$

$$+ r_{i;tf}^2 \cdot [\frac{(3/2 \cdot \pi - 6) \cdot r_{i;tf}^2 + (3/4 \cdot \pi - 3/2) \cdot b_{tf} \cdot r_{i;tf} + b_w \cdot ((3/2 \cdot \pi - 6) \cdot r_{i;tf} + b_{tf})}{EI \cdot (3 \cdot b_{tf} + 2 \cdot b_w)}] \tag{3.18}$$

In appendix A.3 the schematisation of the portal frame model is evaluated by comparing this model (i.e. equation 3.19) with the above derived model that takes the curved transitions into account. This comparison is carried out by varying each parameter that is involved. The deviations appear to be less than 1% (appendix A.3) for rather regular geometrical dimensions and turns out to be significant only in case of members having unrealistic dimensions.

Therefore, it may be concluded that the derived model is a sufficient accurate approximation compared to the model where the curved transition is not ignored.

Chapter 4: Beam on elastic foundation model

This chapter describes the extension of the two-dimensional portal frame model to a three-dimensional model, using the theory of a beam on an elastic foundation.

4.1 Introduction

The portal frame model (as it was presented in chapter 3) can be thought of as a two-dimensional approach in determining the web crippling stiffness: over the length of the member only the length of an infinitely small slice dx under the load bearing plate is taken into account. Actually, the resulting web crippling stiffness can be thought of as the web crippling stiffness of a member with a small length dx. The member is assumed to deform uniformly under this slice dx. This two-dimensional approach underestimates the web crippling stiffness. The main reason for this underestimation is that in reality the whole length of the member L_{span} deforms and not only a slice dx of the member under the load bearing plate. Neglecting the member outside this slice dx results in an underestimation of the force F that is required to deform the whole member. According to equation 3.9 this underestimation of the required force F corresponds with an underestimation of the web crippling stiffness and an overestimation of the web crippling deformations.

Taking the influence of web crippling deformations over the length of the member into account, a better three-dimensional approximation of the web crippling stiffness can be established. Hence, the need for an extension from the two-dimensional portal frame model to a three-dimensional model seems clear.

The influence of web crippling deformations over the length of the member can be modelled in several ways. Probably the simplest extension to a three-dimensional model is established by assuming that the member deforms uniformly over the length of the load bearing plate and does not have any web crippling deformations beside the load bearing plate. This so-called 'uniform web crippling deformation' approach is treated in section 4.2.

A more complicated extension may be derived if it is taken into account that web crippling results in varying deformations over the length of the member. The influence of varying deformations over the length of the member may be modelled by means of the theory of a beam on an elastic foundation. According to this theory the web of the member is thought of as a continuous elastic support (foundation) of the top flange (beam). This approach enables the determination of the resistance of the web as a function of the web crippling deformation. In other words, the web holds up the flange over the whole length by means of a certain foundation stiffness. The use of the theory of a beam on an elastic foundation was first proposed by Bergfelt *(1977)*. Bergfelt has attempted to model the web crippling behaviour of plate girders by considering the flange of a plate girder as an elastic beam on an elastic foundation formed by the web. Tsai *(1987)* developed an analytical model to determine the load-deformation behaviour of cold-formed steel members subjected to the combined action of a concentrated load and a bending moment. In the model of Tsai it has been put forward that the length of the hinge mechanism (figure 2.5) might be approximated using the theory

of a beam on an elastic foundation.

With the use of the theory of a beam on an elastic foundation two extensions to a three-dimensional model are derived within this study, namely an 'effective length' approach and a 'full length' approach. For the sake of clearness, section 4.3 first summarizes the general theory of a beam on an elastic foundation. A general description of the application of this theory in the derivation of the web crippling stiffness of hat sections and first generation deck panels that holds true for both the effective length approach and the full length approach is given in section 4.4

In the effective length approach it is proposed to introduce an effective length, where outside the effective length area the elastic web crippling deformations are assumed to be negligibly small. The magnitude of the effective length has been derive using the theory of a beam on an elastic foundation. The effective length approach is treated in section 4.5.

In the full length approach the variations of the web crippling deformations over the whole length of the member are taken into account and described using the theory of a beam on an elastic foundation. The full length approach is described in section 4.6.

Finally, in section 4.7 the full length approach and the effective length approach as an extension from the portal frame model to a three-dimensional model are evaluated.

4.2 *Uniform web crippling deformation approach*

From test results of Bakker *(1992)*, Reinsch *(1983)* and Tsai *(1987)* it can be concluded that the member after the formation of the (plastic) hinge mechanism shows more or less uniform web crippling deformations underneath the load bearing plate. It can also be concluded that the web crippling deformations decrease beside the load bearing plate to the outer side of the member (figure 1.4). It seems quite reasonable to assume that the rather uniform web crippling deformations under the load bearing plate also appear in the elastic phase of loading.

In the uniform web crippling deformation approach (figure 4.1) it is assumed that the member deforms uniformly under the load bearing plate. The web crippling deformations beside the load bearing plate are neglected.

Since it is assumed that the member deforms uniformly under the load bearing plate, it is relatively simple to extend the portal frame model to the uniform web crippling deformation approach. The two-dimensional web crippling stiffness $k_{\Delta h_w;2D}$ of the portal frame model was derived for a small slice dx under the load bearing plate.

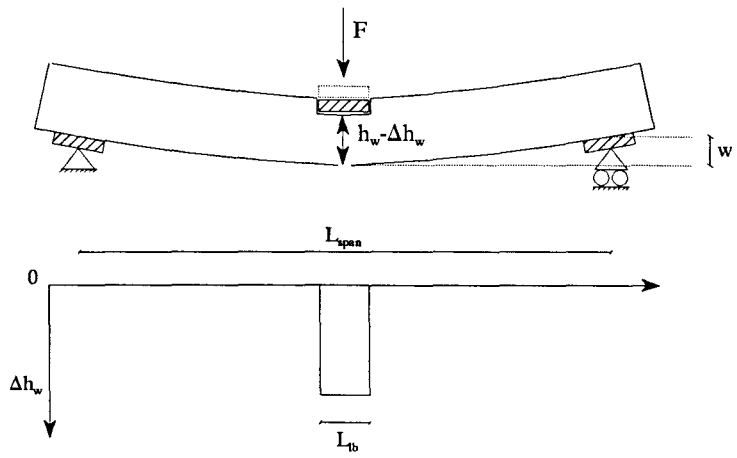

Figure 4.1: *Web crippling deformations in the uniform web crippling deformation approach*

According to the uniform web crippling deformation approach each slice *dx* under the load bearing plate has the same web crippling stiffness and the rest of the member beside the load bearing plate does not contribute to the web crippling stiffness. Hence the three-dimensional web crippling stiffness $k_{\Delta h_w}$ can be derived by multiplying the two-dimensional web crippling stiffness $k_{\Delta h_w;2D}$ with a factor L_{lb}/dx. Using equation 3.10 this gives for hat sections

$$\frac{1}{k_{\Delta h_w}} = \frac{b_w \cdot \sin^2\theta_w}{E \cdot t \cdot L_{lb}} + \frac{\cos\theta_w}{E \cdot t \cdot L_{lb}} \cdot \left[\frac{b_w \cdot \cos\theta_w \cdot (2/3 \cdot b_w + b_{tf}) + \sin\theta_w \cdot r_{i;tf} \cdot b_{tf} - \sin^2\theta_w \cdot r_{i;tf}^2}{b_{tf} + 2/3 \cdot b_w}\right]$$

$$+ \sin^2\theta_w \cdot r_{i;tf}^2 \cdot \left[\frac{b_w \cdot (b_{tf} - 4/3 \cdot \sin\theta_w \cdot r_{i;tf}) + \sin\theta_w \cdot r_{i;tf} \cdot (b_{tf} - 3/2 \cdot \sin\theta_w \cdot r_{i;tf})}{E \cdot t^3 \cdot L_{lb} \cdot (1/4 \cdot b_{tf} + 1/6 \cdot b_w)}\right] \quad (4.1a)$$

Similarly, the web crippling stiffness for first generation deck panels can be specified as

$$\frac{1}{k_{\Delta h_w}} = \frac{b_{bf} \cdot b_w \cdot (3 \cdot b_{tf} + 2 \cdot b_w) + 3 \cdot r_{i;tf} \cdot \sin\theta_w \cdot \cos\theta_w \cdot (b_{bf} + b_w) \cdot (b_{tf} - \sin\theta_w \cdot r_{i;tf}) + b_w^2 \cdot (2 \cdot b_{tf} + b_w)}{E \cdot t \cdot L_{lb} \cdot (b_{bf} \cdot (3 \cdot b_{tf} + 2 \cdot b_w) + b_w \cdot (2 \cdot b_{tf} + b_w))}$$

$$+ \frac{\sin^2\theta_w \cdot r_{i;tf}^2 \cdot b_{bf} \cdot (\sin\theta_w \cdot r_{i;tf} \cdot (6 \cdot b_{tf} - 9 \cdot \sin\theta_w \cdot r_{i;tf}) + b_w \cdot (6 \cdot b_{tf} - 8 \cdot \sin\theta_w \cdot r_{i;tf}))}{1/2 \cdot E \cdot t^3 \cdot L_{lb} \cdot (b_{bf} \cdot (3 \cdot b_{tf} + 2 \cdot b_w) + b_w \cdot (2 \cdot b_{tf} + b_w))}$$

$$+ \frac{\sin^2\theta_w \cdot r_{i;tf}^2 \cdot b_w \cdot (4 \cdot \sin\theta_w \cdot r_{i;tf} \cdot (b_{tf} - b_w) + 3 \cdot b_{tf} \cdot b_w - 6 \cdot \sin^2\theta_w \cdot r_{i;tf}^2)}{1/2 \cdot E \cdot t^3 \cdot L_{lb} \cdot (b_{bf} \cdot (3 \cdot b_{tf} + 2 \cdot b_w) + b_w \cdot (2 \cdot b_{tf} + b_w))} \quad (4.1b)$$

These formulae represent a very rough estimation of the web crippling stiffness but nevertheless give some insight in how the web crippling stiffness depends on the different parameters.
In the uniform web crippling deformation approach the web crippling stiffness is still underestimated, which can be clarified in two different ways.
Firstly, the whole length of the member L_{span} deforms and not only the part of the member under the load bearing plate, as was assumed in the uniform web crippling deformation approach. These deformations beside the load bearing plate require some extra work that is needed to establish the same deformations underneath the load bearing plate. In other words, a larger load F is needed to obtain the same web crippling deformations. Hence, the web crippling stiffness is underestimated.
Secondly, in the uniform web crippling deformation approach the part of the member beside the load bearing plate (i.e. the unloaded part) is not taken into account while in reality the unloaded part of the member will restrain the loaded part of the member and thus decrease the web crippling deformations. Therefore, the uniform web crippling deformation approach underestimates the web crippling stiffness.
In fact, the uniform web crippling deformation approach is only suitable to members which are uniformly deformed over the length of the load bearing plate and not deformed at all beside the load bearing plate. Web crippling results in local deformations that vary along the length of the member. These varying deformations have a maximum magnitude at the centre of the load bearing plate and decrease to the outer sides of the member. Taking the influence of varying deformations over the whole length of the member into account, a better three-dimensional approximation can be established. The variation of the web crippling deformations over the length the member can be described using the theory of a beam on an elastic foundation.

4.3 *General theory of a beam on an elastic foundation*

The theory of the bending of a beam on an elastic foundation has been developed by Winkler *(1867)* and formed the basis of Zimmermann's classical work on the analysis of the railroad track *(1888)*, in which the rails are supported almost along their entire length, by closely spaced sleepers (cross-beams).
In general, the elastic support is provided by a load-bearing medium, referred to as the foundation, distributed continuously along the length of the beam. Though the early investigators thought mainly of soil as the supporting medium, it was later found that there are other fields where the conditions of Winkler's assumption are much more rigorously satisfied, such as in the construction of floor structures for ships, buildings, and bridges and in thin-walled tubes, shells, and domes *(Hetenyi, 1946)*.
In some of the problems the identity of the beam and the foundation can be easily established, as in the case of the railroad track or in the case of actual foundation structures. In other problems however, the concept of beam and foundation is of a more abstract nature. For instance in thin walled tubes and shells, the elastic foundation for the beam part is supplied by the resilience of the adjoining portions of a continuous elastic structure.

The theory is characterized by the fact that when the beam is deflected, the continuously distributed reaction in the foundation at every point is proportional to the deflection at that point. The reaction is independent of reactions or deflections produced elsewhere in the foundation. Such a correlation implies a lack of continuity in the supporting medium, just as if it were made up of rows of closely spaced but independent elastic springs. Under such conditions the reaction per unit length of the beam can be represented by ky, in which y is the deflection and k is a constant usually called the modulus of foundation. This constant denotes the reaction per unit length when the deflection is equal to unity.

Consider an infinitely long prismatic beam supported along its entire length is subjected to a single concentrated load F, as in figure 4.2.

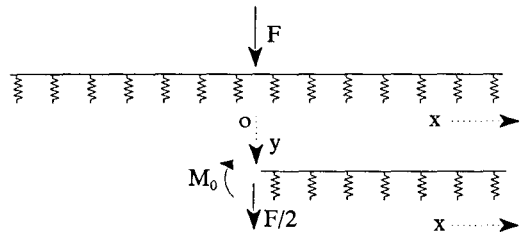

Figure 4.2: *Single concentrated load acting on an infinitely long beam*

It can be derived (appendix B.1) that the deflection curve of the right side ($x \geq 0$) of the beam is given by the function

$$y = \frac{F \cdot \beta}{2 \cdot k} \cdot e^{-\beta x} \cdot (\cos\beta x + \sin\beta x) \tag{4.2a}$$

in which

$$\beta = \sqrt[4]{\frac{k}{4 \cdot EI}} \tag{4.2b}$$

and in which k is the foundation stiffness.

This function with its various derivatives will occur time and again, so that it becomes convenient to introduce the following notations

$$f_1(\beta x) = e^{-\beta x} \cdot (\cos\beta x + \sin\beta x) \tag{4.3a}$$

$$f_2(\beta x) = e^{-\beta x} \cdot \sin\beta x \tag{4.3b}$$

$$f_3(\beta x) = e^{-\beta x}\cdot(\cos\beta x - \sin\beta x) \tag{4.3c}$$

$$f_4(\beta x) = e^{-\beta x}\cdot\cos\beta x \tag{4.3d}$$

With this new notation the solution of the right side of the both way infinite beam subjected to a concentrated load F can be expressed as

$$y = \frac{F\cdot\beta}{2\cdot k}\cdot f_1(\beta x) \tag{4.4a}$$

$$\frac{dy}{dx} = -\frac{F\cdot\beta^2}{k}\cdot f_2(\beta x) \tag{4.4b}$$

$$M = -EI\cdot\frac{d^2y}{dx^2} = \frac{F}{4\cdot\beta}\cdot f_3(\beta x) \tag{4.4c}$$

Equations 4.4 apply only for the right half of the infinite beam; the left half is symmetrical in 4.4a and 4.4c, and antisymmetrical in 4.4b.

The format of the slope (f_1), deflection (f_2) and bending-moment (f_3) diagrams are shown in figure 4.3. Note that these diagrams represent the format of the solutions of a beam which is loaded upwards.

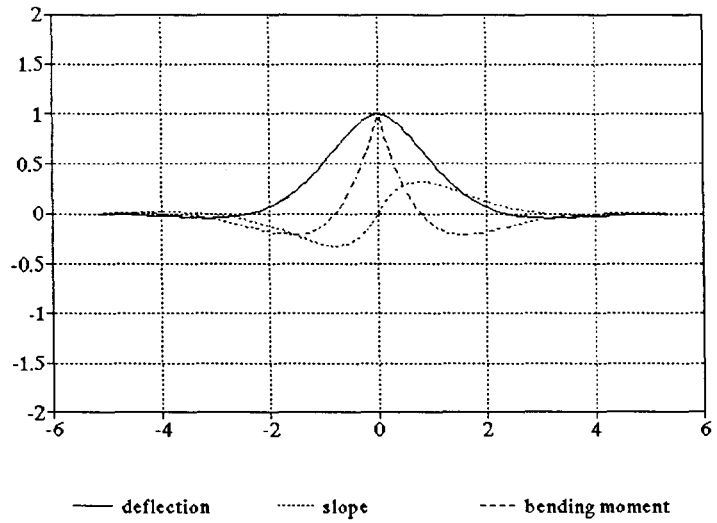

Figure 4.3: *Deflection, Slope and bending-moment diagrams of an infinite beam*

Similarly the solutions of an infinite beam subjected to a bending moment M_0 in the origin can be derived. The solution of such a beam is given by

$$y = \frac{M_0 \cdot \beta^2}{k} \cdot f_2(\beta \cdot x) \tag{4.5a}$$

$$\frac{dy}{dx} = \frac{M_0 \cdot \beta^3}{k} \cdot f_3(\beta \cdot x) \tag{4.5b}$$

$$M = -\frac{M_0}{2} \cdot f_4(\beta \cdot x) \tag{4.5c}$$

The general solutions (equations 4.4 and 4.5) can be used for solving problems of infinite beams loaded with more than one force by superposing the various individual solutions *(Hetenyi,1946)*.
The bending of a beam of finite length on an elastic foundation can also be investigated using equations 4.4 and 4.5 together with the method of superposition. The required solution can then most easily be obtained by superposing the solutions of several infinite beams, that form together the (statical system) of the finite beam.

4.4 *Beam on elastic foundation theory in the determination of the web crippling stiffness*

In this section the general extension from the portal frame model to a three-dimensional model using the theory of a beam on an elastic foundation is described. Eventually, the extension results in two different approaches, namely the effective length approach and the full length approach. However, they are both based on the same principles, that are treated in this section.
To idealize the member to a beam on an elastic foundation, the cross section of the member is divided into a beam and an elastic foundation. The top flange and a part of the web αb_w constitutes the beam, while the elastic foundation consists of the web (figure 4.4).

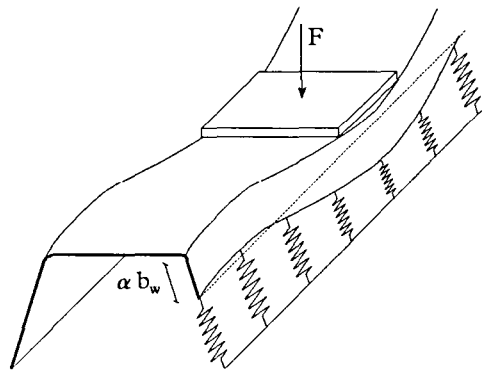

Figure 4.4: *Idealization of the member to a beam on an elastic foundation*

The major reason for this division into a beam and a supporting elastic foundation is the thought that part of the web continuously supports the top flange. The deflection curve of the theory of a beam on an elastic foundation describes the variations of the web crippling deformations over the length of the member and will be used in both the effective length approach and the full length approach.

According to equations 4.2 the deflection curve contains two parameters that have to be clarified.

Firstly, in the theory of a beam on an elastic foundation the resistance of the elastic foundation (i.e. the web) against the beam (top flange and part of the web) is characterized by the foundation stiffness k. In the extension to a three-dimensional model the two-dimensional web crippling stiffness of the portal frame model $k_{\Delta b_w;2D}$ can be thought of as the resistance of the web against deformations of the top flange per slice dx. In the extension from the portal frame model to the three-dimensional model the foundation stiffness k is approximated by the two-dimensional web crippling stiffness of the portal frame model per unit length. Note that this is an important step in the extension from the portal frame model to a three-dimensional model.

Secondly, the flexural rigidity of the beam in the beam on elastic foundation theory is determined by its idealization (figure 4.4). The beam is idealized to consist of the top flange and a part of the web. The influence of the rounding of the top flange corners on the moment of inertia of the cross section of the beam (and thus the flexural rigidity) is neglected in the same way as it was neglected in the portal frame model (section 3.2). This neglect can be justified by a comparison of three different schematisations of the corner radii (figure 4.5) in case of a member with vertical webs.

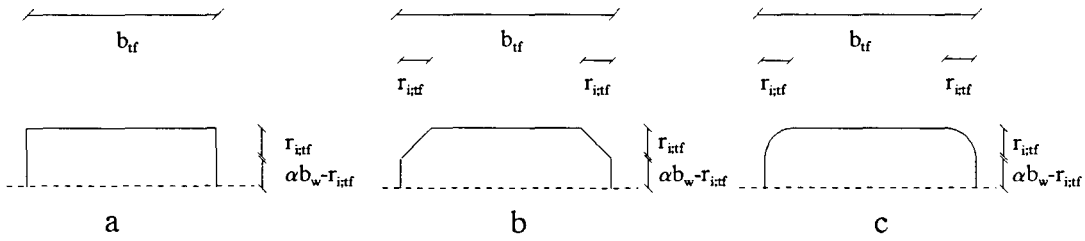

Figure 4.5: *Schematisations of top corner radii*

Schematisation c in figure 4.5 is conform reality. The largest differences between the moments of inertia of the schematisations a, b and c are found for members with narrow top flanges, large top flange corner radii and small values for α. For example, a member with vertical webs, $r_{i;tf}$ = 10 mm, b_{tf} = 20 mm, b_w = 50 mm and α=0.2, will be relatively sensitive for the kind of schematisation that is applied. The moments of inertia of this member for each schematisation are given in table 4.1.

Table 4.1: *Moment of inertia for different schematisations*

Schematisation	*a*	*b*	*c*
Moment of inertia (mm^4)	318	214	298

From table 4.1 it becomes clear that schematisation *a* fits better to reality than schematisation *b*. Furthermore, the differences between schematisation *a* and *c* can be thought of as negligible as far as the accuracy purposes of this study are concerned. For rather regular members ($r_{i;tf}$ << b_{tf}) the difference between schematisation *a* and *c* will be even smaller. Hence, the beam can be schematized as in figure 4.6, thus not taking the rounding of the top flange corners into account.

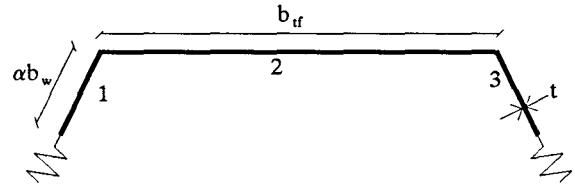

Figure 4.6: *Idealization of the cross section of a beam on an elastic foundation*

From figure 4.6 it can be derived (appendix B.3) that the flexural rigidity of the beam is given by

$$EI = E\cdot[\frac{b_{tf}\cdot t^3}{12} + t\cdot\alpha\cdot b_w\cdot[\frac{\alpha^2\cdot b_w^2+t^2}{12} - \frac{\cos 2\theta_w\cdot(\alpha^2\cdot b_w^2-t^2)}{12} + \frac{t\cdot\alpha\cdot b_w\cdot\sin 2\theta_w}{2}]$$

$$+ b_{tf}\cdot t\cdot(\frac{\alpha^2\cdot b_w^2\cdot\sin\theta_w + t\cdot\alpha\cdot b_w}{b_{tf}+2\cdot\alpha\cdot b_w})^2 + \frac{t\cdot\alpha\cdot b_w}{2}\cdot(\frac{b_{tf}\cdot\alpha\cdot b_w\cdot\sin\theta_w + t\cdot b_{tf}}{b_{tf}+2\cdot\alpha\cdot b_w})^2] \qquad (4.6)$$

Apparently, the magnitude of α highly influences the flexural rigidity of the beam, and thus the resulting web crippling stiffness. There is no clear physical ground on which the magnitude of α might be based. Tsai *(1987)* proposed to use $\alpha = r_{i;tf}/b_w$ in approximating the length of the plastic hinge mechanism.
The reader should note that α can serve as an empirical correction parameter in determining a proper prediction formula for the web crippling stiffness. Furthermore, using α as an empirical correction parameter is the most reasonable possibility to establish a reliable magnitude of α and simultaneously a reliable web crippling stiffness model.
In this research project α has been determined by fitting the model to results from finite element simulations. The finite element simulations as well as the determination of α are treated in chapter 6.
From the general theory of an infinite beam on an elastic foundation subjected to a concentrated load *F*, it is possible to derive the solutions (deflection, slope and bending moment diagrams) of any other finite beam using the method of superposition.
In the determination of the web crippling stiffness the member will be idealized to a beam on an elastic foundation and the web crippling stiffness might be derived using the established deflection curve of the member.
The difference between hat sections and first generation deck panels lies mainly in the fact that the bottom flange can rotate freely in case of hat sections and cannot rotate at all in case of first generation deck panels.

This difference has already resulted in different two-dimensional portal frame models (chapter 3) and will not be of any influence using the theory of a beam on an elastic foundation. Hence, in both the effective length approach and the full length approach only one model will be established which is valid for both hat sections and first generation deck panels. However, note that the resulting model implies the use of two different two-dimensional portal frame models for hat sections and first generation deck panels, that is, the use of two different formulae to determine the foundation stiffness k.

Due to the deflection over the length of the member under the load bearing plate, only two contact points in the length of the member will remain after loading. It is therefore reasonable to idealize the load bearing plate to two concentrated forces in the same way as it has been done in the portal frame model. The resulting schematisation is given in figure 4.7.

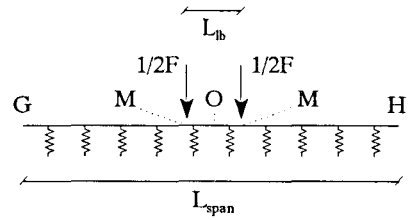

Figure 4.7: *Schematisation of a member to a finite beam on an elastic foundation*

The deflection curve of the beam of figure 4.7 can be obtained by superposing the solutions of several infinite beams, that form together the (statical system) of the finite beam.

This deflection curve represents the web crippling deformation variations of the member. The web crippling deformation within the beam on elastic foundation model $\Delta h_{w;model}$ is defined to be the deflection of the beam at points *M*. The reader should note that the so calculated web crippling deformation $\Delta h_{w;model}$ differs slightly from the web crippling deformation $\Delta h_{w;test}$, measured in the experimental tests by Bakker *(1989)*, being a subtraction of the displacement of the load bearing plate and the maximum deflection of the member. This difference is shown in figure 4.8.

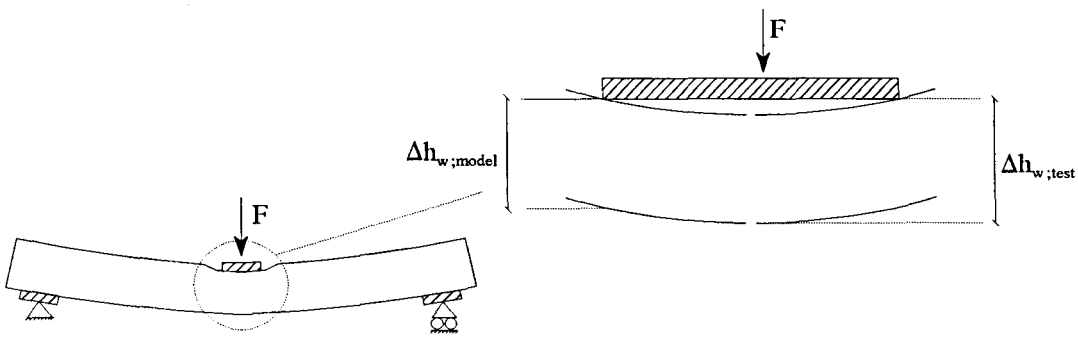

Figure 4.8: *Different definitions of web crippling deformations*

According to figure 4.8 the difference between the two definitions lies in the fact that $\Delta h_{w;model}$ does not take the deflection of the member under the load bearing plate into account, where $\Delta h_{w;test}$ does take this extra deflection of the member into account. The choice to use a web crippling deformation definition in the beam on elastic foundation model that differs from the measured web crippling deformations in experimental tests has two major reasons.

Firstly, it is almost impossible to use a web crippling deformation definition in the beam on elastic foundation model that corresponds completely to the measured web crippling deformation in experimental tests. For $\Delta h_{w;model}$ being the deflection of the beam at points *M*, the difference is pointed out in figure 4.8. If $\Delta h_{w;model}$ was defined to be the maximum deflection at the centre of the member (point *O* in figure 4.7), the definition should neither correspond completely to the measured deformations: $\Delta h_{w;test}$ does not exactly equal the web crippling deformation at the centre of the member because it does not take the downward curling of the top flange underneath the load bearing plate into account. From figure 4.8 it may be concluded that $\Delta h_{w;test}$ does not represent the web crippling deformation at one point of the member and can thus not correspond completely to a web crippling deformation that is defined (and measured) that way.

Secondly, the web crippling deformation definition that is used in the model of Bakker *(1992)* corresponds completely to $\Delta h_{w;model}$. Eventually, the beam on elastic foundation model is developed to establish an analytical model for the web crippling stiffness that can be used in collaboration with the model of Bakker in order to predict the mechanism initiation load. In the development of the beam on elastic foundation model it is obvious to make use of the same web crippling deformation definition as was applied in Bakker's model. For the reasons mentioned above the web crippling stiffness $\Delta h_{w;model}$ is used within the beam on elastic foundation model.

4.5 *Effective length approach*

It has become clear that the magnitude of the elastic web crippling deformations diminishes from the centre of the member towards the supported ends and may even be negligible near these ends. The effective length approach is characterized by the introduction of an effective length L_{ef}, where outside the elastic web crippling deformations are assumed to be negligibly small (figure 4.9). Within the effective length, a certain variation of the web crippling deformations is assumed.

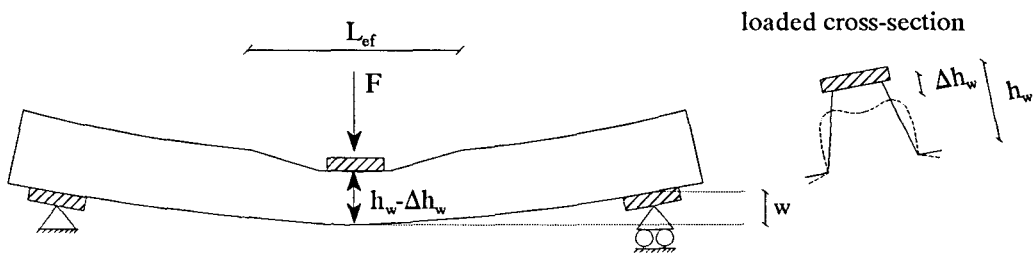

Figure 4.9: Elastic web crippling deformations in the effective length approach

The effective length is determined using the theory of a beam on an elastic foundation. From the deflection curve of a beam loaded by two concentrated forces *1/2F* as shown in figure 4.7, the effective length is chosen rather arbitrary. For example, the effective length can be defined to be the distance between the two points at the left and right side of the beam where the second derivative of the deflection curve equals zero, in which these points thus represent two hinges where the acting bending moment on the beam equals zero. The magnitude of the effective length is mainly influenced by the flexural rigidity of the beam and the foundation stiffness. The latter is specified as the web crippling stiffness of the portal frame model of a portal frame with a width that equals unity, as mentioned in section 4.4. The flexural rigidity is also determined conform section 4.4

Since the derivation of a deflection curve for the finite beam as shown in figure 4.7 is highly complicated, the effective length is determined using a simpler approximation of the statical system of the member. A reasonable good approximation of the effective length can be established using the deflection curve of an infinite beam loaded by two concentrated forces 1/2F, pointed out in figure 4.10.

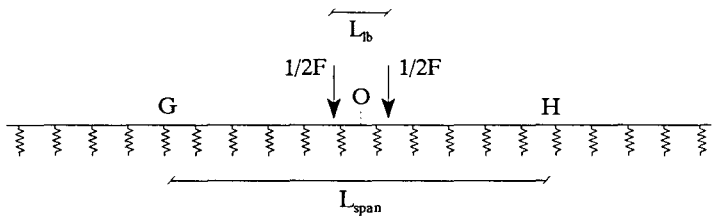

Figure 4.10: *Schematisation of the member to an infinite beam, as used in the effective length approach*

This approximation becomes more accurate with an increasing length of the member and is used in the determination of the effective length.

Using equation 4.4a together with the method of superposition, the deflection curve of the beam of figure 4.10 is given by

$$y = \frac{F \cdot \beta \cdot dx}{4 \cdot k_{\Delta h_w;2D}} \cdot [f_1(\beta \cdot (x - 1/2 \cdot L_{lb})) + f_1(\beta \cdot (x + 1/2 \cdot L_{lb}))] \qquad x > 1/2 \cdot L_{lb} \tag{4.7}$$

in which the origin is situated at point *O* in figure 4.10. Equation 4.7 applies only for the right half of the infinite beam beside the load bearing plate; the left half of the beam is symmetrical in 4.7 and the deflection curve under the load bearing plate is of no importance here. The effective length is chosen as the distance between the two closest points at the left and right side of the beam outside the load bearing plate where the second derivative of the deflection curve equals zero, or

$$\frac{d^2y}{dx^2} = -\frac{F \cdot \beta^3 \cdot dx}{2 \cdot k_{\Delta h_w;2D}} \cdot [f_3(\beta \cdot (x - 1/2 \cdot L_{lb})) + f_3(\beta \cdot (x + 1/2 \cdot L_{lb}))] = 0 \tag{4.8}$$

From equation 4.8 it can be derived that

$$x = \frac{\pi}{4 \cdot \beta} + \frac{n \cdot \pi}{\beta} + 1/2 \cdot L_{lb} \qquad n = 0,1,2,... \tag{4.9}$$

under the condition that

$$L_{lb} = \frac{a \cdot \pi}{\beta} \qquad a = 0,1,2,...$$

The more L_{lb} deviates from $a \cdot \pi/\beta$ the less accurate the approximation of the effective length (according to its definition) will be. However, note that the definition of the effective length was already rather arbitrary, resulting in only a rough estimation of the effective length, which undermines the importance of the above mentioned condition. Hereby, this condition is assumed to hold true, regardless of the length of the load bearing plate and the magnitude of β. The closest point to the origin at the right side of the beam where the second derivative of the deflection curve equals zero is given by equation 4.9 for $n=0$ and equals the distance to the origin of the closest point at the left side of the beam where the second derivative equals zero, due to symmetry. Hence, the effective length can be specified as

$$L_{ef} = L_{lb} + \frac{\pi}{2 \cdot \beta} \tag{4.10}$$

Once the effective length is known, the varying elastic web crippling deformations within this effective length can be calculated. For that purpose the member is divided into infinitely small elements *dx*. The web crippling deformation of such an infinitely small part *dx* under the load bearing plate is approximated using the portal frame model. Assuming a certain variation of the web crippling deformations over the effective length, the concentrated load that causes these deformations can be calculated for each element *dx*. Summarizing these concentrated loads results in the total concentrated load *F* which corresponds with the web crippling deformation under the load bearing plate. Hence, a web crippling stiffness is obtained in which the varying web crippling deformations over the effective length are taken into account. Probably the most simple variation of the web crippling deformations over the effective length is given in figure 4.11.

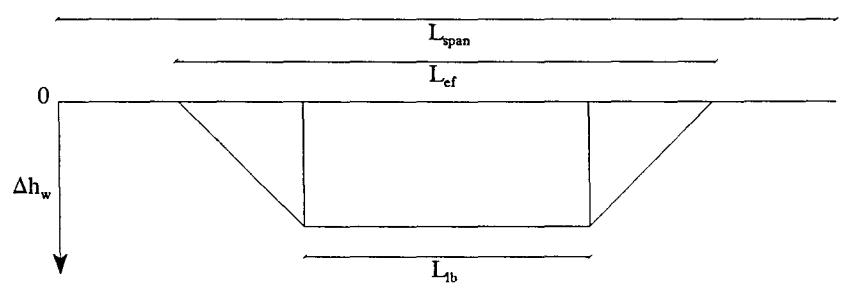

Figure 4.11: *Variation of web crippling deformations over* L_{ef}

Assuming the variation of web crippling deformations of figure 4.11 and using equation 4.10, the resulting web crippling stiffness can be specified as

$$k_{\Delta h_w} = \frac{k_{\Delta h_w;2D} \cdot L_{fb}}{dx} + \frac{\pi}{4} \cdot \sqrt[4]{\frac{4 \cdot EI \cdot k^3_{\Delta h_w;2D}}{dx^3}} \tag{4.11}$$

in which $k_{\Delta h_w;2D}$ is defined to be the web crippling stiffness of the portal frame model for a portal frame with a width that equals dx. The flexural rigidity EI in formula 4.11 is defined to be the flexural rigidity of the beam, which consists of the top flange and a part of the web $\alpha \cdot b_w$ (section 4.4). Evidently, it is also possible to use more complicated descriptions of variations of the web crippling deformations over the effective length. However, this corresponds with highly complicated solutions for the web crippling stiffness and will not further be treated here.

4.6 Full length approach

In the full length approach the variation of the web crippling deformations over the whole length of the member is taken into account. It is assumed that the variation of web crippling deformations over the length of the member can be described properly by the deflection curve according to the beam on elastic foundation theory. The deflection curve is based on the schematisation of the member to a finite beam with hinged ends confirm figure 4.12a. This schematisation implies that the web crippling deformations at the ends of the beam do not necessarily equal zero nor do the rotations. The bending moment at both ends however, needs to equal zero due to the hinged schematisation. Since it is assumed that the variation of web crippling deformations over the length of the member can be approximated by the deflection curve of the beam of figure 4.12a, the web crippling stiffness is given by the quotient of F and the deflection of the beam at point M, as mentioned in section 4.4. In the full length approach the need to derive the whole deflection curve (as in the effective length approach) is avoided this way, because an expression for the deflection at M satisfies the solution. The deflection curve of the beam in figure 4.12a might be established by superposing the solutions for the two kinds of loading of an infinitely beam shown in figure 4.12b and c. In figure 4.12b the two forces $1/2F$ are acting on an infinitely long beam; M_G, M_H denote the bending moments at points G and H of the infinitely long beam in figure 4.12b. In figure 4.12c the infinitely long beam is loaded by bending moments M_0, applied outside the portion GH of the beam, but infinitely close to points G and H which correspond to the hinged ends of the given beam in figure 4.12a.

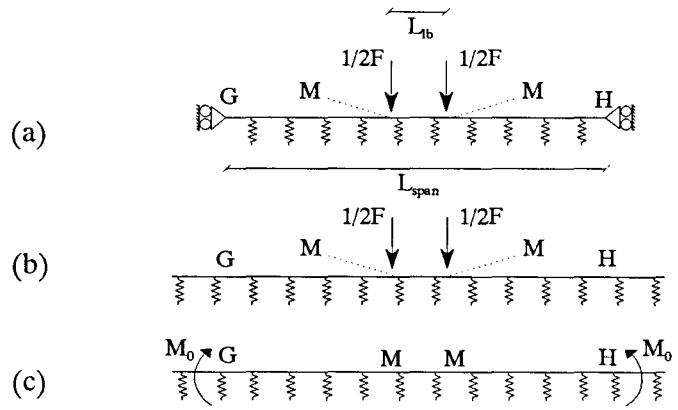

Figure 4.12: *The finite beam (a) as a superposition of infinite beams (b and c)*

It is easy to see that by a proper selection of the bending moment M_0, the bending moment at the cross sections G and H of the resulting infinite beam from superposition of figure 4.12b and c can be made equal to zero. Then the middle portion of the infinite beam will evidently be in the same condition as the finite beam represented in figure 4.12a, and all necessary information regarding bending of the latter beam will be obtained by superposing the cases shown in figure 4.12b and c.

Due to symmetry M_G equals M_H. Hence M_0 must produce $-M_G$ at points G and H on the infinite beam. That is, by equations 4.4 and 4.5, and by superposition of M_0

$$\frac{M_0}{2} \cdot (1 + f_4(\beta \cdot L_{span})) = -M_G \tag{4.12}$$

The bending moment M_G of the infinite beam of figure 4.5b can be obtained using equations 4.4 together with the method of superposition, resulting in

$$M_G = \frac{F}{8 \cdot \beta} \cdot [f_3(1/2 \cdot \beta \cdot (L_{span} - L_{lb})) + f_3(1/2 \cdot \beta \cdot (L_{span} + L_{lb}))] \tag{4.13}$$

Now, the deflection curve of the actual finite beam (figure 4.12a) can be obtained by superposing the deflection curves of the infinite beams of figures 4.12b and c. Moreover, the deflection of the member at point M can be established by superposition of the deflections of the infinite beams of figure 4.11b and c at point M.

The deflection of the infinite beam of figure 4.12b at point M, $y_{M;b}$ can be calculated by superposing the deflections due to the concentrated forces $1/2F$ using equation 4.4a, and is given by

$$y_{M;b} = \frac{F \cdot \beta}{4 \cdot k} \cdot (1 + f_1(\beta \cdot L_{lb})) \tag{4.14}$$

The deflection of the infinite beam of figure 4.12c at point M, $y_{M;c}$ can be calculated by superposing the deflections due to the bending moments M_0 using equations 4.5a, and is given by

$$y_{M;c} = \frac{M_0 \cdot \beta^2}{k} \cdot [f_2(1/2 \cdot \beta \cdot (L_{span} - L_{lb})) + f_2(1/2 \cdot \beta \cdot (L_{span} + L_{lb}))] \tag{4.15}$$

As mentioned above, the deflection of point M of the actual finite beam of figure 4.12a, y_M is given by superposition of the deflections of point M of the infinite beams of figure 4.12b and c, $y_{M;b}$ and $y_{M;c}$. That is by equations 4.14 and 4.15,

$$y_M = \frac{F \cdot \beta}{4 \cdot k} \cdot (1 + f_1(\beta \cdot L_{lb})) + \frac{M_0 \cdot \beta^2}{k} \cdot [f_2(1/2 \cdot \beta \cdot (L_{span} - L_{lb})) + f_2(1/2 \cdot \beta \cdot (L_{span} + L_{lb}))] \tag{4.16}$$

If equations 4.12 and 4.13 are substituted into equation 4.16, the web crippling stiffness can be specified. However, note that the resulting formulae describing the web crippling stiffness becomes rather complex. According to Hetenyi *(1946)* it is possible to classify beams into three groups, depending on the βL_{span} value:

1. Short beams: $\beta L_{span} < \pi/4$;
2. Beams of medium length: $\pi/4 < \beta L_{span} < \pi$;
3. Long beams: $\beta L_{span} > \pi$.

This classification is made from a practical point of view, since it offers the possibility of using approximations and of neglecting certain quantities in particular instances.

The cold-formed hat sections and first generation deck panels which are used in practice, will all belong to the category 'long beams'. Furthermore most of the hat sections on which web crippling tests have been carried out by Bakker *(1992)* belong to this category, although these were relatively short members.

For the sake of clearness it is assumed in this research project that all hat sections and first generation deck panels belong to the category 'long beams'. The reader should note that the approximations that are made as a result of this assumption are not valid for short beams and beams of medium length.

Long beams have a βL_{span} value such that the counter effect which the end-conditioning forces have on each other is a diminishing one. When investigating one end of the beam, it may be assumed that the other end is infinitely far away. In other words, βL_{span} is so large that $f_i(\beta L_{span})$ can be taken zero in all formulae, which greatly simplifies the computations.

Considering this and substituting equation 4.12 into 4.16, the deflection of the actual finite beam (figure 4.11a) can be expressed as

$$y_M = \frac{F \cdot \beta}{4 \cdot k} \cdot (1 + f_1(\beta \cdot L_{lb}) - \frac{2 \cdot \beta^2 \cdot M_G}{k} \cdot [f_2(1/2 \cdot \beta \cdot (L_{span} - L_{lb})) + f_2(1/2 \cdot \beta \cdot (L_{span} + L_{lb}))] \tag{4.17}$$

Substitution of equation 4.13 into equation 4.17 results in

$$y_M = \frac{F \cdot \beta}{4 \cdot k} \cdot [1 + f_1(\beta \cdot L_{lb})$$

$$- (f_2(1/2 \cdot \beta \cdot (L_{span} - L_{lb})) + f_2(1/2 \cdot \beta \cdot (L_{span} + L_{lb}))) \cdot (f_3(1/2 \cdot \beta \cdot (L_{span} - L_{lb})) + f_3(1/2 \cdot \beta \cdot (L_{span} + L_{lb})))] \quad (4.18)$$

After several simplifications and goniometric substitutions (appendix B.2) the web crippling stiffness, which is defined to be F/y_M, can be specified as

$$k_{\Delta h_w} = \frac{\sqrt[4]{1024 \cdot EI \cdot (\frac{k_{\Delta h_w;2D}}{dx})^3}}{1 + f_1(\beta \cdot L_{lb}) - 1/2 \cdot f_1(\beta \cdot (L_{span} - L_{lb})) + 1/2 \cdot e^{-\beta \cdot (L_{span} - L_{lb})}} \quad (4.19)$$

From equation 4.19 it can be seen that the web crippling stiffness in the beam on elastic foundation model is determined by the span length of the beam, the length of the load bearing plate, the flexural rigidity of the beam and the foundation stiffness (i.e. the two-dimensional web crippling stiffness of the portal frame model).

4.7 *Evaluation of the effective length approach and the full length approach*

The effective length approach can be thought of as an approximation of the full length approach. The full length approach takes web crippling deformations over the whole length of the member into account, based on the assumption that the variation of web crippling deformations over the length can be described reasonably well with the beam on elastic foundation theory. The effective length approach takes web crippling deformations over an effective length into account, where outside the web crippling deformations are neglected. Furthermore, the variation of the web crippling deformations over the effective length is taken rather simple (linear), compared to the full length approach. It can be concluded that the effective length approach is more simple but less well-founded than the full length approach.

It is striking that the empirical correction parameter α has a larger influence on the web crippling stiffness of the full length approach than it has on the web crippling stiffness of the effective length approach. For instance, consider a member with vertical webs, L_{span}=290, L_{lb}=50, b_{bf}=60, b_w=50, $r_{i;bf}$=1, $r_{i;tf}$=10 and t=0.68. The web crippling stiffnesses according to the effective length approach and the full length approach are given in table 4.2 for varying values of α, as well as the corresponding experimental test, carried out by Bakker *(1989)*.

Both approaches make use of the portal frame model in the approximation of the foundation stiffness in the beam on elastic foundation model. Furthermore, the approaches both use the same format with which the flexural rigidity of the beam on elastic foundation model is determined.

Table 4.2: Web crippling stiffness of the full length versus the effective length approach

	α=0.2	α=0.5	α=1.0
Full length approach	1536	2418	3617
Effective length approach	649	1169	1551
Experimental test (Bakker)	1960		

In this research project the full length approach is thought to be preferable mainly because this approach is assumed to be a better physical approximation of reality. Henceforward, the full length approach is denoted to as the beam on elastic foundation model throughout this report. However, it is not ruled out that a proper selection of the deformation pattern over the effective length in the effective length approach leads to more reliable results compared to the linear deformation pattern as it is assumed in section 4.5.

Chapter 5: Energy model

The elastic web crippling behaviour of thin-walled cold-formed steel members can be analyzed using the principle of stationary total potential energy. The derivation of the resulting model, that is denoted as 'energy model', is treated here.

5.1 Introduction

From section 4.6 it is clear that the beam on elastic foundation model (i.e. the full length approach in the extension of the portal frame model) is rather complicated. Although it is based on clear physical grounds and might be able to produce reliable predictions of the web crippling stiffness (due to the empirical correction factor α), calculating the web crippling stiffness is cumbersome. With the beam on elastic foundation model the object of this study, the development of an analytical web crippling stiffness model, has probably (the reliability of the model is not clear yet) been satisfied. However, the final aim of this study is a practical prediction method of the mechanism initiation load, which combines Bakker's model and an elastic web crippling stiffness model (figure 1.5) because it might be a reasonable approach to develop design formulae based on the prediction of the mechanism initiation load *(Bakker, 1992)*. The underlying models of these design formulae need to be as simple as possible in order to establish practical prediction formulae. A completely different approach in the derivation of a web crippling stiffness model might result in a more simple model and is thus worth trying. Even if the new model appears to be as complicated as the beam on elastic foundation model (or even more complicated) it still can be useful validating the two models against each other and against the parameter study, whereafter the most reliable model can be chosen as the suitable candidate for the web crippling stiffness model. Therefore, a different model is developed in this chapter, based on the principle of stationary total potential energy.

Basically, this principle asserts that of all the geometrically possible configurations which a mechanical system can take up, the true one, corresponding to the equilibrium between the applied loads and the induced reactions, is identified by a stationary value for the total potential energy *(Richards, 1977)*. The application of this extremum principle points the way towards establishing an energy functional. Substituting assumed deformation functions in the energy functional, involving adjustable parameters, the stationary conditions are determined with respect to these parameters. It is assumed that the geometrical configuration which the member takes up is identified by these stationary conditions. This principle provides a direct method for obtaining approximate solutions to the web crippling stiffness. In this connection the Rayleigh-Ritz method is used in the energy model. Applying the Rayleigh-Ritz method implies the use of kinematic admissible trial functions that approximately describe the displacement solutions of the mechanical system.

Using the principle of stationary total potential energy in combination with the Rayleigh-Ritz method in the derivation of the web crippling stiffness of hat sections and first generation deck panels, several appropriate trial functions can be used. They each result in a different energy functional and consequently in different

solutions for the web crippling stiffness.

For sake of clarity, first the principle of stationary total potential energy is briefly summarized in section 5.2 whereafter the Rayleigh-Ritz method is described in section 5.3. Section 5.4 describes the general assumptions that are made within the energy model. The derivation of the energy model , which is based upon the principle of stationary total potential energy and the Rayleigh-Ritz method, is treated in section 5.5. In this section several descriptions of displacement solutions and their resulting web crippling stiffnesses are summarized. Finally, an evaluation of these different solutions for the web crippling stiffness is given in section 5.6.

5.2 *Principle of stationary total potential energy*

The principle of stationary total potential energy, which applies only to elastic bodies, is developed from the method of virtual work. Elastic bodies are those which recover their original shape completely when disturbing forces are removed. In a complete loading-unloading cycle, the internal forces produce zero net work since the equilibrium configuration thereby follows a closed path: such forces satisfy the law of conservation of energy and consequently are said to be conservative. They have a potential energy of strain or strain energy. The total potential energy of a fully conservative system can be written as

$$V = U + \Omega \tag{5.1}$$

Here, U is the strain energy stored in the system due to internal forces and Ω is the potential energy of the external loads.

The method of virtual work is the means by which the true equilibrium configuration of a mechanical system is identified. It states that a mechanical system is in its equilibrium configuration if the virtual work of all the forces acting on it will be zero for a virtual displacement. When the system contains deformable members, the method of virtual work is given by

$$\delta W_{int} + \delta W_{ext} = 0 \tag{5.2}$$

in which δW_{int} is the virtual work of internal forces and δW_{ext} is the virtual work of external forces. If any deformable bodies are elastic, linear or not, so that Hooke's law or some more complicated load-deformation law is appropriate, the internal forces will have a potential energy and equation 5.2 takes the form

$$\delta W_{ext} = \delta U \tag{5.3}$$

This is the form in which the method of virtual work is frequently quoted in literature on structural analysis.

If the external forces are conservative, it holds that

$$\delta W_{ext} = -\delta \Omega \tag{5.4}$$

and the method of virtual work takes the form

$$\delta V = \delta(U+\Omega) = 0 \tag{5.5}$$

Equation 5.5 is an analytical statement of the principle of stationary total potential energy. The principle asserts that of all the geometrically possible configurations which a mechanical system can take up, the true one, corresponding to the equilibrium between the applied loads and the induced reactions, is identified by a stationary value for the total potential energy *(Richards, 1977)*.

Bodies bounded by flat surfaces whose lateral dimensions are large compared to the separation between these surfaces are called plates. Considering this, a hat section or a first generation deck panel can be thought of as a series of steel plates that are rigidly connected to each other and obey Hooke's law.

For thin plates it is reasonable to assume that the hypothesis of Bernoulli holds. According to this hypothesis lines normal to the midsurface in the undeformed geometry are assumed to remain normal to this surface in the deformed geometry. Such a simplification entails the inclusion of hidden constraints in the plate and the equations of equilibrium resulting from the variation process applied to the total potential energy are accordingly those for a stiffer system than the actual case *(Shames & Dym, 1985)*. The reader should be aware of the fact that, hereby, the energy model will also correspond to a stiffer member than the actual case.

Consider the plate of figure 5.1 with a thickness t, where the xy coordinate plane corresponds to the midplane or middle surface in the undeformed geometry.

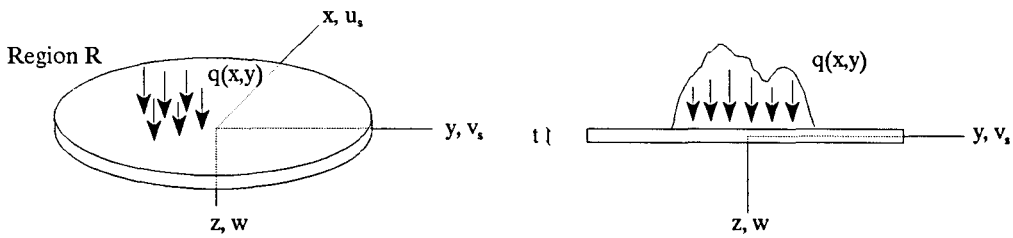

Figure 5.1: *Plate of arbitrair shape*

The strain energy U of the plate in figure 5.1 for linear elastic behaviour is found by evaluating the integral

$$U = \frac{1}{2} \cdot \iint_R \int_{-t/2}^{t/2} \sigma_{ij} \cdot \varepsilon_{ij} dz dx dy \tag{5.6}$$

In case of a plate it is reasonable to assume that $\sigma_{zz} = 0$, despite the fact that the application of transverse loading $q(x,y)$ on the surface $z = -t/2$ leads to a nonzero stress σ_{zz}, and also in spite of the fact that the assumed displacement field with $\varepsilon_{zz} = 0$ is not a case of plane stress (the strain ε_{zz} is assumed to be negligibly small with respect to the rest of the strains, just as in the derivation of the classical theory of plates *(Shames & Dym, 1985)*). Hence, the state of plane stress is employed in evaluating the above expression. From Hooke's law it can be derived that

$$\sigma_{xx} = \frac{E}{1-\mu^2} \cdot (\varepsilon_{xx} + \mu \cdot \varepsilon_{yy}) \tag{5.7a}$$

$$\sigma_{yy} = \frac{E}{1-\mu^2} \cdot (\varepsilon_{yy} + \mu \cdot \varepsilon_{xx}) \tag{5.7b}$$

$$\sigma_{xy} = \frac{E \cdot \varepsilon_{xy}}{(1+\mu)} \tag{5.7c}$$

in which μ is Poisson's ratio. Substituting equations 5.7 into 5.6 results in

$$U = \frac{E}{2 \cdot (1-\mu^2)} \cdot \iint_R \int_{-t/2}^{t/2} [\varepsilon_{xx}^2 + 2 \cdot \mu \cdot \varepsilon_{xx} \cdot \varepsilon_{yy} + \varepsilon_{yy}^2 + 2 \cdot (1-\mu) \cdot \varepsilon_{xy}^2] \, dz dx dy \tag{5.8}$$

The potential energy of the plate in figure 5.1 for the external loads, meanwhile, is given as

$$\Omega = -\iint_R q \cdot w dx dy \tag{5.9}$$

where the loads q are assumed to act on the midplane surface of the plate and in which w represents the deflection of the plate. Both q and w are functions of x and y.
Expressing the strains in terms of displacements, it can be derived *(Shames & Dym, 1985)* that

$$\varepsilon_{xx} = \frac{\partial u_s}{\partial x} - z \cdot \frac{\partial^2 w}{\partial x^2} \tag{5.10a}$$

$$\varepsilon_{yy} = \frac{\partial v_s}{\partial y} - z \cdot \frac{\partial^2 w}{\partial y^2} \tag{5.10b}$$

$$\varepsilon_{xy} = \frac{1}{2} \cdot \left(\frac{\partial u_s}{\partial y} + \frac{\partial v_s}{\partial x}\right) - z \cdot \frac{\partial^2 w}{\partial x \partial y} \tag{5.10c}$$

in which u_s and v_s refer to stretching action of the midsurface. Note that u_s and v_s are functions of x and y. Considering equations 5.8 and 5.9 and substituting equations 5.10, the total potential energy of the plate is given by

$$V=\frac{E}{2\cdot(1-\mu^2)}\int\int_R\int_{-t/2}^{t/2}[(\frac{\partial u_s}{\partial x}-z\cdot\frac{\partial^2 w}{\partial x^2})^2+(\frac{\partial v_s}{\partial y}-z\cdot\frac{\partial^2 w}{\partial y^2})^2+2\cdot\mu\cdot(\frac{\partial u_s}{\partial x}-z\cdot\frac{\partial^2 w}{\partial x^2})\cdot(\frac{\partial v_s}{\partial y}-z\cdot\frac{\partial^2 w}{\partial y^2})$$

$$+2\cdot(1-\mu)\cdot(\frac{1}{2}\cdot(\frac{\partial u_s}{\partial y}+\frac{\partial v_s}{\partial x})-z\cdot\frac{\partial^2 w}{\partial x\partial y})^2]\,dz\,dx\,dy-\int\int_R q\cdot w\,dx\,dy \qquad (5.11)$$

It should be noted that the above energy functional is only valid for displacement functions w satisfying dynamic boundary conditions, otherwise the energy functional should be extended with terms including the moment and shear forces along the plate boundary.

It is well known that trigonometric functions satisfy the dynamic boundary conditions because they are part of the fundamental solution of the biharmonic plate equation. As the selected kinematic admissible (trial) functions resemble the trigonometric functions (see section 5.3) the abovementioned extensions to the energy functional (equation 5.11) can be neglected.

Carrying out the squaring operation and integrating through the thickness while noting that

$$\int_{-t/2}^{t/2}(1,z,z^2)\,dz=(t,0,\frac{t^3}{12})$$

the total potential energy may be obtained in the form

$$V=\frac{E\cdot t}{2\cdot(1-\mu^2)}\cdot\int\int_R[(\frac{\partial u_s}{\partial x})^2+(\frac{\partial v_s}{\partial y})^2+2\cdot\mu\cdot\frac{\partial u_s}{\partial x}\cdot\frac{\partial v_s}{\partial y}+\frac{1-\mu}{2}\cdot(\frac{\partial u_s}{\partial y}+\frac{\partial v_s}{\partial x})^2]\,dx\,dy$$

$$+\frac{E\cdot t^3}{24\cdot(1-\mu^2)}\int\int_R[(\frac{\partial^2 w}{\partial x^2})^2+(\frac{\partial^2 w}{\partial y^2})^2+2\cdot\mu\cdot\frac{\partial^2 w}{\partial x^2}\cdot\frac{\partial^2 w}{\partial y^2}+2\cdot(1-\mu)\cdot(\frac{\partial^2 w}{\partial x\partial y})^2]\,dx\,dy-\int\int_R q\cdot w\,dx\,dy \qquad (5.12a)$$

The total potential energy has three dependent variables: the stretching components u_s and v_s and the vertical displacement variable w. Considering the stresses and moments in the plate as a result of transverse loads only, the strains due to this action will primarily stem from bending effects rather than stretching effects and only the former need to be taken into account. In that case the expression can be rewritten in the following form

$$V=\frac{E\cdot t^3}{24\cdot(1-\mu^2)}\int\int_R[(\frac{\partial^2 w}{\partial x^2})^2+(\frac{\partial^2 w}{\partial y^2})^2+2\cdot\mu\cdot\frac{\partial^2 w}{\partial x^2}\cdot\frac{\partial^2 w}{\partial y^2}+2\cdot(1-\mu)\cdot(\frac{\partial^2 w}{\partial x\partial y})^2]\,dx\,dy-\int\int_R q\cdot w\,dx\,dy \qquad (5.12b)$$

Using the principle of stationary potential energy, the above total potential energy functional (equations 5.12) is minimized. The resulting equations that describe the solution (the stationary conditions for the functional), the so-called Euler-Lagrange equations, correspond to the equilibrium configuration the plate of figure 5.1.

5.3 *Rayleigh-Ritz method*

A mechanical system which has its properties distributed in a continuous manner, such as the plate of figure 5.1, can assume any one of an infinite number of equilibrium configurations. Such a system is said to have an infinite number of degrees of freedom and its response to a given input is given by means of a differential equation corresponding to the energy functional of equation 5.12. The solution to this problem can be derived in two different ways.

Firstly, the formal processes of the calculus of variations to determine the stationary conditions for a functional can be applied. This yields the above mentioned differential equations, the so-called Euler-Lagrange equations, that lead to an exact solution of the problem. It is in the solving of these equations to satisfy prescribed boundary conditions that difficulties are met in engineering analysis.

Secondly, if certain assumptions are made about the nature of deformation, the real system is approximated by one having a finite number of degrees of freedom. This idea seems to have been used first in the 19th century by Lord Rayleigh in his vibration studies. Ritz refined the technique, and what has come to be called the Rayleigh-Ritz method has been very extensively used to obtain numerical solutions to complex engineering problems. Indeed, the finite element method, which can be formulated as a piecewise Rayleigh-Ritz process, is perhaps the most practically significant development in engineering analysis in recent times. In the energy model there is made use of the Rayleigh-Ritz method.

In the Rayleigh-Ritz method the energy functional (equation 5.12) is used to find approximate solutions to the corresponding differential equation. Substituting assumed solutions for the displacement field (the stretching components u_s and v_s and the vertical displacement variable w)into the functional, involving adjustable parameters, and determining the stationary conditions with respect to these parameters, provides approximate solutions to the equilibrium configuration that the mechanical system. Within the Rayleigh-Ritz method the following approximate displacement field components for expressing the total potential energy are employed for a mechanical system such as the plate of figure 5.1:

$$(u_s)_k = \phi_0(x,y,z) + \sum_{i=1}^{k} a_i \cdot \phi_i(x,y,z) \tag{5.13a}$$

$$(v_s)_k = \psi_0(x,y,z) + \sum_{i=1}^{k} b_i \cdot \psi_i(x,y,z) \tag{5.13b}$$

$$w_k = \gamma_0(x,y,z) + \sum_{i=1}^{k} c_i \cdot \gamma_i(x,y,z) \tag{5.13c}$$

The functions with the subscript zero satisfy the boundary conditions. The coefficients a_i, b_i and c_i represent the adjustable parameters which are yet undetermined. The scheme for the Rayleigh-Ritz method is to choose the values of these coefficients so as to minimize the total potential energy. When the values of the coefficients are thus determined they are called Ritz coefficients. The subscript k in equations 5.13 refers to

the number of Ritz coefficients that are involved. It can be shown *(Trefftz, 1928)* that if $k \rightarrow \infty$ in this process, then $(u_s)_k$, $(v_s)_k$ and w_k converge in energy to the exact solution for the problem provided the functions ϕ_i, ψ_i and γ_i are complete. When n is small still very good approximations to the exact solution can be reached if a judicious selection of the functions ϕ_i, ψ_i and γ_i is made.
The procedure is to use $(u_s)_k$, $(v_s)_k$ and w_k to formulate an approximate total potential energy V, which then becomes a function of the $3k$ undetermined constants. V is minimized by imposing the $3k$ requirements:

$$\frac{\partial V}{\partial a_i} = 0 \qquad \frac{\partial V}{\partial b_i} = 0 \qquad \frac{\partial V}{\partial c_i} = 0 \qquad i = 1,2,...,k \tag{5.14}$$

This yields $3k$ equations for the unknown coefficients. The solution of these equations then yields the aforementioned Ritz coefficients.

5.4 *General assumptions*

In the derivation of the energy model certain assumptions are made as far as the application of the principle of stationary potential energy and the Rayleigh-Ritz method is concerned. These assumptions are summarized as follows:

- *Distinction between hat sections and first generation deck panels*

  First generation deck panels can be thought of as a composition of hat sections tied together at the unloaded flange (figure 3.3). Each of these hat sections shows the same web crippling behaviour, because they are loaded similarly. Moreover, each hat section has the same amount of potential energy. Therefore, minimizing the total potential energy of a panel corresponds with minimizing the total potential energy of one hat section and will further be referred to that way, The only difference between hat sections and deck panels is formed by the deformation magnitudes; a difference that finds expression in a factor n which will be discussed later in this section. Although the deformation patterns slightly differ from each other, it will become clear that the same format is used in the description of the deformation variations.

- *Idealization of a member to three plates*

  To apply the principle of stationary total potential energy the hat section is idealized to be built up of a series of plates that are connected to each other. Since hat sections are made out of thin-walled steel sheet, the bottom flange, the web and the top flange can be thought of as plates. The derivation of the energy model is based upon the assumption that $\theta_w > \pm 5^\circ$.

  Web crippling is a local phenomenon that appears near the concentrated load, mainly in the top flange and the webs. It is assumed that these local deformations do not occur within the bottom flange.

Clearly, in case of hat sections the bottom flanges deflect and rotate due to the fact that they are rigidly connected to the webs but it is assumed that the bottom flanges rotate and translate only as a rigid body. This means that the deformation variations (u_s and v_s and w) over the bottom flange equal zero and hence have no strain energy (potential energy). This assumption is confirmed by the results of finite element calculations for members having the following dimensions (mm): L_{span}=0-1560, θ_w=90°, b_{bf}=20-120, b_w=30-100, b_{tf}=20-120, t=0.5-1.3, $r_{i;bf}$ =$r_{i;tf}$=1-10 and L_{lb}=25-300. Their deformation formats are shown in the figures 5.2 and 5.3. Figure 5.2 shows the format of the deformations u_s and v_s and w over the bottom flange, the web and the top flange at the centre of the member, for hat sections that are rather short (relatively long members show a deformation over the length of the member that diminishes within the hinged ends).

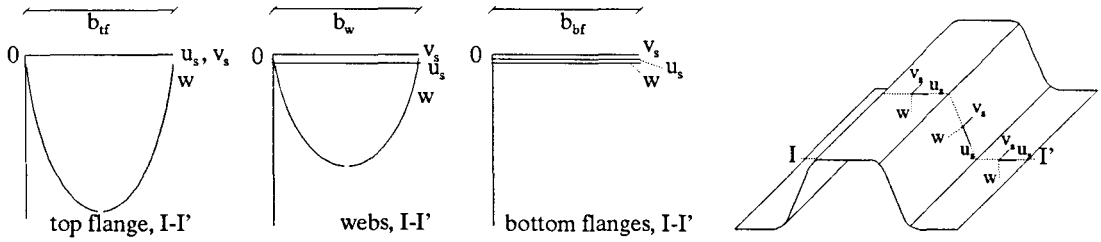

Figure 5.2: *Deformation variations over the cross section of the member in case of hat sections*

Note that u_s, v_s and w are local properties: w, for instance, always represents the deflection of the plate in conformity with figure 5.1, irrespective of the global direction of that deflection. For sake of clarity, the global directions of u_s, v_s and w for each plate are also given in the figures 5.2 and 5.3. Due to symmetry, the deformation pattern of both webs is equal as is the deformation pattern of both bottom flanges.

Figure 5.3 shows the format of the deformations u_s and v_s and w over the length of the member of the midline of the bottom flange, the midline of the web and the midline of the top flange.

From figure 5.2 and 5.3 it may be concluded that the deformation variations over the bottom flange nearly equal zero. The deflection over the length of the bottom flange does show significant variations but these variations are not caused by bending of the bottom flange itself. These variations stem from the stretching actions v_s in the web, which in their turn stem from the bending deflection w in the top flange. A comparison of v_s in the web with w in the bottom flange shows that the deflection of the bottom flange can be thought of as a rigid body translation due to the stretching action v_s in the web, and has thus almost no potential energy. Therefore, the contributions of the bottom flanges to the total potential energy are ignored in case of hat sections and the member is idealized to be built up of three plates, that is one top flange plate and two web plates.

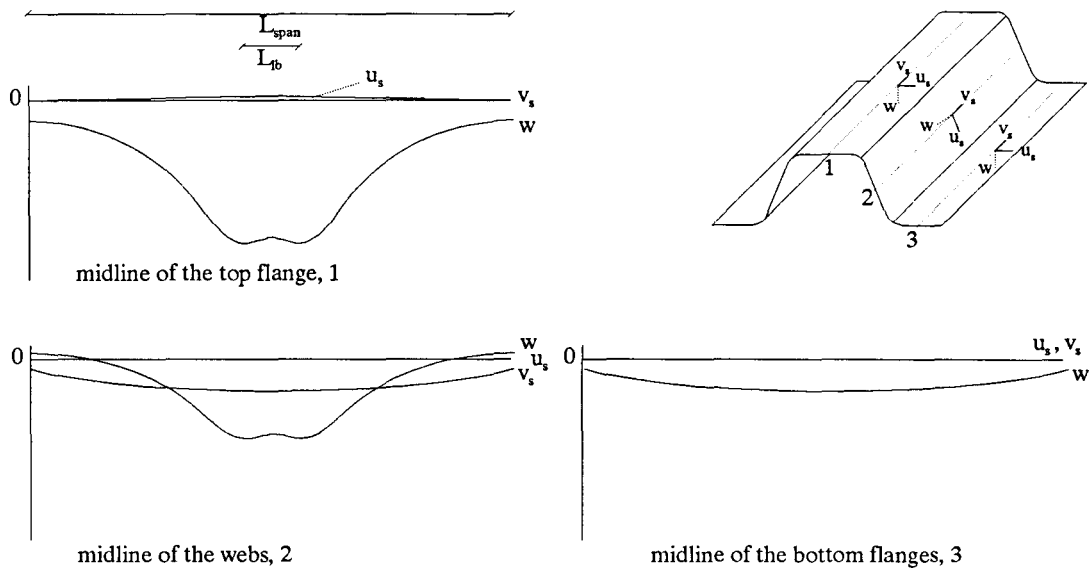

Figure 5.3: *Deformation variations over the length of the member, in case of hat sections*

In case of first generation deck panels it is also assumed that the local deformations occur mainly in the top flange and the webs. Here, the bottom flanges of one hat section cannot rotate and translate freely because their ends are connected to another hat section. Due to compatibility requirements (see for instance section 3.4) the ends of the bottom flanges of one hat section need to have a rotation and horizontal displacements that equal zero. These compatibility requirements result in a slightly different deformation pattern for u_s and v_s over the cross section of the member at the bottom flange, but they have hardly any influence on the deformation pattern of the rest of the cross section and over the length of the member. Considering the deformation pattern of u_s and v_s over the bottom flange in figure 5.2, it can be concluded that the deformation pattern in case of first generation deck panels does not differ significantly from that of hat sections. Therefore, the deformation variations over the bottom flange are also nearly equal to zero in the case of first generation deck panels and the contributions of the bottom flanges to the total potential energy may be ignored. As a result from this assumption first generation deck panels can also be idealized to be built up of three plates (two web plates and a top flange plate).

- *Neglecting the contribution of the stretching actions u_s and v_s*

  For both hat sections and first generation deck panels the contribution of the stretching actions u_s and v_s to the total potential energy of each plate are neglected. This assumption does not imply that no stretching actions occur in the plates. It only states that the variation of the stretching actions in each plate equals zero and that the plates translate as rigid bodies if these stretching actions are considered.

Figure 5.2 and 5.3 show that this assumption is confirmed by finite element calculations: u_s and v_s have almost a constant value over the web and top flange.

- *Ritz coefficients*

Due to the neglect of the contribution of u_s and v_s to the potential energy only the trial function of w_k (equation 5.13c) remains. Hence the potential energy V is minimized by imposing k requirements

$$\frac{\partial V}{\partial c_i} = 0 \qquad i = 1,2,...,k \tag{5.15}$$

for the unknown Ritz coefficients.

The trial function w_k can be expressed as a function of the maximum deflection in the web and the top flange. The maximum deflections are variable and in reality will take up values that belong to the equilibrium configuration corresponding to minimum potential energy. Hence, if the maximum deflection of the top flange is denoted as w_1 and the maximum deflection of the web as w_2, the trial function may be composed of the Ritz coefficients w_1 and w_2 among other Ritz coefficients. Over the length of the member the web crippling variations may extend over the whole member in case of 'short' members, but may also extend over a part of the member in case of 'long' members, as appears from the experimental tests by Bakker and the numerical calculations carried out in this study. In the development of the beam on elastic foundation model it was already proposed to introduce an effective length over which the web crippling deformations extend and where outside the web crippling deformations are assumed to equal zero (section 4.5). The introduction of an effective length L_{ef} is put forward here because the length of the member does not necessarily correspond with the length over which the web crippling deformations extend. An extra parameter L_{ef} is used in the trial function w as a domain over which the web crippling deformations extend in the length direction of the member. Since the bending deformation pattern of the top flange plate in the energy model represent the web crippling deformation pattern, these deformations stretch over the effective length also, and the deformations of the top flange plate outside the effective length area are assumed to be negligibly small and do not contribute to the total potential energy. This deformation pattern over the length of the member is continued over the web. Consequently, the length of the web plates and the top flange plate is taken equal to L_{ef}. Hence, in the development of the energy model three Ritz coefficients are used: L_{ef}, w_1 and w_2.

The use of more Ritz coefficients (probably without any physical interpretation) might produce a more reliable description of the deflection w. However, it is presumed that sufficient accurate approximations can be established with the abovementioned coefficients.

Applying L_{ef} as a Ritz coefficient beneath the coefficients w_1 and w_2 implies an alternative use of the

Rayleigh-Ritz method because the trial function w_k is a product of these coefficients as will become clear in section 5.5. Moreover, in the trial functions L_{ef} may be raised to a certain power. Normally, in the Rayleigh-Ritz procedure is a sum of these coefficients (equation 5.13c).

The reader should be aware of the fact that this alternative use of the Rayleigh-Ritz method implies that the lowest approximation of the web crippling stiffness will not be automatically the most reliable one, while this does hold true if the method is applied in its original form.

- *Constant quotient* $|w_1 / w_2| = n$

  Applying three Ritz coefficients imposes 3 requirements (equation 5.15) and implies three equations that need to be solved simultaneously.

  However, it is assumed that the maximum deflection of the top flange w_1 can be expressed in terms of the maximum deflection of the web w_2. In other words, the quotient $|w_1 / w_2|$ is assumed to equal a factor n that is a function of the geometrical dimensions of the cross section of the member only. Hereby, the number of Ritz coefficients is reduced to two which implies that only two equations need to be solved simultaneously. This greatly simplifies the solution.

  The expression for n is found using the mechanical schematisation of the two-dimensional portal frame model. It is assumed that the maximum deflections of the web and the top flange occur at the middle of the web and the top flange respectively. In the application of the portal frame model this assumption is approximately true, regardless the geometrical dimensions of the member. However, especially in case of the web it is possible that the maximum deflection not exactly occurs at the middle in reality. Due to local deformations in the web, the maximum deflection can be located somewhat nearer the top flange where the loading is applied. Nevertheless, the finite element simulations indicate that the maximum deflection of the web can approximately be taken at the middle (figure 5.2).

  The difference between hat sections and first generation deck panels in the energy model is formed by the factor n. For hat sections (with $\theta_w > \pm 5^\circ$) the statical system of the cross section is given by figure 3.2 and it can be derived that (Appendix C.1)

$$n = \left| \frac{r_{i;tf} \cdot \sin\theta_w \cdot (r_{i;tf} \cdot \sin\theta_w \cdot (9 \cdot b_{tf}^2 - r_{i;tf} \cdot \sin\theta_w \cdot (8 \cdot b_w + 12 \cdot b_{tf})) + 6 \cdot b_w \cdot b_{tf}^2)}{9 \cdot b_w^2 \cdot r_{i;tf} \cdot \sin\theta_w \cdot (r_{i;tf} \cdot \sin\theta_w - b_{tf})} \right| \tag{5.16}$$

  In case of first generation deck panels n is derived the same way. Since the statical system of first generation deck panels (figure 3.4) slightly differs from the statical system of hat sections, a different expression for n is found (Appendix C.2), namely

$$n = \left| \frac{4 \cdot r_{i;tf}^2 \cdot \sin^2\theta_w \cdot (b_w \cdot (b_w + 2 \cdot (b_{tf} + b_{bf})) + 3 \cdot b_{bf} \cdot b_{tf}) - 3 \cdot b_{tf}^2 \cdot (3 \cdot b_{bf} \cdot r_{i;tf} \cdot \sin\theta_w + b_w \cdot (b_w + 2 \cdot (b_{bf} + r_{i;tf} \cdot \sin\theta_w)))}{3 \cdot b_w^2 \cdot (b_{tf} - r_{i;tf} \cdot \sin\theta_w) \cdot (3 \cdot b_{bf} + b_w)} \right| \tag{5.17}$$

As a result from the application of n only two Ritz coefficients remain and the potential energy V is minimized by solving simultaneously

$$\frac{\partial V}{\partial w_2} = 0 \qquad \frac{\partial V}{\partial L_{ef}} = 0 \tag{5.18}$$

both for hat sections and first generation deck panels.

- *Compatibility between the plates*

The three plates that are taken into consideration are connected to each other (without taking the curved transition of the corner radii into account) and hence need to be compatible. These compatibility requirements can be expressed as boundary conditions for each plate. Two different compatibility assumptions are made within the energy model leading to different resulting web crippling stiffnesses. The most obvious compatibility requirement is the assumption that the plates are rigidly connected at their ends (figure 5.4a), thus ignoring eventual rotations of the corner radii that in reality couple the plates. This assumption will be denoted as 'geometrical compatibility'. It states that both the rotations and bending moments at the ends of the plates need to be compatible.

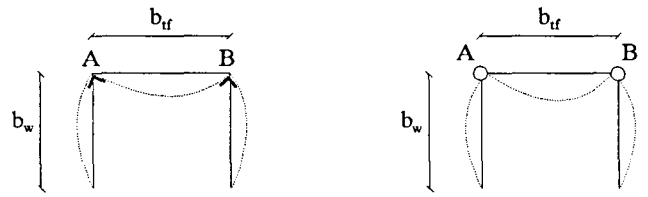

(a): Geometrical compatibility (b): Hinge compatibility

Figure 5.4: *Compatibility approaches in the energy model*

According to figure 5.4a the geometrical compatibility approach analytically implies that

$$\varphi_{w;A} = \varphi_{tf;A} \qquad \varphi_{w;B} = \varphi_{tf;B} \tag{5.19a}$$

$$M_{w;A} = -M_{tf;A} \qquad M_{w;B} = -M_{tf;B} \tag{5.19b}$$

in which the subscripts w and tf refer to web plate and top flange plate respectively.

A less obvious compatibility requirement is formed by the assumption that the plates are connected by hinge-joints (figure 5.4b). This assumption will be denoted as 'hinge compatibility' and implies that the bending moment at the end of each plate equals zero, or

$$M_{w;A} = 0 \qquad M_{tf;A} = 0 \qquad M_{w;B} = 0 \qquad M_{tf;B} = 0 \tag{5.20}$$

There is no physical ground for this assumption but finite element simulations indicate (figure 5.2) that if the bending deflection w of each plate over the cross section is considered, the second derivative of w more or less equals zero at the connection between the plates. This approach is investigated because it is expected to lead to simpler results than the geometrical compatibility approach and therefore deserves attention.

It may be concluded that the geometrical compatibility approach is based on a general assumption that is approximately true for all kind of members while the hinge compatibility approach represents a more specific assumption that appears to be a good approximation for the members with which the finite element simulations are carried out but does not lead necessarily to good results for other members.

For both the hinge and the geometrical compatibility approach it is assumed that in-plane normal and shear deformations can be neglected, which means that the deflections w at the end of each plate necessarily equal zero, thus

$$w_{w;A} = w_{tf;A} = 0 \qquad w_{w;B} = w_{tf;B} = 0$$

According to finite element simulations (figure 5.2) this a reasonable assumption that greatly simplifies the derivation of the web crippling stiffness.

The resulting deformation function $w(x,y)$ for both approaches is treated in section 5.5.

- *Schematisation of the corner radii*

  The member is idealized to be built up out of three plates (i.e. two web plates that have a width b_w and one top flange plate that has a width b_{tf}). In describing the geometry of the cross-section the rounding of the corners is thus ignored, except that the eccentric load application of F which is caused by the top flange corner radii is taken into account. The acceptability of this simplification which is also used in the portal frame model has been discussed already in section 3.5.2.

- *Application of the loads*

  Due to the downward curling of the member underneath the load bearing plate, only four contact points will remain between the top flange and the load bearing plate after initial loading. The transmission of the load F is limited to these points and each contact point transmits $1/4F$. To model the eccentric load application with respect to the web, the contact points are located at a distance $r_{i;tf} \cdot \sin\theta_w$ from the line of intersection of the top flange and web plate (section 3.2). Considering an xy

coordinate plane covering the top flange, that has its origin at the centre of the top flange, the four contact points are thus located at ($1/2L_{lb}$, $1/2b_{tf} - r_{i;tf}\cdot\sin\theta_w$), ($-1/2L_{lb}$, $1/2b_{tf} - r_{i;tf}\cdot\sin\theta_w$), ($1/2L_{lb}$, $-1/2b_{tf} - r_{i;tf}\cdot\sin\theta_w$) and ($-1/2L_{lb}$, $-1/2b_{tf} - r_{i;tf}\cdot\sin\theta_w$). For members with vertical webs this corresponds completely to the application of the loads in the beam on elastic foundation model, where four concentrated loads were applied also (figures 3.1 and 4.11).

- *Definition of the web crippling stiffness*

  Due to the fact that the stretching actions are neglected, the web does not translate vertically. Hence, the web crippling deformation can be taken equal to the deformation of a contact point, just as in the beam in elastic foundation model. If the deformation of the top flange plate is described by w_{tf}, the web crippling stiffness can be specified as

$$k_{\Delta h_w} = \frac{F}{w_{tf}(1/2\cdot L_{lb}, r_{i;tf}\cdot\sin\theta_w)}$$

5.5 *Derivation of the energy model*

As mentioned in section 5.4 two different approaches in the application of the Rayleigh-Ritz method can be distinguished as far as the compatibility of the three plates is concerned, namely the hinge compatibility and the more complicated geometrical compatibility approach. In both approaches the kinematic admissible trial function $w(x,y)$ is defined to be

$$w(x,y) = w(x)\cdot w(y)$$

in which $w(x)$ describes the deformation variations of the plate over the cross-section of the member and $w(y)$ represents the deformation variation of the plate over the length of the member. Ideally, the trial functions should resemble the web crippling deformation pattern as shown in the figures 5.2 and 5.3, but it will be clear that this deformation pattern may only be approximated with varying degrees of accuracy by different trial functions.

Over the cross-section the deformation of both the top flange plate and the web plates is chosen to be described by a fourth degree polynomial, mainly because the second derivatives of the deformation curves of both plates appeared to approximate zero at the ends of the plates (figure 5.2). Describing the deformation curves with a second degree polynomial would imply a second derivative that has a constant value and thus never equals zero. The application of a third degree polynomial is out of the question because of the rather symmetric deformation pattern. Hence, taking into account that the bending moment (i.e. the second derivative of the deformation function) might equal zero somewhere near the connection between the plates,

the most simple deformation variation description is formed by a fourth degree polynomial. In both descriptions the origin is located at the centre of the plate as in figure 5.1. It is assumed that the deformation pattern is symmetrical in the origin resulting in an even function thus without terms of x raised to the first or third power. For the web plates this polynomial is given by

$$w_w(x) = w_2 \cdot (1 + c_{1;w} \cdot \frac{x^2}{b_w^2} + c_{2;w} \cdot \frac{x^4}{b_w^4}) \qquad (-1/2 \cdot b_w \leq x \leq 1/2 \cdot b_w) \tag{5.21a}$$

in which the coefficients $c_{1;w}$ and $c_{2;w}$ are determined by the requirements that are imposed by either the hinge compatibility or the geometrical compatibility approach. These approaches result in different coefficients. For the top flange plate the deformation over the cross-section is given by

$$w_{tf}(x) = w_2 \cdot n \cdot (1 + c_{1;tf} \cdot \frac{x^2}{b_{tf}^2} + c_{2;tf} \cdot \frac{x^4}{b_{tf}^4}) \qquad (-1/2 \cdot b_{tf} \leq x \leq 1/2 \cdot b_{tf}) \tag{5.21b}$$

in which the coefficients $c_{1;tf}$ and $c_{2;tf}$ are determined by either the hinge compatibility or the geometrical compatibility approach also.

The formats of the functions describing the deformation pattern of the web and top flange over the cross-section (equations 5.21) are given in figure 5.5.

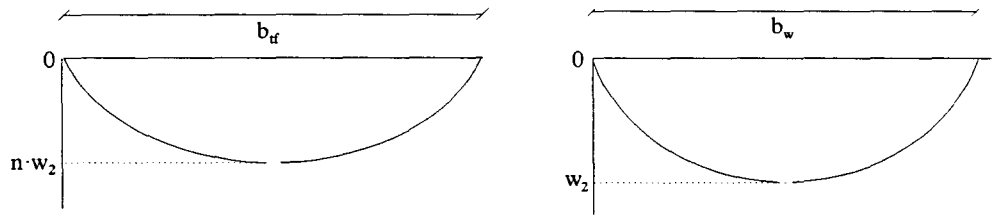

Figure 5.5: *Format of trial functions describing the deformation pattern over the cross-section*

In the following the determination of the abovementioned coefficients for the web plates and the top flange plate is treated for both the hinge compatibility and the geometrical compatibility approach.

Applying the geometrical compatibility approach, equations 5.19 needs to hold true. Noting that

$$\varphi(x) = \frac{dw(x)}{dx}$$

and

$$M(x) = -EI \cdot \frac{d^2 w(x)}{dx^2}$$

substitution of equations 5.21 into 5.19 leads to

$$c_{1;w} = \frac{2 \cdot n \cdot b_w^2 - 5 \cdot b_w \cdot b_{tf} - 3 \cdot b_{tf}^2}{5/8 \cdot b_{tf} \cdot (b_w + b_{tf})} \tag{5.22a}$$

$$c_{2;w} = \frac{b_{tf}^2 + 5 \cdot b_{tf} \cdot b_w - 4 \cdot n \cdot b_w^2}{5/16 \cdot b_{tf} \cdot (b_w + b_{tf})} \tag{5.22b}$$

$$c_{1;tf} = \frac{2 \cdot b_{tf}^2 - 5 \cdot n \cdot b_w \cdot b_{tf} - 3 \cdot n \cdot b_w^2}{5/8 \cdot n \cdot b_w \cdot (b_w + b_{tf})} \tag{5.22c}$$

$$c_{2;tf} = \frac{n \cdot b_w^2 + 5 \cdot n \cdot b_w \cdot b_{tf} - 4 \cdot b_{tf}^2}{5/16 \cdot n \cdot b_w \cdot (b_w + b_{tf})} \tag{5.22d}$$

Within the hinge compatibility approach, equations 5.20 need to hold true. In that case it can be derived that

$$c_{1;w} = c_{1;tf} = -\frac{24}{5} \qquad c_{2;w} = c_{2;tf} = \frac{16}{5} \tag{5.23}$$

Comparing equations 5.22 with equation 5.23 it becomes clear that the hinge compatibility approach is simpler than the geometrical compatibility approach.

Actually, the deformation variations over the cross-section of the member can also be described properly using a sine function for each plate. However, the use of a sine function gives transcendental equations in minimizing the total potential energy, which cannot be solved algebraically.

Over the length of the member the deformation variation is described by *w(y)*. The deformation variation of the top flange plate and the web plates are assumed to obey to the same format, which is justified by figure 5.3. Hereby, the only difference is formed by the maximum deflections of these plates that differ from each other. However, from equations 5.21 it is clear that this difference is accounted for already in the description of the deformation variation over the cross-section of the member *w(x)*. According to equations 5.21 the maximum deflection of the cross-section of the top flange plate and the web plates is respectively $n \cdot w_2$ and w_2. Since *w(x,y)* is defined to be the product of *w(x)* and *w(y)* and the maximum deflection of the top flange plate and the web plates is respectively $n \cdot w_2$ and w_2, the maximum deflection of *w(y)* might simply be taken 1 for both the top flange plate and the web plates. Hence, the deformation variations of the top flange plate and the web plates are described by the same function *w(y)*.

As mentioned in section 5.4 the deformations are assumed to stretch out over the effective length. The magnitude of this effective length might determined by using it as a Ritz coefficient in the application of the Rayleigh-Ritz method. This implies an alternative use of the Rayleigh-Ritz method because the trial function is a product of the Ritz coefficients L_{ef} and w_2 while normally, the Rayleigh-Ritz procedure includes the development of a series of functions γ_i with belonging coefficient c_i that are summarized (equation 5.13c).

Several kinematical admissible trial functions may be applied in describing the deformation variations over the length of the member. The trial functions that are investigated are (with increasing complications):

- Bilinear function $w(y)_1$;
- Trilinear function $w(y)_2$;
- Polynomial of the fourth degree $w(y)_3$.

The formats of the functions describing the (web crippling) deformation pattern of the web and top flange over the effective length of the member are given in figure 5.6.

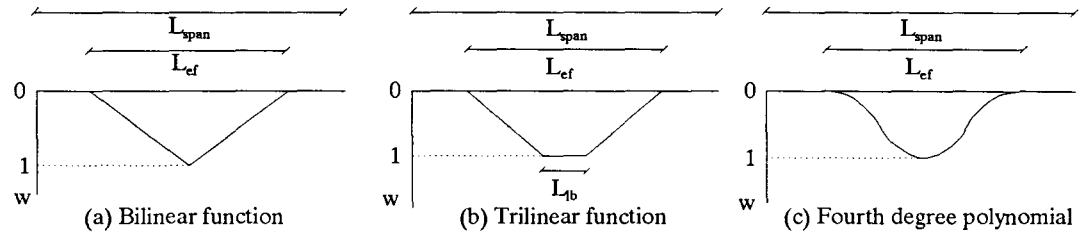

(a) Bilinear function (b) Trilinear function (c) Fourth degree polynomial

Figure 5.6: *Trial functions describing the deformation pattern over the effective length of the member*

If the origin is applied at the centre of the plate, these functions can mathematically be specified as

$$w(y)_1 = 1 - \frac{2 \cdot |y|}{L_{ef}} \qquad |y| < 1/2 \cdot L_{ef} \tag{5.24a}$$

$$w(y)_2 = 1 \qquad |y| < 1/2 \cdot L_{lb}$$

$$w(y)_2 = 1 - \frac{2 \cdot (|y| - 1/2 \cdot L_{lb})}{L_{ef} - L_{lb}} \qquad |y| > 1/2 \cdot L_{lb} \tag{5.24b}$$

$$w(y)_3 = \frac{16}{L_{ef}^4} \cdot (y^2 - 1/4 \cdot L_{ef}^2)^2 \tag{5.24c}$$

and

$$w(y)_1 = w(y)_2 = w(y)_3 = 0 \qquad |y| > 1/2 \cdot L_{ef}$$

Accordingly, the trilinear and fourth degree polynomial trial functions use the Ritz coefficient L_{ef} in another form than is suggested in equation 5.13c, beneath the difference that was already mentioned above. Within the trilinear function the deformation under the load bearing plate are not a function of the Ritz coefficient L_{ef} and the fourth degree polynomial raises L_{ef} to the fourth power. Hence, both the trilinear function and the fourth degree polynomial are not in conformity with equation 5.13c. This alternative use of the Ritz coefficient L_{ef} appears to lead to complicated and sometimes intractable algebraic problems in the derivation

of the web crippling stiffness. In case of the trilinear function the deformation under the load bearing plate and thus under F is not a function of L_{ef} resulting in an external potential energy that is not a function of L_{ef}. Therefore, minimizing the total potential energy with respect to L_{ef} leads to an intractable problem because the external potential energy falls off in the resulting equation (equations 5.18). In case of the fourth degree polynomial describing the (web crippling deformation) the Ritz coefficient L_{ef} is raised to the fourth power, resulting in an intractable equation of the fifth degree in L_{ef} when the total potential energy is minimized with respect to L_{ef}.

A solution for these problems can be found in three different ways.

- Firstly, the parameter L_{ef} can be ignored completely, assuming that the web crippling deformations stretch over the whole length of the member, instead of over the effective length (figure 5.6). In that case, the total potential energy is minimized with respect to w_2 only. It is to be expected that this solution gives poor predictions of the web crippling stiffness in case of longer members, because long members are expected to have negligible web crippling deformations near their hinged ends. This solution is denoted as the full length solution *(fls)*.
- Secondly, the parameter L_{ef} can be approximated using the beam on elastic foundation model. Here, the potential energy is not minimized with respect to L_{ef}, but L_{ef} is used as a parameter describing the length outside where the web crippling deformations are assumed to be negligibly small. Hence the length of the plates in the energy model is approximately defined to be the effective length that stems from the effective length approach within the beam on elastic foundation model. This solution corresponds to the effective length approach and is denoted as the effective length solution *(els)*.
- Thirdly, the web crippling stiffness can be approximated by neglecting some terms of the resulting equations in which the total potential energy is minimized with respect to L_{ef} and w_2. Neglecting some terms in these equations enables the establishment of an algebraically derived solution of the web crippling stiffness. Clearly, this solution can only be applied in case of the fourth degree polynomial description of the deformation over the length of the member because it does not solve the arising problems if the trilinear function is applied. This solution is denoted as the approximate solution *(as)*.

The bilinear function description of the deformations over the length of the member is the only function by which an exact solution for the web crippling stiffness can be determined. Hence, the abovementioned solutions are not applied within the application of the bilinear function; the exact solution that is obtained using the bilinear function is denoted as the exact solution *(es)*. The application of the bilinear function is not expected to produce highly reliable web crippling stiffness formulae. However, it gives clear insight in the way the principle of stationary total potential energy is applied to obtain an exact solution for the web crippling stiffness.

For sake of clarity an overview of the different solutions that can be developed is given in table 5.1.

Table 5.1: Different solutions within the energy model

	$w(y)_1$	$w(y)_2$: *trilinear function*		$w(y)_3$: *fourth degree polynomial*		
approach	*es*	*fls*	*els*	*as*	*fls*	*els*
*hca**	1	3	-	5	-	-
*gca**	2	4	-	6	-	-

** hca: Hinge compatibility approach; gca: Geometrical compatibility approach.*

According to table 5.1 twelve different web crippling stiffness formulae can be established using several combinations of the abovementioned approaches and solutions. Eventually, six of these combinations are investigated in this research project. The application of the effective length solution on the trilinear function is not investigated for the hinge compatibility approach nor for the geometrical compatibility approach because these combinations correspond greatly to the effective length approach within the beam on elastic foundation model. Although they are based on different physical models, the assumed deformation variations over the length of the member are exactly the same, resulting in similar web crippling stiffness formulae as far as the length of the member is concerned. For that, these combinations are not investigated. The application of the effective length solution and the full length solution on the fourth degree polynomial are not investigated for the hinge compatibility approach nor for the geometrical compatibility approach. The full length solution is expected to produce less reliable results compared to the application of the approximate solution for the fourth degree polynomial because the web crippling deformations might not stretch out over the full length, especially in case of long members. The effective length solution will produce highly complicated web crippling stiffness formulae that are not expected to be more reliable than the approximate solution and thus not preferable.

Sections 5.51 to 5.5.3 describe the derivation of the web crippling stiffness for the different trial functions in case hinge compatibility is assumed. First, section 5.5.1 summarizes the derivation of the web crippling stiffness if the deformation variation over the length of the member is described by $w(y)_1$ (combination 1). Thereafter, section 5.5.2 treats the derivation of the web crippling stiffness if $w(y)_2$ is assumed (combination 3). Finally, the web crippling stiffness using $w(y)_3$ is derived in section 5.5.3 (combination 5).

Similarly, the derivation of the web crippling stiffness for these different trial functions in case of the geometrical compatibility approach is summarized in section 5.5.4 to 5.5.6 (the combinations 2, 4 and 6 respectively).

5.5.1 *Combination 1: Bilinear function, hinge compatibility approach & exact solution*

Within combination 1 the deformation variations over the length of the member are described by the bilinear function of figure 5.6a and the hinge compatibility approach is applied (equation 5.23). Minimizing the total potential energy (equation 5.12) with respect to L_{ef} and w_1, it can be derived that (appendix C.3)

$$k_{\Delta h_w} = \frac{27 \cdot D \cdot b_{tf}^5 \cdot L_{lb} \cdot (2 \cdot b_{tf}^3 + 3 \cdot b_w^3 \cdot n^2)}{10 \cdot b_w^3 \cdot n^2 \cdot \sin^2\theta_w \cdot r_{i;tf}^2 \cdot (b_{tf}^3 - 2 \cdot b_{tf} \cdot \sin^2\theta_w \cdot r_{i;tf}^2 \cdot + \sin^3\theta_w \cdot r_{i;tf}^3)^2} \tag{5.25}$$

in which D is called the bending rigidity and given by

$$D = \frac{E \cdot t^3}{12 \cdot (1 - \mu^2)} \tag{5.26}$$

It is striking that the web crippling stiffness is more or less inversely proportional to the squared top flange corner radius. It will become clear that is approximately true for all the combinations.

5.5.2 *Combination 2: Bilinear function, geometrical compatibility approach & exact solution*

In combination 2 the deformation variations over the length of the member are described by the linear function of figure 5.6a, just as in combination 1, but here geometrical compatibility is assumed (equations 5.22). Combination 2 is expected to produce more reliable results than combination 1 because the hinge compatibility approach can be thought of as a special case of the geometrical approach that is only approximately true, where the geometrical approach refers to the true compatibility between the three plates.
For combination 2 the web crippling stiffness can be specified as (appendix C.3)

$$k_{\Delta h_w} = \frac{[9/20 \cdot D \cdot b_{tf}^5 \cdot L_{lb} \cdot (b_{tf}^3 \cdot (b_{tf} \cdot (12 \cdot b_{tf} + 41 \cdot b_w) + 50 \cdot b_w^2)}{[b_w \cdot \sin^2\theta_w \cdot r_{i;tf}^2 \cdot (b_{tf} - \sin\theta_w \cdot r_{i;tf})^2 \cdot (b_{tf}^2 \cdot (b_{tf} \cdot (4 \cdot \sin\theta_w \cdot r_{i;tf} - b_{tf}) - b_w \cdot n \cdot (b_w + 5 \cdot \sin\theta_w \cdot r_{i;tf})}$$

$$\frac{+ b_w^3 \cdot (b_w \cdot n \cdot (6 \cdot b_w \cdot n + 52 \cdot b_{tf}) + b_{tf}^2 \cdot n \cdot (25 \cdot n - 78))]}{-4 \cdot \sin^2\theta_w \cdot r_{i;tf}^2) + b_w \cdot \sin\theta_w \cdot r_{i;tf} \cdot n \cdot (\sin\theta_w \cdot r_{i;tf} \cdot (b_w + 5 \cdot b_{tf}) - b_w \cdot b_{tf}))^2]} \tag{5.27}$$

Apparently, the main difference between combination 1 and 2 is formed by a more complicated use of b_w, b_{tf} and n, due to the different compatibility approaches. Clearly this is caused by the different constants that are used in the description of the deformation of the plates over the cross-section (equations 5.22 and 5.23).

5.5.3 *Combination 3: Trilinear function, hinge compatibility approach & full length solution*

Within combination 3 the deformation variations over the length of the member are described by the trilinear function of figure 5.6b and the hinge compatibility approach is applied. As mentioned before, it is not possible to derive an exact solution for the web crippling stiffness when the total potential energy is minimized with respect to L_{ef} and w_2. Therefore, the total potential energy is only minimized with respect to w_2. Moreover, it is assumed in this combination that the effective length corresponds to the span length of the member L_{span}. The web crippling stiffness is then given by (appendix C.3)

$$k_{\Delta h_w} = \frac{D \cdot b_{tf}^5 \cdot (16 \cdot b_{tf}^3 \cdot b_w \cdot (L_{span} + 3 \cdot L_{lb}) + b_w^4 \cdot n^2 \cdot (8 \cdot L_{span} + 9 \cdot L_{lb}) + b_{tf}^2 \cdot L_{lb} \cdot n^2 \cdot (45 \cdot b_{tf}^2 - 30 \cdot b_w^2))}{20 \cdot b_w^4 \cdot n^2 \cdot \sin^2\theta_w \cdot r_{i;tf}^2 \cdot (b_{tf}^3 - 2 \cdot b_{tf} \cdot \sin^2\theta_w \cdot r_{i;tf}^2 + \sin^3\theta_w \cdot r_{i;tf}^3)^2} \tag{5.28}$$

It is to be expected that the application of the full length solution produces poor predictions in case of rather long members, because this solution assumes that the web crippling deformations stretch out over the length of the member, while in reality the web crippling deformations only appear within a certain region of the load bearing plate. From equation 5.28 it becomes clear that the web crippling stiffness is proportional to the span length of the member.

5.5.4 *Combination 4: Trilinear function, geometrical compatibility approach & full length solution*

The only difference between combination 3 and 4 is formed by the compatibility approach: combination 4 is based on the geometrical compatibility approach where combination 3 uses the hinge compatibility approach. In case of combination 4 it can be derived that

$$k_{\Delta h_w} = \frac{[D\cdot b_{tf}^9\cdot(b_w^4\cdot(L_{fb}\cdot(56/5+7\cdot n-41/4\cdot n^2)+41/15\cdot L_{span})+b_{tf}\cdot b_w^3\cdot(L_{fb}\cdot(12/5+15\cdot n+15/2\cdot n^2)+4/5\cdot L_{span}))}{[b_w^4\cdot\sin^2\theta_w\cdot r_{i;tf}^2\cdot(b_{tf}-\sin\theta_w\cdot r_{i;tf})^2\cdot(b_{tf}^2\cdot(b_{tf}\cdot(4\cdot\sin\theta_w\cdot r_{i;tf}-b_{tf})-b_w\cdot n\cdot(b_w+5\cdot\sin\theta_w\cdot r_{i;tf})-4\cdot\sin^2\theta_w\cdot r_{i;tf}^2)}$$

$$\frac{+D\cdot b_{tf}^8\cdot(b_{tf}^3\cdot L_{fb}\cdot(b_w^2\cdot(25/4\cdot n^2-3\cdot n-4)+b_{tf}\cdot(b_{tf}-5\cdot b_w\cdot n))+10\cdot b_w^5\cdot(L_{fb}\cdot(1-86/50\cdot n-n^2)+1/3\cdot L_{span}))]}{+b_w\cdot\sin\theta_w\cdot r_{i;tf}\cdot n\cdot(\sin\theta_w\cdot r_{i;tf}\cdot(b_w+5\cdot b_{tf})-b_w\cdot b_{tf}))^2]}$$

$$+\frac{[D\cdot b_{tf}^7\cdot b_w^5\cdot n\cdot(-12/5\cdot b_{tf}\cdot L_{span}+b_w\cdot(L_{fb}\cdot(39/4\cdot n-98/5)+L_{span}\cdot(5/3\cdot n-26/5)))}{[b_w^4\cdot\sin^2\theta_w\cdot r_{i;tf}^2\cdot(b_{tf}-\sin\theta_w\cdot r_{i;tf})^2\cdot(b_{tf}^2\cdot(b_{tf}\cdot(4\cdot\sin\theta_w\cdot r_{i;tf}-b_{tf})-b_w\cdot n\cdot(b_w+5\cdot\sin\theta_w\cdot r_{i;tf})-4\cdot\sin^2\theta_w\cdot r_{i;tf}^2)}$$

$$\frac{+D\cdot b_{tf}^5\cdot b_w^7\cdot n^2\cdot(b_{tf}\cdot(129/10\cdot L_{fb}+52/15\cdot L_{span})+2/5\cdot b_w\cdot L_{span}))}{+b_w\cdot\sin\theta_w\cdot r_{i;tf}\cdot n\cdot(\sin\theta_w\cdot r_{i;tf}\cdot(b_w+5\cdot b_{tf})-b_w\cdot b_{tf}))^2]} \qquad (5.29)$$

It is striking that combination 4 results in a far more complicated web crippling stiffness than combination 3. The difference in complexity is much larger than the difference in complexity between combination 1 and 2, that differ from each other only in the compatibility approach also. Note that the denominator of equation 5.29 corresponds almost completely with the denominator of equation 5.27 because they are based upon the same compatibility approach.

5.5.5 *Combination 5: Fourth degree polynomial, hinge compatibility approach & approximate solution*

Combination 5 makes use of the fourth degree polynomial that describes the deformations over the length of the member. It is based upon the hinge compatibility approach and the total potential energy is minimized with respect to L_{ef} and w_2. As mentioned before it is not possible to derive an exact solution for the web crippling stiffness. Therefore, the web crippling stiffness is approximately determined by neglecting some terms in the expression of the total potential energy functional which have low energy compared to other terms. An overview of the terms that are ignored and the derivation of the resulting web crippling stiffness is

given in appendix C.3.

The web crippling stiffness is calculated as

$$k_{\Delta h_w} = [\frac{512 \cdot D \cdot \sqrt{2 \cdot b_{tf}^3 + b_w^3 \cdot n^2} \cdot (b_{tf}^3 \cdot (34 \cdot b_w^2 + 252 \cdot L_{fb}^2) + b_w^3 \cdot n^2 \cdot (17 \cdot b_{tf}^2 + 126 \cdot L_{fb}^2))}{525 \sqrt{7} \cdot b_{tf} \cdot \sin^2\theta_w \cdot r_{i;tf}^2 \cdot b_w^3 \cdot n \cdot (b_{tf}^3 \cdot (34 \cdot b_w^2 + 490 \cdot L_{fb}^2) + b_w^3 \cdot n^2 \cdot (17 \cdot b_{tf}^2 + 245 \cdot L_{fb}^2))^4}]$$

$$\cdot [b_{tf}^3 \cdot (34 \cdot b_w^2 + 504 \cdot L_{fb}^2) + b_w^3 \cdot n^2 \cdot (17 \cdot b_{tf}^2 + 252 \cdot L_{fb}^2)]^{7/2} \qquad (5.30)$$

It is remarkable that combination 5 results in a relatively simple web crippling stiffness formula compared to combination 4, while combination 5 is based upon a deformation variation over the length of the member that is far more complicated.

5.5.6 *Combination 6: Fourth degree polynomial, geometrical compatibility approach & approximate solution*

Combination 6 can be thought of as the most complicated and reliable combination. The deformations over the length of the member are described by the fourth degree polynomial and the coupling between the plates is established using the geometrical compatibility approach. This combination is expected to be the most accurate approximation of all combinations. Just as in combination 5 it is not possible to derive an exact solution for the web crippling stiffness. Therefore, the web crippling stiffness is approximately determined by neglecting some terms in the expression of the total potential energy functional which have low energy compared to other terms, just as in case of combination 5. Moreover, in the derivation of the effective length (minimizing the total potential energy with respect to the effective length) it turns out to be impossible to determine the effective length analytically, even after the ignorance of the terms mentioned above. This is because an equation of the effective length in the fifth degree remains to be solved after this ignorance, while combination 5 consists of a less complicated total potential energy functional, resulting in an equation of the effective length in the second degree, that can be solved analytically which is the aim of this work. The difference in complexity stems from the unknown magnitude of the constants $c_{1;w}$, $c_{2;w}$, $c_{1;f}$ and $c_{2;f}$ in case of combination 6, resulting in an impossibility to ignore certain terms. As stated before, the kinematical admissible trial function $w(x,y)$ is defined to be the product of two separate functions $w(x)$ and $w(y)$. The deformation over the length of the member for combination 5 and 6 are described by the same fourth degree polynomial $w(y)$. The only difference is formed by the compatibility approach and thus by the descriptions of the deformations over the cross-section of the member $w(x)$. Only $w(y)$ is a function of the effective length. Hereby, $w(x)$ can be thought of as a constant in minimizing the total potential energy with respect to the effective length, resulting in the same kind of equation (with different constants) for combination 5 and 6, from which the effective length can be solved. It is assumed that the difference in the description of $w(x)$ has no significant influence on the resulting effective length. Henceforth, the effective length in combination 6 is

taken equal to the effective length of combination 5. Now, it is possible to determine the web crippling stiffness as (appendix C.3)

$$k_{\Delta h_w} = \frac{D \cdot b_{tf}^2 \cdot L_{ef}^5}{1575 \cdot (L_{lb}^2 - L_{ef}^2)^4 \cdot (b_{tf}^2 + b_w^2 \cdot n)}$$

$$\cdot[\frac{[b_{tf}^4 \cdot (b_w^3 \cdot L_{ef}^2 \cdot (8640 + 2400 \cdot n) + 5248 \cdot L_{ef}^4 \cdot b_w + b_{tf} \cdot (L_{ef}^2 \cdot (1536 \cdot L_{ef}^2 + 3936 \cdot b_w^2 + 2400 \cdot b_w^2 \cdot n))}{[b_w \cdot \sin^2\theta_w \cdot r_{i;tf}^2 \cdot (\sin\theta_w \cdot r_{i;tf} - b_{tf}) \cdot (b_{tf}^2 \cdot (b_{tf} \cdot (4 \cdot \sin\theta_w \cdot r_{i;tf} - b_{tf}) - b_w \cdot n \cdot (b_w + 5 \cdot \sin\theta_w \cdot r_{i;tf}) - 4 \cdot \sin^2\theta_w \cdot r_{i;tf}^2)}$$

$$\frac{+ b_{tf}^5 \cdot b_w^3 \cdot (b_w \cdot (3150 + 15750 \cdot n^2) + 7875 \cdot b_{tf} \cdot n^2) + b_w^4 \cdot (b_{tf}^3 \cdot L_{ef}^2 \cdot (2400 \cdot n^2 - 768 \cdot n + 8800) + 6656 \cdot b_{tf} \cdot L_{ef}^4 \cdot n^2)]}{+ b_w \cdot \sin\theta_w \cdot r_{i;tf} \cdot n \cdot (\sin\theta_w \cdot r_{i;tf} \cdot (b_w + 5 \cdot b_{tf}) - b_w \cdot b_{tf}))]}$$

$$+ \frac{[b_w^5 \cdot (L_{ef}^2 \cdot n^2 \cdot (768 \cdot L_{ef}^2 + 2400 \cdot b_{tf}^2) + b_{tf}^2 \cdot n \cdot (7875 \cdot b_{tf}^2 \cdot n - 8960 \cdot L_{ef}^2) - 2100 \cdot b_{tf}^4 + 4096 \cdot b_w \cdot b_{tf} \cdot L_{ef}^2 \cdot n^2)}{[b_w \cdot \sin^2\theta_w \cdot r_{i;tf}^2 \cdot (\sin\theta_w \cdot r_{i;tf} - b_{tf}) \cdot (b_{tf}^2 \cdot (b_{tf} \cdot (4 \cdot \sin\theta_w \cdot r_{i;tf} - b_{tf}) - b_w \cdot n \cdot (b_w + 5 \cdot \sin\theta_w \cdot r_{i;tf}) - 4 \cdot \sin^2\theta_w \cdot r_{i;tf}^2)}$$

$$\frac{+ b_{tf}^2 \cdot (b_w^6 \cdot (8400 \cdot n \cdot (b_{tf} + b_w) - 5250 \cdot b_{tf}) + L_{ef}^4 \cdot b_w^2 \cdot (b_w \cdot n \cdot (3200 \cdot n - 9984) - b_{tf} \cdot (4608 \cdot n - 6400)))]}{+ b_w \cdot \sin\theta_w \cdot r_{i;tf} \cdot n \cdot (\sin\theta_w \cdot r_{i;tf} \cdot (b_w + 5 \cdot b_{tf}) - b_w \cdot b_{tf}))]}] \qquad (5.31)$$

in which

$$L_{ef} = \sqrt{\frac{b_{tf}^3 \cdot (34 \cdot b_w^2 + 504 \cdot L_{lb}^2) + b_w^3 \cdot n^2 \cdot (17 \cdot b_{tf}^2 + 252 \cdot L_{lb}^2)}{14 \cdot b_{tf}^3 + 7 \cdot b_w^3 \cdot n^2}} \qquad (5.32)$$

Evidently, the resulting web crippling stiffness of combination 6 is the most complicated formula of the six combinations. Note that the denominator of equation 5.31 corresponds almost completely with the denominator of the equations 5.27 and 5.29 because they are based upon the same compatibility approach.

5.6 *Evaluation of the different solutions for the web crippling stiffness*

In section 5.5 six different solutions for the web crippling stiffness are derived, based on different combinations of the compatibility approaches and the kinematical admissible trial functions (combinations 1 to 6 in table 5.1). As mentioned in section 5.4 it is to be expected that the combinations which are based upon the geometrical approach (combinations 2, 4 and 6) produce more accurate results than the combinations which are based upon the hinge compatibility approach (combination 1, 3 and 5). Nevertheless, the latter may also produce fairly reliable results within certain dimensions of the web and the bottom and top flange. Their advantage lies within the complexity of the resulting web crippling stiffness formulae, which are relatively simple compared to the ones that are based upon the geometrical approach. The validation of these combinations against the finite element model (chapter 7) is meant to point out the dimension areas in which

the hinge compatibility approach may be applied without significant reduction of accuracy. Therefore, the discussion on the kind of compatibility approach is treated in chapter 7 as well.

Combination 1 and 2 are based upon the bilinear trial function of figure 5.6a and are not expected to produce very reliable approximations of the web crippling stiffness. However, these combinations result in relatively simple web crippling stiffness formulae and give clear insight in how the web crippling stiffness depends on each parameter, which is certainly not true in case of the other combinations. Moreover, it is not ruled out that these combinations can produce accurate predictions of the web crippling stiffness if an empirical correction factor is added. The derivation of this factor is beyond the scope of this study but it is put forward that these combinations produce elegant web crippling stiffness formulae that should be paid attention to.

Combination 3 and 4 make use of the trilinear trial function of figure 5.6b and apply the full length solution in deriving the web crippling stiffness. It is expected that these combinations produce poor predictions in case of rather long members. It seems clear that they produce the most accurate results if the span length more or less equals the effective length, whose magnitude can be approximated using equation 5.32. Note that it is also possible to use combinations 3 and 4 together with the effective length of combinations 5 and 6 (equation 5.32). This implies an extra combination that might be considered in the development of a relatively simple web crippling stiffness formula, but is further not treated in this study.

Finally, combination 5 and 6 use the most reliable description of the deformation variations of the length of the member: the fourth degree polynomial. They apply the approximate solution in the deviation of the web crippling stiffness. Despite the neglect of several terms in the total potential energy functional, they apparently still result in complex solutions for the web crippling stiffness. However, some factors of these solutions are negligible for certain dimensions of the hat sections or deck panels. Hereby, it might be possible to simplify the solution within certain dimension areas of each parameter but the derivation of these simplified solutions and the determination under which conditions they hold true is beyond the scope of this study.

Chapter 6: Finite element model

In this chapter an overview is given of the developed finite element model that is used in the evaluation and the development of the beam on elastic foundation model and the energy model.

6.1 *Introduction*

The developed analytical models describing the web crippling stiffness (i.e. the beam on elastic foundation model and the energy model) have to be validated against test results. Test results are also needed for the empirical determination of the parameter α in the beam on elastic foundation model. These test results may be obtained in two different ways.

Firstly, the results may be obtained from experimental tests. Bakker (*1992*) carried out an experimental study in which the load-deformation behaviour of hat sections subjected to a concentrated load and a bending moment was studied. The test program of Bakker included about 60 tests. For each test the web crippling stiffness was determined. The analytical models can hence be validated with the experimental results of Bakker but this validation is not made within this study because of existing measuring-inaccuracies in the experimental tests. The reader is referred to section 6.3 where a more detailed description of these measuring-inaccuracies is given.

Secondly, test results may be obtained from numerical simulations, using numerical models. In this study, the numerical models have been confined to finite element models. The elastic web crippling behaviour has been simulated numerically with the finite element program ANSYS. The finite element model is described in section 6.2. This model is validated against the experimental test results of Bakker in order to investigate the possibility of simulating elastic web crippling tests (section 6.3).

The developed model has been used for a parameter study to validate the analytical models. This parameter study will be described in chapter 7.

6.2 *Specifications of the finite element model*

The finite element model has been developed within the finite element program ANSYS, version 5.0A. Finite element calculations have been carried out both on hat sections and first generation deck panels. To establish a finite element model of a first generation deck panel, it is idealized to a hat section with extra boundary conditions, just as has been done in the portal frame model (section 3.4).

The finite element model is characterized by several aspects, such as:

- element type;
- element shape;
- modelling of the load application;
- modelling of the supports;
- use of symmetry;

- definition of the web crippling stiffness;
- modelling of the corner radii;
- mesh density;
- difference between hat sections and first generation deck panels.

In the following each of the above mentioned aspects will be discussed.

6.2.1 *Element type*

Since web crippling occurs only in thin-walled members whose webs and flanges have a large width-to-thickness ratio, the finite element model can be compiled of shell elements. Web crippling results in local deformations (in the web and top flange) that can be described properly either by using a mesh of elements with a quadratic deformation shape, or by using a more refined mesh of elements with a linear deformation shape. The former requires less memory capacity (1/8=12.5%) if the same density of nodes is used and is thus preferred. In the entire model SHELL93 elements are used. SHELL93 is an isoparametric shell element that has both bending and membrane capabilities. The element consists of eight nodes (figure 6.1). Hence, the deformation shapes are quadratic in both in-plane directions.

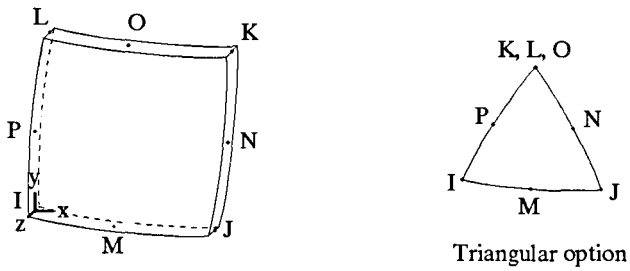

Figure 6.1: *The SHELL93-element (ANSYS manual)*

SHELL93 has six degrees of freedom in each node: translations in the nodal x, y and z directions and rotations about the nodal x, y and z axes. The element is defined by the thickness and the orthotropic material properties. It is particularly well suited to model curved shells, such as the rounding of the corners, because it is an isoparametric element.

6.2.2 *Element shape*

The choice between rectangular and triangular elements is rather arbitrarily. In the literature, examples can be found of finite element models describing the web crippling behaviour which are composed of rectangular elements (for instance *Tsai, 1987*), as well as models which are composed of triangular elements *(Santaputra, 1986)*. In this study the use of both rectangular and triangular elements has been investigated. No difference in the deformation pattern, web crippling stiffness or whatsoever could be observed. Eventually, the finite

element model is chosen to be made up of rectangular elements, because this results in a simpler mesh.

6.2.3. *Modelling of the load application*

The developed analytical models in previous sections are based upon the assumption that the member is loaded by a load bearing plate that is infinitely stiff. Due to the downward curling of the member underneath the load bearing plate, only four contact points between the member and the load bearing plate will remain after initial loading and each of these four contact points transmits a concentrated load *1/4F* (sections 3.2 and 4.3). The experimental study of Bakker is carried out with a load bearing plate that can be thought of as infinitely stiff as well. As the finite element model is developed to serve both the analytical models and the experimental study of Bakker, the loading is established by four concentrated loads *1/4F*, that are applied at the four contact points.

6.2.4 *Modelling of the supports*

In the modelling of the supports a distinction is made between the general finite element model, with which the parameter study is carried out, and a more specific model that is used to verify the experimental results of Bakker. The latter will be discussed in section 6.3.

The schematisation of the general finite element model is according to figure 1.4, namely a member with hinged ends. Over the width of the member the hinged ends are modelled as a continuous hinge over the width of the bottom flange. However, the bottom flange corner radii are assumed to be able to rotate and translate freely and do not belong to the continuous hinge. It is not quite sure if this is in conformity with reality but the schematisation of the hinges at the ends of the member has hardly any influence on the web crippling behaviour (web crippling is a local phenomenon).

6.2.5 *Use of symmetry*

In the calculation of the web crippling stiffness of hat sections and first generation deck panels, only one quarter of the member needs to be modelled. Due to symmetry in two directions (in the *xy*-plane and the *yz*-plane which both contain the midpoint of the top flange, point *B* in figure 6.2) the deflections and web crippling deformations of the rest of the member are similar to the part that is modelled. Taking only one quarter of the member into account implies additional boundary conditions that provide compatibility with the other three quarters. These additional boundary conditions are numbered 1 and 2 in figure 6.2. Besides, the additional boundary conditions which are used in case of first generation deck panels are also shown in this figure (number 3). For more detailed information about the modelling of these panels, the reader is referred to section 6.2.9.

Clearly also one quarter of the load bearing plate is modelled for both hat sections and first generation deck panels, and only one concentrated load *1/4F* remains.

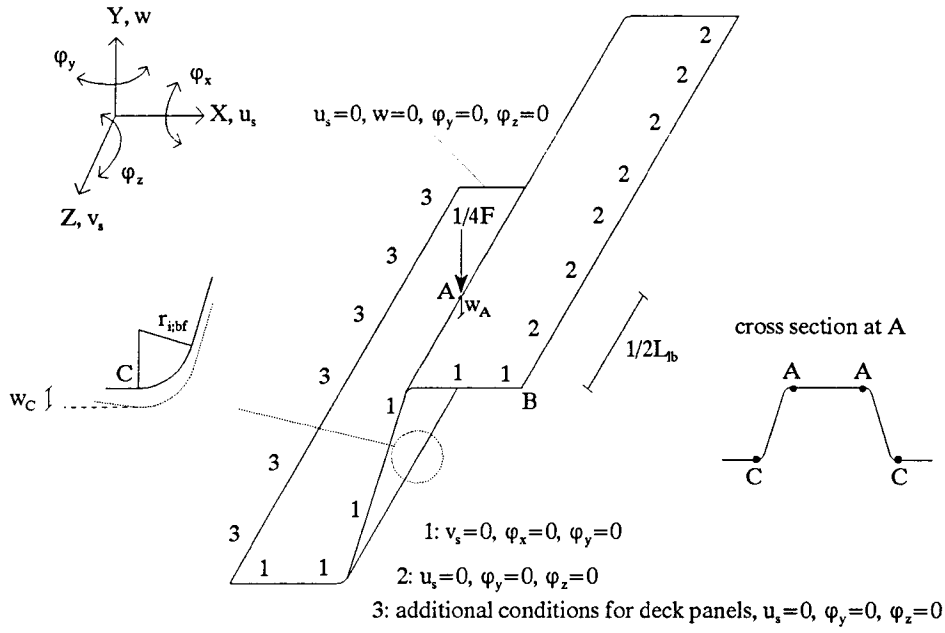

Figure 6.2: Boundary conditions and the measurement of the web crippling deformations

6.2.6 *Definition of the web crippling stiffness*

The web crippling deformation in the general finite element model is calculated straightforward as the displacement of point *A*, w_A, with respect to the one of point *C*, w_C. Henceforth, the web crippling stiffness is given by

$$k_{\Delta h_w} = \frac{F}{w_A - w_C} \tag{6.1}$$

Note that this corresponds with $\Delta h_{w;model}$ in figure 4.8. From equation 6.1 and figure 6.2 it follows that the web crippling stiffness is calculated roughly in the same way as in the analytical models.

6.2.7 *Modelling of the corner radii*

Three different possible representations of the corner radii in the finite element model have been investigated. These three representations are shown for the top flange corner radii in figure 6.3.

Representation *a* models the eccentricity of the applied load due to the corner radii but ignores the rounding of the corners. This representation is also used in the portal frame model. In representation *b* the rounding of the corner radii is modelled by a straight line under an angle of 45° with the web and the top flange, while in representation *c* the rounding is modelled by a circle segment.

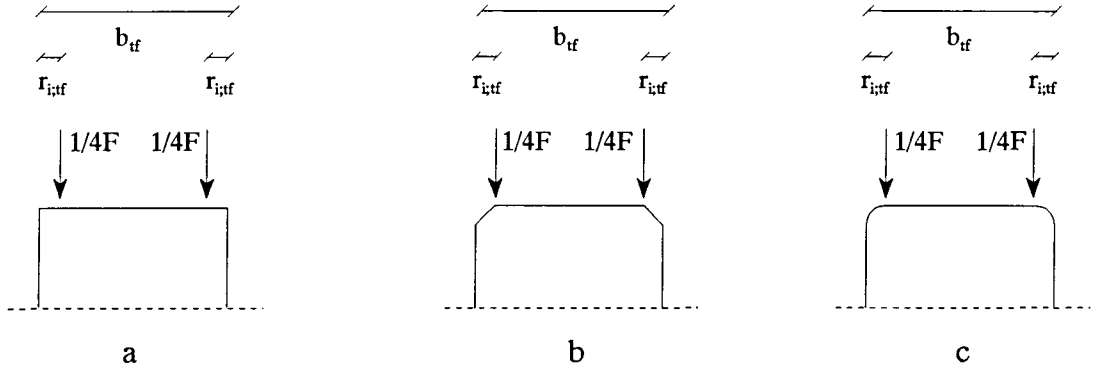

Figure 6.3: Representation of the corner radii

Several finite element simulations are carried out with the above mentioned representations in order to compare the resulting web crippling stiffnesses and to evaluate the reliability of each representation for both the top flange and the bottom flange corner radii.

It is to be expected that the differences between the representations vary with the magnitudes of the corner radii on which the representations are applied. Therefore, the simulations are carried out on three hat sections that differ only from each other in the magnitude of their corner radii:

- member A $r_{i;bf}=r_{i;tf}=10$ mm;
- member B $r_{i;bf}=1$, $r_{i;tf}=10$ mm;
- member C $r_{i;bf}=r_{i;tf}=1$ mm.

Considering the rest of the member, these three members have the same following geometrical properties: $L_{span}=290$, $\theta_w=90°$, $b_{bf}=100$, $b_w=50$, $b_{tf}=60$, $t=0.68$ and $L_{lb}=50$. It is assumed that the influence of the representations on hat sections does not differ much from the influence on first generation deck panels. The results of the simulations are given in table 6.1.

Table 6.1: The influence of the representation of the corner radii on the web crippling stiffness

representation of corner radii			member A		member B		member C	
test nr.	$r_{i;bf}$	$r_{i;tf}$	$r_{i;bf}=r_{i;tf}=10$	index	$r_{i;bf}=1$, $r_{i;tf}=10$	index	$r_{i;bf}=r_{i;tf}=1$	index
1	*a*	*c*	1993	49	1993	96	35597	76
2	*b*	*c*	3791	93	2128	102	46280	99
3	*c*	*c*	4065	100	2077	100	46871	100
4	*c*	*a*	1379	34	1138	55	37629	80
5	*c*	*b*	4662	115	2534	122	49164	105

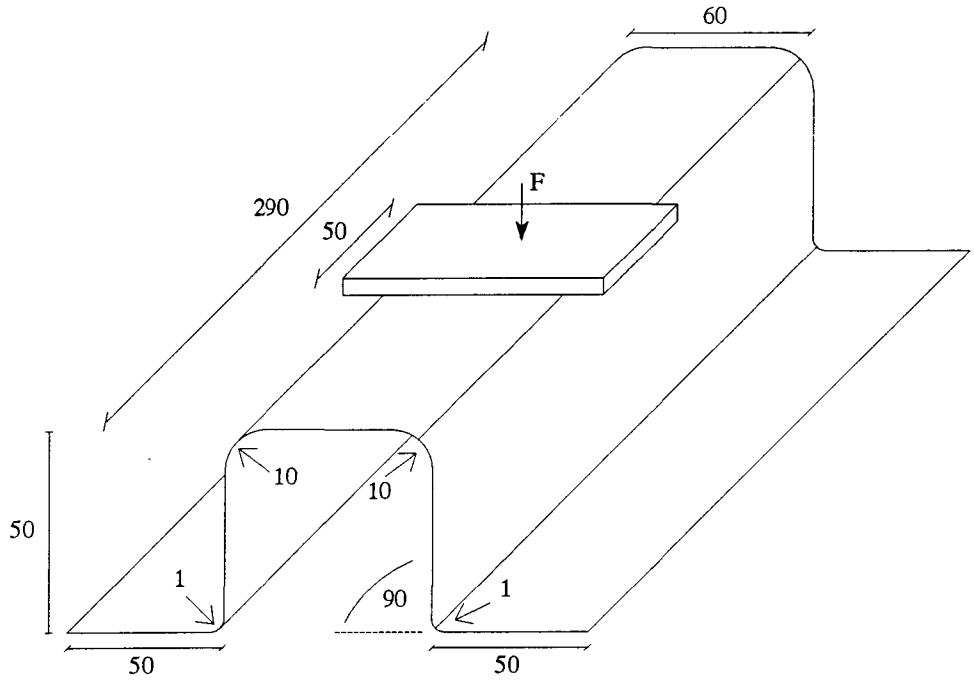

Figure 6.4: *Geometrical properties of the member B corresponding to table 6.1*

The geometrical properties of member B are once more shown in figure 6.4 as an example.
The simulations for each member differ from each other in the kind of representations that are used for the bottom flange corner radius ($r_{i;bf}$) and the top flange corner radius ($r_{i;tf}$). Each member is composed of more or less square elements that have a width of 8 mm. An exception is made for the corner radii where two elements are used over the width of the curved transitions in case of corner radii of 1 mm, and six elements in case of corner radii of 10 mm.
In representation *c*, the rounding of the corner radii is modelled most accurately. Thus, the tests A3, B3 and C3 produce the most reliable and accurate simulations for the test series on the members A, B and C respectively. Comparison of A1, B1 and C1 with A3, B3 and C3 shows that applying representation *a* for the bottom flange corner radii underestimates the web crippling stiffness significantly, especially if the top flange and bottom flange corner radii have the same magnitude. The application of representation *b* for the bottom flange corner radii gives fairly accurate approximations of the web crippling stiffness for members having small bottom flange corner radii. However, the difference between the tests A.2 and A.3 indicate that representation *b* for the bottom flange corner radii is less reliable for large bottom flange corner radii.
The deviations of the tests 4 from the tests 3 in case of the series A, B and C point out that representation *a* for the top flange corner radii implies significant underestimations of the web crippling stiffness, thus representing a less stiff description of the rounding of the corners compared to representation *c*. Finally, a

comparison between the tests 5 and 3 for all the test series indicates that representation *b* for the top flange corner radii produces poor results, especially in case of large top flange corner radii. It is striking that the representation of the bottom flange corner radii has a different influence on the web crippling stiffness than the representation of the top flange corner radii.

Note that the larger the top flange corner radii, the larger the influence of different representations on the web crippling stiffness will be. It may be concluded that the representations *a* and *b* cannot be used properly for the top flange corner radii, nor for the bottom flange corner radii. Henceforth, representation *c* is used throughout the finite element model for each corner radius.

In the finite element model the representations *a* and *c* differ from each other significantly considering the resulting web crippling stiffnessses, while in the beam on elastic foundation model representation *a* approximately corresponds to *c* and has thus been used in describing the rounding of the corners. This might be caused by the fact that representation *c* within the finite element model provides additional stiffness over the length of the member at the rounding of the corners, compared to representation *a*. This additional stiffness results in smaller deformations w_C and w_A. Clearly, this does not take place in the portal frame model, which is confined to the cross-section of a small slice of the member. Although this additonal stiffness is also provided in the three-dimensional extension of the portal frame model in case of representation *c*, it has less influence on the resulting web crippling stiffness because only a part of the cross-section is taken into account (the top flange and a part of the web) while the difference between *a* and *c* has also significant influence on the rest of the cross-section (i.e. on the deformation w_C). Hence, the representations *a* and *c* may greatly differ from each other in the finite element model, while this difference is less significant in the beam on elastic foundation model.

It is remarkable that these finite element simulations point out that the magnitude of the bottom flange corner radius may have a significant influence on the web crippling stiffness. The results for the test series A and B show great deviations for almost every test. It could have been possible that these deviations diminish in case of longer (more regular) members. However, if the same simulations of table 6.1 are carried out for a member with a span length of 1560 mm and the rest of the parameters are held at the same value, these deviations appear to remain large. Hence, the disregarding of the bottom flange corner radii in both the energy model and the beam on elastic foundation model turns out to be rather questionable. The reader is referred to chapter 7 where this disregarding is discussed on the basis of the results of the parameter study.

6.2.8 *Mesh density*

In the establishment of the mesh density three aspects are distinguished explicitly:

- the element size that is used throughout the entire model (*esize*), except at the corner radii, the supports and the load application;
- the number of elements that are used over the rounding of the corners ($n(r_{i;tf})$ and $n(r_{i;tf})$);

- the element size at the supports and the load application.

Within ANSYS it is possible to determine the maximum magnitude of the length and width of each element throughout the finite element model. The size of the elements *(esize)* refers to the longest dimension of each element (i.e. the length or the width) that is applied in the finite element model. Some finite element tests are carried out for members having relatively small corner radii (1 mm). To preclude the creation of only one element over the rounding of the corners in case of small top flange corner radii, implying a poor representation of the curved transitions, the number of elements is determined separately at these roundings ($n(r_{i;bf})$ and $n(r_{i;tf})$). On the other hand, a large number of elements over the rounding of the corners promotes the existence of poorly shaped elements (elements having a length-to-width ratio that exceeds 8), because these elements have a rather small width while their length more or less equals the element size. To avoid the above mentioned problems, two solutions remain. Firstly, it is possible to use a small element size throughout the model. This offers the opportunity of to use a number of elements over the rounding of the corners without creating poorly shaped elements. However, this solution implies a very fine mesh that requires much memory capacity, especially in case of small corner radii. Secondly, the number of elements over the rounding of the corners can be adjusted proportionally to the magnitude of the corresponding corner radii. In other words, the larger the corner radii the more elements are used over the rounding of the corners. This solution is based upon the knowledge that the representation of large corner radii has a relatively large influence on the web crippling stiffness compared to small corner radii (table 6.1). It is to be expected that this holds also true for the mesh density at the rounding of the corners. However, this solution implies the use of few elements in case of small corner radii.

The third aspect refers to the problems that might arise at the application of a concentrated load, thus at the supports and the load application. The use of concentrated loads might cause sensitivity for the mesh density around the locations where these loads are introduced.

The influence of the general mesh density, the mesh density at the introduction of concentrated loads and the number of elements over the rounding of the corners ($n(r_{i;bf})$ and $n(r_{i;tf})$) is investigated for the members B and C. Several finite element tests are carried out for these members varying the element size *(esize)*, which is proportional to the mesh density, and $n(r_{i;bf})$ and $n(r_{i;tf})$. For all tests representation *c* is applied for both the top flange and the bottom flange corner radii. The results are shown in table 6.2.

Member B has bottom flange corner radii of 1 mm. In the test series B the number of elements over the rounding of the bottom flange corners is varied as well as the element size throughout the model. Comparison of B1 with B2 shows that halving the element size reduces the web crippling stiffness with less than 1%. Hereby, it is shown that the mesh density barely correlates to the accuracy of the results, starting from a relatively fine mesh (*esize*=10 mm). Evaluating the tests B2, B3 and B4 on the influence of the number of elements over the rounding of the corners, it becomes clear that it is possible to use few elements over the rounding of the corners without significant loss of accuracy, in case of small corner radii.

Table 6.2: The influence of the mesh fineness on the web crippling stiffness

	esize (mm)	$n(r_{i;bf})$	$n(r_{i;tf})$	refinement	$k_{\Delta h_w}$	index
B1	10	1	6	-	2143	101
B2	5	1	6	-	2134	100
B3	5	2	6	-	2132	100
B4	5	3	6	-	2132	100
C1	15	3	3	-	56833	111
C2	7.5	3	3	-	51282	100
C3	15	3	3	F, 1*	54645	107
C4	10	3	3	F & S, 3**	54750	107

** F, 1: Refinement at the application of F with element size 1;*

*** F & S, 3: Refinement at the application of F and at the Supports with element size 3.*

Considering the test series C, C2 represents the most reliable and accurate simulation because it has the finest mesh density. Furthermore, C2 produces the lowest approximation of the web crippling stiffness for the test series C. From a physical point of view it can easily be seen that a mesh refinement, implying a more accurate approximation, corresponds to a reduction of the web crippling stiffness: a reduction of the web crippling stiffness implies a reduction of the deflection of the member w_C . ANSYS calculates the deformations and deflection using the principle of minimum total potential energy. A reduction of the deflection implies a lower amount of total potential energy that is required to achieve the deflection. This lower amount of total potential energy is always a better approximation of the absolute minimum of total potential energy that is requisite in reality.

Comparison of C1 with C2 shows that halving the element size here reduces the web crippling stiffness by 11%. However, a further refinement of the mesh appeared not to be possible with the current software at the Eindhoven University of Technology: the maximum wavefront of 400 was exceeded that way. The maximum wavefront corresponds to the maximum number of equations that can be solved simultaneously. This should not be confused with the maximum number of degrees of freedom of the model because ANSYS does not solve all the equations at the same time. Comparing these results with the results of the mesh refinement of test series B it becomes clear that a further refinement of the mesh density is not expected to give significant more accurate results.

With the aid of 'submodelling', a technique within ANSYS that provides local mesh refinements, the influence of mesh refinements at locations of the member that have large stress variations is investigated starting from C.1. These large stress variations are caused by the introduction of concentrated loads: they occur at the loading application and at the supports. The test C3 can be thought of as a refinement of C1, namely at the application of F with an element size that equals 1. Apparently C3 produces slightly more

accurate results than C1. Generally, it can be concluded that a local refinement of the mesh might influence the resulting web crippling stiffness slightly. Note however that a decrease in the element size has a larger influence on the web crippling stiffness than has a local refinement. From the results of C4 it becomes clear that a mesh refinement at the application of the supports does not contribute to a better approximation of the web crippling stiffness.

Eventually, the number of elements over the corner radii in the finite element model is varied from 2, in case of corner radii that equal unity, to 6, in case of corner radii of 10 mm. No local mesh refinements are applied in the finite element model because of the results in table 6.2, indicating that the best approximations might be established by using a small element size (7 to 10), rather than applying local refinements. The element size in the numerical simulations is varied from 5 to 10, depending on the capacity restrictions (the maximum wavefront). An example of the eventual mesh of member B, with the corresponding deformation plots, is given in the figures 6.5 and 6.6. In figure 6.5 the deformation is shown with respect to the undeformed member (the dotted line).

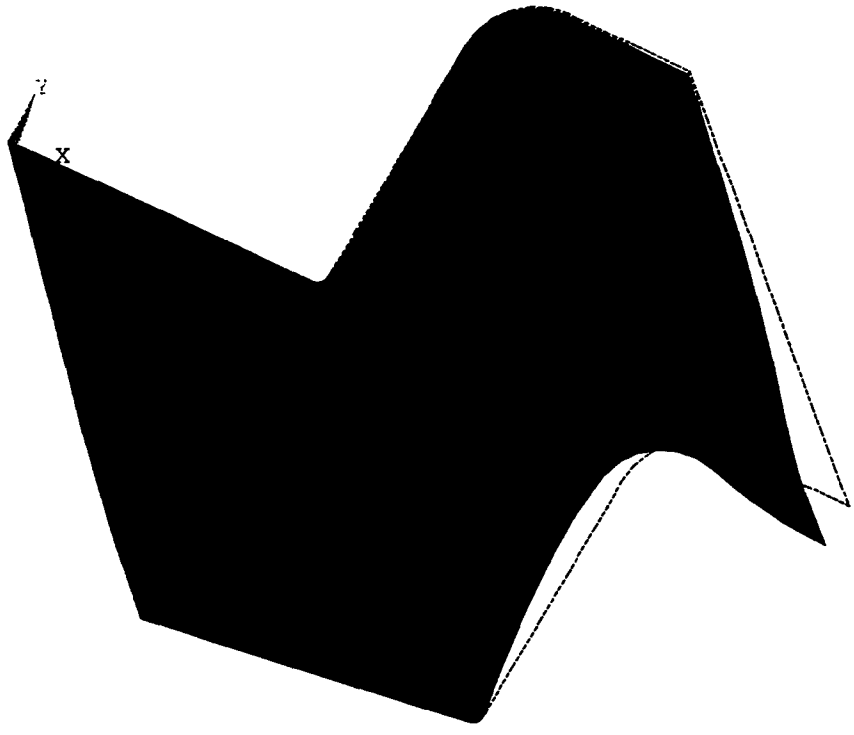

Figure 6.5: *Finite element deformation plot of member B*

A contour plot of the deformations in the *y* direction is given in figure 6.6. Some general remarks can be made about this plot. It becomes clear that the axial deformations in the web are indeed negligibly small. The colour transitions mark the deformation variations. The deformations of the top flange are concentrated within a small region. For w_c apparently being negligibly small, this indicates the existence of an effective length: the deformations of the rounding of the top flange corner radius approach zero near the end of the member.

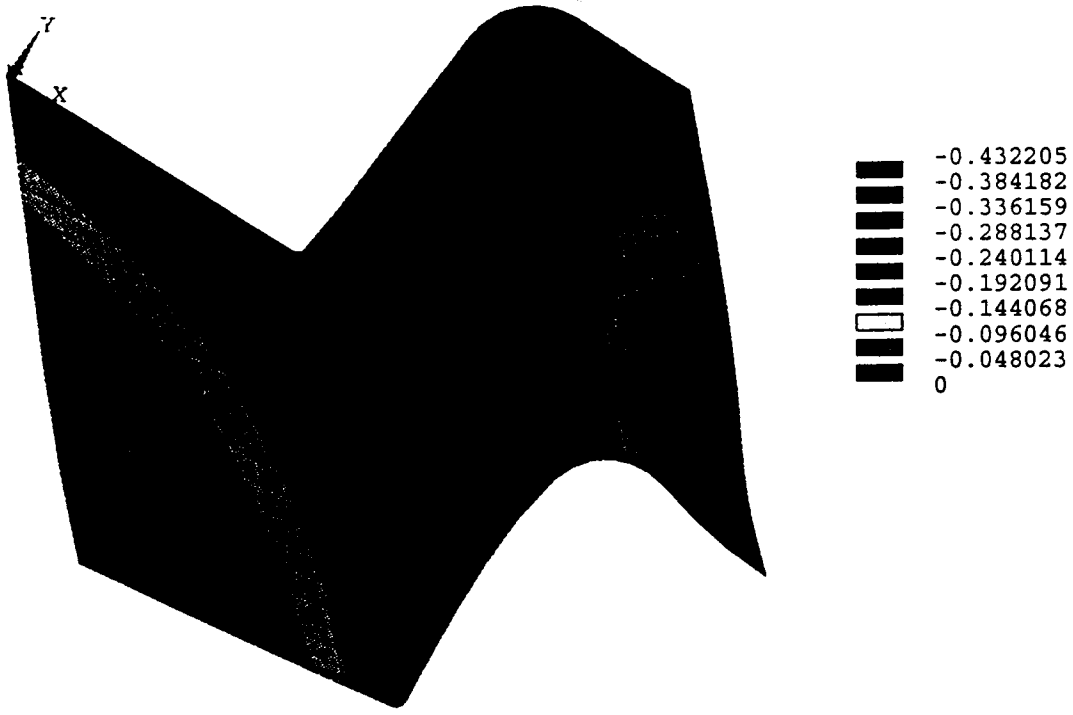

Figure 6.6: Finite element contour deformation plot (y direction) of member B

6.2.9 *Difference between hat sections and first generation deck panels*

First generation deck panels can be thought of as a composition of hat sections that are uniformly loaded and tied together at the unloaded flanges (figure 3.3 in section 3.4). It is assumed that each of these hat sections shows the same physical behaviour, because they are loaded similarly. Note however that the outer hat sections are not tied together at their outer unloaded flange, resulting in a slightly different web crippling behaviour. However, this different behaviour is not expected to have a significant influence on the overall behaviour of the panel. Therefore, the simulation of a web crippling test for a first generation deck panel may be reduced to the simulation of a web crippling test for a hat section under the condition that the ends of the unloaded flanges maintain the continuity of the deck panel. In other words, the rotations φ_y, φ_z and the horizontal displacement u_x need to equal zero at the ends of the bottom flanges over the whole length of the hat section if the web crippling test of a first generation deck panel is considered. These additional boundary conditions are shown in figure 6.2 (number 3).

6.3 *Validation of the finite element model against the experimental tests of Bakker*

The finite element model is validated against the experimental tests of Bakker *(Bakker, 1992, Bakker & v. Esch, 1989)*. To establish a reliable validation the finite element model as described in section 6.2 is adjusted to the specific conditions under which the experimental tests of Bakker were carried out. These conditions are described in section 6.3.1. The adjustments that are made within the finite element model are treated in

section 6.3.2. Finally, an overview of the validation of the adjusted finite element model against the experimental tests of Bakker is given in section 6.3.3.

6.3.1 *The experimental test setup of Bakker*

The experimental study of Bakker was designed to enable the determination of the influence of the various parameters on the web crippling behaviour, including the post-failure behaviour. In the tests carried out in this experimental study among other things the load and web crippling deformation were measured from which the (initial) web crippling stiffness was determined. The web crippling behaviour was studied in three-point bending tests. The test program was restricted to hat sections with doubly supported compression flanges without intermediate stiffeners in the flange or web elements. Altogether, 73 tests were performed with varying geometrical dimensions.

Four different materials were used for forming test specimens. Materials 1 and 2 were zinc coated steel sheets as normally used for cold-formed deck panels. Materials 3 and 4 were uncoated, gradually yielding steel sheets.

The test specimen was fastened on two reaction bearing plates with a length of 40 mm each. The reaction bearing plates had a very large stiffness compared to the test specimens and were hinged to allow for rotations in the longitudinal direction of the test specimen. The support conditions at the reaction bearing plates are shown in figure 6.7.

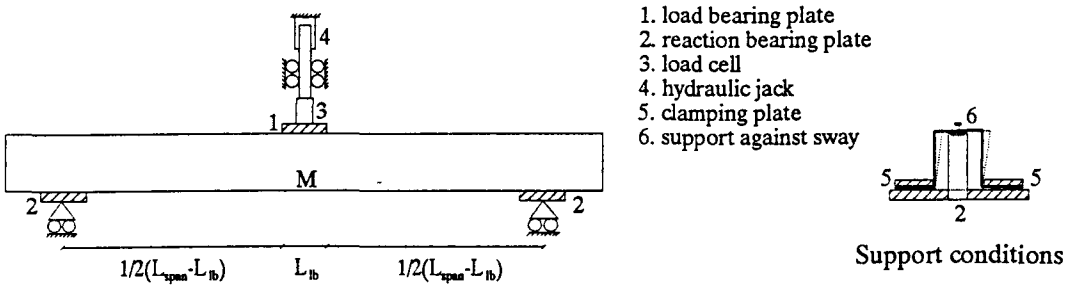

Figure 6.7: Experimental test setup and support conditions (Bakker, 1992)

The bottom flanges were clamped between the reaction bearing plate and a clamping plate. Sway of the test specimen was prevented at the supports by restraining the top flange from moving sideways by means of a screw through the top flange. Spreading of the webs was prevented only at the supports.

In the tests the load was applied by a hydraulic jack, operated by a hand pump (figure 6.7). The magnitude of the applied force was measured by a load cell between the hydraulic jack and the load bearing plate. The load bearing plate had a very large stiffness compared to the test specimens. The width of the load bearing plate was chosen to be larger than the width of the top flange of the test specimen. The load bearing plate was not fastened to the test specimen. Consequently, in all tests, the first clearly visible deformation of the

member was the downward curling of the flange underneath the load bearing plate, caused by the eccentric application of the concentrated load on the web. As a result the load bearing plate was supported only by the webs of the member, just as assumed in the portal frame model and the energy model. From figure 6.7 it becomes clear that in the tests of Bakker the length of the member exceeds the span length.

In the experimental study of Bakker the web crippling deformation was measured as the displacement of the load bearing plate w_A with respect to the rounding of the bottom flange corners underneath it (the bottom of the web) at the centre of the specimen w_M (see point M in figure 6.7 and $\Delta h_{w;test}$ in figure 4.8). For members with small corner radii (1 mm), having small elastic deformations, the web crippling deformation was difficult to determine. The measurements of w_A and w_M have an absolute inaccuracy of 0.01 mm. In case of small deformations w_A and w_M this inaccuracy has a large influence on the resulting web crippling deformations. Hereby, these web crippling deformations are relatively inaccurate. It may be concluded that the tests of Bakker on members with small corner radii contain inaccuracies.

The hat sections used as test specimens were made by press braking from steel sheets. The geometrical dimensions involved were set at certain (varying) values, but due to machine inaccuracies these values sometimes deviated slightly from the ones they were set on. After the manufacture of the test specimens the geometrical dimensions were measured with sufficient accuracy (0.01-0.1 mm). The magnitudes of the corner radii however, were very difficult to measure accurately. The accuracy in forming the corner radii is estimated to be ±0.5 mm. Especially, in case of small top flange corner radii, and to a less extent in case of small bottom flange corner radii, such a deviation might have a large influence on the web crippling stiffness. The actual inaccuracy in the magnitude of the corner radii might even exceed this estimated inaccuracy.

6.3.2 *Adjustments within the finite element model*

Comparing the general setup of the finite element model with the experimental test setup of Bakker it becomes clear that certain adjustments within the finite element model need to be made in order to approximate the experimental test setup of Bakker as accurately as possible.

A zinc coated steel cross-section (materials 1 and 2) can be regarded as a composite cross-section. In principle the properties of such a cross-section can be calculated from the properties of the composite materials (zinc and steel). However, little is known of the mechanical properties of the zinc layer, and it is difficult to determine these properties accurately. It is normal practice to idealize a zinc coated steel cross-section to a homogeneous cross-section. In this study the most common idealization is used, based on the core thickness. Hence, the stress in the cross-section is determined by dividing the load on the zinc coated test specimen by the area of the steel core. Not only the stress, but also the modulus of elasticity of a composite cross-section depends on the composition of the cross-section. For the zinc coated sheets used in practice, it can be shown that the influence of the zinc layer on the stiffness is rather small. Therefore the modulus of elasticity of the composite cross-section (referring to the core thickness is simply taken equal to

the steel modulus of elasticity (210000 N/mm^2), regardless of the zinc coating.

As mentioned in section 6.3.1 the length of the member exceeds the span length in the tests of Bakker. This extra length outside the hinged supports has not been modelled in the general finite element model. This extra length might slightly influence the resulting web crippling stiffness because it holds up the member against web crippling deformations. Therefore, in the validation of the finite element model against the experimental tests of Bakker the finite element model is adjusted by modelling this extra length outside the hinged supports also. The extra length outside both hinges (figure 6.6) equals $1/2 \cdot L_{rb} + 4 \cdot b_w$.

The finite element model has been developed with continuous hinged supports over the whole length of the bottom flange while over the length of the member the dimension of the hinges is infinitely small (figure 6.2). This does not correspond with the reaction bearing plate that was used in the experimental tests of Bakker (figure 6.6), which had a length of 40 mm. Hence, the hinges in the finite element model are adjusted to the dimensions of the reaction bearing plate in order to establish a better validation: they have a length of 40 mm and are applied continuously over the whole width of the bottom flange (figure 6.8).

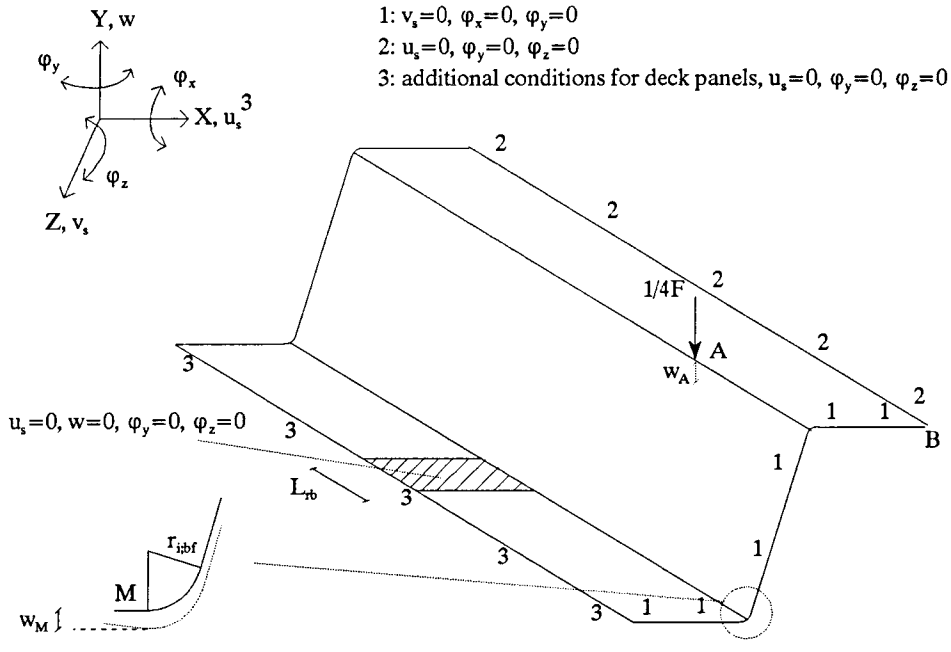

Figure 6.8: *Boundary conditions for the adjusted finite element model, in validating experimental tests*

In the experimental tests of Bakker the web crippling deformation is calculated as the displacement of the load bearing plate with respect to the bottom of the web underneath it at the middle of the specimen (point *M* in figure 6.8), while the general finite element model calculates the web crippling deformation as the displacement of the load bearing plate with respect to the bottom of the web underneath it at the edge of the load bearing plate (point *C* in figure 6.2). For that reason, in the validation the finite element model is

adapted to the experimental tests and the web crippling deformation is defined to be w_A - w_M.

6.3.3 *The adjusted finite element model versus the experimental tests of Bakker*

A selection of the experimental tests of Bakker has been simulated within the finite element model to get insight in the reliability of the finite element simulations and the possibility to simulate web crippling tests numerically with a finite element program. As mentioned in section 6.3.1 the magnitude of the corner radii has an estimated inaccuracy of ±0.5mm. This might have a large influence on the resulting web crippling stiffness in case of members with small corner radii. Hence, it is possible that a finite element simulation deviates significantly from the experimental test due to inaccuracies within the experimental test. Therefore, all the experimental tests of Bakker that are considered in the validation, are carried out twice within the finite element model: once with the lower limit of the corner radii magnitudes (simulation *a*) and once with the upper limit of the corner radii magnitudes (simulation *b*). For instance, a top flange corner radius of 5 mm in an experimental test is taken 5 mm in simulation *a* and 5.5 mm in simulation *b*. By that, the web crippling stiffness of every experimental test of Bakker that is simulated with the finite element model is compared with the web crippling stiffnesses of two simulations *a* and *b* that enclose the domain wherein the measured web crippling stiffness of the experimental tests is expected to lie assuming that the finite element model is a good representation of the experimental tests. Table 6.3 shows the results of the validation of the finite element model against a number of experimental tests carried out by Bakker. Note that each experimental test had a bottom flange corner radius of 1 mm and that they are thus taken automatically 1 mm in each numerical simulation *a* and 1.5 mm in each simulation *b*. The measuring inaccuracy of the corner radii has a large influence on the resulting web crippling stiffnesses, especially in case of hat sections with small corner radii (1 mm). The simulations *a* and *b* of both test 11 and 69 include a rather large domain wherein the web crippling stiffnesses of the experimental tests 11 and 69 lie. However, this holds not true for the tests 52, 60 and 69. These simulations deviate greatly from the experimental tests but it was already stated in section 6.3.1 that the inaccuracy of the dimensions of the corner radii is only estimated to be +0.5 mm and may be larger. Moreover, in the experimental tests it turned out to be difficult to measure the deformations accurately, resulting in relatively large inaccuracies for web crippling deformations in case of members having small corner radii (see section 6.3.1). It is assumed that the deviations of the simulations from the tests 52, 60 and 69 are caused either by an even larger measuring inaccuracy of the corner radii, or by measuring inaccuracies of the deformations of the member. It should be noted that the validity of the experimental test 69 is questionable. The member that is used in this test corresponds completely to the member of test 49, except that the latter has a smaller span length *(Bakker, 1992)*. Since the web crippling stiffness is expected to be independent of the span length (which is confirmed by the parameter study), these tests should produce more or less the same web crippling stiffnesses. However, the web crippling stiffness corresponding to test 49 is almost twice as large as the one of test 69.

Table 6.3: Validation of the finite element model against experimental tests of Bakker

Experimental tests										Simulations			
test *	*mat.**	t	θ_w	b_w	b_{tf}	L_{span}	L_{lb}	$r_{i;tf}$	$k_{\Delta h_w}$	a	*index*	b	*index*
11	1	0.68	90	50	60	290	50	1	37094	53057	143	33112	89
14	1	0.68	90	50	60	290	50	5	4298	5344	124	4496	105
17	1	0.68	90	50	60	290	50	10	1960	2188	112	2120	108
18	1	0.68	90	50	60	190	50	10	1965	2218	113	2140	109
52	2	0.62	90	50	60	265	25	1	15615	34566	221	21366	137
53	2	0.62	90	50	60	265	25	5	3048	3297	108	3002	98
54	2	0.62	90	50	60	265	25	10	1150	1443	125	1403	122
60	3	0.58	90	100	160	490	50	1	10579	25582	242	15396	146
61	3	0.58	90	100	160	490	50	10	813	1247	153	1185	146
62	4	0.97	90	50	60	290	50	1	44560	90233	202	32554	73
63	4	0.97	90	50	60	290	50	10	4460	5652	127	5464	123
69	2	0.62	90	100	160	940	100	1	12316	40306	327	23419	190
70	2	0.62	90	100	160	940	100	5	3088	3100	100	2793	90
71	2	0.62	90	100	160	940	100	10	1034	1127	109	1077	104
73	2	0.62	60	100	160	540	100	5	4332	7182	166	6527	151
74	2	0.62	60	100	160	540	100	10	1966	2319	118	2186	111

t, b_w, b_{tf}, L_{span}, L_{lb} and $r_{i;tf}$ in mm; $k_{\Delta h_w}$, a and b in N/mm; θ_w in °; index: simulation with respect to experimental test

** test: Numbering of experimental tests according to Bakker; mat.: Type of material according to Bakker (section 6.3.1).*

The best approximations of the web crippling stiffness are established for members having corner radii of 5 mm. The deviations of the finite element simulations from these experimental tests are smaller than 5% in case of members having vertical webs. It is striking that the member with inclined webs (test 73) greatly overestimates the web crippling stiffness.

Finally, the simulations of hat sections with corner radii of 10 mm overestimate the web crippling stiffness, up to 23%. An exception has to be made for test 61 (material 3) where the overestimation appears to be 45%. Note that this test has a significant smaller wall thickness than the other tests.

On the whole it appears to be difficult to verify the web crippling behaviour of experimental tests with finite element simulations. Nevertheless, from the performance of the simulations of members having corner radii of 5, and to a less extent 10 mm, it may be concluded that the finite element model is capable of simulating web crippling tests reasonably well.

Chapter 7: Parameter study

The energy model and the beam on elastic foundation model have been validated against finite element simulations using a parameter study. The specifications of the parameter study and the corresponding validations are treated here, as well as the development of an empirical correction factor γ within the energy model and the determination of the factor α in the beam on elastic foundation model..

7.1 Introduction

Within the energy model six different solutions for the web crippling stiffness have been developed, based upon different combinations of the compatibility approach and the description of deformation variations over the length of the member (section 5.5). These combinations need to be evaluated on their web crippling stiffness prediction capabilities. The beam on elastic foundation model (i.e. the full length approach) contains a correction factor α whose magnitude has to be derived empirically by evaluating the model for several magnitudes of α. For this purpose a parameter study is carried out with the finite element model described in chapter 6.

Section 7.2 describes the specifications of the parameter study. It gives an overview of which parameters are involved and the ranges within which they are varied. In section 7.3 the results of the finite element simulations are compared to those of the analytical models. From this comparison it becomes clear that the beam on elastic foundation model performs best if α made is proportional to the magnitude of the corner radii, rather than α having a constant value. Basically, all combinations of the energy model tend to show a web crippling stiffness that deviates significantly from the finite element simulations for small corner radii (1-3 mm) and large corner radii (7-10 mm). However, it is possible to add an empirical correction factor γ to the energy model which takes away these deviations, resulting in considerable better predictions of the web crippling stiffness. Both the determination of this factor γ and the determination of the empirical factor α, are treated in section 7.4, resulting in an adjusted energy and beam on elastic foundation model. In section 7.5 the results of the finite element simulations are compared to those of the adjusted energy and beam on elastic foundation model. Finally, in section 7.6 some concluding remarks on the different models are noted.

7.2 Specifications of the parameter study

The parameter study is confined to first generation deck panels because they are used in practice more frequently than hat sections. The following parameters are involved: L_{span}, θ_w, b_{bf}, b_w, b_{tf}, $r_{i;bf}$, $r_{i;tf}$, t and L_{lb}. Due to the manufacturing process $r_{i;bf}$ usually equals $r_{i;tf}$ in practice. Hereby, $r_{i;bf}$ is taken equal to $r_{i;tf}$ for all tests in the parameter study. The influence of each parameter on the web crippling stiffness is investigated emanating from three different general members in which each parameter is varied separately. These three general members differ from each other only in the magnitudes of their corner radii: they have bottom and

top flange corner radii of 1, 5 and 10 mm respectively. Hence, the whole parameter study is carried out for three members with small, medium and large corner radii. The geometrical dimensions (in mm) of the general members are:

- general member 1: L_{span}=1560, θ_w=90°, b_{bf}=60, b_w=65, b_{tf}=60, $r_{i;bf}$=1, $r_{i;tf}$=1, t=0.7 and L_{lb}=100;
- general member 2: L_{span}=1560, θ_w=90°, b_{bf}=60, b_w=65, b_{tf}=60, $r_{i;bf}$=5, $r_{i;tf}$=5, t=0.7 and L_{lb}=100;
- general member 3: L_{span}=1560, θ_w=90°, b_{bf}=60, b_w=65, b_{tf}=60, $r_{i;bf}$=10, $r_{i;tf}$=10, t=0.7 and L_{lb}=100.

For each member the parameters (except the corner radii) are varied as follows (in mm):

- L_{span}: 520, 1040, 1560, 2080, 2600;
- θ_w: 50°, 60°, 70°, 80°, 90°;
- b_{bf}: 20, 40, 60, 80, 100, 120;
- b_w: 30, 50, 65, 80, 100;
- b_{tf}: 20, 40, 60, 80, 100, 120;
- t: 0.5, 0.7, 0.9, 1.1, 1.3, 1.5;
- L_{lb}: 25, 50, 100, 150, 200, 250, 300.

Besides, the influence of the corner radii is once more investigated by varying $r_{i;tf}$(and thus $r_{i;bf}$) from 1 to 10 mm (steps of 1 mm) using the geometrical dimensions of the above mentioned general members (except for the corner radii). The test program included 106 tests.

The ranges of each parameter are based upon the geometrical dimensions of first generation deck panels that are commonly used in practice. Moreover, the parameters are varied under the condition that the span length-to-height of the web ratio varies between 8 and 40. The performed three point bending tests described in chapter 6 can be regarded as a simulation of the behaviour of a part of a continuous member at an interior support, provided the span length L_{test} in the test is chosen in such a way that the occurring M_{test}/F_{test} ratio corresponds to the M/F ratio at the interior support of the continuous member. For a two-span member with two identical spans (with a length L_{span}), loaded by a uniformly distributed load, it can be derived *(Bakker, 1992)* that this span length L_{test} can approximately taken equal to $0.4 \cdot L_{span}$. The range of the span length in the tests stems from the assumption that first generation deck panels have a span of ±1000-6000 mm when hey are used as structural elements, such as roof, floor and wall elements. The modulus of elasticity is taken 210000 N/mm^2.

7.3 *Discussion of the results*

As mentioned before, the parameter study is carried out on the finite element model (Fem), the energy model and the beam on elastic foundation model. For the energy model, all six combinations are involved. However, in the discussion of the results the emphasis will lie on the combinations which are based upon the geometrical compatibility approach (gca) because the hinge compatibility approach (hca) can be thought of as

a simplification of this approach. The beam on elastic foundation model (which will be abbreviated as boef model) is evaluated for four different values of α, namely 0.2, 0.4, 0.6 and 0.8. For sake of clarity the six combinations of the energy model are once more given below.

- Combination 1: Bilinear deformation pattern over the length of the member (bilinear), hca;
- Combination 2: Bilinear deformation pattern over the length of the member (bilinear), gca;
- Combination 3: Trilinear deformation pattern over the length of the member (trilinear), hca;
- Combination 4: Trilinear deformation pattern over the length of the member (trilinear), gca;
- Combination 5: Fourth degree polynomial deformation pattern over the length of the member (fdp), hca;
- Combination 6: Fourth degree polynomial deformation pattern over the length of the member (fdp), gca.

In the sections 7.3.1 to 7.3.8, the results of the parameter study for both the energy model and the beam on elastic foundation model are discussed per parameter (for all three general members). For a more detailed description of the results the reader is referred to appendix D.1.

7.3.1 Results concerning the corner radii

The results of the energy model (only the combinations which are based upon the geometrical compatibility approach) for the general member with varying corner radii is given in the figures 7.1 and 7.2.

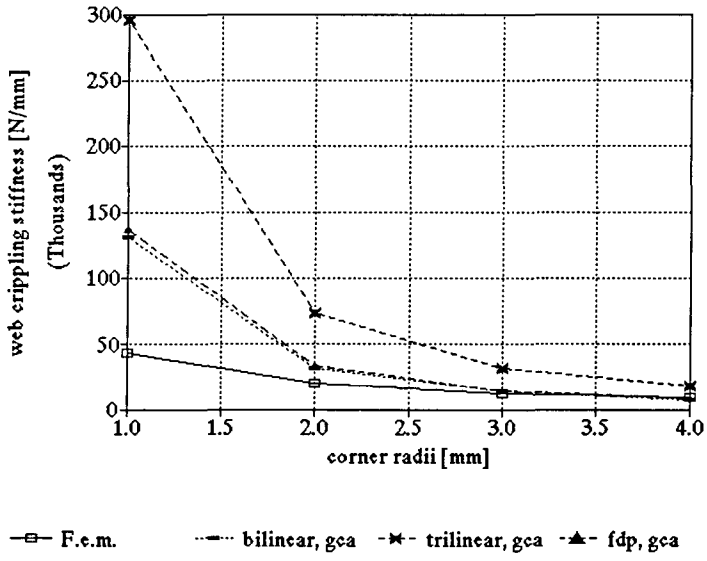

Figure 7.1: *Web crippling stiffness for varying corner radii (1-4 mm)*

According to the figures 7.1 and 7.2 all geometrical compatibility combinations of the energy model perform poorly in predicting the web crippling stiffness. Moreover, the hinge compatibility combinations perform poor as well (appendix D.1).

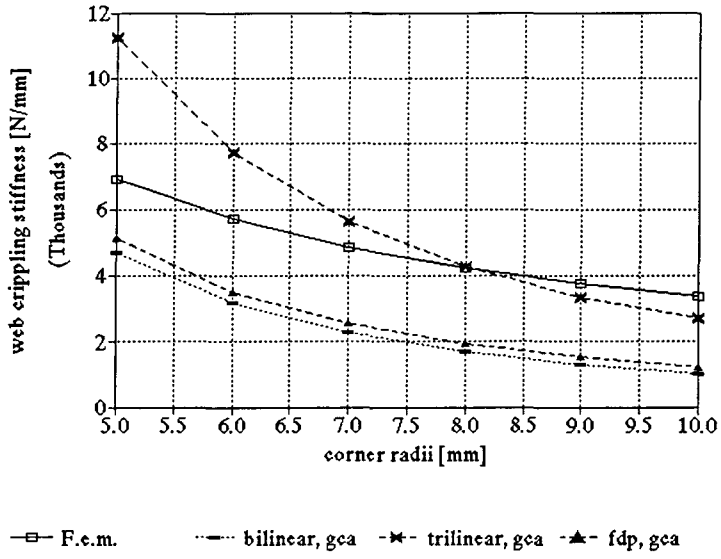

Figure 7.2: *Web crippling stiffness for varying corner radii (5-10 mm)*

Combination 6 which is based upon the fourth degree polynomial description of the deformations over the length of the member performs relatively best for small corner radii, while combination 3 which is based upon the trilinear description of the deformations over the length of the member perform relatively best for large corner radii. It may be concluded that the corner radii are not very well accounted for throughout the energy model. The energy models result in a web crippling stiffness that is inversely proportional to the square corner radii while the finite element simulations tend to show a behaviour in which the web crippling stiffness is more or less inversely proportional to the corner radii. This poor performance of each combination of the energy model in case of varying corner radii, can be clarified in two different ways.

Firstly, it might be caused by the chosen descriptions of the deformations over the cross-section of the member, which are taken equal for each combination. Especially, the deformation variation over the height of the web is rather questionable because it is assumed that the maximum deformation of the web occurs at the centre of the web, regardless of the magnitude of the corner radii. In reality, it is possible that the maximum deformation of the web is located somewhat higher in the web, nearer to the application of the load. The location of the maximum deformation of the web might also depend on the magnitude of the corner radii. It is plausible that the larger the top flange corner radii, the more the deformations are concentrated at the curvatures, resulting a maximum deformation (of the web) that is located somewhat higher in the web. Future research might be directed to the development of proper deformation descriptions, making use of the existing solutions for similar local problems in other fields of construction, for instance buckling.

Secondly, the energy model ignores the geometrical dimensions of the bottom flange corner radii. This

neglect is based upon the statement that the load is transmitted mainly via the web. The top flange corner radii bring about an eccentrical load application at the load bearing plate but the bottom flange corner radii only cause an eccentrical application at the supports. It is at these supports that the web crippling deformations are assumed to be negligibly small. The extra bending deformations that occur at the supports due to this eccentrical are expected to have almost no influence on the centre of the member, just as the eccentrical loading application has almost no influence on the supports. However, according to the finite element simulations on the members A and B (section 6.2.7), the bottom flange corner radii have a significant influence on the web crippling stiffness. The members A and B only differ from each other in the magnitude of their bottom flange corner radii, having a bottom flange corner radius of 10 and 1 mm respectively. Comparing their web crippling stiffnesses on the most reliable representation (test 3) it becomes clear that a member with a bottom flange of 10 mm has a web crippling stiffness that is more or less twice as large as the web crippling stiffness of the same member with a bottom flange corner radius of 1 mm. Hence, neglecting the bottom flange corner radii in case of member A ($r_{i;bf}=10$), and thus assuming zero eccentricity of the bottom flange with respect to the web might implies an even larger deviation from the real web crippling stiffness. Table 6.1 indicates that the disregarding of the bottom flange corner radii results in an significant underestimation of the web crippling stiffness for members with large corner radii. According to the results from the parameter study the web crippling stiffness of members with large bottom flange corner radii is systematically underestimated throughout the energy model. This clearly supports the above mentioned statement. In future research it might be useful to investigate the role of the bottom flange corner radius

separately. The results of the beam on elastic foundation model for the general member with varying corner radii is given in the figures 7.3 and 7.4. From the figures 7.3 and 7.4 it becomes clear that the beam on elastic foundation model performs somewhat better than the energy model in varying the top flange corner radii. A small value of α turns out to produce good approximations of the web crippling stiffness in case of members with small corner radii, while the web crippling stiffness of members with large corner radii is approximated best by using a large α. Hence, the web crippling stiffness can only be approximated properly for α being a function of the corner radii, instead of α having a constant value. This can be clarified in two ways. Firstly, the bottom flange corner radii are in this model not taken into account either, bringing about the same problems as in case of the energy model. Secondly, it is plausible that the transmission of the concentrated load occurs differently for different magnitudes of the corner radii. Hereby, the part of the web that belongs to the beam (and actually transmits the load) depends on the top flange corner radii.
In a way this behaviour more or less resembles to the thought in the energy model that the location of the maximum deformation of the web might be a function of the corner radii, because in both cases the web crippling deformation behaviour of the web is thought to be a function of the magnitude of the corner radii. In other words, in the beam in elastic foundation model the poor covering of the top flange corner radii might

also be caused by a poor description of the deformation variations over the height of the web. Anyhow, the results on the beam on the elastic foundation model indicate that the corner radii are not covered very well, for α having a constant value.

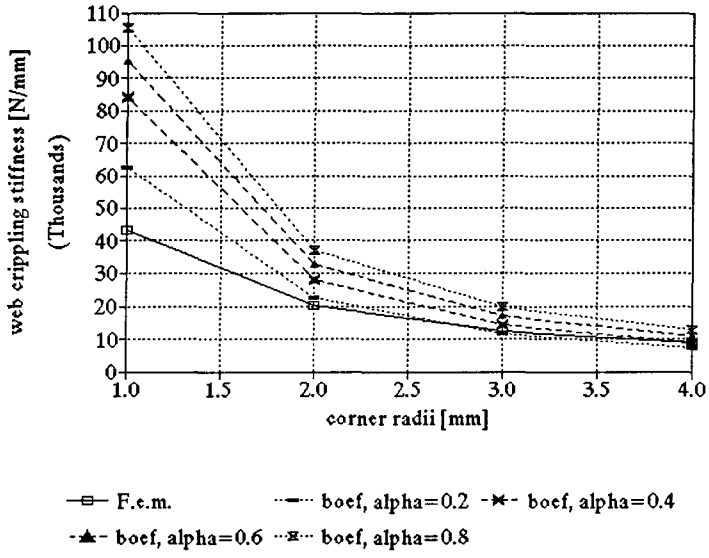

Figure 7.3: *Web crippling stiffness for varying corner radii (1-4 mm)*

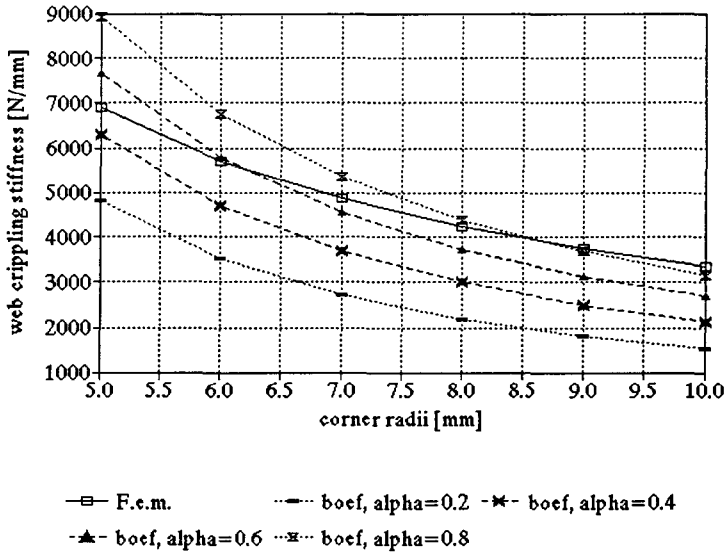

Figure 7.4: *Web crippling stiffness for varying corner radii (5-10 mm)*

The energy model and the beam on elastic foundation model on the one hand, and the finite element simulations on the other, may deviate greatly from each other due to the poor treatment of the corner radii of the former. Especially, in case of the general members 1 and 3 (with corner radii of 1 and 10 mm respectively) these deviations appear to be very large, anyhow resulting in large deviations for each parameter test of these members. Evidently, this does not imply that the other parameters perform poorly also.
The performance of the rest of the parameters is merely determined by investigating to which extent the deviations between the analytical models and the finite element simulations vary.

7.3.2 *Results concerning the bottom flange*

According to the finite element simulations, the web crippling stiffness slightly increases with an increasing width of the bottom flange. The influence of the bottom flange on the web crippling stiffness is covered reasonably well throughout the energy model. All six combinations tend to show constant deviations from the finite element simulations for the whole range over which the length of the width of the bottom flange is varied. These constant deviations occur for all general members (see appendix D.1 for a plot of this behaviour). Hereby, the neglect of the deformation variations of the bottom flanges in the development of the energy model is justified. Apparently, taking the influence of the bottom flange into account, only in describing the ratio of the maximum deflection of the top flange and the web, is a fair assumption of the energy model.
Considering the beam on elastic foundation model, the influence of the bottom flange on the web crippling stiffness is modelled reasonably well, especially in case of large corner radii (the general members 2 and 3). The application of several magnitudes of α in the parameter study points out that using a small value of α in case of small corner radii (general member 1) and a large value of α in case of large corner radii (general member 3) gives the best approximations of the web crippling stiffness.

7.3.3 *Results concerning the top flange*

The finite element simulations tend to show a slightly decreasing web crippling stiffness with an increasing width of the top flange. The performance of the energy model in varying the widths of the top flange differ for each combination. Only combination 6 results in more or less constant deviations of the finite element simulations for the whole range over which the width of the top flange is varied. An exception has to be made for members having small corner radii and small top flanges, where increasing deviations from the finite element simulations occur. To a less extent the combinations 1 and 2 (bilinear description of the deformation variations over the length of the member) produce reliable results also, but only for top flanges larger than 30 mm. Although combination 5 is based upon the same effective length as combination 6, it shows a completely different dependence of the width of the top flange than the latter. Accordingly, the hinge compatibility approach differs greatly from the geometrical compatibility approach, in case of the fourth

degree polynomial description of the deformation variations over the length of the member. The hinge compatibility approach is no longer valid if the magnitude of the top flange is varied strongly. This can be clarified by considering the portal frame of the portal frame model. If the length of the top flange is varied it is clear that the bending moment at the connection between the top flange and the web will vary also and definitely not necessarily equal zero.

In the beam on elastic foundation model the influence of the top flange is covered reasonably well. However, for members having small corner radii this model shows a larger dependence of the width of the top flange than the finite element simulations.

Both the energy model and the beam on elastic foundation model perform better for large corner radii than for small corner radii as far as the top flange is concerned. This indicates that the schematisation of the portal frame model corresponds better to reality in case of larger corner radii. They both perform reasonably well for top flanges larger than 30 mm and smaller than 110 mm.

7.3.4 Results concerning the web

The finite element simulations show a decreasing web crippling stiffness with an increasing height of the web. Considering the energy model, only the combinations 2 and 6 correspond reasonably to the behaviour of the finite element simulations when the magnitude of the web is varied (they have almost constant deviations for webs larger than 40 mm). It is remarkable that a different description of the deformation variations over the length of the member implies greatly different performances on parameters of the cross-section, just as occurred in case of the bottom flanges. This is clarified by the application of the principle of minimum total potential energy: the second derivatives of the descriptions of the deformations over the length of the member interact with the descriptions of the deformations over the cross-section (equation 5.12).

In general, the beam on elastic foundation model produces a web crippling stiffness that slightly decreases with an increasing height of the web, a behaviour that barely corresponds to the finite element simulations. Within the beam on elastic foundation model different values of α show a slightly different dependence for the web crippling stiffness of the height of the web, especially for members with small corner radii. This might be caused by the schematisation of the beam. The larger α, the bigger the influence the web has on the web crippling stiffness because a large value of α implies a large influence of the second moment of area of the beam on the resulting web crippling stiffness and the magnitude of the second moment of area depends mainly on the web. Besides, the web crippling stiffness is dependent on the two-dimensional web crippling stiffness, that is also a function of the web. Hence, it is possible that the influence of the web differs with varying magnitudes of α.

7.3.5 Results concerning the web angle

The finite element simulations point out that the web crippling stiffness increases with a decreasing web

angle. Hence, a member with inclined webs has a larger web crippling stiffness than the same member with vertical webs. The dependence of the web angle appears to vary with varying corner radii.
In varying the web angle, both the energy model and the beam on elastic foundation model are only capable of proper predictions of the web crippling stiffness for members having web angles larger than 80°. This is caused by a poor performance of these models on the web angle in case of members having small corner radii. Note that in case of small corner radii the web crippling stiffness quite different depends on the web angle than for large corner radii, according to the finite element simulations: it has a decreasing gradient with decreasing web angles, while this holds definitely not true for larger corner radii. In case of the energy model the most obvious reason for this lack of reliability for members having inclined webs is that the assumption of the maximum deflection of the web occurring at the centre is no longer valid. This would imply that the factor n is no longer valid nor are the deformation descriptions in the energy model over the cross-section. Considering the beam on elastic foundation model it is plausible that the part of the web that belongs to the beam should depend on the web angle because different web angles imply a different transmission of the load F through the web. For α being dependent of the web angle a better treatment of the web angle might be established.

7.3.6 Results concerning the load bearing plate

According to the finite element simulations, the web crippling stiffness is proportional to the length of small load bearing plates (smaller than 100 a 150 mm) and is independent of the length of long load bearing plates (longer than 150 mm). Apparently, the length of the load bearing plate where the independence is initiated increases with increasing corner radii (appendix D.1). This type of behaviour can be explained by the deformation variation configuration that the top flange takes up. The downward curling of the top flange under the load bearing plate causes the proportionality between the web crippling stiffness and the length of the load bearing plate for small load bearing plates: the larger the load bearing plate, the more work that has to be carried out (due to the extra downward curling) to achieve the same web crippling deformations at the edge of the load bearing plate. In case of longer load bearing plates however, some significant upward curling occurs under the centre of the load bearing plate (figure 5.3). Hence, the downward curling does not take place, so that no extra work is brought about. This results in a web crippling stiffness that is independent of the length of long load bearing plates.
The energy model has a web crippling stiffness that is more or less proportional to the length of the load bearing plate. Hence, it may be concluded that the load bearing plate is poorly covered in the energy model. This is caused by the chosen deformation descriptions over the length of the member: in these descriptions it is assumed that the deformations continuously increase under the load bearing plate, except by the trilinear description, that assumes a constant deformation under the load bearing plate. It is this trilinear description that relatively produces the best results. For the energy model not taking the upward curling of the top flange

under the load bearing plate into account, it seems quite logical that the larger the load bearing plate the worse the energy model predicts the web crippling stiffness.

The beam on elastic foundation model does not take the upward curling of the top flange into account either, but uses a different description of the deformation variations over the length of the member than the energy model. Apparently, in the beam on elastic foundation model the web crippling stiffness is more or less independent of the length of the load bearing plate for small values of α. However, this is contradictory to the other parameters for which the beam on elastic foundation model corresponds best to the finite element simulations for α being proportional to the corner radii.

7.3.7 *Results concerning the span length*

The finite element simulations point out that the web crippling stiffness is independent of the span length of the member.

The combinations 1, 2, 5 and 6 are based upon the assumption that the web crippling deformations stretch out over an effective length that is a function only of the magnitudes of the bottom and top flanges and the web. Therefore, these combinations perform well in describing the influence of the span length on the web crippling stiffness. In case of the combinations 3 and 4, the web crippling stiffness is proportional to the span length. Within these combinations the full length solution is applied in which the effective length is taken equal to the span length.

From these results it may be concluded that it is justified to introduce an effective length where outside the web crippling deformations are assumed to equal zero.

Despite the fact that the beam on elastic foundation model does take web crippling deformations over the span length into account, the resulting web crippling stiffnesses appear to be more or less independent of the span length also. Hereby, it follows that the web crippling deformation variations over the length of the member can be described properly by the deflection curve of a beam on an elastic foundation.

7.3.8 *Results concerning the wall thickness*

The finite element simulations show that the web crippling stiffness is proportional to the wall thickness raised to (about) the 5/2 power (appendix D.1). Throughout the energy model the web crippling stiffness is proportional with the wall thickness raised to the third power. It may be concluded that the treatment of the wall thickness is not quite so well within the energy model. This is caused by the neglect of the axial deformations in the member in this model (only bending deformations are taken into account). Generally, it holds true that the larger the wall thickness, the larger the influence of the axial deformations on the resulting web crippling stiffness. The axial web crippling deformations are inversely proportional to the wall thickness while the web crippling deformations due to bending actions are inversely proportional to the wall thickness raised to the third power. Hence, the relative influence of the axial web crippling deformations on the web

crippling stiffness increases with an increasing wall thickness. For example, consider the portal frame model for first generation deck panels (equation 3.16). From figure A.20 it becomes clear that the axial web crippling deformations in this model may have a considerable influence on the two dimensional web crippling stiffness, in case of large wall thicknesses. It should be noted that this influence decreases with an increasing top flange corner radius, because the web crippling deformations due to bending action are far more larger than the ones due to axial forces in case of larger corner radii.

In the beam on elastic foundation model the web crippling stiffness is more or less proportional to the wall thickness raised to the 5/2 power, as are the finite element simulations. In this model the wall thickness appears to be fairly accounted for. Note that here, the axial bending deformations are taken into account explicitly, namely within the portal frame model. This confirms the argumentation of the poor treatment of the wall thickness in the energy model.

7.4 *Adjustment of the energy model and the beam on elastic foundation model*

The energy model and the beam on elastic foundation model (for α having a constant value) perform poorly on several parameters (section 7.3). Some of the parameters can be better accounted for by simple adjustments. In this section these adjustments are treated for both the energy model (section 7.4.1) and the beam on elastic foundation model (section 7.4.2).

7.4.1 Energy model

The development of the adjusted energy model is confined to combination 6 because this is the only combination within the energy model that produces reasonable results for most of the parameters. Principally, the derivation of this factor for other combinations is similar.

In the energy the corner radii, the length of the load bearing plate, the wall thickness and the web angle are poorly accounted for.

In section 7.3 and appendix D.1 it has become clear that the poor treatment of the corner radii in the energy and model enlarges the deviations of those models from the finite element simulations in case of several other parameters. In the energy model the covering the of the corner radii is improved by the addition of a correction factor which is empirically determined.

According to section 7.3 the wall thickness is poorly accounted for due to the neglect of axial (web crippling) deformations. Taking these stretching action into account would greatly improve the energy model concerning the wall thickness. However, this also highly complicates the resulting web crippling stiffness. The treatment of the wall thickness can be improved relatively simple by adding an empirical correction factor. In the current situation this means that the web crippling stiffness should be divided by roughly the square root of the wall thickness.

The correction factor on the corner radii and the wall thickness has been established using a trial and error

method with the aid of a spreadsheet program that calculates the consequences of the application of the correction factor for each test of the parameter study. Eventually, this resulted in a correction factor γ with which the web crippling stiffness has to be multiplied. For combination 6 γ is given by

$$\gamma = \frac{r_{i;tf}^{0.92}}{4.035 \cdot t^{0.65}} \tag{7.1}$$

As mentioned before, the poor covering of the length of the load bearing plate stems from the disregarding of the upward curling underneath it. This a lack of the model that can be solved on physical grounds by adjusting the deformation description of the top flange over the length of the member. The most simple solution is to assume that the deformations have a constant value underneath the load bearing plate, applying the fourth degree polynomial only outside the plate. A more complicated but physically more relevant solution lies in the description of the upward curling of the top flange underneath the load bearing plate. If it is possible to establish an appropriate deformation description of the upward curling, the influence of the load bearing plate would be covered much better. Finally, a more provisional solution can be applied making use of the fact that the web crippling stiffness is independent of L_{lb}, if L_{lb}>100 mm. Hence, it is possible to replace L_{lb} by a constant value. In the adjusted model the length of the load bearing plate is replaced by a constant value of 100 mm.

No adjustment is made on the covering of the web angle. It is recommended to improve the treatment of the web angle by using a different deformation description (and thus a different value for n) over the cross-section.

In the adjusted energy model (combination 6) the web crippling stiffness is given by

$$k_{\Delta h_w} = \frac{D \cdot b_{tf}^2 \cdot L_{ef}^5 \cdot r_{i;tf}^{0.92}}{6355 \cdot t^{0.65} \cdot (100^2 - L_{ef}^2)^4 \cdot (b_{tf}^2 + b_w^2 \cdot n)}$$

$$\cdot [\frac{[b_{tf}^4 \cdot (b_w^3 \cdot L_{ef}^2 \cdot (8640 + 2400 \cdot n) + 5248 \cdot L_{ef}^4 \cdot b_w + b_{tf} \cdot (L_{ef}^2 \cdot (1536 \cdot L_{ef}^2 + 3936 \cdot b_w^2 + 2400 \cdot b_w^2 \cdot n))}{[b_w \cdot \sin^2\theta_w \cdot r_{i;tf}^2 \cdot (\sin\theta_w \cdot r_{i;tf} - b_{tf}) \cdot (b_{tf}^2 \cdot (b_{tf} \cdot (4 \cdot \sin\theta_w \cdot r_{i;tf} - b_{tf}) - b_w \cdot n \cdot (b_w + 5 \cdot \sin\theta_w \cdot r_{i;tf}) - 4 \cdot \sin^2\theta_w \cdot r_{i;tf}^2)}$$

$$\frac{+ b_{tf}^5 \cdot b_w^3 \cdot (b_w \cdot (3150 + 15750 \cdot n^2) + 7875 \cdot b_{tf} \cdot n^2) + b_w^4 \cdot (b_{tf}^3 \cdot L_{ef}^2 \cdot (2400 \cdot n^2 - 768 \cdot n + 8800) + 6656 \cdot b_{tf} \cdot L_{ef}^4 \cdot n^2)]}{+ b_w \cdot \sin\theta_w \cdot r_{i;tf} \cdot n \cdot (\sin\theta_w \cdot r_{i;tf} \cdot (b_w + 5 \cdot b_{tf}) - b_w \cdot b_{tf}))]}$$

$$+ \frac{[b_w^5 \cdot (L_{ef}^2 \cdot n^2 \cdot (768 \cdot L_{ef}^2 + 2400 \cdot b_{tf}^2) + b_{tf}^2 \cdot n \cdot (7875 \cdot b_{tf}^2 \cdot n - 8960 \cdot L_{ef}^2) - 2100 \cdot b_{tf}^4 + 4096 \cdot b_w \cdot b_{tf} \cdot L_{ef}^2 \cdot n^2)}{[b_w \cdot \sin^2\theta_w \cdot r_{i;tf}^2 \cdot (\sin\theta_w \cdot r_{i;tf} - b_{tf}) \cdot (b_{tf}^2 \cdot (b_{tf} \cdot (4 \cdot \sin\theta_w \cdot r_{i;tf} - b_{tf}) - b_w \cdot n \cdot (b_w + 5 \cdot \sin\theta_w \cdot r_{i;tf}) - 4 \cdot \sin^2\theta_w \cdot r_{i;tf}^2)}$$

$$\frac{+ b_{tf}^2 \cdot (b_w^6 \cdot (8400 \cdot n \cdot (b_{tf} + b_w) - 5250 \cdot b_{tf}) + L_{ef}^4 \cdot b_w^2 \cdot (b_w \cdot n \cdot (3200 \cdot n - 9984) - b_{tf} \cdot (4608 \cdot n - 6400)))]}{+ b_w \cdot \sin\theta_w \cdot r_{i;tf} \cdot n \cdot (\sin\theta_w \cdot r_{i;tf} \cdot (b_w + 5 \cdot b_{tf}) - b_w \cdot b_{tf}))]}] \tag{7.2}$$

in which

$$L_{ef} = \sqrt{\frac{b_{tf}^3 \cdot (34 \cdot b_w^2 + 504 \cdot 10^4) + b_w^3 \cdot n^2 \cdot (17 \cdot b_{tf}^2 + 252 \cdot 10^4)}{14 \cdot b_{tf}^3 + 7 \cdot b_w^3 \cdot n^2}} \tag{7.3}$$

7.4.2 Beam on elastic foundation model

In the beam on elastic foundation model the corner radii, the web and the web angle are poorly accounted for. For this model including already a correction factor α, it is unnecessary to add an extra factor with which the web crippling stiffness need to be multiplied in order to improve the treatment of the corner radii. It is more obvious to determine α, so, that a better treatment of the corner radii is established. According to the results of the parameter study, the magnitude of α which provides the best approximations is proportional to the magnitude of the corner radii. In deriving a formula for α that provides the best approximations for all parameters, a difficulty is formed by the fact that some parameters are contradictory in their optimum for α. Therefore, the derivation of this formula turns out to be impossible. Within this project, the derivation of α is limited to optimize the treatment of the corner radii. Several formulae can be applied, providing solutions that differ from each other in the value of the corner radii where they perform best. The chosen solution is directed to the medium and large corner radii as those are thought to be most relevant in practice. The solution for α is given by

$$\alpha = 0.118 \cdot r_{i;tf}^{0.89} \tag{7.2}$$

It is difficult to adjust the model as far as the treatment of the web is concerned. The web has a different function for each value of α, that in the circumstances cannot be changed easily, without affecting the fundamental basis on which the model has been developed. The factor α could be adjusted to the magnitude of the web angle. However, it is recommended to get first clear physical insight in how α depends on this parameter. Hence, no adjustments are made for the treatment of these parameters.

7.5 Results concerning the adjusted energy and beam on elastic foundation model

To investigate the influence of the adjustments in section 7.4, the whole parameter study is carried out once more for the adjusted combination 6 of the energy model and for the beam on elastic foundation model with the adjusted formula for α.

7.5.1 Results concerning the corner radii

For varying the magnitude of the corner radii the performance of both adjusted models is given in the figures 7.5 and 7.6.

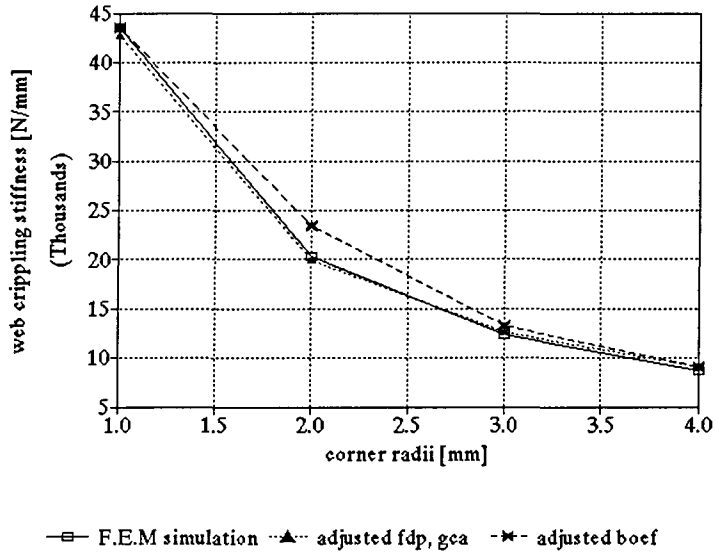

Figure 7.5: *Web crippling stiffness for varying corner radii (1-4 mm)*

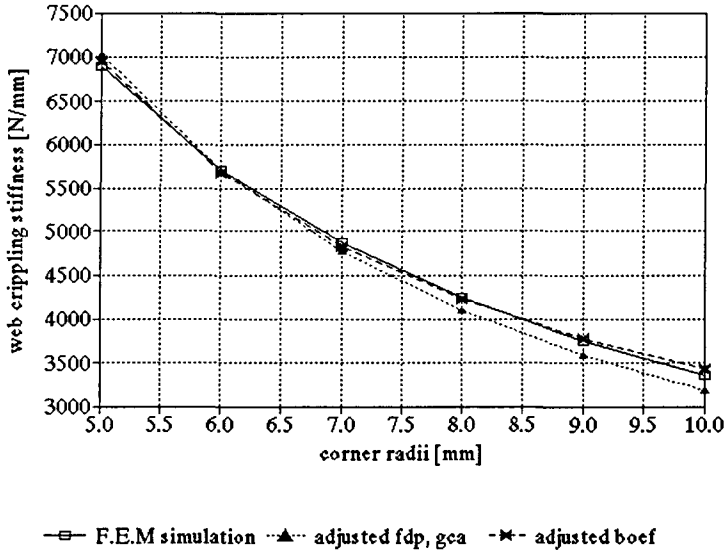

Figure 7.6: *Web crippling stiffness for varying corner radii (5-10 mm)*

The adjustments result in very good performances for varying the corner radii. For these corner radii being the most important parameter in the determination of the web crippling stiffness this is an important result. The only exception is formed by members having a corner radius of about 2 mm weir web crippling stiffness

is predicted by the beam on elastic foundation model. However, it was already noted that the adjustment within this model is directed to somewhat larger corner radii.

7.5.2 *Results concerning the bottom flange*

For the energy model the results on the bottom flanges are reasonably well. The deviations of the energy model from the finite element simulations remain within acceptable limits throughout the whole range in which the width of the bottom flange is varied, for the members 1, 2 and 3. On the other hand, the beam on elastic foundation model shows quite different dependencies of the bottom flange for the members 1, 2 and 3, while the finite element simulations tend to show merely one characteristic behaviour, regardless of the corner radii. It is concluded that the beam on elastic foundation model performs reasonably well also in the description of the influence of the bottom flange. The finite element simulations point out that the web crippling stiffness increases with an increasing width of the bottom flange. However, the gradient of this increase diminishes for large corner radii. Although the beam on elastic foundation model exhibits an even decreasing web crippling stiffness with increasing bottom flanges in case of members having large corner radii, the differences between the model and the simulations remain small over the whole range for which the width of the bottom flange is varied. To illustrate this, the web crippling stiffness for varying bottom flanges in case of member 2 is given in figure 7.7. The other results are given in appendix E.

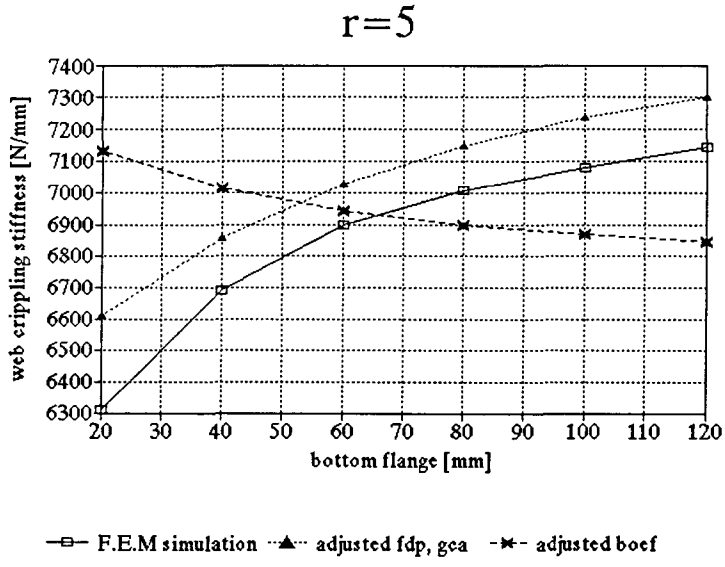

Figure 7.7: Web crippling stiffness for varying bottom flanges

Note that the energy model performs better for members with large corner radii than for members with small corner radii, considering the influence of the bottom flange (appendix E).

7.5.3 *Results concerning the top flange*

Both the beam on elastic foundation model and the energy model performs reasonably well for the members 1, 2 and 3 in varying the magnitude of the width of the top flange, except that the web crippling stiffness for small top flanges is overestimated. However, for members having top flanges larger than about 35 mm the energy model is capable of producing reliable results for varying top flanges. The results on member 1 are given in figure 7.8. Note that the energy model, the beam on elastic foundation model as well as the finite element model show that dependence of the web crippling stiffness on the top flange is the roughly the same throughout the members 1, 2 and 3. (appendix E).

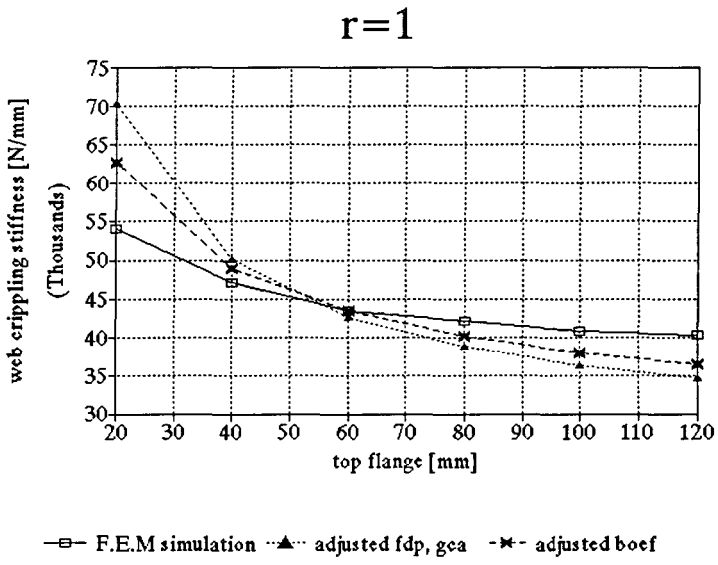

Figure 7.8: Web crippling stiffness for varying top flanges

7.5.4 *Results concerning the web*

Considering variations in the height of the web, the predictions of the adjusted combination 6 of the energy model are sufficient accurate, except that the predictions increasingly deviate from the finite element simulations for members with small corner radii and small webs (less than 50 mm).

It was already noticed in the original parameter study that the influence of the web on the web crippling stiffness is poorly covered within the beam on elastic foundation model. Figure 7.9 shows the plot corresponding to the variations of the height in the web for member 3.

Varying the factor α, corresponds to varying the role of the web in the beam on elastic foundation model. Hence, it is not surprising that the adjusted beam on elastic foundation model exhibits a different kind of behaviour for the members 1, 2 and 3 (they have different corner radii and thus different values for α).

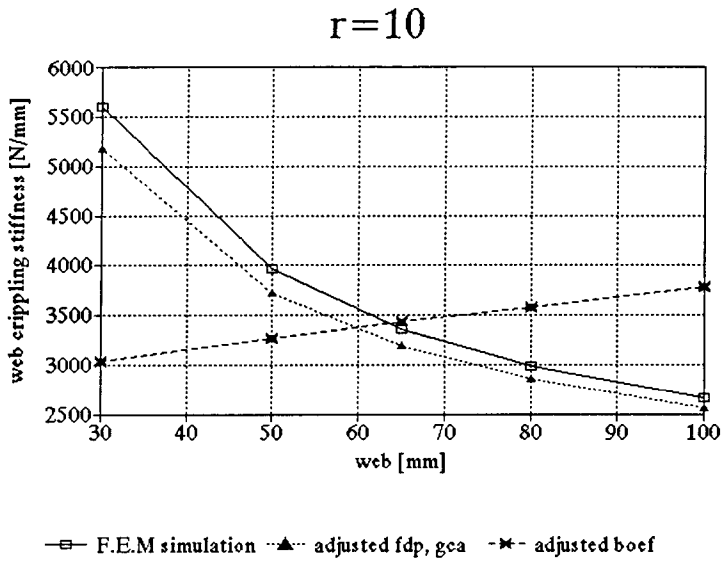

Figure 7.9: *Web crippling stiffness for varying webs*

7.5.5 Results concerning the web angle

The energy model and the beam on elastic foundation model behave rather similar in varying the web angles of member 1, 2 and 3. They exhibit a slightly increasing web crippling stiffness with a decreasing web angle.

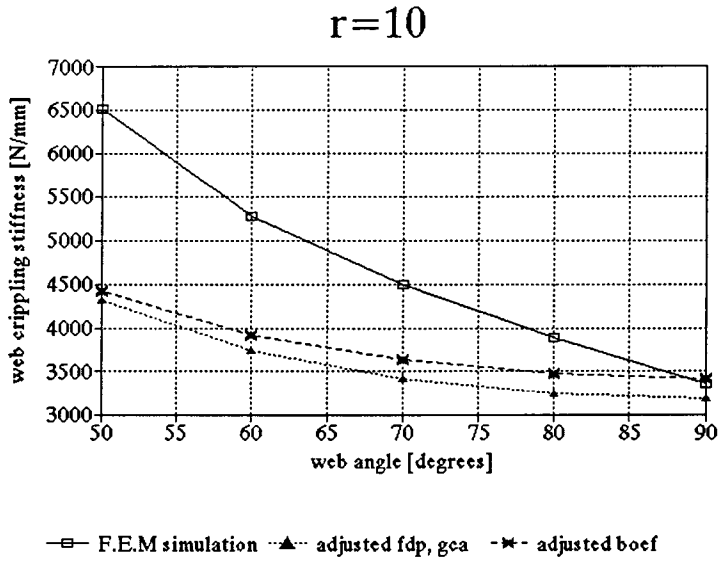

Figure 7.10: *Web crippling stiffness for varying web angles*

The finite element simulations on the other hand show a stronger correlation. For members having vertical webs the deviations between the analytical models and the finite element simulations remain small. The deviations tend to increase however, with a decreasing web angle. Hence, the adjusted models are only capable of producing reliable results for web angles larger than 80°, just as the original models. It is striking that both the energy model and the beam on elastic foundation model perform better for large corner radii than for small corner radii as far as the influence of the web angle is concerned, mainly because the web crippling stiffness has a rather strange bend at an web angle of 60°.
The characteristic behaviour is shown in figure 7.10 for member 3.

7.5.6 *Results concerning the load bearing plate*

In the adjusted energy model the influence of the load bearing plate is fairly treated. Only in case of small load bearing plates (L_{lb}<100 mm) significant deviations from the finite element simulations occur. A solution for this might be found in applying a different description of the deformation of the top flange underneath the load bearing plate in the energy model (section 7.4).

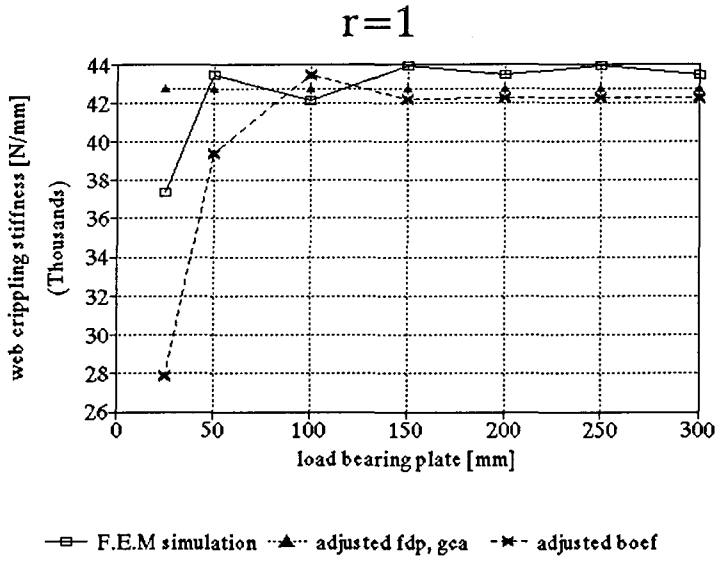

Figure 7.11: *Web crippling stiffness for varying load bearing plates*

The beam on elastic foundation model uses a different description for the deformation variations over the length of the member and performs somewhat better, considering the load bearing plate. However, in case of members with corner radii of about 5 mm, it is to be expected that the web crippling stiffness approximations of the beam on elastic foundation model satisfy neither in case of load bearing plates longer than 150 mm. The differences between the models are illustrated using member 1 (figure 7.11).

7.5.7 *Results concerning the span length*

Both the energy model and the beam on elastic foundation model perform well, considering the span length of the member. As mentioned in appendix D, the web crippling stiffness appears to be almost independent of the span length of the member. The adjustment of the models has not changed the web crippling stiffness behaviour with regard to the span length. In figure 7.12 the results are given for member 2.

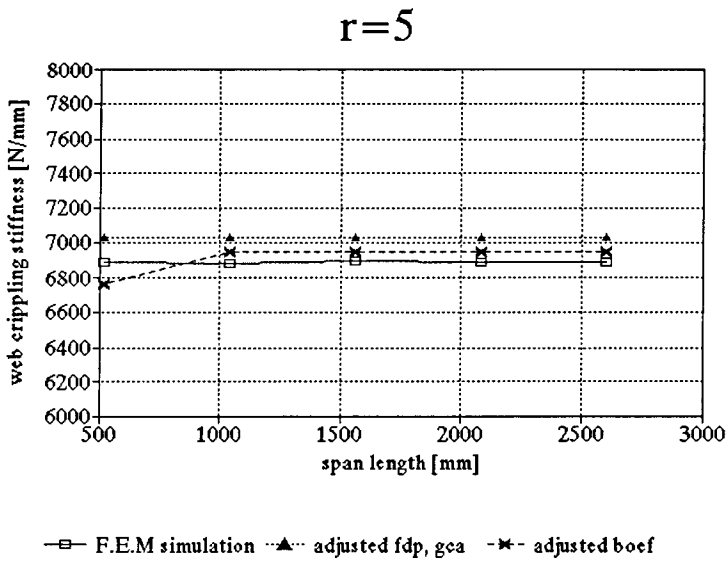

Figure 7.9: Web crippling stiffness for varying span lengths

7.5.8 *Results concerning the wall thickness*

The wall thickness is treated reasonably well within the adjusted energy model. Only for large wall thicknesses (t >1.1 mm) the model shows increasing deviations from the finite element simulations. Especially in case of members having small corner radii great deviations occur for a large wall thicknesses. This is caused by the fact that the treatment of the wall thickness has been improved by adding a simple correction factor for t that is independent of the magnitude of the corner radii. However, it was already noted in section 7.3 that not taking the axial deformations into account has varying influences on the resulting web crippling stiffness with varying values of the corner radii (in case of small corner radii the axial deformations have a relatively large influence on the web crippling stiffness). Hence, the correction factor has a slightly different influence on members with different corner radii.

The beam on elastic foundation model performs very well on the wall thickness, regardless the magnitude of the corner radii. For general member 2 the results concerning the wall thickness are given in figure 7.13.

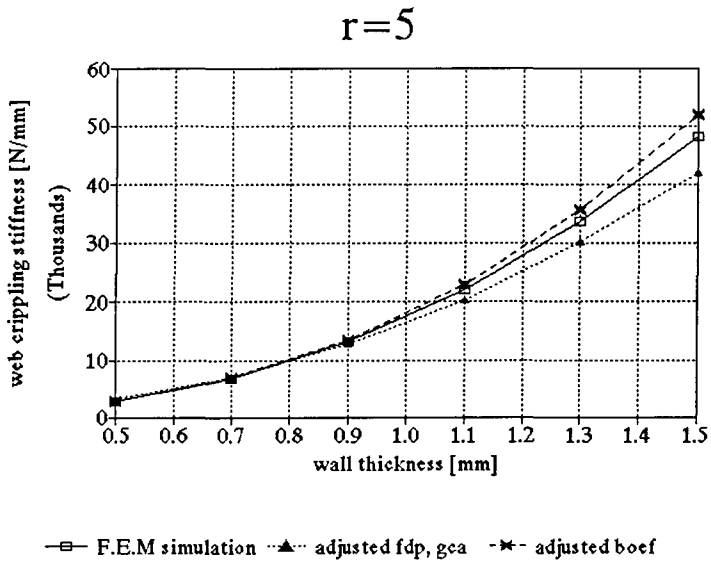

Figure 7.13: Web crippling stiffness for varying wall thicknesses

7.6 *Concluding remarks*

It can briefly be stated that the adjusted energy model performs well on the corner radii, the web, the bottom and the top flange, the load bearing plate, the span length and to a less extent the wall thickness, while the beam on elastic foundation model performs well on the corner radii, the bottom flange, the wall thickness and to a less extent the top flange and the load bearing plate.

At first sight it seems difficult to adjust the beam on elastic foundation model. The difficulty in adjusting the beam on elastic foundation model is formed by the web. Actually, the web has a different function for each α, that in the circumstances cannot be changed easily, without affecting the fundamental basis on which the model is developed. Besides, the beam on elastic foundation model needs to be adjusted on the influence of the web angle. The factor α might be made dependent of the magnitude of the web angle.

Considering the adjusted energy model, the first priority should be to improve the treatment of the web angle. The most obvious reason for this lack of reliability in case of members having inclined webs is that the assumption of the maximum deflection of the web occurring at the centre is no longer valid. This would imply that the factor n is no longer valid nor are the deformation descriptions in the energy model over the cross-section. It is possible to derive an extra model for members with small web angles that is based upon different descriptions of the deformation variations. Furthermore, it is also possible to develop a more complicated model that is based on a more general deformation variations description, which appears to be valid, regardless of the magnitude of the web angle. For instance, a new parameter might be introduced that

represents the location of the maximum deformation of the web. This location can be determined by minimizing with the maximum deformation of the web respect to this parameter. Hereby, the deformation descriptions of the web over the cross-section of the member are determined by this extra parameter.
In the adjusted energy model the load bearing plate and the wall thickness are treated fairly well, except that the model tends to show increasing deviations from the finite element simulations in case of small load bearing plates and large wall thicknesses. It is very well possible to apply some further adjustments by which these deviations might be taken way. In case of the covering of the load bearing plate a more complicated but physically more relevant solution lies in the description of the upward curling of the top flange underneath the load bearing plate. Considering the treatment of the wall thickness, the energy model might be improved by taking the stretching actions in the plate into account. However, the current adjusted energy model is simply not valid for members having small load bearing plates (L_{lb}<100 mm) or large wall thicknesses (t >1.1 mm).

Chapter 8: Conclusions and recommendations

This final chapter gives an overview of the conclusions that can be made as a result from this research project. Besides, some recommendations for future research are pointed out.

8.1 Introduction

On account of this research project on the web crippling stiffness of hat sections and first generation deck panels some conclusions can be made. Firstly, section 8.2 describes some conclusions that relate to the general characteristics of web crippling stiffness. Secondly, some conclusions can be drawn that are related to the simulation of web crippling behaviour using a finite element model (section 8.3). Thirdly, conclusions that relate to the beam on elastic foundation model are given in section 8.4. Finally, some conclusions can be made, considering the development of the energy model (section 8.5). In section 8.6 a provisional web crippling stiffness formula is given, with which the web crippling stiffness can be approximately be determined. In addition, some recommendations for future research on web crippling behaviour can be made and are summarized in section 8.7.

8.2 General conclusions concerning the web crippling stiffness

From the finite element simulations it is possible to draw some general conclusions on the web crippling stiffness behaviour, particularly the behaviour of first generation deck panels. The most important ones are summarized here.

- *Web crippling is a local phenomenon, which influences the deformation configuration of a member only within a certain region (the effective length), and which is independent of the span length of the member.*
The web crippling stiffness appears to be independent of the span length of the member. In other words, the length of the member does not affect the web crippling behaviour of the member below the load bearing plate. Only, in case of short members the web crippling stiffness shows some slight dependence of the span length. This indicates the existence of an effective length over which the web crippling deformations stretch. Note that this is in conformity with the results of Bakker *(1992)*.

- *The web crippling stiffness is influenced mostly by the corner radii and by the wall thickness.*
Finite element simulations show that the web crippling stiffness is more or less inversely proportional to the top flange corner radius. Especially in case of members having small corner radii, this implies that the web crippling stiffness is highly sensitive to the magnitude of the corner radii.
The treatment of the corner radii in an analytical model greatly contributes to the general validity of it.
Note that this conclusion promotes the use of members having small corner radii, as far as the elastic web crippling behaviour is concerned (the failing on web crippling is not considered).

The web crippling stiffness appears to be proportional to the wall thickness raised to the 5/2 power. This large influence of the wall thickness is not quite surprising. Consider a member to be built up of several plates. The moment of inertia of each of these plates is proportional to the wall thickness raised to the third power. Bending deformations of plates are inversely proportional to their moment of inertia. Since the web crippling stiffness mainly depends on the magnitudes of bending deformations, the web crippling stiffness is expected to be proportional to the wall thickness raised to about the third power.

- The web crippling stiffness is proportional to the length of the load bearing plate in case of small load bearing plates and independent of it in case of large load bearing plates.

This type of behaviour can be clarified by the deformation configuration that the top flange takes up. The downward curling of the top flange under the load bearing plate causes the proportionality between the web crippling stiffness and the length of the load bearing plate for small load bearing plates: i.e. the larger the load bearing plate, the more work that has to be carried out (due to the extra downward curling) to achieve the same web crippling deformations at the edge of the load bearing plate. In the case of longer load bearing plates however, some significant upward curling occurs underneath the centre of the load bearing plate (figure 5.3). Hence, the downward curling does not take place, so that no extra work is brought about. This results in a web crippling stiffness that is independent of the length of long load bearing plates.

8.3 *Conclusions related to the finite element model*

On the simulations of elastic web crippling behaviour in a finite element program, particularly within ANSYS version 5.0A, the following conclusions can be made.

- The rounding of the corners can best be modelled by circle segments.

For the corner radii being the most important parameter determining the web crippling stiffness, special attention needs to be paid to the modelling of the rounding of the corners in the finite element model. The rounding of the corners can be modelled in several ways (figure 6.3), for instance by reducing them to straight lines under angle of 45° with the web and the flange. However, it may be concluded (table 6.1) that a representation of the rounding of the corners by a circle segment, which is conform reality, produces the most accurate results. It is not quite surprising that the differences between this representation and other, more simplified representations increase with increasing magnitudes of the corner radii.

- The first generation deck panels can be meshed properly with a constant element size, except at the corner radii.

The finite element model can be built up out of elements that have more or less the same dimensions. The influence of local refinements at areas where large stress variations occur, such as at the loading application

and at the supports, is investigated using the 'submodelling' technique within ANSYS. Apparently, these local refinements have no large influence on the web crippling stiffness (table 6.2). Hence, the model can be meshed properly using elements of the same size throughout the model. An exception is made at the rounding of the corners. To preclude the creation of only one element over the rounding of the corners in case of small corner radii, implying a poor representation of the curved transitions, the element size is determined separately at these rounding. Hence, on one hand relatively small elements should be used at the rounding for the abovementioned reason of representation of the curved transitions. On the other hand, a large number of elements over the rounding of the corners promotes the existence of poorly shaped elements (elements having a length-to-width ratio that exceeds 8), because these elements have a rather small width while their length more or less equals the element size that is used throughout the model. A solution to this problem is found by adjusting the number of elements over the rounding of the corners proportionally to the magnitude of the corresponding corner radii. This solution is based upon the knowledge that the representation of large corner radii has a relatively large influence on the web crippling stiffness, compared to small corner radii.

- The load bearing plate may be modelled by four concentrated loads.

Due to the downward curling of the top flange underneath the load bearing plate, only four contact points between the load bearing plate and the top flange will remain after initial loading. These four contact points each transmit one quarter of the total loading that is applied. Note that this idealization of the load bearing plate is also used within the portal frame model, the beam on elastic foundation model and the energy model.

- ANSYS is very well suited for the purpose of parameter studies.

The finite element program ANSYS offers the possibility of carrying out finite element tests in the interactive mode as well as on the background by using batch files (passive mode). Within ANSYS it is possible to describe parameters by symbols. After attaching values to these symbols the web crippling tests are carried out. Now, with the usement of batch files it is relatively simple to carry out a parameter study using one and the same batch file for all tests, except that different values are attached to the symbols.

8.4 Conclusions related to the beam on elastic foundation model

On the ability of the beam on elastic foundation model to produce reliable approximations of the web crippling stiffness, the following conclusions, which are confined to first generation deck panels, can be made.

- The corner radii are poorly accounted for within the beam on elastic foundation model.

The web crippling stiffness of finite element simulations tends to show a significant different dependence of the corner radii than the beam on elastic foundation model. The underlying reasons for this poor treatment are

twofold. Firstly, the bottom flange corner radii are not taken into account within the beam on elastic foundation model, while they appear to have significant influence on the web crippling stiffness. They are neglected because otherwise the deformation description of the web in the portal frame model is not conform reality. Secondly, the part of the web that is considered to belong to the beam in the application of the beam on elastic foundation theory (the factor α) might depend on the magnitude of the corner radii. This is plausible because the transmission of the concentrated load occurs differently for different magnitudes of the (top flange) corner radii. In the adjusted beam on elastic foundation model, the factor of α is defined to depend on the corner radii. Hereby, the covering of the corner radii is greatly improved, resulting in satisfactory results as far as the covering of the corner radii is considered.

- *The influence of the web and the web angle is poorly described in the beam on elastic foundation model.*
The beam on elastic foundation model covers the influence of the web poorly. According to the model the web crippling stiffness is more or less proportional to the height of the web while the finite element simulations exhibit a decreasing web crippling stiffness with an increasing height of the web. This poor treatment might be caused by the definition that a part of the web belongs to the beam while the whole web continuously supports the beam in the application of the theory of a beam on an elastic foundation. Hence, varying the height of the web influences the role of the beam.
Both the beam on elastic foundation model and the finite element simulations point out that the web crippling stiffness increases with a decreasing web angle. However, finite element simulations tend to show a stronger dependence. The beam on elastic foundation model is only capable of acceptable predictions (as far as the web angle is concerned) for members having a web angle larger than 80°. It is plausible that the part of the web that belongs to the beam should depend on the web angle because different web angles imply a different transmission of the load F through the web. For α being dependent of the web angle a better treatment of the web angle might be established.

- *The results of the beam on elastic foundation model with respect to the bottom and top flanges, the load bearing plate, the span length and the wall thickness are reasonably well.*
The finite element simulations point out that the web crippling stiffness increases with an increasing width of the bottom flange. However, the gradient of this increase diminishes for large corner radii. Although the beam on elastic foundation model exhibits a decrease of the web crippling stiffness for increasing bottom flanges in case of members having large corner radii, the differences between the model and the simulations remain small over the whole range for which the width of the bottom flange is varied.
The influence of the top flange is fairly well described by the beam on elastic foundation model. Both the model and the simulations show that the web crippling stiffness depends on the width of the top flange in a decreasing manner when increasing the width. The larger the corner radii, the better this performance turns

out to be.

According to the finite element simulations the web crippling stiffness is proportional to the length of the load bearing plate for small load bearing plates and becomes independent of it for larger load bearing plates. This behaviour is reasonably well covered in the beam on elastic foundation model, especially in case of members having small corner radii.

Both the model and the simulations show that the web crippling stiffness is independent of the span length of the member. This indicates that it is very well possible to apply the theory of a beam on an elastic foundation in describing the variations of deformation over the length of the member.

8.5 *Conclusions related to the energy model*

Six different combinations have been developed within the energy model. They differ from each other in the deformation description over the length of the member and the compatibility between the plates. Two compatibility approaches can be distinguished, namely the hinge compatibility approach (hca) and the geometrical compatibility approach. The latter is based upon the assumption that the top flange and web plates are rigidly connected to each other, while the former assumes hinge connections between the plates. For sake of clarity the six combinations of the energy model are given below.

- Combination 1: Bilinear deformation pattern over the length of the member (bilinear), hca;
- Combination 2: Bilinear deformation pattern over the length of the member (bilinear), gca;
- Combination 3: Trilinear deformation pattern over the length of the member (trilinear), hca;
- Combination 4: Trilinear deformation pattern over the length of the member (trilinear), gca;
- Combination 5: Fourth degree polynomial deformation pattern over the length of the member (fdp), hca;
- Combination 6: Fourth degree polynomial deformation pattern over the length of the member (fdp), gca.

Eventually, combination 6 of the energy model has been adjusted in order to improve the treatment of the corner radii, the length of the load bearing plate and the wall thickness. On the ability of the energy model (all combinations and the adjusted model) to produce reliable approximations of the web crippling stiffness, the following conclusions, which are confined to first generation deck panels, can be made.

- *The corner radii are poorly accounted for within the energy model for all combinations.*

The web crippling stiffness of the finite element simulations exhibits a significant different dependence of the corner radii than the energy model does. The underlying reasons for this poor treatment are twofold.

Firstly, the bottom flange corner radii are not taken into account within the beam on elastic foundation model, while they appear to have a significant influence on the web crippling stiffness.

Secondly, it might be caused by the chosen descriptions of the deformations over the cross-section of the member, especially the description of these variations over the height of the web. These descriptions are based on the assumption that the maximum deformation occurs at the centre of the webs and top flange.

Moreover, they are established by trial functions which are independent of the corner radii. It is possible that in reality the maximum deformation of the web is located somewhat higher in the web, thus nearer to the point of load application. Furthermore, the location of the maximum deformation of the web might depend on the magnitude of the corner radii because it is plausible that the larger the corner radii, the more the deformations are concentrated at the rounding of the corners instead of at the web.
In the adjusted model a correction factor γ is added to the original model. This factor γ is a function of the corner radii (and the wall thickness). Throughout the adjusted energy model the treatment of the corner radii is greatly improved, resulting in satisfactory results as far as the covering of the corner radii is considered.

- *The energy model covers the web angle, the load bearing plate and the wall thickness poorly.*

The dependence of the web angle within the energy model corresponds to this dependence in the beam on elastic foundation model. Hence, the finite element simulations tend to depend stronger on the web angle, just as is the case in the beam on elastic foundation model. The energy model is only capable of proper predictions (as far as the web angle is concerned) for members having a web angle larger than 80°. The most obvious reason for this lack of reliability for members having inclined webs is that the assumption of the maximum deflection of the web occurring at the centre is no longer valid. This would imply that the factor n is no longer valid nor are the deformation descriptions in the energy model over the cross-section. The factor n is defined to be the quotient of the maximum deflections of the top flange and the web and used in the description of the deformation variations over the cross-section of the member.
According to the energy model, the web crippling stiffness is proportional to the length of the load bearing plate, regardless the length of the load bearing plate. Clearly, this does not correspond not very well to the simulations, especially in case of long load bearing plates. The combinations 1, 2, 5 and 6, which consider an increase of the deformations underneath the load bearing plate, produce very poor predictions in varying the length of the load bearing plate. The combinations 3 and 4, which imply a constant deformation underneath the load bearing plate) relatively perform best. For the energy model not taking the upward curling underneath the load bearing plate into account in case of all combinations, it seems quite logical that the larger the load bearing plate the worse the energy model predicts the web crippling stiffness.
Each combination performs the same varying the wall thickness, as the wall thickness is uniformly accounted for throughout the energy model. According to the energy model, the web crippling stiffness is proportional to the wall thickness raised to the third power, while the finite element simulations point out that it is proportional to the wall thickness raised to roughly the 5/2 power. However, this poor treatment only has a large influence on the resulting web crippling stiffness for members with wall thicknesses larger than 1 mm. It is caused by the neglect of axial deformations in throughout the member.
In the adjusted energy model the influence of the load bearing plate and the wall thickness is better described than in the original model. The web crippling stiffness is made independent of the length of the load bearing

plate. In the adjusted model the treatment of the length of the load bearing plate is very well for load bearing plates larger than about 75 mm. Considering the treatment of the wall thickness, an empirical correction factor (γ) is added, whereafter the influence of the wall thickness is described accurately for wall thicknesses smaller than 1.1 mm.

- In the energy model the bottom and top flange, the web and the span length are accounted for reasonably well for several combinations.

Considering the bottom flange, the energy model does very well on each combination throughout the whole range over which the width of the bottom flange is varied. Therefore, the neglect of the deformation variations over the bottom flange, resulting in a description of the member only by one top flange plate and two web plates, is justified. Moreover, the introduction of the factor n in the development of the energy model is justified also, for members having vertical webs. Since, the deformation variations of the bottom flange are neglected, the influence of the bottom flange on the web crippling stiffness is represented by n.
The performances of the energy model with respect to the top flange differ for each combination. Only combination 6 performs reasonably well, regardless of the magnitude of the corner radii. The other combinations show a performance that varies with varying magnitudes of the corner radii.
Only combination 2 and 6 cover the web considerably well, regardless the magnitude of the corner radii.
The combinations 1, 2, 5 and 6 are based upon the assumption that the web crippling deformations stretch out over an effective length that is only a function of the bottom and top flange and the web. Hence, these combinations produce web crippling stiffnesses which are independent of the span length, just as the finite element simulations indicate. The combinations 3 and 4 apply the so-called full length solution in determining the web crippling stiffness. This solution states that the effective length equals the span length and show a web crippling stiffness that is proportional to the span length. From the results it may be concluded that the introduction of the effective length is justified.

- The geometrical compatibility approach is preferred to the hinge compatibility approach.

According to the results of the parameter study, the hinge compatibility approach, which is based upon the assumption that the web and top flange plates are connected to each other by hinges, only produces reliable results for few parameters. This indicates that the hinge compatibility approach cannot be applied in the derivation of a web crippling stiffness model that should be able to produce reliable predictions of the web crippling stiffness. The hinge compatibility approach is based upon the assumption that the plates are rigidly connected, where the bending moment at these connections not necessarily equals zero Hence, the geometrical approach, which can be thought of as a generalization of the hinge compatibility approach, is preferred to the hinge compatibility approach.

- A fourth degree polynomial description of the deformation variations over the length of the member, combined with the geometrical compatibility approach (combination 6), produces the most reliable approximations of the web crippling stiffness, throughout the parameter study.

Of all combinations that have been investigated, combination 6 appears to produce the most reliable results. This was to be expected because combination 6 represents the most progressive description of the deformation variations over the length of the member. After application of the adjustments, this model even treats all parameters considerably well, except that the web angle is poorly accounted for. It should be noted that the energy model is very sensitive to the description of the deformation variations over the length of the member according to the large deviations between the results of the various combinations.

- The energy model results in rather complicated web crippling stiffness formulae.

Compared to the beam on elastic foundation model, the energy model produces web crippling stiffness formulae which are far more complicated. Especially combination 6 gives very complicated formulae which are not easy to use.

8.6 *Provisional web crippling stiffness formulae*

Comparing the beam on elastic foundation model and the energy model, it has become clear that the energy model can be adjusted in order to improve the treatment of certain parameters, while the treatment of the web in the beam on elastic foundation model cannot be improved easily without affecting the fundamental basis of the model. Hence, the energy model is preferred to the beam on elastic foundation model.

So far, the web crippling stiffness described most properly by the adjusted energy model (combination 6), in which the web crippling stiffness is given by

$$k_{\Delta h_w} = \frac{D \cdot b_{tf}^2 \cdot L_{ef}^5 \cdot r_{i;tf}^{0.92}}{6355 \cdot t^{0.65} \cdot (100^2 - L_{ef}^2)^4 \cdot (b_{tf}^2 + b_w^2 \cdot n)}$$

$$\cdot [\frac{[b_{tf}^4 \cdot (b_w^3 \cdot L_{ef}^2 \cdot (8640 + 2400 \cdot n) + 5248 \cdot L_{ef}^4 \cdot b_w + b_{tf} \cdot (L_{ef}^2 \cdot (1536 \cdot L_{ef}^2 + 3936 \cdot b_w^2 + 2400 \cdot b_w^2 \cdot n))}{[b_w \cdot \sin^2\theta_w \cdot r_{i;tf}^2 \cdot (\sin\theta_w \cdot r_{i;tf} - b_{tf}) \cdot (b_{tf}^2 \cdot (b_{tf} \cdot (4 \cdot \sin\theta_w \cdot r_{i;tf} - b_{tf}) - b_w \cdot n \cdot (b_w + 5 \cdot \sin\theta_w \cdot r_{i;tf}) - 4 \cdot \sin^2\theta_w \cdot r_{i;tf}^2)}$$

$$\frac{+ b_{tf}^5 \cdot b_w^3 \cdot (b_w \cdot (3150 + 15750 \cdot n^2) + 7875 \cdot b_{tf} \cdot n^2) + b_w^4 \cdot (b_{tf}^3 \cdot L_{ef}^2 \cdot (2400 \cdot n^2 - 768 \cdot n + 8800) + 6656 \cdot b_{tf} \cdot L_{ef}^4 \cdot n^2)]}{+ b_w \cdot \sin\theta_w \cdot r_{i;tf} \cdot n \cdot (\sin\theta_w \cdot r_{i;tf} \cdot (b_w + 5 \cdot b_{tf}) - b_w \cdot b_{tf}))]}$$

$$+ \frac{[b_w^5 \cdot (L_{ef}^2 \cdot n^2 \cdot (768 \cdot L_{ef}^2 + 2400 \cdot b_{tf}^2) + b_{tf}^2 \cdot n \cdot (7875 \cdot b_{tf}^2 \cdot n - 8960 \cdot L_{ef}^2) - 2100 \cdot b_{tf}^4 + 4096 \cdot b_w \cdot b_{tf} \cdot L_{ef}^2 \cdot n^2)}{[b_w \cdot \sin^2\theta_w \cdot r_{i;tf}^2 \cdot (\sin\theta_w \cdot r_{i;tf} - b_{tf}) \cdot (b_{tf}^2 \cdot (b_{tf} \cdot (4 \cdot \sin\theta_w \cdot r_{i;tf} - b_{tf}) - b_w \cdot n \cdot (b_w + 5 \cdot \sin\theta_w \cdot r_{i;tf}) - 4 \cdot \sin^2\theta_w \cdot r_{i;tf}^2)}$$

$$+ b_{tf}^2 \cdot (b_w^6 \cdot (8400 \cdot n \cdot (b_{tf} + b_w) - 5250 \cdot b_{tf}) + L_{ef}^4 \cdot b_w^2 \cdot (b_w \cdot n \cdot (3200 \cdot n - 9984) - b_{tf} \cdot (4608 \cdot n - 6400)))] \Big/ \left[+ b_w \cdot \sin\theta_w \cdot r_{i;tf} \cdot n \cdot (\sin\theta_w \cdot r_{i;tf} \cdot (b_w + 5 \cdot b_{tf}) - b_w \cdot b_{tf}))\right] \quad (8.1)$$

in which

$$L_{ef} = \sqrt{\frac{b_{tf}^3 \cdot (34 \cdot b_w^2 + 504 \cdot 10^4) + b_w^3 \cdot n^2 \cdot (17 \cdot b_{tf}^2 + 252 \cdot 10^4)}{14 \cdot b_{tf}^3 + 7 \cdot b_w^3 \cdot n^2}} \quad (8.2)$$

This model is capable of predicting the web crippling stiffness with an accuracy of about 10%, within the following dimension ranges (in mm):

r_i=1-10, b_w=50-80, b_{bf}=20-120, b_{tf}=40-100, L_{span}=520-2600, θ_w=80-90°, t=0.5-1.1 and L_{lb}=100-300.

8.7 *Recommendations*

Some recommendations for future research are given below.

- *Improvement of the energy model by a better treatment of the web angle.*

In the development of an analytical web crippling stiffness model, both the energy model and the beam on elastic foundation model might be adjusted on the treatment of several parameters, in order to establish reliable web crippling stiffness formulae. It is recommended to improve the energy model rather than the beam on elastic foundation model for the following reason. The beam on elastic foundation model cannot be improved easily on the influence of the web, without affecting the fundamental basis on which the model is developed. As mentioned before, within the beam on elastic foundation model the web has a function that is twofold due to the fact that a part of it belongs to the beam and the whole web belongs to the elastic foundation in the application of the beam on elastic foundation theory.

The energy model should primarily be improved on the influence of the web angle because it performs poorly for web angles smaller than 80°. The most obvious reason for this lack of reliability for rather small web angles is that the assumption of the maximum deflection of the web occurring at the centre is no longer valid. This would imply that the factor n is no longer valid nor are the deformation descriptions in the energy model over the cross-section. It is possible to derive an extra model for members with small web angles that is based upon different descriptions of the deformation variations. Furthermore, it is also possible to develop a more complicated model that is based on a more general deformation variations description, which appears to be valid, regardless of the magnitude of the web angle. It is less convenient to improve the energy model analytically (instead of empirical adjustments), concerning the influence of the load bearing plate and the wall thickness. In case of the load bearing plate this might be established by using a different description of the deformation variations over the length of the member, taking the upward curling underneath the load bearing plate into account. Considering the wall thickness, the energy model might be improved by taking the axial deformations in the plates into account. However, both adjustments are complicated

- Simplification of the energy model.

A disadvantage of the (adjusted) energy model is formed by its complexity. The resulting web crippling stiffness formulae are not very practicable. It is very useful to investigate the contribution of each term of the energy model on the web crippling stiffness for a series of members. Hereby, it might be possible to simplify the energy model for members having parameters weir magnitude lies between prescribed limits, by neglecting several terms of the original model.

-Tuning of the application of the energy model together with Bakker's model describing the rigid-plastic mechanism initiation curve.

Failure by web crippling occurs after the development of a spatial rigid-plastic mechanism *(Bakker, 1992).* The rigid-plastic mechanism initiation curve, for which a mathematical description is derived in Bakker's model, contains all load-deformation combinations where the rigid-plastic mechanism is initiated. The corresponding load is denoted as the mechanism initiation load. Bakker argued that it might be a reasonable approach to develop design formulae based on the prediction of the mechanism initiation load instead of the ultimate load. The mechanism initiation load is the point of intersection between the mechanism initiation curve and the elastic curve, which is fully described by its slope the web crippling stiffness. The future design formulae might be based upon a combination of Bakker's model and an analytical web crippling stiffness model. Two different possible developments can be distinguished. On one hand it is possible to join both models, whereafter the resulting web crippling model is simplified in order to establish a practical formula. On the other hand, the models may be simplified separately first, after which they are united to one resulting web crippling model. Both possibilities should be investigated in further research.

References

Abramowicz, W. and Wierzbicki, T., 1979; **A kinematic approach to crushing of shell structures.** In: *Third international conference of vehicle structural mechanics.* Warrendale, SAE.

Alfutov, N.A. and Balabukh, L.I., 1967; **On the possibility of solving plate stability problems without a preliminary determination of the initial state of stress.** In: *Applied Mathematics and Mechanics*, PMM, Vol. 31, No. 4, pp. 716-722.

Argyris, J.H. and Kelsey, S., 1960; **Energy theorems and structural analysis.** London: Butterworth & Co. Ltd.

Baehre, R. et al., 1982; **Cold-formed steel applications abroad.** In: *Recent research and developments in cold-formed steel design and construction. Sixth International Specialty Conference on Cold-Formed Steel Structures.* Edited by W.W. Yu and J.H. Senne. Rolla, Missouri: University of Missouri-Rolla, Department of Civil engineering.

Bakker, M.C.M., 1992; **Web crippling of cold-formed steel members.** Ph.D. Thesis. Eindhoven: Eindhoven University of technology, Department of Building construction.

Bakker, M.C.M. and Esch, W.J.H. van, 1989; **Experimenteel onderzoek naar het belastingvervormingsgedrag van koudgevormde stalen hoedprofielen onderworpen aan een lijfkreukelbelasting.** TUE-BKO-89.01 & TUE-BKO-89.02. Eindhoven, University of technology, Department of Building construction.

Bakker, M.C.M. and Peköz, T., 1985; **Comparison and evaluation of web crippling prediction formulas.** EUT-report 86-B-01. Eindhoven: Eindhoven University of technology, Department of Building construction.

Bergfelt, A., 1977; **The behaviour and design of slender webs under partial edge loading.** In: *Steel plated structures. An International Symposium.* Edited by P.J. Dowling, J.E. Harding and P.A. Frieze. London: Crosby Lockwood Staples.

Bhat, S.U. and Xirouchakis, P.C., 1986; **Plastic analysis of floating beams.** In: *Journal of Engineering Mechanics*, Vol. 112, No. 2, pp. 199-214.

Cook, R.D., 1974; **Concepts and Applications of Finite Element Analysis.** New York: John Wiley & Sons, Inc.

Fenner, R.T., 1986; **Engineering elasticity**. Chichester: Ellis Horwood Limited Publisher.

Gere, J.M. and Timoshenko, S.P., 1987; **Mechanics of materials**. Second edition. Boston, Massachusetts: Van Nostrand Reinhold (International) Co. Ltd.

Hartog, J.P. den, 1952; **Advanced strength of materials**. New York: McGraw-Hill book company.

Koiter, W.T., 1972; **Stijfheid en sterkte 1, Grondslagen**. Haarlem: Scheltema & Holkema N.V.

Kreyszig, E., 1988; **Advanced engineering mathematics**. Sixth edition. New York: John Wiley & Sons, Inc.

Reinsch, W., 1983; **Das Kantenbeulen zur rechnerischen Ermittlung von Stahltrapezblech-Trägern**. Dissertation D17. Darmstadt: Technische Hochschule Darmstadt.

Richards, T.H., 1977; **Energy methods in stress analysis**. Chichester: Ellis Horwood Limited Publisher.

Salmi, P. and Talja, A., 1992; **Bending strength of beams with non-linear analysis**. In: *Eleventh International Specialty Conference on Cold-Formed Steel Structures*. St. Louis, Missouri.

Santaputra, C. and Yu, W.W., 1986; **Design of automotive structural components using high strength sheet steels; web crippling of cold-formed steel beams**. Rolla, Missouri: University of Missouri-Rolla, Department of Civil engineering.

Shames, I.H. and Dym, C.L., 1985; **Energy and finite element methods in structural mechanics**. Hemisphere Publishing Corporation.

Sharp, M.L., 1989; **Behaviour of Plates Under Partial Edge Loading**. In: *Steel Structure Proceedings Structures Congress '89*. San Francisco, ASCE

Timoshenko, S., 1930; **Strength of materials Part I, Elementary Theory and Problems**. Third edition. Princeton, New Jersey: D. van Nostrand company, Inc.

Timoshenko, S., 1930; **Strength of materials Part II, Advanced Theory and Problems**. Third edition. Princeton, New Jersey: D. van Nostrand company, Inc.

Trefftz, E., 1928; **Handbüch der Physik**. Berlin: Springer-Verlag.

Tsai, Y.M. and Crisinel, M., 1986; **Moment redistribution in continuous profiled sheeting**. In: *Thin-walled metal structures in buildings*. IABSE proceedings, Vol. 49, pp. 107-114. Zurich: IABSE- AIPC- IVBH.

Tsai, Y.M., 1987; **Comportement sur appuis de tôles minces formées à froid**. Thèse No. 689. Lausanne: Ecole Polytechnique Fédérale de Lausanne.

Vlasov, V.Z. and Leontev, U.N., 1966; **Beams, plates and shells on elastic foundations**. Edited by Pelz, T., M. Sc. Jerusalem: Wiener Bindery Ltd.

Wilkesmann, F.W., 1960; **Stegblechbeulung bei Längsrandbelastung**. In: *Der Stahlbau*, Vol. 29, No. 10, pp. 314-322.

Winkler, E., 1867; **Die Lehre von der Elastizität und Festigkeit**. Prag.

Wolfram, S., 1988; **Mathematica, a system for doing mathematics by computer**. Second edition. Redwood City, California: Addison-Wesley Publishing Company, Inc.

Zimmermann, H., 1888; **Die Berechnung des Eisenbahnoberbaues**. Berlin.

Appendix A

In this appendix a detailed description is given of the establishment of the portal frame model both of hat sections and deck panels, as well as the influence of the curvatures and the web crippling deformations due to axial forces on the resulting web crippling formulae.

A.1 Establishment of the portal frame model of hat sections

A detailed derivation of the portal frame model of hat sections will be given.

According the assumptions as stated in section 3.2, the cross section of an infinitely small element *dx* of the loaded part of the member can be idealized as depicted in figure A.1.

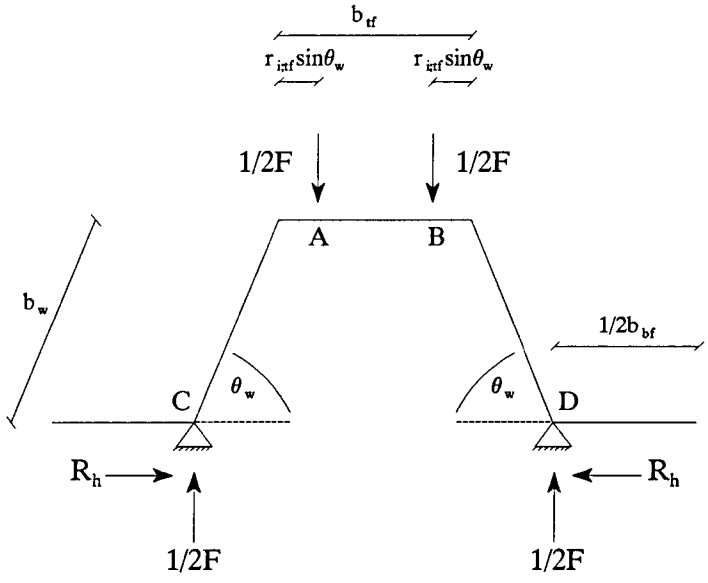

Figure A.1: *Statical system of the portal frame model of hat sections*

From figure A.1 it becomes clear that the curvatures between the webs and the top flange are taken into account by means of an eccentric application of the loads. Hence, the bending deformations due to this eccentric application are taken into account while the curvatures themselves are neglected. For more detailed information about the schematisation of an infinitely small slice *dx* of the loaded part of the member to a portal frame, the reader is referred to section 3.2.

In the portal frame model the (two-dimensional) web crippling deformation is given by the displacement of the points A and B with respect to the supports. The displacement of *A* (which equals the displacement of *B*) can be calculated using Castigliano's law. This law points out that the displacement of any point *j* in the direction of a concentrated force F_j at point *j* can be calculated by differentiating the external work (which equals the internal work) with respect to this force F_j. The general format of this law is given by

$$\frac{\partial W}{\partial F_j} = w_j \tag{A.1}$$

Furthermore, the rotation of any point j is can be calculated by differentiating the external work with respect to the bending moment at j M_j, or

$$\frac{\partial W}{\partial M_j} = \varphi_j \tag{A.2}$$

In the elastic stadium, the internal work of a beam with a length l equals the amount of accumulated elastic energy in the beam. The accumulated energy can be specified with the help of the acting forces on each cross section of the beam and is given by

$$E_i = \frac{1}{2} \cdot \int_0^l \left(\frac{N^2}{EA} + \eta \cdot \frac{V^2}{GA} + \frac{T^2}{GI_{wr}} + \frac{M^2}{EI_y}\right) dx \tag{A.3}$$

In the model shear deformations have not been taken into account and torsion does not to take place due to symmetry. Therefore in equation A.3 these terms may be neglected, resulting in

$$E_i = W = \frac{1}{2} \cdot \int_0^l \left(\frac{N^2}{EA} + \frac{M^2}{EI_y}\right) dx \tag{A.4}$$

In a portal frame which is divided in n different continuous beams with a certain length l_i, the displacement of j can thus be calculated as

$$w_j = \frac{\partial}{\partial F_j} \sum_{i=1}^{n} \frac{1}{2} \cdot \int_0^{l_i} \left(\frac{N^2}{EA} + \frac{M^2}{EI}\right) dx \tag{A.5a}$$

or

$$w_j = \sum_{i=1}^{n} \int_0^{l_i} \left(\frac{N^2}{EA} \cdot \frac{\partial N}{\partial F_j} + \frac{M^2}{EI} \cdot \frac{\partial M}{\partial F_j}\right) dx \tag{A.5b}$$

To establish the displacement of point A in the portal frame of figure A.1, it is necessary to determine the internal work W of the portal frame first. Due to symmetry, the portal frame may be divided in four different continuous beams which all appear twice in the portal frame itself, as shown in figure A.2. Note that the vertical reaction forces at the supports have a magnitude of 1/2F, due to symmetry.

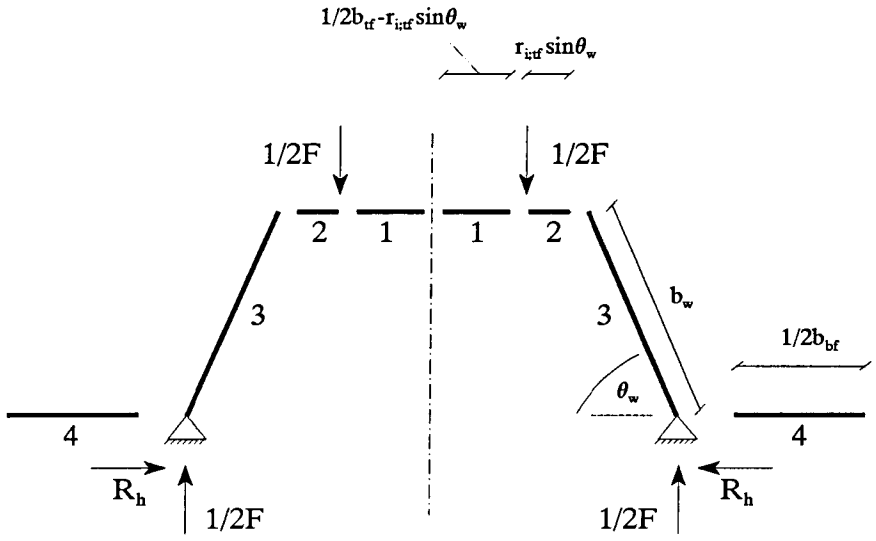

Figure A.2: *Division of portal frame into four different beams*

Now, the acting forces and bending moments on the ends of each beam can be derived from the overall equilibrium of the portal frame and are given in figure A.3.

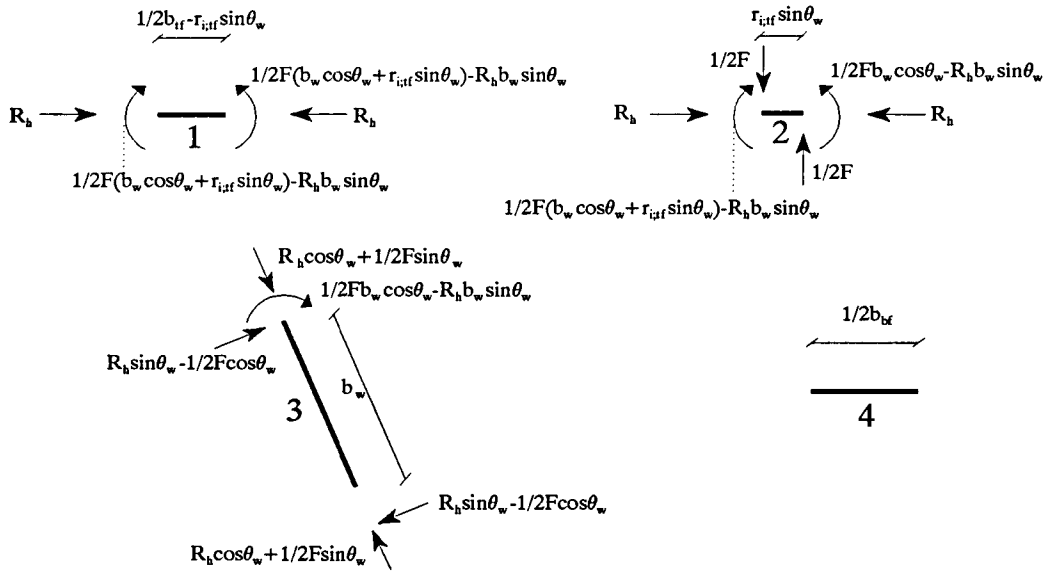

Figure A.3: *Acting forces and bending moments on the five different beams (hat sections)*

The internal work of the portal frame can be calculated by summarizing the internal work of the four

different beams of figure A.3, and double it, as each beam appears twice in the portal frame. Using equation A.4 the internal work of the portal frame can then be specified as

$$W = \int_0^{b_w} [\frac{(R_h \cdot \cos\theta_w + 1/2 \cdot F \cdot \sin\theta_w)^2}{EA} + \frac{(R_h \cdot x \cdot \sin\theta_w - 1/2 \cdot F \cdot x \cdot \cos\theta_w)^2}{EI}] dx$$

$$+ \int_0^{r_{i;tf} \cdot \sin\theta_w} [\frac{R_h^2}{EA} + \frac{(1/2 \cdot F \cdot x - R_h \cdot b_w \cdot \sin\theta_w + 1/2 \cdot F \cdot b_w \cdot \cos\theta_w)^2}{EI}] dx$$

$$+ \int_0^{1/2 \cdot b_{tf} - r_{i;tf} \cdot \sin\theta_w} [\frac{R_h^2}{EA} + \frac{(1/2 \cdot F \cdot b_w \cdot \cos\theta_w - R_h \cdot b_w \cdot \sin\theta_w + 1/2 \cdot F \cdot r_{i;tf} \cdot \sin\theta_w)^2}{EI}] dx \quad (A.6)$$

To calculate the vertical displacement of point A in figure A.1, w_A, it is necessary to calculate the reaction force at the supports first.

The portal frame is onefold statically undetermined and the horizontal reaction force at C and D, R_h, can be derived with Castigliano's law, using the condition

$$u_C = u_D = 0 \quad (A.7)$$

in which u_i represents the horizontal displacement of point i. Combining equations A.1 and A.7, the reaction force R_h can be calculated by solving

$$\frac{\partial W}{\partial R_h} = u_D = 0 \quad (A.8)$$

Using equation A.6, equation A.8 can be expressed as

$$\frac{\partial W}{\partial R_h} = 0 = 2 \cdot \int_0^{b_w} [\frac{\cos\theta_w \cdot (R_h \cdot \cos\theta_w + 1/2 \cdot F \cdot \sin\theta_w)}{EA} + \frac{x \cdot \sin\theta_w \cdot (R_h \cdot x \cdot \sin\theta_w - 1/2 \cdot F \cdot x \cdot \cos\theta_w)}{EI}] dx$$

$$+ 2 \cdot \int_0^{r_{i;tf} \cdot \sin\theta_w} [\frac{R_h}{EA} + \frac{b_w \cdot \sin\theta_w \cdot (R_h \cdot b_w \cdot \sin\theta_w - 1/2 \cdot F \cdot (x + b_w \cdot \cos\theta_w))}{EI}] dx$$

$$+ 2 \cdot \int_0^{1/2 \cdot b_{tf} - r_{i;tf} \cdot \sin\theta_w} [\frac{R_h}{EA} + \frac{b_w \cdot \sin\theta_w \cdot (R_h \cdot b_w \cdot \sin\theta_w - 1/2 \cdot F \cdot (b_w \cdot \cos\theta_w + r_{i;tf} \cdot \sin\theta_w))}{EI}] dx \quad (A.9)$$

From equation A.9 it follows that

$$\frac{2\cdot R_h\cdot(1/2\cdot b_{tf}+b_w\cdot\cos^2\theta_w)+F\cdot b_w\cdot\sin\theta_w\cdot\cos\theta_w}{EA}+\frac{b_w^3\sin\theta_w\cdot(2/3\cdot R_h\cdot\sin\theta_w-1/3\cdot F\cdot\cos\theta_w)}{EI}$$

$$+\frac{b_w\cdot\sin^2\theta_w\cdot r_{i;tf}\cdot(2\cdot R_h\cdot b_w\cdot\sin\theta_w-3/2\cdot F\cdot(r_{i;tf}\cdot\sin\theta_w+2\cdot b_w\cdot\cos\theta_w)}{EI}$$

$$+\frac{b_w\cdot\sin\theta_w\cdot(R_h\cdot b_w\cdot\sin\theta_w\cdot(b_{tf}-2\cdot r_{i;tf}\cdot\sin\theta_w)-1/2\cdot F\cdot(r_{i;tf}\cdot b_{tf}\cdot\sin\theta_w+b_w\cdot\cos\theta_w\cdot(b_{tf}-2\cdot r_{i;tf}\cdot\sin\theta_w)))}{EI}=0 \quad \text{(A.10)}$$

from where it can be derived that

$$R_h=\frac{F\cdot\sin\theta_w\cdot(EA\cdot(b_w\cdot\cos\theta_w\cdot(3\cdot b_{tf}+2\cdot b_w)-3\cdot r_{i;tf}\cdot\sin\theta_w\cdot(r_{i;tf}\cdot\sin\theta_w-b_{tf}))-6\cdot EI\cdot\cos\theta_w)}{2\cdot(EA\cdot b_w^2\cdot\sin^2\theta_w\cdot(3\cdot b_{tf}+2\cdot b_w)+3\cdot EI\cdot(2\cdot b_w\cdot\cos^2\theta_w+b_{tf}))} \quad \text{(A.11a)}$$

From equation A.11a it becomes clear that R_h approaches zero if θ_w approaches zero. This is as expected; in this case the problem is reduced to a four-point-bending-test where R_h is zero.
Unfortunately the expression for R_h is rather complex, due to both bending deformations and deformations due to axial forces. However, for rather regular hat sections, with a wall thickness $t \ll b_{tf}$ and $t \ll b_w$, and with $\theta_w \geq 5°$, the deformations due to axial forces are negligible compared to the bending deformations. Hence, equation A.10 might be simplified by not taking the deformations due to axial forces into account, which results in a more simple expression for R_h, namely

$$R_h=\frac{F}{4\cdot b_w\cdot\sin\theta_w}\cdot\left[\frac{b_w\cdot\cos\theta_w\cdot(2/3\cdot b_w+b_{tf})+r_{i;tf}\cdot b_{tf}\cdot\sin\theta_w-r_{i;tf}^2\cdot\sin^2\theta_w}{1/2\cdot b_{tf}+1/3\cdot b_w}\right] \quad ;\ \theta_w\geq 5° \quad \text{(A.11b)}$$

Using equation A.1 the (two-dimensional) web crippling deformation (and thus the vertical displacement of point A) can be expressed as

$$\Delta h_w;2D=w_A=\frac{\partial W}{\partial 1/2\cdot F} \quad \text{(A.12)}$$

Therefore, the web crippling deformation can be derived by differentiating equation A.6 with respect to the applied force at A, which gives

$$\Delta h_w;2D=2\cdot\int_0^{b_w}\left[\frac{\sin\theta_w\cdot(R_h\cdot\cos\theta_w+1/2\cdot F\cdot\sin\theta_w)}{EA}+\frac{x\cdot\cos\theta_w\cdot(1/2\cdot F\cdot x\cdot\cos\theta_w-R_h\cdot x\cdot\sin\theta_w)}{EI}\right]dx$$

$$+2\cdot\int_0^{r_{i;tf}\cdot\sin\theta_w}\left[\frac{(x+b_w\cdot\cos\theta_w)\cdot(1/2\cdot F\cdot(x+b_w\cdot\cos\theta_w)-R_h\cdot b_w\cdot\sin\theta_w)}{EI}\right]dx$$

$$+2\cdot\int_{0}^{1/2\cdot b_{tf}-r_{i;tf}\cdot\sin\theta_w}\left[\frac{(b_w\cdot\cos\theta_w+r_{i;tf}\cdot\sin\theta_w)\cdot(1/2\cdot F\cdot(b_w\cdot\cos\theta_w+r_{i;tf}\cdot\sin\theta_w)-R_h\cdot b_w\cdot\sin\theta_w)}{EI}\right]dx \qquad (A.13)$$

After integration this results in

$$\Delta h_w;2D=\frac{b_w\cdot\sin\theta_w}{EA}\cdot[2\cdot R_h\cdot\cos\theta_w+F\cdot\sin\theta_w]+\frac{F}{EI}\cdot[1/3\cdot b_w^3\cdot\cos\theta_w+1/2\cdot b_{tf}\cdot b_w^2\cdot\cos^2\theta_w]$$

$$+\frac{F}{EI}\cdot[r_{i;tf}\cdot b_{tf}\cdot b_w\cdot\cos\theta_w\cdot\sin\theta_w-r_{i;tf}^2\cdot b_w\cdot\cos\theta_w\cdot\sin^2\theta_w+r_{i;tf}^2\cdot\sin^2\theta_w\cdot(1/2\cdot b_{tf}-2/3\,r_{i;tf}\cdot\sin\theta_w]$$

$$-\frac{R_h\cdot b_w\cdot\sin\theta_w}{EI}\cdot[2/3\cdot b_w^2\cdot\cos\theta_w-r_{i;tf}^2\cdot\sin^2\theta_w+b_{tf}\cdot r_{i;tf}\cdot\sin\theta_w+b_{tf}\cdot b_w\cdot\cos\theta_w] \qquad (A.14)$$

Substitution of equation A.11b into equation A.14 gives

$$\Delta h_w;2D=\frac{F\cdot b_w\cdot\sin^2\theta_w}{EA}+\frac{F\cdot\cos\theta_w}{EA}\cdot\left[\frac{2/3\cdot b_w^2\cdot\cos\theta_w+r_{i;tf}\cdot b_{tf}\cdot\sin\theta_w+b_{tf}\cdot b_w\cdot\cos\theta_w-r_{i;tf}^2\cdot\sin^2\theta_w}{b_{tf}+2/3\cdot b_w}\right]$$

$$+\frac{F}{EI}\cdot\left[\frac{b_w\cdot r_{i;tf}^2\cdot\sin^2\theta_w\cdot(b_{tf}-4/3\cdot r_{i;tf}\cdot\sin\theta_w)+r_{i;tf}^3\cdot\sin^3\theta_w\cdot(b_{tf}-3/2\cdot r_{i;tf}\cdot\sin\theta_w)}{3\cdot b_{tf}+2\cdot b_w}\right] \qquad (A.15)$$

Since it is defined that

$$k_{\Delta h_w;2D}=\frac{F}{\Delta h_w;2D} \qquad (A.16)$$

the reciproke two-dimensional web crippling stiffness can be specified as

$$\frac{1}{k_{\Delta h_w;2D}}=\frac{b_w\cdot\sin^2\theta_w}{EA}+\frac{\cos\theta_w}{EA}\cdot\left[\frac{b_w\cdot\cos\theta_w\cdot(2/3\cdot b_w+b_{tf})+r_{i;tf}\cdot b_{tf}\cdot\sin\theta_w-r_{i;tf}^2\cdot\sin^2\theta_w}{b_{tf}+2/3\cdot b_w}\right]$$

$$+r_{i;tf}^2\cdot\sin^2\theta_w\cdot\left[\frac{b_w\cdot(b_{tf}-4/3\cdot r_{i;tf}\cdot\sin\theta_w)+r_{i;tf}\cdot\sin\theta_w\cdot(b_{tf}-3/2\cdot r_{i;tf}\cdot\sin\theta_w)}{EI\cdot(3\cdot b_{tf}+2\cdot b_w)}\right] \qquad (A.17)$$

For hat sections with vertical webs (θ_w=90°) equation 3.10 can be reduced to

$$\frac{1}{k_{\Delta h_w;2D}}=\frac{b_w}{EA}+r_{i;tf}^2\cdot\sin^2\theta_w\cdot\left[\frac{b_w\cdot(b_{tf}-4/3\cdot r_{i;tf}\cdot\sin\theta_w)+r_{i;tf}\cdot\sin\theta_w\cdot(b_{tf}-3/2\cdot r_{i;tf}\cdot\sin\theta_w)}{EI\cdot(3\cdot b_{tf}+2\cdot b_w)}\right] \qquad (A.18)$$

A.2 *Establishment of the portal frame model of first generation deck panels*

In this section a detailed derivation of the portal frame model of first generation deck panels will be given. According to the assumptions as stated in section 3.2, the cross section of an infinitely small element *dx* of the loaded part of the member can be idealized to figure A.4.

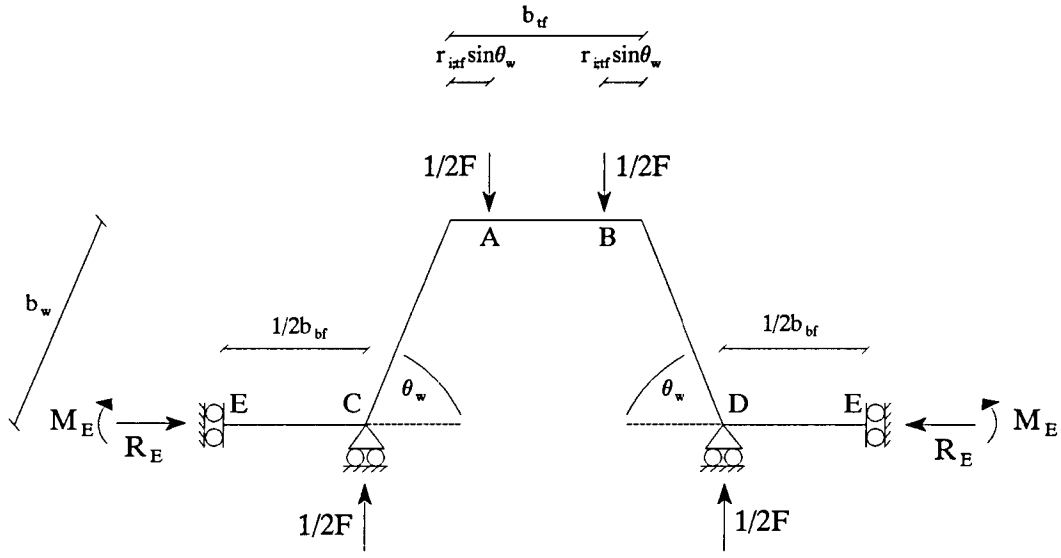

Figure A.4: *Statical system of the portal frame model of first generation deck panels*

The bending moment M_E and the horizontal reaction force R_E maintain the continuity of the deck panel.
The portal frame of figure A.4 is twofold statically undetermined and the determination of R_E and M_E can be established using Castigliano's law (equations A.1 and A.2), where after the web crippling deformation can be calculated with the same law.
In this model (as well as in the model of hat sections) shear deformations have not been taken into account and torsion does not take place due to symmetry. Hence M_E, R_E and the web crippling deformation can be determined using equations A.4 and A.5.
Due to symmetry, the portal frame of figure A.4 may be divided in four different continuous beams that all appear twice in the portal frame itself (i.e. the same division as in the portal frame model of hat sections; see also figure A.2 for the format of this division). Note that the vertical reaction forces at the supports have a magnitude of 1/2F, due to symmetry. The acting forces and bending moments on the ends of each beam can be derived from the overall equilibrium of the portal frame and are given in figure A.5.
The internal work of the portal frame can be calculated by summarizing the internal work of the four different beams of figure A.5, and double it, as each beam appears twice in the portal frame.

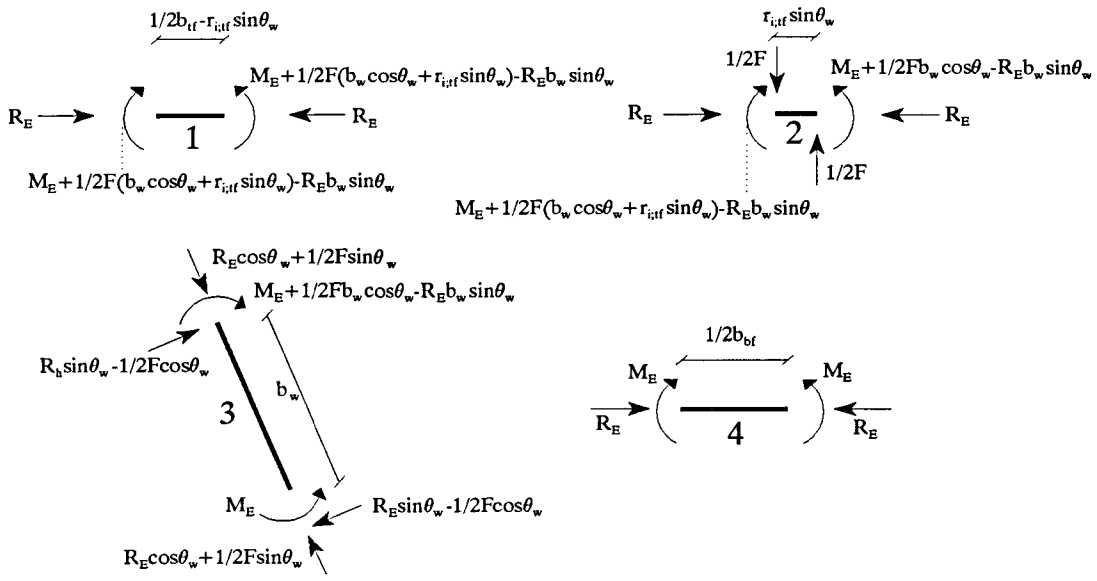

Figure A.5: *Acting forces and bending moments on the four different beams (deck panels)*

Using equation A.4 the internal work of the portal frame can then be specified as

$$W = \int_0^{1/2\cdot b_{bf}} \left[\frac{R_E^2}{EA} + \frac{M_E^2}{EI}\right] dx + \int_0^{b_w} \left[\frac{(R_E\cdot\cos\theta_w + 1/2\cdot F\cdot\sin\theta_w)^2}{EA} + \frac{(R_E\cdot x\cdot\sin\theta_w - 1/2\cdot Fx\cos\theta_w - M_E)^2}{EI}\right] dx$$

$$+ \int_0^{r_{i,tf}\cdot\sin\theta_w} \left[\frac{R_E^2}{EA} + \frac{(1/2\cdot F\cdot x - R_E\cdot b_w\cdot\sin\theta_w + 1/2\cdot F\cdot b_w\cdot\cos\theta_w + M_E)^2}{EI}\right] dx$$

$$+ \int_0^{1/2\cdot b_{tf} - r_{i,tf}\cdot\sin\theta_w} \left[\frac{R_E^2}{EA} + \frac{(1/2\cdot F\cdot(b_w\cdot\cos\theta_w + r_{i,tf}\cdot\sin\theta_w) - R_E\cdot b_w\cdot\sin\theta_w + M_E)^2}{EI}\right] dx \qquad \text{(A.19)}$$

To calculate the vertical displacement of point A in figure A.4, w_A, it is necessary to calculate the reaction forces and moments at the supports first. R_E and M_E can be found by solving the equations

$$\frac{\partial W}{\partial R_E} = u_E = 0 \qquad \text{(A.20a)}$$

and

$$\frac{\partial W}{\partial M_E} = \varphi_E = 0 \qquad \text{(A.20b)}$$

Using equation A.19, equation A.20a can be expressed as

$$\frac{\partial W}{\partial R_E} = 0 = 2 \cdot \int_0^{1/2 \cdot b_{bf}} \frac{R_E}{EA} dx + 2 \cdot \int_0^{b_w} [\frac{\cos\theta_w \cdot (R_E \cdot \cos\theta_w + 1/2 \cdot F \cdot \sin\theta_w)}{EA}] dx$$

$$+ 2 \cdot \int_0^{b_w} [\frac{x \cdot \sin\theta_w \cdot (R_E \cdot x \cdot \sin\theta_w - 1/2 \cdot Fx \cdot \cos\theta_w - M_E)}{EI}] dx$$

$$+ 2 \cdot \int_0^{r_{i;tf} \cdot \sin\theta_w} [\frac{R_E}{EA} + \frac{b_w \cdot \sin\theta_w \cdot (R_E \cdot b_w \cdot \sin\theta_w - 1/2 \cdot F \cdot x - 1/2 \cdot F \cdot b_w \cdot \cos\theta_w - M_E)}{EI}] dx$$

$$+ 2 \cdot \int_0^{1/2 \cdot b_{tf} - r_{i;tf} \cdot \sin\theta_w} [\frac{R_E}{EA} + \frac{b_w \cdot \sin\theta_w \cdot (R_E \cdot b_w \cdot \sin\theta_w - 1/2 \cdot F \cdot (b_w \cdot \cos\theta_w + r_{i;tf} \cdot \sin\theta_w) - M_E)}{EI}] dx \quad \text{(A.21)}$$

For rather regular first generation deck panels, with a wall thickness $t \ll b_{tf}$ and $t \ll b_w$, and with $\theta_w \geq 5°$, the deformations due to axial forces are negligible compared to the bending deformations. Hence, equation A.21 might be simplified by not taking the deformations due to axial forces into account, which has also been done in determining the reaction force in case of the hat sections.

Now, after integration equation A.21 becomes

$$R_E = \frac{F \cdot (b_w \cdot \cos\theta_w (1/3 \cdot b_w + 1/2 \cdot b_{tf}) + 1/2 \cdot r_{i;tf} \cdot \sin\theta_w \cdot (b_{tf} - r_{i;tf} \cdot \sin\theta_w)) + M_E \cdot (b_w + b_{tf})}{b_w \cdot \sin\theta_w \cdot (2/3 \cdot b_w + b_{tf})} \quad \text{(A.22)}$$

Similarly, using equation A.19, equation A.20b can be expressed as

$$\frac{\partial W}{\partial M_E} = 0 = 2 \cdot \int_0^{1/2 \cdot b_{bf}} \frac{M_E}{EI} dx + 2 \cdot \int_0^{b_w} [\frac{(M_E - R_E \cdot x \cdot \sin\theta_w + 1/2 \cdot Fx \cdot \cos\theta_w)}{EI}] dx$$

$$+ 2 \cdot \int_0^{r_{i;tf} \cdot \sin\theta_w} [\frac{M_E - R_E \cdot b_w \cdot \sin\theta_w + 1/2 \cdot F \cdot x + 1/2 \cdot F \cdot b_w \cdot \cos\theta_w)}{EI}] dx$$

$$+ 2 \cdot \int_0^{1/2 \cdot b_{tf} - r_{i;tf} \cdot \sin\theta_w} [\frac{M_E - R_E \cdot b_w \cdot \sin\theta_w + 1/2 \cdot F \cdot (b_w \cdot \cos\theta_w + r_{i;tf} \cdot \sin\theta_w)}{EI}] dx \quad \text{(A.23)}$$

After integration M_E can be specified as

$$M_E = \frac{R_E \cdot b_w \cdot \sin\theta_w \cdot (b_w + b_{tf}) - F \cdot (1/2 \cdot b_w \cdot \cos\theta_w \cdot (b_w + b_{tf}) + 1/2 \cdot r_{i;tf} \cdot \sin\theta_w \cdot (b_{tf} - r_{i;tf} \cdot \sin\theta_w))}{(b_{bf} + 2 \cdot b_w + b_{tf})} \quad \text{(A.24)}$$

Equations A.22 and A.24 can be thought of as two equations with two unknown parameters R_E and M_E. After proper substitutions of these equations it follows that

$$R_E = \frac{F\cdot(b_w\cdot\cos\theta_w\cdot(b_{bf}\cdot(3\cdot b_{tf}+2\cdot b_w)+b_w\cdot(2\cdot b_{tf}+b_w))-3\cdot r_{i;tf}\cdot\sin\theta_w\cdot(b_{bf}+b_w)\cdot(r_{i;tf}\cdot\sin\theta_w-b_{tf}))}{2\cdot b_w\cdot\sin\theta_w\cdot(b_{bf}\cdot(3\cdot b_{tf}+2\cdot b_w)+b_w\cdot(2\cdot b_{tf}+b_w))} \quad \text{(A.25a)}$$

and

$$M_E = -\frac{F\cdot r_{i;tf}\cdot b_w\cdot\sin\theta_w\cdot(r_{i;tf}\cdot\sin\theta_w-b_{tf}))}{2\cdot(b_{bf}\cdot(3\cdot b_{tf}+2\cdot b_w)+b_w\cdot(2\cdot b_{tf}+b_w))} \quad \text{(A.25b)}$$

Now, the web crippling deformation (e.g. the displacement of point A with respect to the supports) can be calculated by differentiating equation A.19 (the internal work) with respect to the applied force at A, which results in

$$\Delta h_w;2D = \frac{\partial W}{\partial 1/2\cdot F} = 2\cdot\int_0^{b_w}[\frac{\sin\theta_w\cdot(R_E\cdot\cos\theta_w+1/2\cdot F\cdot\sin\theta_w)}{EA}]\,dx$$

$$+2\cdot\int_0^{b_w}[\frac{x\cdot\cos\theta_w\cdot(M_E-R_E\cdot x\cdot\sin\theta_w+1/2\cdot F\cdot x\cdot\cos\theta_w)}{EI}]\,dx$$

$$+2\cdot\int_0^{r_{i;tf}\cdot\sin\theta_w}[\frac{(x+b_w\cdot\cos\theta_w)\cdot(M_E-R_E\cdot b_w\cdot\sin\theta_w+1/2\cdot F\cdot x+1/2\cdot F\cdot b_w\cdot\cos\theta_w)}{EI}]\,dx$$

$$+2\cdot\int_0^{1/2\cdot b_{tf}-r_{i;tf}\cdot\sin\theta_w}[\frac{(b_w\cdot\cos\theta_w+r_{i;tf}\cdot\sin\theta_w)\cdot(M_E-R_E\cdot b_w\cdot\sin\theta_w+1/2\cdot F\cdot(b_w\cdot\cos\theta_w+r_{i;tf}\cdot\sin\theta_w))}{EI}]\,dx \quad \text{(A.26)}$$

which after integration becomes

$$\Delta h_w;2D = \frac{b_w\cdot\sin\theta_w}{EA}\cdot(2\cdot R_E\cdot\cos\theta_w+F\cdot\sin\theta_w)+\frac{F}{EI}\cdot(1/3\cdot b_w^3\cdot\cos^2\theta_w)$$

$$+\frac{F}{EI}\cdot(1/2\cdot b_{tf}\cdot b_w^2\cdot\cos^2\theta_w+b_w\cdot r_{i;tf}\cdot\cos\theta_w\cdot\sin\theta_w\cdot(b_{tf}-r_{i;tf}\cdot\sin\theta_w)+1/2\cdot b_{tf}\cdot r_{i;tf}^2\cdot\sin^2\theta_w-2/3\cdot r_{i;tf}^3\cdot\sin^3\theta_w)$$

$$+\frac{M_E}{EI}\cdot(b_w\cdot\cos\theta_w\cdot(b_w+2\cdot r_{i;tf}\cdot\sin\theta_w)+r_{i;tf}^2\cdot\sin^2\theta_w+2\cdot(r_{i;tf}\cdot\sin\theta_w+b_w\cdot\cos\theta_w)\cdot(1/2\cdot b_{tf}-r_{i;tf}\cdot\sin\theta_w))$$

$$-\frac{R_E\cdot b_w\cdot\sin\theta_w}{EI}\cdot(2/3\cdot b_w^2\cdot\cos\theta_w-r_{i;tf}^2\cdot\sin^2\theta_w+b_{tf}\cdot(r_{i;tf}\cdot\sin\theta_w+b_w\cdot\cos\theta_w)) \quad \text{(A.27)}$$

Using equation A.16 and substituting equations A.25a and A.25b into equation A.27 gives

$$\frac{1}{k_{\Delta b_w;2D}} = \frac{b_{bf}\cdot b_w\cdot(3\cdot b_{tf}+2\cdot b_w)+3\cdot r_{i;tf}\cdot\sin\theta_w\cdot\cos\theta_w\cdot(b_{bf}+b_w)\cdot(b_{tf}-r_{i;tf}\cdot\sin\theta_w)+b_w^2\cdot(2\cdot b_{tf}+b_w)}{EA\cdot(b_{bf}\cdot(3\cdot b_{tf}+2\cdot b_w)+b_w\cdot(2\cdot b_{tf}+b_w))}$$

$$+\frac{r_{i;tf}^2\cdot\sin^2\theta_w\cdot b_{bf}\cdot(r_{i;tf}\cdot\sin\theta_w\cdot(6\cdot b_{tf}-9\cdot r_{i;tf}\cdot\sin\theta_w)+b_w\cdot(6\cdot b_{tf}-8\cdot r_{i;tf}\cdot\sin\theta_w))}{6\cdot EI\cdot(b_{bf}\cdot(3\cdot b_{tf}+2\cdot b_w)+b_w\cdot(2\cdot b_{tf}+b_w))}$$

$$+\frac{b_w\cdot r_{i;tf}^2\cdot\sin^2\theta_w\cdot(4\cdot r_{i;tf}\cdot\sin\theta_w\cdot(b_{tf}-b_w)+3\cdot b_{tf}\cdot b_w-6\cdot r_{i;tf}^2\cdot\sin^2\theta_w)}{6\cdot EI\cdot(b_{bf}\cdot(3\cdot b_{tf}+2\cdot b_w)+b_w\cdot(2\cdot b_{tf}+b_w))} \qquad \text{(A.28)}$$

A.3 Influence of the rounding of the corners

In the derived model the corner radii are taken into account by means of an eccentric application of the loads. However, the rounding of the corners is ignored as can be seen in figure A.1 and A.4. In this section it is shown that the influence of the rounding of the corners is negligibly small and may therefore be neglected. Only hat sections will be considered, since it is assumed that the influence in first generation deck panels will not differ much from that in hat sections. If the rounding of the top flange corners is taken into account a different and more complicate approximation of the web crippling stiffness will be obtained. This is caused by a different transmission of the concentrated load at the curved transitions compared to the linear schematisation of figure A.1.

The influence of the rounding of the corners is only investigated for hat sections with vertical webs (θ_w=90°). For members having inclined webs the horizontal reaction force R_h will be larger, which may imply a larger influence of the rounding of the corners on the resulting web crippling stiffness. However, for rather regular members ($\theta_w \geq 45°$) this influence is only slightly larger. Hence, if the influence appears to be negligibly small for members having vertical webs, this holds also approximately true for members having inclined webs. According to the derived model, where the rounding of the corners is ignored, the web crippling stiffness of is given by

$$\frac{1}{k_{\Delta b_w;2D}} = \frac{b_w}{EA} + r_{i;tf}^2\cdot\left[\frac{b_w\cdot(b_{tf}-4/3\cdot r_{i;tf})+r_{i;tf}\cdot(b_{tf}-3/2\cdot r_{i;tf})}{EI\cdot(3\cdot b_{tf}+2\cdot b_w)}\right] \qquad \text{(A.29)}$$

If the rounding of the top flange corners is taken into account, the portal frame with vertical webs may be schematised as in figure A.6.

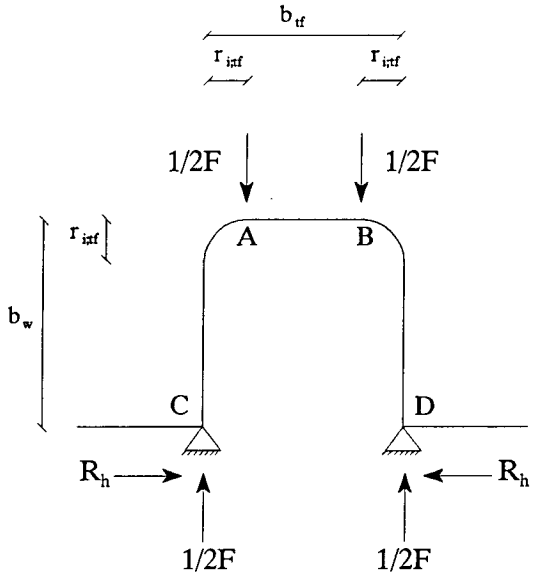

Figure A.6: *Statical system of the portal frame with curvatures*

The displacement of point A (i.e. the web crippling deformation) may be calculated using Castiglianos's law. Therefore, the portal frame of figure A.6 is divided in four different beams, all appearing twice in the portal frame itself, as shown in figure A.7.

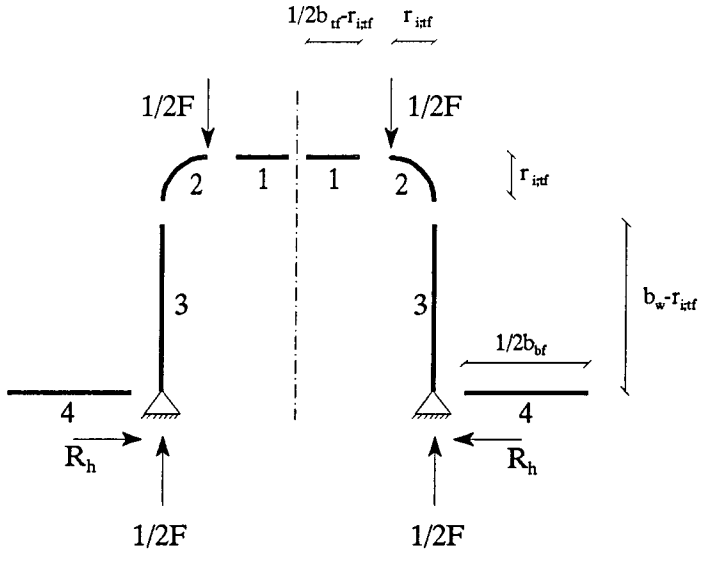

Figure A.7: *Division of portal frame into four beams, taking the rounding of the corners into account*

Now, the acting forces and bending moments on the end of each beam can be derived from the overall equilibrium of the portal frame and are given in figure A.8.

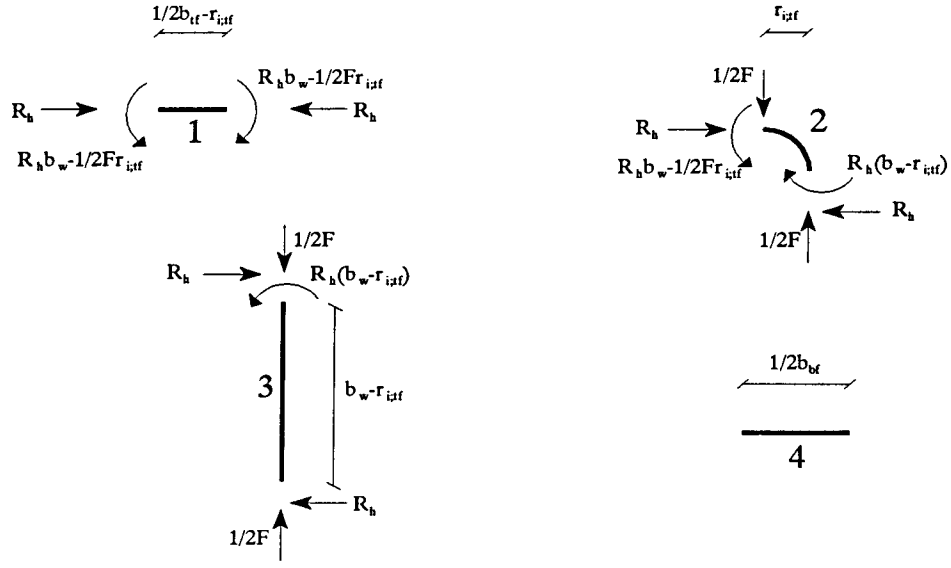

Figure A.8: *Acting forces and bending moments on the four different beams*

The internal work of the portal frame can be calculated by summarizing the internal work of the four different beams of figure A.7, and double it, as each beam appears twice in the portal frame. Using equation A.4 the internal work of the portal frame can then be specified as

$$W = \int_0^{b_w - r_{i;tf}} \left[\frac{(1/2 \cdot F)^2}{EA} + \frac{(R_h \cdot x)^2}{EI}\right] dx + \int_0^{1/2 \cdot b_{tf} - r_{i;tf}} \left[\frac{R_h^2}{EA} + \frac{(R_h \cdot b_w - 1/2 \cdot F \cdot r_{i;tf})^2}{EI}\right] dx$$

$$+ \int_0^{1/2 \cdot \pi} \left[\frac{(\sin\varphi \cdot (R_h + 1/2 \cdot F))^2}{EA} + \frac{(1/2 \cdot F \cdot r_{i;tf} \cdot (1 - \cos\varphi) - R_h \cdot r_{i;tf} \cdot \sin\varphi - R_h \cdot (b_w - r_{i;tf}))^2}{EI}\right] \cdot r_{i;tf}\, d\varphi \qquad \text{(A.30)}$$

The web crippling deformations may be determined using equation A.12, which gives

$$\Delta h_w; 2D = 2 \cdot \int_0^{b_w - r_{i;tf}} \left[\frac{1/2 \cdot F}{EA}\right] dx + 2 \cdot \int_0^{1/2 \cdot b_{tf} - r_{i;tf}} \left[\frac{r_{i;tf} \cdot (1/2 \cdot F \cdot r_{i;tf} - R_h \cdot b_w)}{EI}\right] dx + 2 \cdot \int_0^{1/2 \cdot \pi} \left[\frac{\sin^2\varphi \cdot (R_h + 1/2 \cdot F)}{EA}\right] \cdot r_{i;tf}\, d\varphi$$

$$+ 2 \cdot \int_0^{1/2 \cdot \pi} \left[\frac{(1 - \cos\varphi) \cdot (1/2 \cdot F \cdot r_{i;tf} \cdot (1 - \cos\varphi) - R_h \cdot (r_{i;tf} \cdot \sin\varphi - b_w + r_{i;tf}))}{EI}\right] \cdot r_{i;tf}^2\, d\varphi \qquad \text{(A.31)}$$

Making use of the goniometrical equation

$$\cos^2\varphi = \frac{\cos(2 \cdot \varphi) + 1}{2}$$

equation A.31 becomes after integration

$$\Delta h_w;2D = \frac{r_{i;tf}\cdot(1/2\cdot\pi\cdot R_h+(1/4\cdot\pi-1)\cdot F)+F\cdot b_w}{EA}$$

$$+\frac{r_{i;tf}\cdot(r_{i;tf}^2\cdot(3/4\cdot\pi-3)\cdot F+(\pi-3)\cdot R_h)+r_{i;tf}\cdot(1/2\cdot F\cdot b_{tf}+(4-\pi)\cdot R_h\cdot b_w)-R_h\cdot b_w\cdot b_{tf})}{EI} \qquad \text{(A.32)}$$

Using equation A.16 and substituting equation A.11b, the web crippling stiffness may be given by

$$\frac{1}{k_{\Delta h_w;2D}} = \frac{3\cdot\pi\cdot r_{i;tf}^2}{4\cdot b_w\cdot EA}\cdot\left[\frac{b_{tf}-r_{i;tf}}{3\cdot b_{tf}+2\cdot b_w}\right]+\frac{(1/4\cdot\pi-1)\cdot r_{i;tf}+b_w}{EA}+\frac{3/2\cdot(\pi-3)}{b_w\cdot EI}\cdot\left[\frac{r_{i;tf}^4\cdot(b_{tf}-r_{i;tf})}{3\cdot b_{tf}+2\cdot b_w}\right]$$

$$+r_{i;tf}^2\cdot\left[\frac{(3/2\cdot\pi-6)\cdot r_{i;tf}^2+(3/4\cdot\pi-3/2)\cdot b_{tf}\cdot r_{i;tf}+b_w\cdot((3/2\cdot\pi-6)\cdot r_{i;tf}+b_{tf})}{EI\cdot(3\cdot b_{tf}+2\cdot b_w)}\right] \qquad \text{(A.33)}$$

Comparing equation A.29 with equation A.33, the influence of the curvatures can be determined. The influence of the curvatures on the web crippling stiffness may be expressed as the percentual deviation of the web crippling stiffness if the curvatures are taken into account *(pdwcs)*, or

$$pdwcs = \frac{k_{\Delta h_w;2D}(A.33)-k_{\Delta h_w;2D}(A.29)}{k_{\Delta h_w;2D}(A.33)}$$

The influence of the curvatures may only be neglected if *pdwcs* is less than 1 to 5 % for rather regular hat sections. The magnitude of *pdwcs* may be investigated by the determination of the web crippling stiffness, varying each geometrical parameter. Combining the influences of each geometrical parameter, the maximum magnitude of *pdwcs* might be established. The influence of each parameter on *pdwcs* is given in figures A.9 to A.12. In the investigation of the influence of each parameter, the top flange corner radius has been varied from 1 to 10 mm and the other parameters have been set a constant value, b_{tf}=60, b_w=50, θ_w=90° and t=0.68.

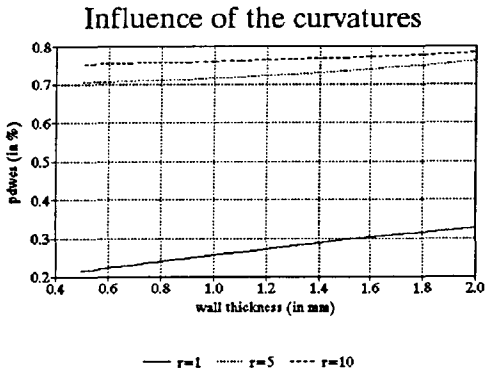

Figure A.9: Influence of t on pdwcs

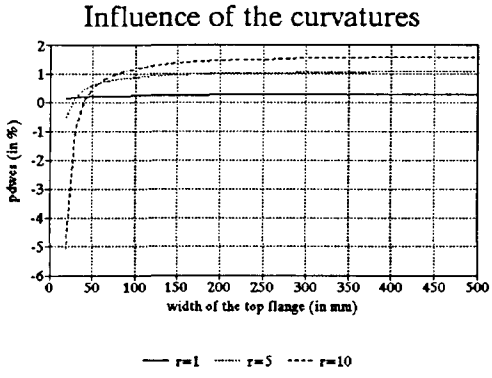

Figure A.10: Influence of b_{tf} on pdwcs

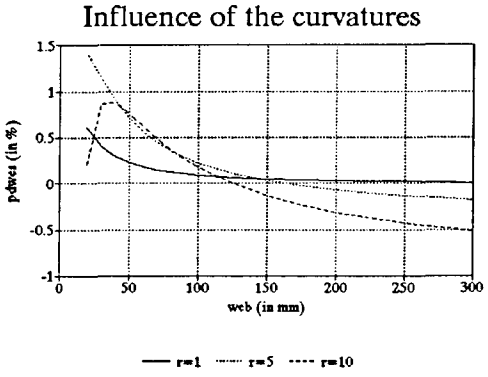

Figure A.11: Influence of b_w on pdwcs

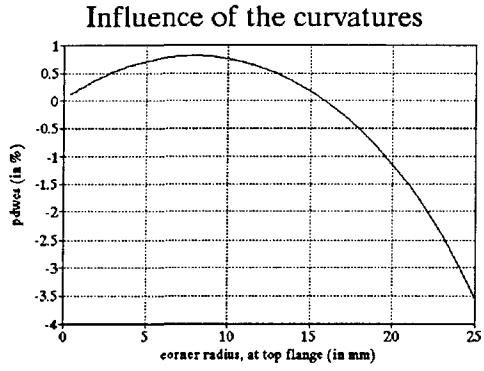

Figure A.12: Influence of $r_{i;tf}$ on pdwcs

From figures A.9 to A.12 it becomes clear that the influence of the top flange corners is negligibly small (considering the accuracy purposes of this study) if $r_{i;tf}$ < 20 mm and b_w > 20 mm. Since it has already been stated that the influence of the rounding of the corners only slightly increases with a decreasing web angle θ_w, they may also be neglected for hat sections with inclined webs, where $r_{i;tf}$ < 20 mm and b_w > 20 mm. Finally, the influence of the rounding of the corners in case of hat sections is not assumed to differ significantly from the influence in case of first generation deck panels, so there they may be neglected under the same conditions, too.

A.4 Neglect of the web crippling deformations due to axial forces in case of hat sections

The deformations due to axial forces in both equations A.17 and A.18 are relatively small compared to the bending deformations. In fact, they appear to be negligibly small, particurally in case of hat sections with rather large corner radii (about 10 mm). To investigate the influence of web crippling deformations due to

axial forces on the overall web crippling deformations and thus on the web crippling stiffness, the web crippling deformations due to axial forces are calculated as a percentage of the overall web crippling deformations for various hat sections. In the investigation of the influence of each parameter, the top flange corner radius has been varied from 1 to 10 mm and the other parameters have been set a constant value, b_{tf}=60, b_w=50, θ_w=90° and t=0.68. The results are given in the figures A.13 to A.17.

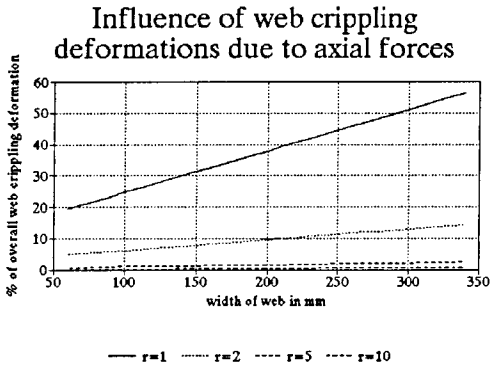

Figure A.13: Influence of b_w

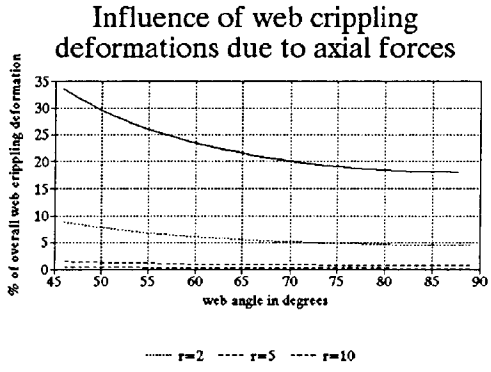

Figure A.14: Influence of θ_w

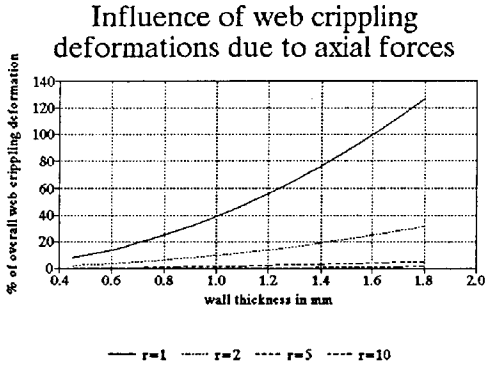

Figure A.15: Influence of t

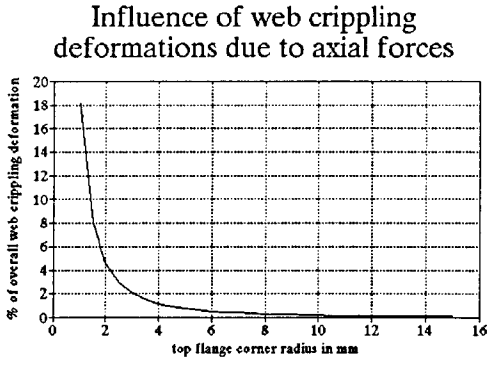

Figure A.16: Influence of $r_{i;tf}$

The figures A.13 to A.17 show an influence of the axial deformations that is rather large for members having top flange corner radii of 1mm (up to 140%) in case of various parameters. However, for members having top flange corner radii larger than 2 mm the influence is smaller than 10% for every parameter, except that members with very large wall thicknesses have relatively large axial deformations. Hence, the influence of web crippling deformations due to axial forces on the overall web crippling deformations mainly depends on the magnitude of the corner radii and the wall thickness. The deformations due to axial forces in case of hat

sections are less than one-tenth of the overall deformations if $r_{i:tf}$ > 2 mm and t < 2 mm. Considering the accuracy purposes of this study they may be neglected in that case.

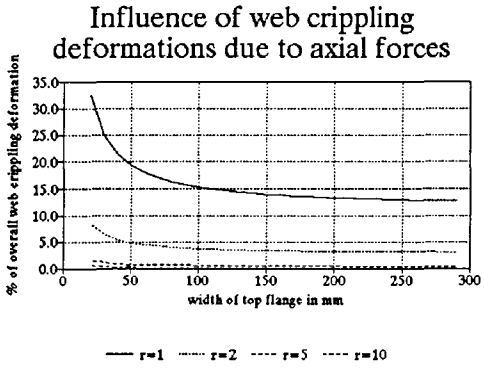

Figure A.17: *Influence of b_{tf}*

A.5 Neglect of the web crippling deformations due to axial forces in case of deck panels

The deformations due to axial forces in equation A.28 are relatively small compared to the bending deformations. In fact, they appear to be negligibly small, particurally in case of hat sections with rather large corner radii (about 10 mm). To investigate the influence of web crippling deformations due to axial forces on the overall web crippling deformations and thus on the web crippling stiffness, the web crippling deformations due to axial forces are calculated as a percentage of the overall web crippling deformations for various first generation deck panels. In the investigation of the influence of each parameter, the top flange corner radius has been varied from 1 to 10 mm and the other parameters have been set a constant value, b_{tf}=60, b_w=50, θ_w=90° and t=0.68. The results are given in the figures A.18 to A.22.

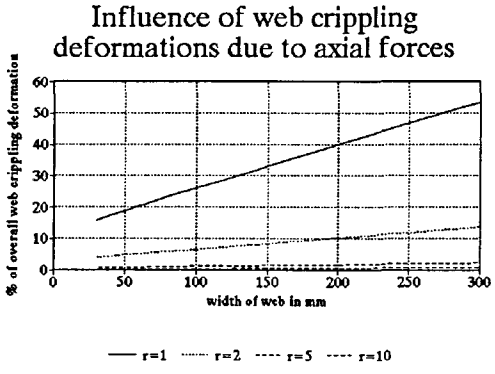

Figure A.18: *Influence of b_w*

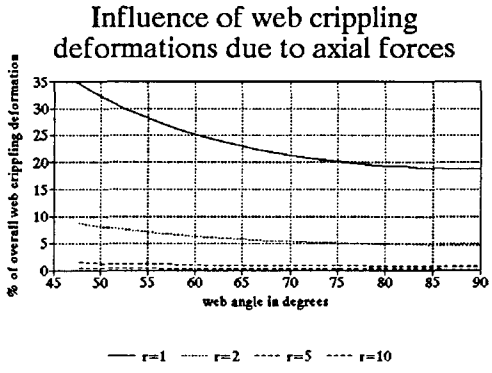

Figure A.19: *Influence of θ_w*

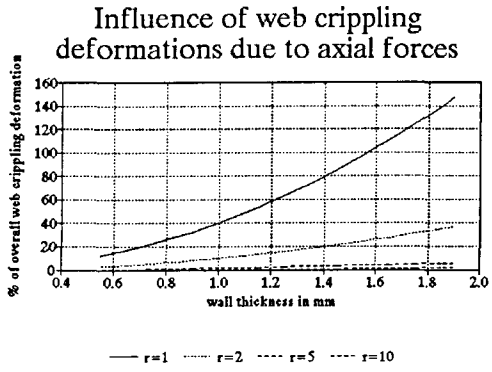

Figure A.20: Influence of t

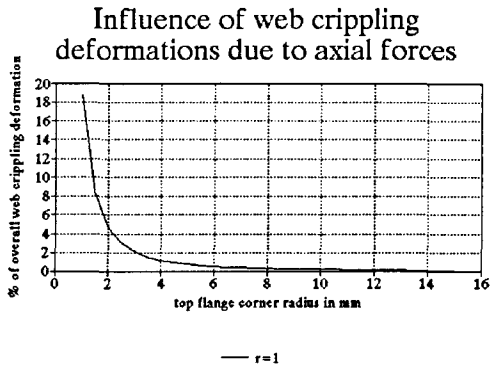

Figure A.21: Influence of $r_{i;tf}$

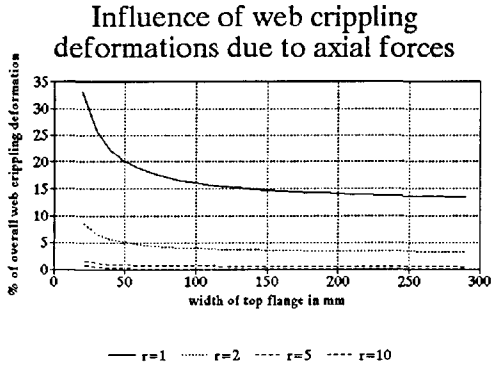

Figure A.22: Influence of b_w

Figures A.18, to A.22 show an influence of the axial deformations that is rather large for members having top flange corner radii of 1mm in case of various parameters. However, for members having top flange corner radii larger than 2 mm the influence is smaller than 10% for every parameter, except that members with very large wall thicknesses have relatively large axial deformationsIt may be concluded that here also the influence of the deformations due to axial forces on the web crippling stiffness mainly depends on the magnitude of the corner radii and the wall thickness. The deformations due to axial forces in case of first generation deck panels may be neglected if $r_{i;tf} > 2$ mm and $t < 2$ mm.

Appendix B

This appendix gives an overview of the general theory of beams on elastic foundations and describes the derivation of the web crippling stiffness of the beam on elastic foundation model. Finally, this appendix deals with the derivation of the flexural rigidity of the beam in the latter model.

B.1 General theory of beams on elastic foundations

Consider a straight beam supported along its entire length and subjected to vertical forces q, acting in the plane of the symmetrical cross section. Because of these forces the beam will deflect, producing continuously distributed reaction forces in the supporting medium. If an infinitely small element is taken under consideration, which is enclosed between two vertical cross sections a distance dx apart, the forces acting on such an element can be given by figure B.1. Note that it is assumed that the slope is so small compared to unity that cross sections (normal to the elastic line) can be replaced by vertical cross sections.

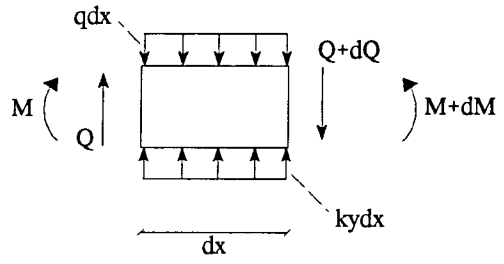

Figure B.1: *Forces acting on an infinitely small element of a beam on an elastic foundation*

Considering the vertical equilibrium of the element in figure 4.3, it follows that

$$\frac{dQ}{dx} = k \cdot y - q \tag{B.1}$$

Making use of the relation

$$Q = \frac{dM}{dx}$$

equation B.1 can be expressed as

$$\frac{dQ}{dx} = \frac{d^2M}{dx^2} = k \cdot y - q \tag{B.2}$$

Using the differential equation of a beam in bending,

$$EI \cdot \frac{d^2Y}{dx^2} = -M$$

and differentiating it twice, it can be obtained that

$$EI \cdot \frac{d^4y}{dx^4} = -\frac{d^2M}{dx^2} = -k \cdot y + q \tag{B.3}$$

This is the differential equation for the deflection curve of a beam supported on an elastic foundation. Along the unloaded parts of the beam, where no distributed load is acting, $q=0$, equation B.3 will take the form

$$EI \cdot \frac{d^4}{dx^4} = -k \cdot y \tag{B.4}$$

Introducing a parameter β with

$$\beta = \sqrt[4]{\frac{k}{4 \cdot EI}} \tag{B.5}$$

the general solution of equation B.4 can be represented as follows:

$$y = e^{\beta x} \cdot (A \cdot \cos\beta x + B \cdot \sin\beta x) + e^{-\beta x} \cdot (C \cdot \cos\beta x + D \cdot \sin\beta x) \tag{B.6}$$

In particular cases the constants A, B, C and D of the solution must be determined from the known conditions at certain points.

Consider the case of a single concentrated load F acting on an infinitely long prismatic beam, taking the origin of coordinates at the point of application of F. Because of the apparent symmetry of the deflection curve, only that part of the beam to the right of F needs to be considered (figure B.2).

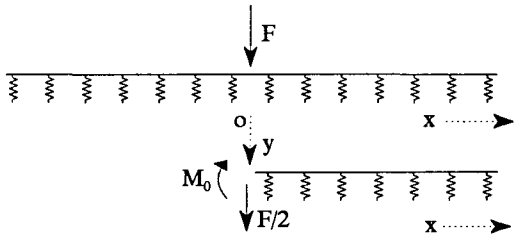

Figure B.2: *Single concentrated load acting on an infinitely long beam*

In applying the general solution, equation B.6, to this case, the arbitrary constants must be found first. It is reasonable to assume that at points infinitely distant from the force F the deflection approaches zero. This condition can be fulfilled only if the constants A and B in equation B.6 are taken equal to zero.

The two remaining constants C and D are found from the condition at the origin, $x=0$. At this point, from the condition of symmetry, the deflection curve must have a horizontal tangent; therefore

$$[\frac{dy}{dx}]_{x=0} = 0$$

or using equation 4.7 and the condition that $A=B=0$,

$$e^{-\beta x}\cdot(C\cdot\cos\beta x + D\cdot\sin\beta x + C\cdot\sin\beta x - D\cdot\cos\beta x)_{x=0} = 0$$

from which it becomes clear that $C=D$. The constant C can be obtained from the consideration that the sum of reaction forces will keep equilibrium with the load F, that is,

$$2\cdot\int_0^{\infty} k\cdot y\ dx = F$$

After substitution of equation B.6 and integration, this results in

$$C = \frac{F\cdot\beta}{2\cdot k} \tag{B.7}$$

Substituting equation B.7 in B.6 and using $A=B=0$ as well as $C=D$, the deflection curve of the right side ($x\geq 0$) of the beam is given by

$$y = \frac{F\cdot\beta}{2\cdot k}\cdot e^{-\beta x}\cdot(\cos\beta x + \sin\beta x) \tag{B.8}$$

The left half of the beam is symmetrical with the right half in y.

B.2 *Establishment of the full length approach in the beam on elastic foundation model*

The portal frame model is extended to a three dimensional model using the theory of a beam on an elastic foundation. In order to take the varying web crippling deformations over the length of the member into account, the member is idealized to a beam (top flange and part of the web) on an elastic foundation (the rest of the web) as shown in figure B.3.

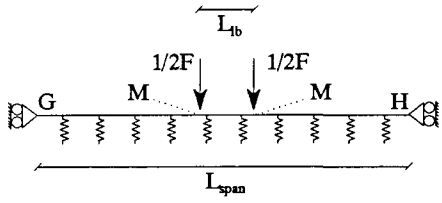

Figure B.3: *Idealization of a member to a beam on an elastic foundation*

Substituting the two-dimensional web crippling stiffness for the foundation stiffness, it can be derived (section 4.3) that for the finite beam of figure B.3 the deflection at point *M* is given by (equation 4.18)

$$y_M = \frac{F \cdot \beta \cdot dx}{4 \cdot k_{\Delta h_w:2D}} \cdot [1 + f_1(\beta \cdot L_{lb})$$

$$- (f_2(1/2 \cdot \beta \cdot (L_{span} - L_{lb})) + f_2(1/2 \cdot \beta \cdot (L_{span} + L_{lb}))) \cdot (f_3(1/2 \cdot \beta \cdot (L_{span} - L_{lb})) + f_3(1/2 \cdot \beta \cdot (L_{span} + L_{lb})))] \quad \text{(B.9)}$$

in which

$$f_1(\beta x) = e^{-\beta x} \cdot (\cos \beta x + \sin \beta x) \quad \text{(B.10a)}$$

$$f_2(\beta x) = e^{-\beta x} \cdot \sin \beta x \quad \text{(B.10b)}$$

$$f_3(\beta x) = e^{-\beta x} \cdot (\cos \beta x - \sin \beta x) \quad \text{(B.10c)}$$

Substitution of equations B.10 into equation B.9 results in

$$y_M = \frac{F \cdot \beta \cdot dx}{4 \cdot k_{\Delta h_w:2D}} \cdot [e^{-\beta \cdot L_{lb}} \cdot (\cos(\beta \cdot L_{lb}) + \sin(\beta \cdot L_{lb}))$$

$$- (e^{-1/2 \cdot \beta \cdot (L_{span} - L_{lb})} \cdot \sin(1/2 \cdot \beta \cdot (L_{span} - L_{lb})) + e^{-1/2 \cdot \beta \cdot (L_{span} + L_{lb})} \cdot \sin(1/2 \cdot \beta \cdot (L_{span} + L_{lb})))$$

$$\cdot (e^{-1/2 \cdot \beta \cdot (L_{span} - L_{lb})} \cdot (\cos(1/2 \cdot \beta \cdot (L_{span} - L_{lb})) - \sin(1/2 \cdot \beta \cdot (L_{span} - L_{lb})))$$

$$+ e^{-1/2 \cdot \beta \cdot (L_{span} + L_{lb})} \cdot (\cos(1/2 \cdot \beta \cdot (L_{span} + L_{lb})) - \sin(1/2 \cdot \beta \cdot (L_{span} + L_{lb})))] \quad \text{(B.11)}$$

which becomes after expanding

$$y_M = \frac{F\cdot\beta\cdot dx}{4\cdot k_{\Delta h_w;2D}}\cdot[1+e^{-\beta\cdot L_{lb}}\cdot(\cos(\beta\cdot L_{lb})+\sin(\beta\cdot L_{lb}))$$

$$-[e^{-\beta\cdot(L_{span}-L_{lb})}\cdot\sin(1/2\cdot\beta\cdot(L_{span}-L_{lb}))\cdot(\cos(1/2\cdot\beta\cdot(L_{span}-L_{lb}))-\sin(1/2\cdot\beta\cdot(L_{span}-L_{lb})))$$

$$+e^{-\beta\cdot L_{span}}\cdot\sin(1/2\cdot\beta\cdot(L_{span}+L_{lb}))\cdot(\cos(1/2\cdot\beta\cdot(L_{span}-L_{lb}))-\sin(1/2\cdot\beta\cdot(L_{span}-L_{lb})))$$

$$+e^{-\beta\cdot L_{span}}\cdot\sin(1/2\cdot\beta\cdot(L_{span}-L_{lb}))\cdot(\cos(1/2\cdot\beta\cdot(L_{span}+L_{lb}))-\sin(1/2\cdot\beta\cdot(L_{span}+L_{lb})))$$

$$+e^{-\beta(L_{span}+L_{lb})}\cdot\sin(1/2\cdot\beta\cdot(L_{span}+L-lb))\cdot(\cos(1/2\cdot\beta\cdot(L_{span}+L_{lb}))-\sin(1/2\cdot\beta\cdot(L_{span}+L_{lb})))] \quad \text{(B.12)}$$

Noting that

$$\sin\alpha\cdot(\cos\alpha-\sin\alpha)=\frac{1}{2}\cdot(\sin(2\cdot\alpha)+\cos(2\cdot\alpha)-1),$$

$$\sin(\alpha+\gamma)=\sin\alpha\cdot\cos\gamma+\cos\alpha\cdot\sin\gamma$$

and

$$\sin\alpha\cdot\sin\gamma=\frac{1}{2}\cdot(\cos(\alpha-\gamma)-\cos(\alpha+\gamma))$$

equation B.12 may be simplified to

$$y_M = \frac{\cdot\beta\cdot d}{4\cdot k_{\Delta h\ ;2D}}\cdot[1+e^{-\beta\cdot L_{lb}}\cdot(\cos(\beta\cdot L_{lb})+\sin(\beta\cdot L_{lb}))$$

$$-[1/2\cdot e^{-\beta\cdot(L_{span}-L_{lb})}\cdot(\sin(\beta\cdot(L_{span}-L_{lb}))+\cos(\beta\cdot(L_{span}-L_{lb}))-1)$$

$$+e^{-\beta\cdot L_{span}}\cdot(\sin(\beta\cdot L_{span})+\cos(\beta\cdot L_{span})-\cos(\beta\cdot L_{lb}))$$

$$+1/2\cdot e^{-\beta\cdot(L_{span}+L_{lb})}\cdot(\sin(\beta\cdot(L_{span}+L_{lb}))+\cos(\beta\cdot(L_{span}+L_{lb}))-1)] \quad \text{(B.13)}$$

Using the notation of equations B.10, the deflection at point *M* is given by

$$y_M = \frac{F\cdot\beta\cdot dx}{4\cdot k_{\Delta h_w;2D}}\cdot[1+f_1(\beta\cdot L_{lb})-1/2\cdot f_1(\beta\cdot(L_{span}-L_{lb}))+1/2\cdot e^{-\beta\cdot(L_{span}-L_{lb})}-f_1(\beta\cdot L_{span})+e^{-\beta\cdot L_{span}}\cdot\cos(\beta\cdot L_{lb})$$

$$-1/2\cdot f_1(\beta\cdot(L_{span}+L_{lb}))+1/2\cdot e^{-\beta\cdot(L_{span}+L_{lb})}] \quad \text{(B.14)}$$

It is assumed that the cold-formed hat sections and first generation deck panels which are used in practice, belong to the category 'long beams' (section 4.3), according to the classification of Hetenyi *(1946)*. Long beams have a βL_{span} value such that the counter effect which the end-conditioning forces have on each other is a diminishing one. When investigating one end of the beam, it may be assumed that the other end is infinitely far away. In other words, βL_{span} is so large that $f_i(\beta L_{span})$ can be taken zero in all formulae. Hence $f_i(\beta x)$ in which $x > \beta L_{span}$ can also be taken zero. Therefore equation B.14 may be reduced to

$$y_M = \frac{F \cdot \beta \cdot dx}{4 \cdot k_{\Delta h_w;2D}} \cdot [1 + f_1(\beta \cdot L_{fb}) - 1/2 \cdot f_1(\beta \cdot (L_{span} - L_{fb})) + 1/2 \cdot e^{-\beta \cdot (L_{span} - L_{fb})}]$$

$$- 1/2 \cdot f_1(\beta \cdot (L_{span} + L_{fb})) + 1/2 \cdot e^{-\beta \cdot (L_{span} + L_{fb})}] \qquad \text{(B.15)}$$

The web crippling stiffness in the beam on elastic foundation model is defined as

$$k_{\Delta h_w} = \frac{F}{y_M}$$

Using equation B.14 and substituting equation B.5 into B.14, the web crippling stiffness can be expressed as

$$k_{\Delta h_w} = \frac{\sqrt[4]{1024 \cdot EI \cdot (\frac{k_{\Delta h_w;2D}}{dx})^3}}{1 + f_1(\beta \cdot L_{fb}) - 1/2 \cdot f_1(\beta \cdot (L_{span} - L_{fb})) + 1/2 \cdot e^{-\beta \cdot (L_{span} - L_{fb})}} \qquad \text{(B.16)}$$

B.3 *Derivation of the flexural rigidity of a beam in the beam on elastic foundation model*

In the beam on elastic foundation model the beam is idealized to consist of the top flange and part of the web, as in figure B.4.

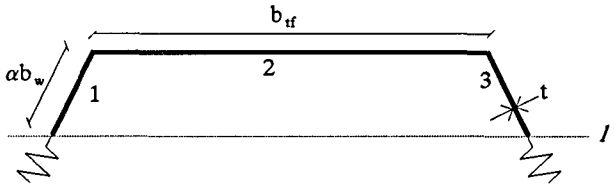

Figure B.4: *Idealization of the beam on an elastic foundation*

To calculate the flexural rigidity *EI* of the beam in figure B.4, the distance between line *l* and the centre of gravity of the beam, z, needs to be determined first. Dividing the beam into three pieces, the centre of gravity can be found by solving

$$\sum_{i=1}^{3} d_i \cdot A_i = z \cdot \sum_{i=1}^{3} A_i \tag{B.17}$$

in which d_i represents the distance between the centre of gravity of part i and line l.
For the beam in figure B.4 equation B.17 can be specified as

$$t \cdot b_{tf} \cdot (\alpha \cdot b_w \cdot \sin\theta_w + 1/2 \cdot t) + \alpha^2 \cdot b_w^2 \cdot \sin\theta_w \cdot t = z \cdot t \cdot (b_{tf} + 2 \cdot \alpha \cdot b_w)$$

from which it follows that

$$z = \frac{\alpha^2 \cdot b_w^2 \cdot \sin\theta_w + b_{tf} \cdot (\alpha \cdot b_w \cdot \sin\theta_w + 1/2 \cdot t)}{b_{tf} + 2 \cdot \alpha \cdot b_w} \tag{B.18}$$

Now, the moment of inertia I, can be calculated using the same division of the beam into three pieces and is given by

$$I = \sum_{i=1}^{3} (I_i + a_i^2 \cdot A_i) \tag{B.19}$$

in which a_i represents the distance between the centre of gravity of part i and the centre of gravity of the beam itself and in which I_i is defined to be the moment of inertia of the centre line of piece i that is parallel to line l. For the parts 1 and 3 I_i can be calculated as *(Gere & Timoshenko, 1987)*

$$I_1 = I_3 = t \cdot \alpha \cdot b_w \cdot [\frac{\alpha^2 \cdot b_w^2 + t^2}{24} - \frac{\cos 2\theta_w \cdot (\alpha^2 \cdot b_w^2 - t^2)}{24} + \frac{t \cdot \alpha \cdot b_w \cdot \sin 2\theta_w}{4}] \tag{B.20}$$

Using equation B.19 and equation B.20 it follows for the beam of figure B.4 that

$$I = \frac{b_{tf} \cdot t^3}{12} + t \cdot \alpha \cdot b_w \cdot [\frac{\alpha^2 \cdot b_w^2 + t^2}{12} - \frac{\cos 2\theta_w \cdot (\alpha^2 \cdot b_w^2 - t^2)}{12} + \frac{t \cdot \alpha \cdot b_w \cdot \sin 2\theta_w}{2}]$$

$$+ b_{tf} \cdot t \cdot (\alpha \cdot b_w \cdot \sin\theta_w + 1/2 \cdot t - z)^2 + 2 \cdot \alpha \cdot b_w \cdot t \cdot (1/2 \cdot \alpha \cdot b_w \cdot \sin\theta - z)^2 \tag{B.21}$$

After substitution of equation B.18 into equation B.21, the flexural rigidity can be expressed as

$$EI = E \cdot [\frac{b_{tf} \cdot t^3}{12} + t \cdot \alpha \cdot b_w \cdot [\frac{\alpha^2 \cdot b_w^2 + t^2}{12} - \frac{\cos 2\theta_w \cdot (\alpha^2 \cdot b_w^2 - t^2)}{12} + \frac{t \cdot \alpha \cdot b_w \cdot \sin 2\theta_w}{2}]$$

$$+ b_{tf} \cdot t \cdot (\frac{\alpha^2 \cdot b_w^2 \cdot \sin\theta_w + t \cdot \alpha \cdot b_w}{b_{tf} + 2 \cdot \alpha \cdot b_w})^2 + \frac{t \cdot \alpha \cdot b_w}{2} \cdot (\frac{b_{tf} \cdot \alpha \cdot b_w \cdot \sin\theta_w + t \cdot b_{tf}}{b_{tf} + 2 \cdot \alpha \cdot b_w})^2] \tag{B.22}$$

Appendix C

The derivation of the factor n for both hat sections and first generation deck panels is described in this appendix. A detailed description of the derivation of the energy model in case of several kinematical admissible trial functions is also given here.

C.1 Derivation of n for hat sections

According to section 5.4 it is assumed that the quotient of the maximum deflection of the top flange w_1 and the web w_2 equals a factor n that is a function of the geometrical dimensions of the member. Due to the fact that both w_1 and w_2 are located at the centre of the member and lie within the same cross-section, only the geometrical dimensions of that cross-section are involved in a description of n. The cross-section at the centre of the member was already schematised properly in the derivation of the portal frame model. Hence, an expression for n can be found using the mechanical schematisation of the two-dimensional portal frame model. The underlying assumptions to this schematisation are stated in section 3.2 and assumed to hold here too, for the same reasons. The mechanical schematisation in case of hat sections is given in figure C.1.

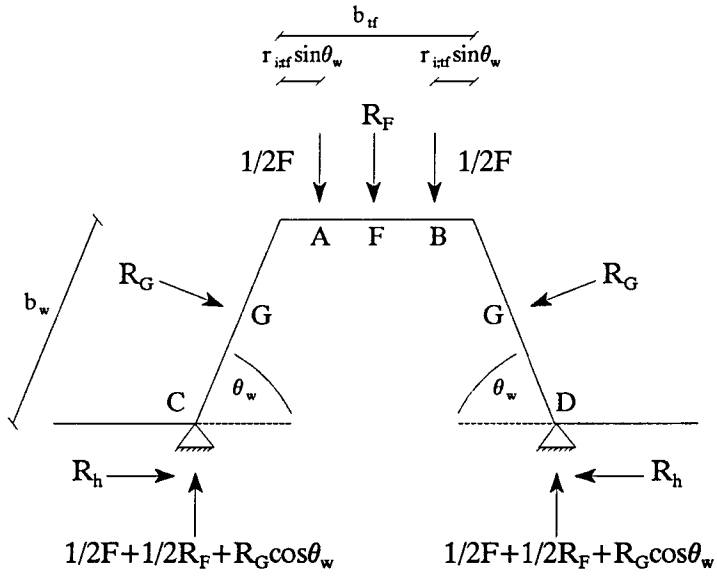

Figure C.1: *Portal frame schematisation in the derivation of n for hat sections*

In this model n is defined to be

$$n = \left|\frac{w_1}{w_2}\right| = \left|\frac{w_F}{w_G}\right| \tag{C.1}$$

in which w_F and w_G represent the displacement perpendicular to the top flange at point F and perpendicular to the web at point G respectively (figure C.1). The displacement of F and G can be calculated by introducing

two fictive forces R_F and R_G that both equal zero, as in figure C.1. Now, Castigliano's law (appendix A.1) states that

$$\frac{\partial W}{\partial R_F} = w_F \tag{C.2}$$

and

$$\frac{\partial W}{\partial R_G} = w_G \tag{C.3}$$

and w_F and w_G can be derived similar to w_A in appendix A.1.

The internal work W of the portal frame of figure C.1 needs to be determined first. Due to symmetry the portal frame may be divided in five different continuous beams that all appear twice in the portal frame itself, as shown in figure C.2.

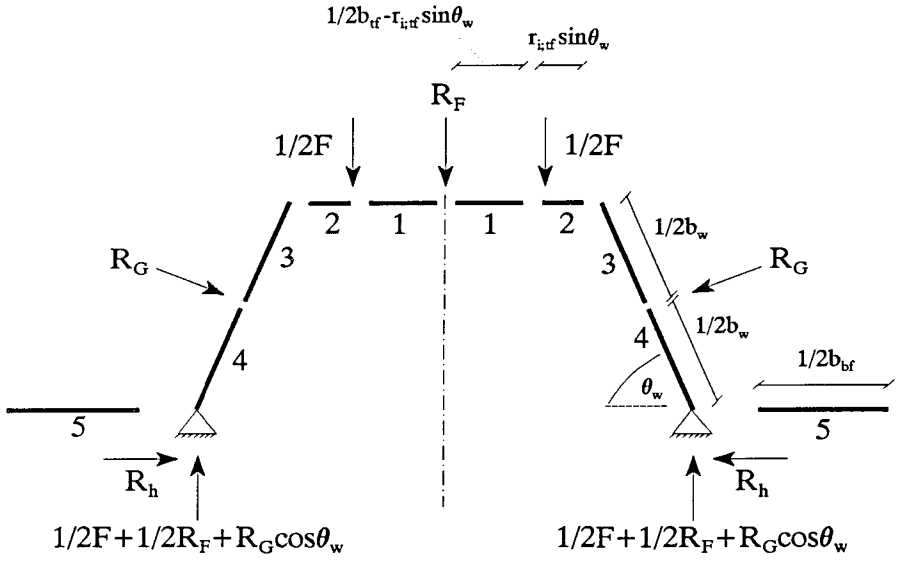

Figure C.2: *Division of portal frame into six different beams*

Note that the vertical reaction forces at the supports have a magnitude of $\frac{1}{2}\cdot F+\frac{1}{2}\cdot R_F+R_G\cdot\cos\theta_w$ due to symmetry.

The acting forces and bending moments on the ends of each beam can be determined from the overall equilibrium of the portal frame and are given in figure C.3.

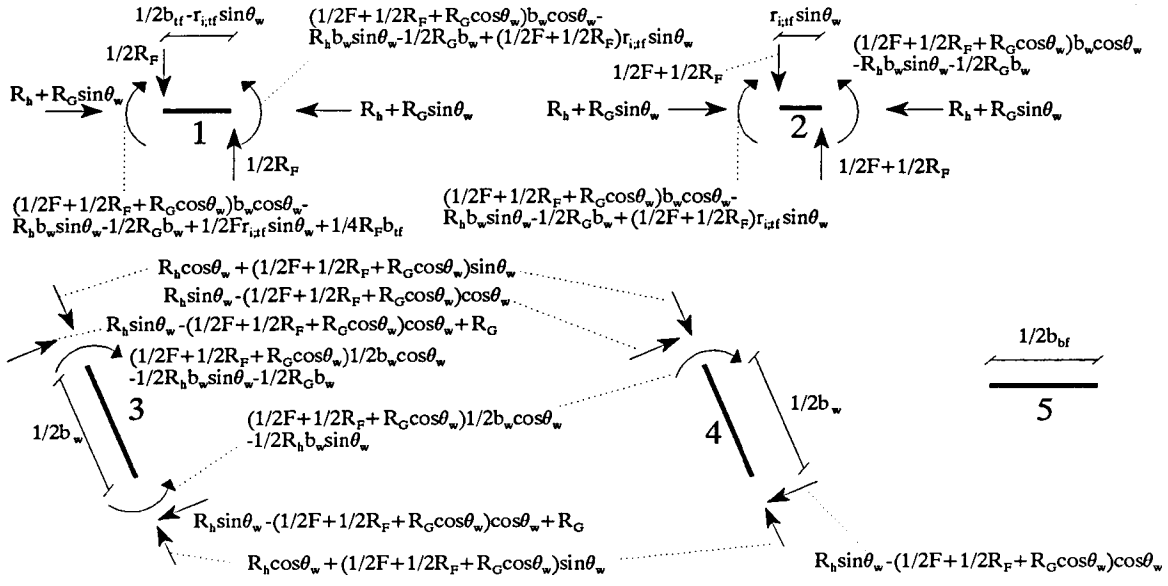

Figure C.3: Acting forces and bending moments on the different beams (hat sections)

The internal work of the portal frame can be calculated by summarizing the internal work of the five different continuous beams of figure C.3 and double it, as each beam appears twice in the portal frame. Using equation A.4 (appendix A.1) and gathering the terms of beam 3 and 4 under the same integral, the internal work of the portal frame is specified as

$$W = \int_0^{1/2 \cdot b_w} [2 \cdot \frac{(R_h \cdot \cos\theta_w + (1/2 \cdot F + 1/2 \cdot R_F + R_G \cdot \cos\theta_w) \cdot \sin\theta_w)^2}{EA}$$

$$+ \frac{(R_h \cdot x \cdot \sin\theta_w - x \cdot \cos\theta_w \cdot (1/2 \cdot F + 1/2 \cdot R_F + R_G \cdot \cos\theta_w))^2}{EI}$$

$$+ \frac{(R_h \cdot x \cdot \sin\theta_w - (1/2 \cdot F + 1/2 \cdot R_F + R_G \cdot \cos\theta_w) \cdot (x \cdot \cos\theta_w + 1/2 \cdot b_w \cdot \cos\theta_w) + R_G \cdot x + 1/2 \cdot R_h \cdot b_w \cdot \sin\theta_w)^2}{EI}] dx$$

$$+ \int_0^{r_{i,tf} \cdot \sin\theta_w} [\frac{(b_w \cdot \cos\theta_w \cdot (1/2 \cdot F + 1/2 \cdot R_F + R_G \cdot \cos\theta_w) - 1/2 \cdot R_G \cdot b_w - R_h \cdot b_w \cdot \sin\theta_w + 1/2 \cdot x \cdot (F + R_F))^2}{EI}$$

$$+ \frac{(R_h + R_G \cdot \sin\theta_w)^2}{EA}] dx + \int_0^{1/2 \cdot b_{tf} - r_{i,tf} \cdot \sin\theta_w} [\frac{(R_h + R_G \cdot \sin\theta_w)^2}{EA}$$

$$+\frac{(b_w\cdot\cos\theta_w\cdot(1/2\cdot F+1/2\cdot R_F+R_G\cdot\cos\theta_w)-b_w\cdot(1/2\cdot R_G+R_h\cdot\sin\theta_w)+1/2\cdot(r_{i;tf}\cdot\sin\theta_w\cdot(F+R_F)+R_F\cdot x))^2}{EI}]\,dx \quad \text{(C.4)}$$

In the derivation of w_F and w_G the reaction force at the supports R_h needs to be calculated first. The reaction force R_h can be determined just as this force was calculated in appendix A.1. Hence, using equations A.7 and A.8, the derivation of R_h is established by solving

$$\frac{\partial W}{\partial R_h}=0=2\cdot\int_0^{1/2\cdot b_w}[2\cdot\frac{\cos\theta_w\cdot(R_h\cdot\cos\theta_w+(1/2\cdot F+1/2\cdot R_F+R_G\cdot\cos\theta_w)\cdot\sin\theta_w)}{EA}$$

$$+\frac{x\cdot\sin\theta_w(R_h\cdot x\cdot\sin\theta_w-x\cdot\cos\theta_w\cdot(1/2\cdot F+1/2\cdot R_F+R_G\cdot\cos\theta_w))+1/2\cdot R_h\cdot b_w\cdot\sin^2\theta_w\cdot(x+1/2\cdot b_w)}{EI}$$

$$+\frac{\sin\theta_w\cdot(x+1/2\cdot b_w)\cdot(R_h\cdot x\cdot\sin\theta_w-(1/2\cdot F+1/2\cdot R_F+R_G\cdot\cos\theta_w)\cdot(x\cdot\cos\theta_w+1/2\cdot b_w\cdot\cos\theta_w)+R_G\cdot x)}{EI}]\,dx$$

$$+2\cdot\int_0^{r_{i;tf}\cdot\sin\theta_w}[\frac{b_w\cdot\sin\theta_w\cdot(1/2\cdot R_G\cdot b_w+R_h\cdot b_w\cdot\sin\theta_w-b_w\cdot\cos\theta_w\cdot(1/2\cdot F+1/2\cdot R_F+R_G\cdot\cos\theta_w)-1/2\cdot x\cdot(F+R_F))}{EI}$$

$$+\frac{R_h+R_G\cdot\sin\theta_w}{EA}]\,dx+2\cdot\int_0^{1/2\cdot b_{tf}-r_{i;tf}\cdot\sin\theta_w}[\frac{(R_h+R_G\cdot\sin\theta_w)}{EA}-\frac{1/2\cdot b_w\cdot\sin\theta_w\cdot(r_{i;tf}\cdot\sin\theta_w\cdot(F+R_F)+R_F\cdot x)}{EI}$$

$$+\frac{b_w\cdot\sin\theta_w\cdot(1/2\cdot R_G\cdot b_w+R_h\cdot b_w\cdot\sin\theta_w-b_w\cdot\cos\theta_w\cdot(1/2\cdot F+1/2\cdot R_F+R_G\cdot\cos\theta_w))}{EI}]\,dx \quad \text{(C.5)}$$

From equation C.5 it can be derived that

$$R_h=\frac{R_F\cdot\sin\theta_w\cdot b_w\cdot(EA\cdot(3\cdot b_{tf}^2+b_w\cdot\cos\theta_w\cdot(12\cdot b_{tf}+8\cdot b_w))-24\cdot EI\cdot\cos\theta_w)}{8\cdot(EA\cdot b_w^2\cdot\sin^2\theta_w\cdot(2\cdot b_w+3\cdot b_{tf})+3\cdot EI\cdot(b_{tf}+2\cdot b_w\cdot\cos^2\theta_w))}$$

$$+\frac{R_G\cdot\sin\theta_w\cdot(EA\cdot b_w\cdot(1/4\cdot b_w^2+b_w\cdot\cos2\theta_w\cdot(2/3\cdot b_w+b_{tf}))-2\cdot EI\cdot(b_{tf}+b_w(1+\cos2\theta_w)))}{2/3\cdot(EA\cdot b_w^2\cdot\sin^2\theta_w\cdot(2\cdot b_w+3\cdot b_{tf})+3\cdot EI\cdot(b_{tf}+2\cdot b_w\cdot\cos^2\theta_w))}$$

$$+\frac{F\cdot b_w\cdot\sin\theta_w\cdot(EA\cdot(r_{i;tf}\cdot\sin\theta_w\cdot(b_{tf}-r_{i;tf}\cdot\sin\theta_w)+b_{tf}\cdot b_w\cdot\cos\theta_w+2/3\cdot b_w^2\cdot\cos\theta_w)-2\cdot EI\cdot\cos\theta_w)}{2/3\cdot(EA\cdot b_w^2\cdot\sin^2\theta_w\cdot(2\cdot b_w+3\cdot b_{tf})+3\cdot EI\cdot(b_{tf}+2\cdot b_w\cdot\cos^2\theta_w))} \quad \text{(C.6a)}$$

For rather regular hat sections with $t<<b_{tf}$ and $t<<b_w$, and with $\theta_w\geq5°$, the deformations due to axial forces are negligible compared to the bending deformations and equation C.6 might be simplified to

$$R_h = \frac{R_G \cdot b_w \cdot (1/4 \cdot b_w + \cos 2\theta_w \cdot (b_{tf} + 2/3 \cdot b_w)) + F \cdot (r_{i;tf} \cdot \sin\theta_w \cdot (b_{tf} - r_{i;tf} \cdot \sin\theta_w) + b_w \cdot \cos\theta_w \cdot (b_{tf} + 2/3 \cdot b_w))}{2/3 \cdot b_w \cdot \sin\theta_w \cdot (3 \cdot b_{tf} + 2 \cdot b_w)}$$

$$+ \frac{R_F \cdot (1/4 \cdot b_{tf}^2 + b_w \cdot \cos\theta_w \cdot (b_{tf} + 2/3 \cdot b_w))}{2/3 \cdot b_w \cdot \sin\theta_w \cdot (3 \cdot b_{tf} + 2 \cdot b_w)} \qquad \text{(C.6b)}$$

Taking into consideration that both R_F and R_G equal zero, equations C.6 correspond to equations A.11 in appendix A.1.

Using equation C.2 the maximum deflection of the top flange w_F can be derived by differentiating equation C.4 with respect to R_F, resulting in

$$w_F = \int_0^{1/2 \cdot b_w} [\frac{2 \cdot \sin\theta_w \cdot (R_h \cdot \cos\theta_w + (1/2 \cdot F + 1/2 \cdot R_F + R_G \cdot \cos\theta_w) \cdot \sin\theta_w)}{EA}$$

$$+ \frac{x \cdot \cos\theta_w \cdot (x \cdot \cos\theta_w \cdot (1/2 \cdot F + 1/2 \cdot R_F + R_G \cdot \cos\theta_w) - R_h \cdot x \cdot \sin\theta_w)}{EI}$$

$$+ \frac{(x \cdot \cos\theta_w + 1/2 \cdot b_w \cdot \cos\theta_w) \cdot ((1/2 \cdot F + 1/2 \cdot R_F + R_G \cdot \cos\theta_w) \cdot (x \cdot \cos\theta_w + 1/2 \cdot b_w \cdot \cos\theta_w) - R_h \cdot x \cdot \sin\theta_w)}{EI}$$

$$- \frac{(x \cdot \cos\theta_w + 1/2 \cdot b_w \cdot \cos\theta_w) \cdot (R_G \cdot x + 1/2 \cdot R_h \cdot b_w \cdot \sin\theta_w)}{EI}] \, dx$$

$$+ \int_0^{r_{i;tf} \cdot \sin\theta_w} [\frac{(b_w \cdot \cos\theta_w + x) \cdot (b_w \cdot \cos\theta_w \cdot (1/2 \cdot F + 1/2 \cdot R_F + R_G \cdot \cos\theta_w) - 1/2 \cdot R_G \cdot b_w - R_h \cdot b_w \cdot \sin\theta_w + 1/2 \cdot x \cdot (F + R_F))}{EI}$$

$$+ \int_0^{1/2 \cdot b_{tf} - r_{i;tf} \cdot \sin\theta_w} [\frac{(b_w \cdot \cos\theta_w + r_{i;tf} \cdot \sin\theta_w + x) \cdot (1/2 \cdot r_{i;tf} \cdot \sin\theta_w \cdot (F + R_F) + 1/2 \cdot R_F \cdot x)}{EI}$$

$$+ \frac{(b_w \cdot \cos\theta_w + r_{i;tf} \cdot \sin\theta_w + x) \cdot (b_w \cdot \cos\theta_w \cdot (1/2 \cdot F + 1/2 \cdot R_F + R_G \cdot \cos\theta_w) - 1/2 \cdot R_G \cdot b_w - R_h \cdot b_w \cdot \sin\theta_w)}{EI}] \, dx \qquad \text{(C.7)}$$

Taking into consideration that both R_F and R_G equal zero, equation C.7 after integration becomes

$$w_F = \frac{EA \cdot F \cdot b_w^2 \cdot (4 \cdot b_w + 6 \cdot b_{tf}) + 24 \cdot EI \cdot R_h \cdot b_w \cdot \sin 2\theta_w + 3 \cdot EA \cdot F \cdot b_{tf}^2 \cdot r_{i;tf} \cdot \sin\theta_w}{48 \cdot EA \cdot EI}$$

$$+\frac{F\cdot(b_w\cdot\cos\theta_w\cdot(3\cdot b_{tf}^2+12\cdot r_{i;tf}\cdot\sin\theta_w\cdot(b_{tf}-r_{i;tf}\cdot\sin\theta_w))+4\cdot r_{i;tf}^3\cdot\sin^3\theta_w+b_w^2\cdot\cos 2\theta_w\cdot(4\cdot b_w+6\cdot b_{tf}))}{48\cdot EI}$$

$$+\frac{12\cdot EI\cdot F\cdot b_w\cdot(1-\cos 2\theta_w)-6\cdot EA\cdot R_h\cdot b_w\cdot(\sin\theta_w\cdot b_{tf}^2+b_w\cdot\sin 2\theta_w\cdot(4/3\cdot b_w+2\cdot b_{tf}))}{48\cdot EA\cdot EI} \qquad \text{(C.8)}$$

Similarly, the maximum deflection of the web w_G is derived by differentiating equation C.4 with respect to R_G, resulting in

$$w_G=\int_0^{1/2\cdot b_w}[\frac{4\cdot\cos\theta_w\cdot\sin\theta_w\cdot(\sin\theta_w\cdot(1/2\cdot F+1/2\cdot R_F+R_G\cdot\cos\theta_w)+\cos\theta_w\cdot R_h)}{EA}$$

$$+\frac{2\cdot x\cdot\cos^2\theta_w\cdot(x\cdot\cos\theta_w\cdot(1/2\cdot F+1/2\cdot R_F+R_G\cdot\cos\theta_w)-R_h\cdot x\cdot\sin\theta_w)}{EI}$$

$$+\frac{2\cdot(\cos\theta_w\cdot(x\cdot\cos\theta_w+1/2\cdot b_w\cdot\cos\theta_w)-x)\cdot(1/2\cdot F+1/2\cdot R_F+R_G\cdot\cos\theta_w)\cdot(x\cdot\cos\theta_w+1/2\cdot b_w\cdot\cos\theta_w)}{EI}$$

$$-\frac{2\cdot(\cos\theta_w\cdot(x\cdot\cos\theta_w+1/2\cdot b_w\cdot\cos\theta_w)-x)\cdot(R_G\cdot x+R_h\cdot\sin\theta_w\cdot(1/2\cdot b_w+x))}{EI}]\,dx$$

$$+\int_0^{r_{i;tf}\cdot\sin\theta_w}[\frac{2\cdot b_w\cdot(\cos^2\theta_w-1/2)\cdot(b_w\cdot\cos\theta_w\cdot(1/2\cdot F+1/2\cdot R_F+R_G\cdot\cos\theta_w)-1/2\cdot R_G\cdot b_w)}{EI}$$

$$+\frac{2\cdot b_w\cdot(\cos^2\theta_w-1/2)\cdot(1/2\cdot x\cdot(F+R_F)-R_h\cdot b_w\cdot\sin\theta_w)}{EI}]\,dx+\int_0^{1/2\cdot b_{tf}}[\frac{2\cdot\sin\theta_w\cdot(R_h+R_G\cdot\sin\theta_w)}{EA}]\,dx$$

$$+\int_0^{1/2\cdot b_{tf}-r_{i;tf}\cdot\sin\theta_w}[\frac{2\cdot b_w\cdot(\cos^2\theta_w-1/2)\cdot(b_w\cdot\cos\theta_w\cdot(1/2\cdot F+1/2\cdot R_F+R_G\cdot\cos\theta_w)-1/2\cdot R_G\cdot b_w)}{EI}$$

$$+\frac{2\cdot b_w\cdot(\cos^2\theta_w-1/2)\cdot(1/2\cdot r_{i;tf}\cdot\sin\theta_w\cdot(F+R_F)+1/2\cdot R_F\cdot x-R_h\cdot b_w\cdot\sin\theta_w)}{EI}]\,dx \qquad \text{(C.9)}$$

Taking into consideration that both R_F and R_G equal zero, it may be verified that

$$w_G=\frac{F\cdot b_w\cdot(b_w\cdot(7\cdot b_w\cdot\cos\theta_w+6\cdot b_{tf})+12\cdot r_{i;tf}\cdot\sin\theta_w\cdot\cos 2\theta_w\cdot(b_{tf}-r_{i;tf}\cdot\sin\theta_w)+b_w\cdot\cos 3\theta_w\cdot(4\cdot b_w+6\cdot b_{tf}))}{48\cdot EI}$$

$$+\frac{R_h \cdot b_w \cdot (b_w \cdot \sin\theta_w \cdot (b_w + 6 \cdot b_{tf}) - b_w \cdot \sin 3\theta_w \cdot (4 \cdot b_w + 6 \cdot b_{tf}))}{24 \cdot EI}$$

$$+\frac{F \cdot b_w \cdot (\cos\theta_w - \cos 3\theta_w) + 2 \cdot R_h \cdot (\sin\theta_w \cdot (b_w + 2 \cdot b_{tf}) + b_w \cdot \sin 3\theta_w)}{4 \cdot EA} \qquad \text{(C.10)}$$

For rather regular hat sections with $t << b_{tf}$ and $t << b_w$, and with $\theta_w \geq 5°$, the deformations due to axial forces are negligible compared to the bending deformations. Neglecting the deformations due to axial forces and substituting equations C.6b, C.8 and C.10 into equation C.1 while noting that R_F and R_G equal zero, n can be specified as

$$n = \left| \frac{r_{i;tf} \cdot \sin\theta_w \cdot (r_{i;tf} \cdot \sin\theta_w \cdot (9 \cdot b_{tf}^2 - r_{i;tf} \cdot \sin\theta_w \cdot (8 \cdot b_w + 12 \cdot b_{tf})) + 6 \cdot b_w \cdot b_{tf}^2)}{9 \cdot b_w^2 \cdot r_{i;tf} \cdot \sin\theta_w \cdot (r_{i;tf} \cdot \sin\theta_w - b_{tf})} \right| \qquad \text{(C.11)}$$

C.2 *Derivation of n for first generation deck panels*

The factor n for first generation deck panels is derived in the same way as it was derived for hat sections in appendix C.1. Moreover, its derivation is analogous to the derivation of the web crippling deformation in the portal frame model for first generation deck panels that is treated in appendix A.2. A first generation deck panel can be thought of as a series of hat sections that are tied together at the unloaded flanges. Each of these hat sections is loaded similarly and shows the same deformation pattern. Obviously, this implies that their maximum deflections of the top flange and webs are the same also. Hence, only one such a hat section need to be taken into account explicitly. The mechanical schematisation of the cross-section of such a hat section out of which the first generation deck panels are composed is given in figure C.4.

The bending moment M_E and the horizontal reaction force R_E maintain the continuity of the deck panel. The portal frame is twofold statically undetermined and M_E and R_E can be derived using Castigliano's law, whereafter w_F and w_G can be calculated with that same law.

The portal frame can be derived in the same way as it was derived in the derivation of n for hat sections (figure C.2) and the vertical reaction forces at the supports have a magnitude of $\frac{1}{2} \cdot F + \frac{1}{2} \cdot R_F + R_G \cdot \cos\theta_w$ due to symmetry.

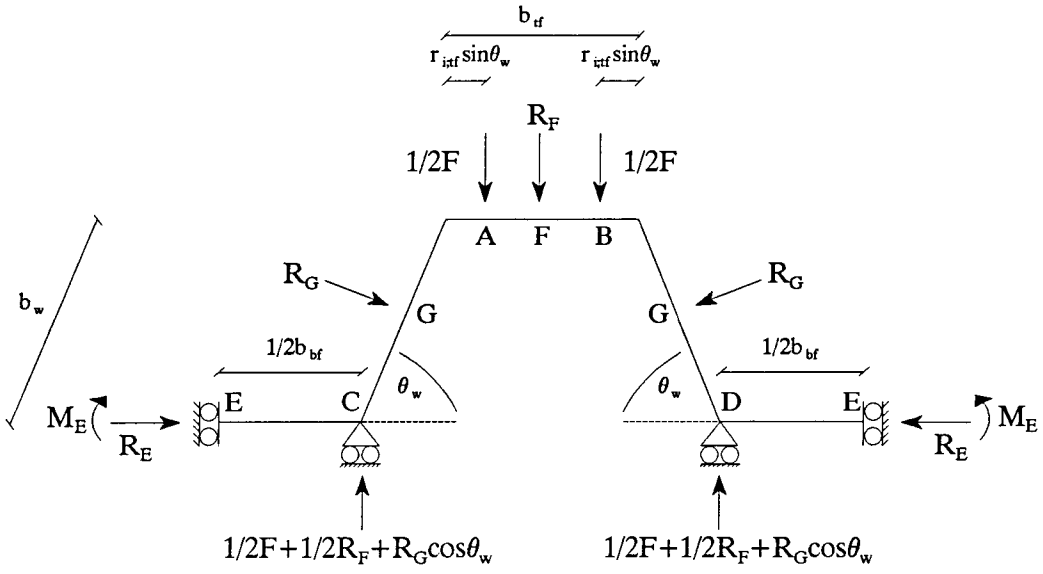

Figure C.4: *Portal frame schematisation in the derivation of n for first generation deck panels*

The acting forces and bending moments on the ends of each of the five beams can be derived from the overall equilibrium and are given in figure C.5.

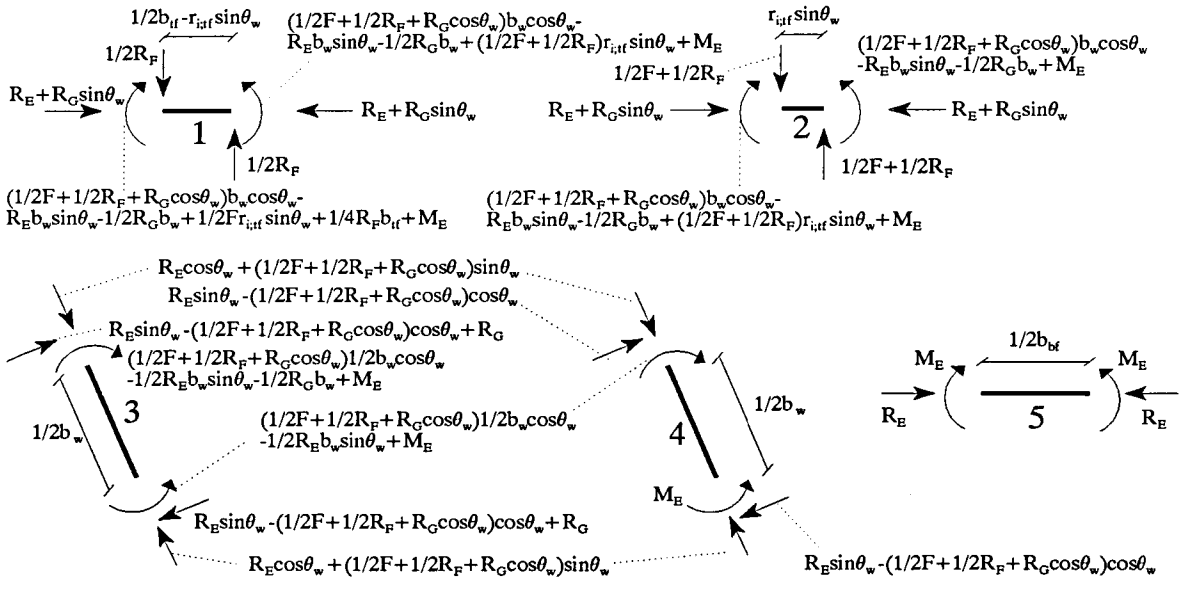

Figure C.5: *Acting forces and bending moments on the different beams (first generation deck panels)*

Since each beam appears twice in the portal frame, the internal work of the frame can be calculated by summarizing the internal work of each beam in figure C.5 and double it. Using equation A.4 and gathering the terms of the beams 3 and 4, this results in

$$W=\int_0^{1/2\cdot b_{bf}}\left[\frac{R_E^2}{EA}+\frac{M_E^2}{EI}\right]dx+\int_0^{1/2\cdot b_w}\left[2\cdot\frac{(R_E\cdot\cos\theta_w+(1/2\cdot F+1/2\cdot R_F+R_G\cdot\cos\theta_w)\cdot\sin\theta_w)^2}{EA}\right.$$

$$+\frac{(R_E\cdot x\cdot\sin\theta_w-x\cdot\cos\theta_w\cdot(1/2\cdot F+1/2\cdot R_F+R_G\cdot\cos\theta_w)-M_E)^2}{EI}$$

$$\left.+\frac{((x+1/2\cdot b_w)\cdot(R_E\cdot\sin\theta_w-\cos\theta_w\cdot(1/2\cdot F+1/2\cdot R_F+R_G\cdot\cos\theta_w))+R_G\cdot x-M_E)^2}{EI}\right]dx$$

$$+\int_0^{r_{i,tf}\cdot\sin\theta_w}\left[\frac{(b_w\cdot\cos\theta_w\cdot(1/2\cdot F+1/2\cdot R_F+R_G\cdot\cos\theta_w)-1/2\cdot R_G\cdot b_w-R_E\cdot b_w\cdot\sin\theta_w+1/2\cdot x\cdot(F+R_F)+M_E)^2}{EI}\right.$$

$$\left.+\frac{(R_E+R_G\cdot\sin\theta_w)^2}{EA}\right]dx+\int_0^{1/2\cdot b_{tf}-r_{i,tf}\cdot\sin\theta_w}\left[\frac{(R_E+R_G\cdot\sin\theta_w)^2}{EA}\right.$$

$$\left.+\frac{(b_w\cdot\cos\theta_w\cdot(1/2\cdot F+1/2\cdot R_F+R_G\cdot\cos\theta_w)-b_w\cdot(1/2\cdot R_G+R_E\cdot\sin\theta_w)+1/2\cdot(r_{i,tf}\cdot\sin\theta_w\cdot(F+R_F)+R_F\cdot x)+M_E)^2}{EI}\right]dx \tag{C.12}$$

Now, R_E and M_E can be determined, using equations A.20 and C.12. Hence, R_E can be calculated by solving

$$\frac{\partial W}{\partial R_E}=0=2\cdot\int_0^{1/2\cdot b_{bf}}\frac{R_E}{EA}dx+2\cdot\int_0^{1/2\cdot b_w}\left[2\cdot\frac{\cos\theta_w\cdot(R_E\cdot\cos\theta_w+(1/2\cdot F+1/2\cdot R_F+R_G\cdot\cos\theta_w)\cdot\sin\theta_w)}{EA}\right.$$

$$+\frac{x\cdot\sin\theta_w(R_E\cdot x\cdot\sin\theta_w-x\cdot\cos\theta_w\cdot(1/2\cdot F+1/2\cdot R_F+R_G\cdot\cos\theta_w)-M_E)+1/2\cdot R_E\cdot b_w\cdot\sin^2\theta_w\cdot(x+1/2\cdot b_w)}{EI}$$

$$\left.+\frac{\sin\theta_w\cdot(x+1/2\cdot b_w)\cdot(R_E\cdot x\cdot\sin\theta_w-\cos\theta_w\cdot(x+1/2\cdot b_w)\cdot(1/2\cdot F+1/2\cdot R_F+R_G\cdot\cos\theta_w)+R_G\cdot x-M_E)}{EI}\right]dx$$

$$+2\cdot\int_0^{r_{i,tf}\cdot\sin\theta_w}\left[\frac{b_w\cdot\sin\theta_w\cdot(1/2\cdot R_G\cdot b_w+R_E\cdot b_w\cdot\sin\theta_w-b_w\cdot\cos\theta_w\cdot(1/2\cdot F+1/2\cdot R_F+R_G\cdot\cos\theta_w)-1/2\cdot x\cdot(F+R_F))}{EI}\right.$$

$$\left.-\frac{b_w\cdot\sin\theta_w\cdot M_E}{EI}+\frac{R_E+R_G\cdot\sin\theta_w}{EA}\right]dx+2\cdot\int_0^{1/2\cdot b_{tf}-r_{i,tf}\cdot\sin\theta_w}\left[\frac{(R_h+R_G\cdot\sin\theta_w)}{EA}-\frac{1/2\cdot b_w\cdot r_{i,tf}\cdot\sin^2\theta_w\cdot(F+R_F)}{EI}\right.$$

$$\left.+\frac{b_w\cdot\sin\theta_w\cdot(1/2\cdot R_G\cdot b_w+R_E\cdot b_w\cdot\sin\theta_w-1/2\cdot R_F\cdot x-b_w\cdot\cos\theta_w\cdot(1/2\cdot F+1/2\cdot R_F+R_G\cdot\cos\theta_w)-M_E)}{EI}\right]dx \tag{C.13}$$

From equation C.13 it can be derived that

$$R_E = \frac{F \cdot b_w \cdot \sin\theta_w \cdot (EA \cdot (r_{i;tf} \cdot \sin\theta_w \cdot (b_{tf} - r_{i;tf} \cdot \sin\theta_w) + b_{tf} \cdot b_w \cdot \cos\theta_w + 2/3 \cdot b_w^2 \cdot \cos\theta_w) - 2 \cdot EI \cdot \cos\theta_w)}{2/3 \cdot (EA \cdot b_w^2 \cdot \sin^2\theta_w \cdot (2 \cdot b_w + 3 \cdot b_{tf}) + 3 \cdot EI \cdot (b_{bf} + b_{tf} + 2 \cdot b_w \cdot \cos^2\theta_w))}$$

$$+ \frac{R_G \cdot \sin\theta_w \cdot (EA \cdot b_w \cdot (1/4 \cdot b_w^2 + b_w \cdot \cos 2\theta_w \cdot (2/3 \cdot b_w + b_{tf})) - 2 \cdot EI \cdot (b_{tf} + b_w (1 + \cos 2\theta_w)))}{2/3 \cdot (EA \cdot b_w^2 \cdot \sin^2\theta_w \cdot (2 \cdot b_w + 3 \cdot b_{tf}) + 3 \cdot EI \cdot (b_{bf} + b_{tf} + 2 \cdot b_w \cdot \cos^2\theta_w))}$$

$$+ \frac{R_F \cdot \sin\theta_w \cdot b_w \cdot (EA \cdot (1/4 \cdot b_{tf}^2 + b_w \cdot \cos\theta_w \cdot (b_{tf} + 2/3 \cdot b_w)) - 2 \cdot EI \cdot \cos\theta_w) + 2 \cdot EA \cdot M_E \cdot b_w \cdot (b_w + b_{tf})}{2/3 \cdot (EA \cdot b_w^2 \cdot \sin^2\theta_w \cdot (2 \cdot b_w + 3 \cdot b_{tf}) + 3 \cdot EI \cdot (b_{bf} + b_{tf} + 2 \cdot b_w \cdot \cos^2\theta_w))} \qquad \text{(C.14a)}$$

For rather regular hat sections with $t << b_{tf}$ and $t << b_w$, and with $\theta_w \geq 5°$, the deformations due to axial forces are negligible compared to the bending deformations and equation C.14a might be simplified to

$$R_E = \frac{R_F \cdot (1/4 \cdot b_{tf}^2 + b_w \cdot \cos\theta_w \cdot (b_{tf} + 2/3 \cdot b_w)) + 2 \cdot M_E \cdot b_w \cdot (b_w + b_{tf})}{2/3 \cdot b_w \cdot \sin\theta_w \cdot (3 \cdot b_{tf} + 2 \cdot b_w)}$$

$$+ \frac{R_G \cdot b_w \cdot (1/4 \cdot b_w + \cos 2\theta_w \cdot (b_{tf} + 2/3 \cdot b_w)) + F \cdot (r_{i;tf} \cdot \sin\theta_w \cdot (b_{tf} - r_{i;tf} \cdot \sin\theta_w) + b_w \cdot \cos\theta_w \cdot (b_{tf} + 2/3 \cdot b_w))}{2/3 \cdot b_w \cdot \sin\theta_w \cdot (3 \cdot b_{tf} + 2 \cdot b_w)} \qquad \text{(C.14b)}$$

Taking into consideration that both R_F and R_G equal zero, equations C.14b correspond to equation A.22 in appendix A.1.

Similarly, using equation C.12, equation A.20b can be expressed as

$$\frac{\partial W}{\partial M_E} = 2 \cdot \int_0^{1/2 \cdot b_{bf}} \frac{M_E}{EI} dx + 2 \cdot \int_0^{1/2 \cdot b_w} [\frac{M_E - R_E \cdot x \cdot \sin\theta_w + x \cdot \cos\theta_w \cdot (1/2 \cdot F + 1/2 \cdot R_F + R_G \cdot \cos\theta_w)}{EI}$$

$$+ \frac{M_E - (x + 1/2 \cdot b_w) \cdot (R_E \cdot \sin\theta_w - (1/2 \cdot F + 1/2 \cdot R_F + R_G \cdot \cos\theta_w) \cdot (x + 1/2 \cdot b_w)) - R_G \cdot x}{EI}] dx$$

$$+ 2 \cdot \int_0^{r_{i;tf} \cdot \sin\theta_w} [\frac{b_w \cdot \cos\theta_w \cdot (1/2 \cdot F + 1/2 \cdot R_F + R_G \cdot \cos\theta_w) - 1/2 \cdot R_G \cdot b_w - R_E \cdot b_w \cdot \sin\theta_w + 1/2 \cdot x \cdot (F + R_F) + M_E}{EI}] dx$$

$$+ 2 \cdot \int_0^{1/2 \cdot b_{tf} - r_{i;tf} \cdot \sin\theta_w} [\frac{b_w \cdot (\cos\theta_w \cdot (1/2 \cdot F + 1/2 \cdot R_F + R_G \cdot \cos\theta_w) - 1/2 \cdot R_G - R_E \cdot \sin\theta_w)}{EI}$$

$$+ \frac{1/2 \cdot (r_{i;tf} \cdot \sin\theta_w \cdot (F + R_F) + R_F \cdot x) + M_E}{EI}] dx \qquad \text{(C.15)}$$

After integration M_E can be specified as

$$M_E = \frac{R_E \cdot b_w \cdot \sin\theta_w \cdot (b_w + b_{tf}) - F \cdot (1/2 \cdot b_w \cdot \cos\theta_w \cdot (b_w + b_{tf}) + 1/2 \cdot r_{i;tf} \cdot \sin\theta_w \cdot (b_{tf} - r_{i;tf} \cdot \sin\theta_w))}{(b_{bf} + 2 \cdot b_w + b_{tf})}$$

$$- \frac{R_F \cdot (1/8 \cdot b_{tf}^2 + 1/2 \cdot b_w \cdot \cos\theta_w \cdot (b_w + b_{tf})) + R_G \cdot b_w \cdot (1/4 \cdot b_w + 1/2 \cdot \cos 2\theta_w \cdot (b_w + b_{tf}))}{b_{bf} + 2 \cdot b_w + b_{tf}} \qquad \text{(C.16)}$$

in which R_F and R_G both equal zero. Equations C.14b and C.16 can be thought of as two equations with two unknown parameters R_E and M_E. After proper substitutions of these equations it follows that

$$R_E = \frac{F \cdot (b_w \cdot \cos\theta_w \cdot (b_{bf} \cdot (3 \cdot b_{tf} + 2 \cdot b_w) + b_w \cdot (2 \cdot b_{tf} + b_w)) - 3 \cdot r_{i;tf} \cdot \sin\theta_w \cdot (b_w + b_{bf}) \cdot (r_{i;tf} \cdot \sin\theta_w - b_{tf}))}{2 \cdot b_w \cdot \sin\theta_w \cdot (b_{bf} \cdot (3 \cdot b_{tf} + 2 \cdot b_w) + b_w \cdot (2 \cdot b_{tf} + b_w))} \qquad \text{(C.17a)}$$

and

$$M_E = - \frac{F \cdot r_{i;tf} \cdot b_w \cdot \sin\theta_w \cdot (r_{i;tf} \cdot \sin\theta_w - b_{tf})}{2 \cdot (b_{bf} \cdot (3 \cdot b_{tf} + 2 \cdot b_w) + b_w \cdot (2 \cdot b_{tf} + b_w))} \qquad \text{(C.17b)}$$

Using equation C.2 the maximum deflection of the top flange w_F is derived by differentiating the internal work (equation C.12) with respect to R_F, resulting in

$$w_F = \int_0^{1/2 \cdot b_w} [\frac{2 \cdot \sin\theta_w \cdot (R_E \cdot \cos\theta_w + \sin\theta_w \cdot (1/2 \cdot (F + R_F) + R_G \cdot \cos\theta_w))}{EA}$$

$$+ \frac{x \cdot \cos\theta_w \cdot (x \cdot \cos\theta_w \cdot (1/2 \cdot F + 1/2 \cdot R_F + R_G \cdot \cos\theta_w) - R_E \cdot x \cdot \sin\theta_w + M_E)}{EI}$$

$$+ \frac{\cos\theta_w \cdot (x + 1/2 \cdot b_w) \cdot (\cos\theta_w \cdot (x + 1/2 \cdot b_w) \cdot (1/2 \cdot F + 1/2 \cdot R_F + R_G \cdot \cos\theta_w) - R_E \cdot x \cdot \sin\theta_w)}{EI}$$

$$- \frac{\cos\theta_w \cdot (x + 1/2 \cdot b_w) \cdot (R_G \cdot x + 1/2 \cdot R_E \cdot b_w \cdot \sin\theta_w - M_E)}{EI}] \, dx$$

$$+ \int_0^{r_{i;tf} \cdot \sin\theta_w} [\frac{(b_w \cdot \cos\theta_w + x) \cdot (b_w \cdot \cos\theta_w \cdot (1/2 \cdot F + 1/2 \cdot R_F + R_G \cdot \cos\theta_w) - 1/2 \cdot R_G \cdot b_w - R_E \cdot b_w \cdot \sin\theta_w)}{EI}$$

$$+ \frac{(b_w \cdot \cos\theta_w + x) \cdot (1/2 \cdot x \cdot (F + R_F) + M_E)}{EI}] \, dx + \int_0^{1/2 \cdot b_{tf} - r_{i;tf} \cdot \sin\theta_w} [\frac{1/2 \cdot r_{i;tf} \cdot \sin\theta_w \cdot (F + R_F) \cdot (b_w \cdot \cos\theta_w + r_{i;tf} \cdot \sin\theta_w + x)}{EI}$$

$$+\frac{(b_w\cdot\cos\theta_w + r_{i;tf}\cdot\sin\theta_w + x)\cdot(b_w\cdot\cos\theta_w\cdot(1/2\cdot F + 1/2\cdot R_F + R_G\cdot\cos\theta_w) - b_w\cdot(1/2\cdot R_G + R_E\cdot\sin\theta_w) + M_E + R_F\cdot x)}{EI}]\,dx \tag{C.18}$$

which after integration gives

$$w_F = \frac{F\cdot(3\cdot b_{tf}^2\cdot r_{i;tf}\cdot\sin\theta_w + b_w\cdot\cos\theta_w\cdot(3\cdot b_{tf}^2 + 12\cdot r_{i;tf}\cdot\sin\theta_w\cdot(b_{tf} - r_{i;tf}\cdot\sin\theta_w)) + b_w^2\cdot(1+\cos 2\theta_w)\cdot(4\cdot b_w + 6\cdot b_{tf}))}{48\cdot EI}$$

$$+\frac{12\cdot EI\cdot F\cdot b_w\cdot(1-\cos 2\theta_w) - 6\cdot EA\cdot R_E\cdot b_w\cdot b_{tf}^2\cdot\sin\theta_w + b_w\cdot\sin 2\theta_w\cdot(4/3\cdot b_w + 2\cdot b_{tf})) + 4\cdot EA\cdot F\cdot r_{i;tf}^3\cdot\sin^3\theta_w}{48\cdot EA\cdot EI}$$

$$+\frac{M_E\cdot(1/4\cdot b_{tf}^2 + b_w\cdot\cos\theta_w\cdot(b_w + b_{tf}))}{2\cdot EI} + \frac{R_E\cdot b_w\cdot\sin 2\theta_w}{2\cdot EA} \tag{C.19}$$

Similarly, the maximum deflection of the web w_G is derived by differentiating the internal work with respect to R_G, resulting in

$$w_G = \int_0^{1/2\cdot b_w}[\frac{4\cdot\cos\theta_w\cdot\sin\theta_w\cdot(\sin\theta_w\cdot(1/2\cdot F + 1/2\cdot R_F + R_G\cdot\cos\theta_w) + R_E\cdot\cos\theta_w)}{EA}$$

$$+\frac{2\cdot x\cdot\cos^2\theta_w\cdot(x\cdot\cos\theta_w\cdot(1/2\cdot(F+R_F) + R_G\cdot\cos\theta_w) - R_E\cdot x\cdot\sin\theta_w + M_E)}{EI}$$

$$+\frac{2\cdot(\cos\theta_w\cdot(x\cdot\cos\theta_w + 1/2\cdot b_w\cdot\cos\theta_w) - x)\cdot(1/2\cdot F + 1/2\cdot R_F + R_G\cdot\cos\theta_w)\cdot(x\cdot\cos\theta_w + 1/2\cdot b_w\cdot\cos\theta_w)}{EI}$$

$$-\frac{2\cdot(\cos\theta_w\cdot(x\cdot\cos\theta_w + 1/2\cdot b_w\cdot\cos\theta_w) - x)\cdot(R_G\cdot x + R_E\cdot\sin\theta_w\cdot(1/2\cdot b_w + x) - M_E)}{EI}]\,dx$$

$$+\int_0^{r_{i;tf}\cdot\sin\theta_w}[\frac{2\cdot b_w\cdot(\cos^2\theta_w - 1/2)\cdot(b_w\cdot\cos\theta_w\cdot(1/2\cdot F + 1/2\cdot R_F + R_G\cdot\cos\theta_w) - 1/2\cdot R_G\cdot b_w + M_E)}{EI}$$

$$+\frac{2\cdot b_w\cdot(\cos^2\theta_w - 1/2)\cdot(1/2\cdot x\cdot(F+R_F) - R_E\cdot b_w\cdot\sin\theta_w)}{EI}]\,dx + \int_0^{1/2\cdot b_{tf}}[\frac{2\cdot\sin\theta_w\cdot(R_E + R_G\cdot\sin\theta_w)}{EA}]\,dx$$

$$+\int_0^{1/2\cdot b_{tf} - r_{i;tf}\cdot\sin\theta_w}[\frac{2\cdot b_w\cdot(\cos^2\theta_w - 1/2)\cdot(b_w\cdot\cos\theta_w\cdot(1/2\cdot F + 1/2\cdot R_F + R_G\cdot\cos\theta_w) - 1/2\cdot R_G\cdot b_w)}{EI}$$

$$+\frac{2\cdot b_w\cdot(\cos^2\theta_w-1/2)\cdot(1/2\cdot r_{i;tf}\cdot\sin\theta_w\cdot(F+R_F)+1/2\cdot R_F\cdot x-R_E\cdot b_w\cdot\sin\theta_w+M_E)}{EI}]\,dx \qquad (C.20)$$

From equation C.20 it follows that

$$w_G=\frac{F\cdot b_w\cdot(b_w\cdot(7\cdot b_w\cdot\cos\theta_w+6\cdot b_{tf})+12\cdot r_{i;tf}\cdot\cos 2\theta_w\cdot\sin\theta_w\cdot(b_{tf}-r_{i;tf}\cdot\sin\theta_w)+b_w\cdot\cos 3\theta_w\cdot(4\cdot b_w+6\cdot b_{tf}))}{48\cdot EI}$$

$$+\frac{R_E\cdot b_w\cdot(b_w\cdot\sin\theta_w\cdot(b_w+6\cdot b_{tf})-b_w\cdot\sin 3\theta_w\cdot(4\cdot b_w+6\cdot b_{tf}))+12\cdot M_E\cdot b_w\cdot(\cos 2\theta_w\cdot(b_w+b_{tf})+1/2\cdot b_w)}{24\cdot EI}$$

$$+\frac{F\cdot b_w\cdot(\cos\theta_w-\cos 3\theta_w)+2\cdot R_E\cdot(\sin\theta_w\cdot(b_w+2\cdot b_{tf})+b_w\cdot\sin 3\theta_w)}{4\cdot EA} \qquad (C.21)$$

Considering equation C.1 and substituting equations C.19 and C.21, it may readily be verified that

$$n=\left|\frac{4\cdot r_{i;tf}^2\cdot\sin^2\theta_w\cdot(b_w\cdot(b_w+2\cdot(b_{tf}+b_{bf}))+3\cdot b_{bf}\cdot b_{tf})-3\cdot b_{tf}^2\cdot(3\cdot b_{bf}\cdot r_{i;tf}\cdot\sin\theta_w+b_w\cdot(b_w+2\cdot(b_{bf}+r_{i;tf}\cdot\sin\theta_w)))}{3\cdot b_w^2\cdot(b_{tf}-r_{i;tf}\cdot\sin\theta_w)\cdot(3\cdot b_{bf}+b_w)}\right| \qquad (C.22)$$

It is striking that the web crippling stiffness is more or less inversely proportional to the squared top flange corner radius. It will become clear that is approximately true for all the combinations.

C.3 *Derivation of the energy model*

The derivation of the six combinations of the energy model is established with the aid of the computer program Mathematica *(Wolfram, 1988)*. This program is used in minimizing the total potential energy with respect to the coefficients w_2 and L_{ef}. The program is capable of solving algebraic equations and integrals. First, the working of this program has been checked by making use of it in the derivation of the two-dimensional web crippling stiffness in the portal frame model.

The derivation of the web crippling stiffness for the combinations 1 to 6 of the energy model is briefly summarized in the sections C.3.1 to C.3.6.

C.3.1 Combination 1: Bilinear function, hinge compatibility approach & exact solution

Within combination 1 the deformation variations over the length of the member are described by the bilinear function of figure 5.6a and the hinge compatibility approach is applied. Taking into account that

$$w_w(x,y) = w_w(x)\cdot w(y) \qquad W_{tf}(x,y) = w_{tf}(x)\cdot w(y) \qquad (C.23)$$

and combining the equations 5.21 and 5.24, the deformation functions $w_w(x,y)$ and $w_{tf}(x,y)$ for combination 1 are given by

$$w_w(x,y) = w_2 \cdot (1 + c_{1;w} \cdot \frac{x^2}{b_w^2} + c_{2;w} \cdot \frac{x^4}{b_w^4}) \cdot (1 - \frac{2 \cdot |y|}{L_{ef}}) \qquad (|x| \le 1/2 \cdot b_w \cap |y| \le 1/2 \cdot L_{ef}) \qquad \text{(C.24a)}$$

$$w_{tf}(x,y) = w_2 \cdot n \cdot (1 + c_{1;tf} \cdot \frac{x^2}{b_{tf}^2} + c_{2;tf} \cdot \frac{x^4}{b_{tf}^4}) \cdot (1 - \frac{2 \cdot |y|}{L_{ef}}) \qquad (|x| \le 1/2 \cdot b_{tf} \cap |y| \le 1/2 \cdot L_{ef}) \qquad \text{(C.24b)}$$

in which

$$c_{1;w} = c_{1;tf} = -\frac{24}{5} \qquad c_{2;w} = c_{2;tf} = \frac{16}{5} \qquad \text{(C.24d)}$$

Note that the deformations equal zero for x or y having values that are not within the abovementioned specifications. This holds true for every combination in the energy model and will not further be mentioned explicitly in the derivation of each combination. The total potential energy is given by (equation 5.12)

$$V = 1/2 \cdot D \cdot \int\int_R [(\frac{\partial^2 W}{\partial x^2})^2 + (\frac{\partial^2 W}{\partial y^2})^2 + 2 \cdot \mu \cdot \frac{\partial^2 W}{\partial x^2} \cdot \frac{\partial^2 W}{\partial y^2} + 2 \cdot (1 - \mu) \cdot (\frac{\partial^2 W}{\partial x \partial y})^2] \, dxdy - \int\int_R q \cdot w \, dxdy \qquad \text{(C.25a)}$$

in which D is called the bending rigidity and given by

$$D = \frac{E \cdot t^3}{12 \cdot (1 - \mu^2)} \qquad \text{(C.25b)}$$

The strain energy of the member is formed by the strain energy of the two web plates and the top flange plate. The potential energy of the member for external loads is formed by four concentrated loads which are located at $(1/2L_{lb},\ 1/2b_{tf} - \sin\theta_w \cdot r_{i;tf})$, $(-1/2L_{lb},\ 1/2b_{tf} - \sin\theta_w \cdot r_{i;tf})$, $(1/2L_{lb},\ -1/2b_{tf} - \sin\theta_w \cdot r_{i;tf})$ and $(-1/2L_{lb},\ -1/2b_{tf} - \sin\theta_w \cdot r_{i;tf})$. Due to symmetry the magnitudes of the four loads as well as their corresponding deformations equal each other. From here, the total potential energy can be specified as (equation 5.12)

$$V = D \cdot \int_{-1/2 \cdot L_{ef}}^{1/2 \cdot L_{ef}} \int_{-1/2 \cdot b_w}^{1/2 \cdot b_w} [(\frac{\partial^2 w_w(x,y)}{\partial x^2})^2 + 2 \cdot \frac{\partial^4 w_w(x,y)}{\partial x^2 \partial y^2} + (\frac{\partial^2 w_w(x,y)}{\partial y^2})^2] \, dxdy$$

$$+ 1/2 \cdot D \cdot \int_{-1/2 \cdot L_{ef}}^{1/2 \cdot L_{ef}} \int_{-1/2 \cdot b_{tf}}^{1/2 \cdot b_{tf}} [(\frac{\partial^2 w_{tf}(x,y)}{\partial x^2})^2 + 2 \cdot \frac{\partial^4 w_{tf}(x,y)}{\partial x^2 \partial y^2} + (\frac{\partial^2 w_{tf}(x,y)}{\partial y^2})^2] \, dxdy - F \cdot w_{tf}(1/2 \cdot L_{fb}, 1/2 \cdot b_{tf} - r_{i;tf} \cdot \sin\theta_w) \qquad \text{(C.26)}$$

After substitution of the equations C.24 into equation C.26, the total potential energy can be written as

$$V = \frac{2048 \cdot w_2^2 \cdot D \cdot L_{ef}}{125 \cdot b_w^3} + \frac{1024 \cdot w_2^2 \cdot D \cdot n^2 \cdot L_{ef}}{125 \cdot b_{tf}^3}$$

$$-\frac{64\cdot F\cdot w_2\cdot n\cdot r_{i;tf}\cdot\sin\theta_w\cdot(1-L_{fb}/L_{ef})\cdot(b_{tf}^3-2\cdot b_{tf}\cdot r_{i;tf}^2\cdot\sin^2\theta_w+r_{i;tf}^3\cdot\sin^3\theta_w)}{5\cdot b_{tf}^4} \tag{C.27}$$

Now, the total potential energy needs to be minimized with respect to the coefficients w_2 and L_{ef}. Minimizing the total potential energy with respect to w_2 gives

$$\frac{4096\cdot w_2\cdot D\cdot L_{ef}}{125\cdot b_w^3}+\frac{2048\cdot w_2\cdot D\cdot n^2\cdot L_{ef}}{125\cdot b_{tf}^3}$$

$$-\frac{64\cdot F\cdot n\cdot r_{i;tf}\cdot\sin\theta_w\cdot(1-L_{fb}/L_{ef})\cdot(b_{tf}^3-2\cdot b_{tf}\cdot r_{i;tf}^2\cdot\sin^2\theta_w+r_{i;tf}^3\cdot\sin^3\theta_w)}{5\cdot b_{tf}^4}=0 \tag{C.28}$$

Minimizing the total potential energy (equation C.27) with respect to L_{ef} results in

$$\frac{2048\cdot w_2^2\cdot D}{125\cdot b_w^3}+\frac{1024\cdot w_2^2\cdot D\cdot n^2}{125\cdot b_{tf}^3}-\frac{64\cdot F\cdot w_2\cdot n\cdot r_{i;tf}\cdot\sin\theta_w\cdot L_{fb}\cdot(b_{tf}^3-2\cdot b_{tf}\cdot r_{i;tf}^2\cdot\sin^2\theta_w+r_{i;tf}^3\cdot\sin^3\theta_w)}{5\cdot b_{tf}^4\cdot L_{ef}^2}=0 \tag{C.29}$$

After solving the equations C.28 and C.29 simultaneously with respect to the coefficients w_2 and L_{ef}, these coefficients can be specified as

$$L_{ef}=3\cdot L_{fb} \tag{C.30a}$$

and

$$w_2=\frac{25\cdot F\cdot b_w^3\cdot n\cdot r_{i;tf}\cdot\sin\theta_w\cdot(b_{tf}^3-2\cdot b_{tf}\cdot r_{i;tf}^2\cdot\sin^2\theta_w+r_{i;tf}^3\cdot\sin^3\theta_w)}{144\cdot D\cdot b_{tf}\cdot L_{fb}\cdot(2\cdot b_{tf}^3+b_w^3\cdot n^2)} \tag{C.30b}$$

The web crippling stiffness is defined to be

$$k_{\Delta h_w}=\frac{F}{w_{tf}(1/2\cdot L_{fb},r_{i;tf}\cdot\sin\theta_w)} \tag{C.31}$$

After substitution of the equations C.30 into equation C.24b, it may be readily verified that, according to the abovementioned definition,

$$k_{\Delta h_w}=\frac{27\cdot D\cdot b_{tf}^5\cdot L_{fb}\cdot(2\cdot b_{tf}^3+3\cdot b_w^3\cdot n^2)}{10\cdot b_w^3\cdot n^2\cdot\sin^2\theta_w\cdot r_{i;tf}^2\cdot(b_{tf}^3-2\cdot b_{tf}\cdot\sin^2\theta_w\cdot r_{i;tf}^2\cdot+\sin^3\theta_w\cdot r_{i;tf}^3)^2} \tag{C.32}$$

C.3.2 *Combination 2: Bilinear function, geometrical compatibility approach & exact solution*

In combination 2 the deformation variations over the length of the member are described by the linear function of figure 5.6a, just as in combination 1, but here geometrical compatibility is assumed.

The deformation functions $w_w(x,y)$ and $w_{tf}(x,y)$ for combination 2 are given by

$$w_w(x,y) = w_2 \cdot (1 + c_{1;w} \cdot \frac{x^2}{b_w^2} + c_{2;w} \cdot \frac{x^4}{b_w^4}) \cdot (1 - \frac{2 \cdot |y|}{L_{ef}}) \qquad (|x| \le 1/2 \cdot b_w \cap |y| \le 1/2 \cdot L_{ef}) \qquad \text{(C.33a)}$$

$$w_{tf}(x,y) = w_2 \cdot n \cdot (1 + c_{1;tf} \cdot \frac{x^2}{b_{tf}^2} + c_{2;tf} \cdot \frac{x^4}{b_{tf}^4}) \cdot (1 - \frac{2 \cdot |y|}{L_{ef}}) \qquad (|x| \le 1/2 \cdot b_{tf} \cap |y| \le 1/2 \cdot L_{ef}) \qquad \text{(C.33b)}$$

in which

$$c_{1;w} = \frac{2 \cdot n \cdot b_w^2 - 5 \cdot b_w \cdot b_{tf} - 3 \cdot b_{tf}^2}{5/8 \cdot b_{tf} \cdot (b_w + b_{tf})} \qquad \text{(C.33d)}$$

$$c_{2;w} = \frac{b_{tf}^2 + 5 \cdot b_{tf} \cdot b_w - 4 \cdot n \cdot b_w^2}{5/16 \cdot b_{tf} \cdot (b_w + b_{tf})} \qquad \text{(C.33e)}$$

$$c_{1;tf} = \frac{2 \cdot b_{tf}^2 - 5 \cdot n \cdot b_w \cdot b_{tf} - 3 \cdot n \cdot b_w^2}{5/8 \cdot n \cdot b_w \cdot (b_w + b_{tf})} \qquad \text{(C.33f)}$$

$$c_{2;tf} = \frac{n \cdot b_w^2 + 5 \cdot n \cdot b_w \cdot b_{tf} - 4 \cdot b_{tf}^2}{5/16 \cdot n \cdot b_w \cdot (b_w + b_{tf})} \qquad \text{(C.33g)}$$

Substituting the deformation functions of equations C.33a to C.33c into the total potential energy (equation C.26) gives

$$V = \frac{D \cdot L_{ef} \cdot w_2^2 \cdot (20 \cdot c_{1;w}^2 + 20 \cdot c_{1;w} \cdot c_{2;w} + 9 \cdot c_{2;w}^2)}{15 \cdot b_w^3} + \frac{D \cdot L_{ef} \cdot n^2 \cdot w_2^2 \cdot (20 \cdot c_{1;tf}^2 + 20 \cdot c_{1;tf} \cdot c_{2;tf} + 9 \cdot c_{2;tf}^2)}{30 \cdot b_{tf}^3}$$

$$- 4 \cdot F \cdot w_2 \cdot n \cdot (1 - L_{fb}/L_{ef}) \cdot (1 + \frac{c_{1;tf} \cdot (1/2 \cdot b_{tf} - r_{i;tf} \cdot \sin\theta_w)^2}{b_{tf}^2} + \frac{c_{2;tf} \cdot (1/2 \cdot b_{tf} - r_{i;tf} \cdot \sin\theta_w)^4}{b_{tf}^4}) \qquad \text{(C.34)}$$

Similar to combination 1, the total potential energy (equation C.34) is minimized with respect to the coefficients w_2 and L_{ef}. After proper calculations it may be derived that

$$L_{ef} = 3 \cdot L_{fb} \qquad \text{(C.35a)}$$

and

$$w_2 = \frac{5 \cdot F \cdot b_w^3 \cdot n \cdot (b_{tf}^4 \cdot (16 + 4 \cdot c_{1;tf} + c_{2;tf}) - 8 \cdot b_{tf}^3 \cdot r_{i;tf} \cdot \sin\theta_w \cdot (2 \cdot c_{1;tf} + c_{2;tf}))}{6 \cdot D \cdot b_{tf} \cdot L_{lb} \cdot (b_{tf}^3 \cdot (4\Delta \cdot c_{1;w}^2 + 40 c_{1;w} \cdot c_{2;w} + 18 c_{2;w}^2) + b_w^3 \cdot n^2 \cdot (20 c_{1;tf}^2 + 20 c_{1;tf} \cdot c_{2;tf} + 9 \cdot c_{2;tf}^2))}$$

$$+ \frac{5 \cdot F \cdot b_w^3 \cdot n \cdot (b_{tf}^2 \cdot r_{i;tf}^2 \cdot \sin^2\theta_w \cdot (16 \cdot c_{1;tf} + 24 \cdot c_{2;tf}) - 32 \cdot b_{tf} \cdot c_{2;tf} \cdot r_{i;tf}^3 \cdot \sin^3\theta_w + 16 \cdot c_{2;tf} \cdot r_{i;tf}^4 \cdot \sin^4\theta_w)}{6 \cdot D \cdot b_{tf} \cdot L_{lb} \cdot (b_{tf}^3 \cdot (40 \cdot c_{1;w}^2 + 40 \cdot c_{1;w} \cdot c_{2;w} + 18 \cdot c_{2;w}^2) + b_w^3 \cdot n^2 \cdot (20 \cdot c_{1;tf}^2 + 20 \cdot c_{1;tf} \cdot c_{2;tf} + 9 \cdot c_{2;tf}^2))} \qquad \text{(C.35b)}$$

Substitution of the equations C.35 into C.33b and using equation C.31 results in

$$k_{\Delta h_w} = \frac{[9/20 \cdot D \cdot b_{tf}^5 \cdot L_{lb} \cdot (b_{tf}^3 \cdot (b_{tf} \cdot (12 \cdot b_{tf} + 41 \cdot b_w) + 50 \cdot b_w^2)}{[b_w \cdot \sin^2\theta_w \cdot r_{i;tf}^2 \cdot (b_{tf} - \sin\theta_w \cdot r_{i;tf})^2 \cdot (b_{tf}^2 \cdot (b_{tf} \cdot (4 \cdot \sin\theta_w \cdot r_{i;tf} - b_{tf}) - b_w \cdot n \cdot (b_w + 5 \cdot \sin\theta_w \cdot r_{i;tf})}$$

$$\frac{+ b_w^3 \cdot (b_w \cdot n \cdot (6 \cdot b_w \cdot n + 52 \cdot b_{tf}) + b_{tf}^2 \cdot n \cdot (25 \cdot n - 78))]}{-4 \cdot \sin^2\theta_w \cdot r_{i;tf}^2) + b_w \cdot \sin\theta_w \cdot r_{i;tf} \cdot n \cdot (\sin\theta_w \cdot r_{i;tf} \cdot (b_w + 5 \cdot b_{tf}) - b_w \cdot b_{tf}))^2]} \qquad \text{(C.36)}$$

C.3.3 Combination 3: Trilinear function, hinge compatibility approach & full length solution

Within combination 3 the deformation variations over the length of the member are described by the trilinear function of figure 5.6b and the hinge compatibility approach is applied.

It is not possible to derive an exact solution for the web crippling stiffness when the total potential energy is minimized with respect to L_{ef} and w_2. Therefore, the total potential energy is only minimized with respect to w_2. Moreover, it is assumed in this combination that the effective length corresponds to the span length of the member L_{span}.

The deformation functions $w_w(x,y)$ and $w_{tf}(x,y)$ for combination 3 are given by

$$w_w(x,y) = w_2 \cdot (1 - 24/5 \cdot \frac{x^2}{b_w^2} + 16/5 \cdot \frac{x^4}{b_w^4}) \cdot (1 - \frac{2 \cdot (|y| - 1/2 \cdot L_{lb})}{L_{span} - L_{lb}}) \qquad (|x| \le 1/2 \cdot b_w \cap |y| > 1/2 \cdot L_{lb}) \qquad \text{(C.37a)}$$

$$w_{tf}(x,y) = w_2 \cdot n \cdot (1 - 24/5 \cdot \frac{x^2}{b_{tf}^2} + 16/5 \cdot \frac{x^4}{b_{tf}^4}) \cdot (1 - \frac{2 \cdot (|y| - 1/2 \cdot L_{lb})}{L_{span} - L_{lb}}) \qquad (|x| \le 1/2 \cdot b_{tf} \cap |y| > 1/2 \cdot L_{lb}) \qquad \text{(C.37b)}$$

$$w_w(x,y) = w_2 \cdot (1 - 24/5 \cdot \frac{x^2}{b_w^2} + 16/5 \cdot \frac{x^4}{b_w^4}) \qquad (|x| \le 1/2 \cdot b_w \cap |y| \le 1/2 \cdot L_{lb}) \qquad \text{(C.37c)}$$

$$w_{tf}(x,y) = w_2 \cdot n \cdot (1 - 24/5 \cdot \frac{x^2}{b_{tf}^2} + 16/5 \cdot \frac{x^4}{b_{tf}^4}) \qquad (|x| \le 1/2 \cdot b_{tf} \cap |y| \le 1/2 \cdot L_{lb}) \qquad \text{(C.37d)}$$

After substitution of the equations C.37 into equation C.26 and substituting L_{ef} for L_{span}, the total potential energy can be written as

$$V = \frac{2048 \cdot w_2^2 \cdot D \cdot (L_{span} + 3 \cdot L_{lb})}{125 \cdot b_w^3} + \frac{128 \cdot w_2^2 \cdot D \cdot n^2 \cdot (b_w^4 \cdot (8 \cdot L_{span} + 9 \cdot L_{lb}) + L_{lb} \cdot (45 \cdot b_{tf}^4 - 30 \cdot b_{tf}^2 \cdot b_w^2)}{125 \cdot b_{tf}^3 \cdot b_w^4}$$

$$- \frac{64 \cdot F \cdot w_2 \cdot n \cdot r_{i;tf} \cdot \sin\theta_w \cdot (b_{tf}^3 - 2 \cdot b_{tf} \cdot r_{i;tf}^2 \cdot \sin^2\theta_w + r_{i;tf}^3 \cdot \sin^3\theta_w)}{5 \cdot b_{tf}^4} \qquad \text{(C.38)}$$

Now, the total potential energy needs to be minimized with respect to w_2, resulting in

$$\frac{4096 \cdot w_2 \cdot D \cdot (L_{span} + 3 \cdot L_{lb})}{125 \cdot b_w^3} + \frac{256 \cdot w_2 \cdot D \cdot n^2 \cdot (b_w^4 \cdot (8 \cdot L_{span} + 9 \cdot L_{lb}) + L_{lb} \cdot (45 \cdot b_{tf}^4 - 30 \cdot b_{tf}^2 \cdot b_w^2)}{125 \cdot b_{tf}^3 \cdot b_w^4}$$

$$- \frac{64 \cdot F \cdot n \cdot r_{i;tf} \cdot \sin\theta_w \cdot (b_{tf}^3 - 2 \cdot b_{tf} \cdot r_{i;tf}^2 \cdot \sin^2\theta_w + r_{i;tf}^3 \cdot \sin^3\theta_w)}{5 \cdot b_{tf}^4} = 0 \qquad \text{(C.39)}$$

From equation C.39 it follows that

$$w_2 = \frac{25 \cdot F \cdot b_w^4 \cdot n \cdot r_{i;tf} \cdot \sin\theta_w \cdot (b_{tf}^3 - 2 \cdot b_{tf} \cdot r_{i;tf}^2 \cdot \sin^2\theta_w + r_{i;tf}^3 \cdot \sin^3\theta_w)}{4 \cdot D \cdot b_{tf} \cdot (16 \cdot b_{tf}^3 \cdot b_w \cdot (L_{span} + 3 \cdot L_{Lb}) + b_w^4 \cdot n^2 \cdot (8 \cdot L_{span} + 9 \cdot L_{lb}) + L_{lb} \cdot b_{tf}^2 \cdot n^2 \cdot (45 \cdot b_{tf}^2 - 30 \cdot b_w^2))} \qquad \text{(C.40)}$$

Substituting equation C.40 into equation C.37d and using equation C.31, the web crippling stiffness can be calculated as

$$k_{\Delta h_w} = \frac{D \cdot b_{tf}^5 \cdot (16 \cdot b_{tf}^3 \cdot b_w \cdot (L_{span} + 3 \cdot L_{lb}) + b_w^4 \cdot n^2 \cdot (8 \cdot L_{span} + 9 \cdot L_{lb}) + b_{tf}^2 \cdot L_{lb} \cdot n^2 \cdot (45 \cdot b_{tf}^2 - 30 \cdot b_w^2))}{20 \cdot b_w^4 \cdot n^2 \cdot \sin^2\theta_w \cdot r_{i;tf}^2 \cdot (b_{tf}^3 - 2 \cdot b_{tf} \cdot \sin^2\theta_w \cdot r_{i;tf}^2 + \sin^3\theta_w \cdot r_{i;tf}^3)^2} \qquad \text{(C.41)}$$

C.3.4 Combination 4: Trilinear function, geometrical compatibility approach & full length solution

The only difference between combination 3 and 4 is formed by the compatibility approach: combination 4 is based on the geometrical compatibility approach where combination 3 uses the hinge compatibility approach. Just as in case of combination 3, it is not possible to derive an exact solution for the web crippling stiffness when the total potential energy is minimized with respect to L_{ef} and w_2. Therefore, the total potential energy is only minimized with respect to w_2. Moreover, it is assumed in this combination that the effective length corresponds to the span length of the member L_{span} (full length solution).

The deformation functions $w_w(x,y)$ and $w_{tf}(x,y)$ for combination 4 are given by

$$w_w(x,y) = w_2 \cdot (1 + c_{1;w} \cdot \frac{x^2}{b_w^2} + c_{2;w} \cdot \frac{x^4}{b_w^4}) \cdot (1 - \frac{2 \cdot (|y| - 1/2 \cdot L_{lb})}{L_{span} - L_{lb}}) \qquad (|x| \le 1/2 \cdot b_w \cap |y| > 1/2 \cdot L_{lb}) \qquad \text{(C.42a)}$$

$$w_{tf}(x,y) = w_2 \cdot n \cdot (1 + c_{1;tf} \cdot \frac{x^2}{b_{tf}^2} + c_{2;tf} \cdot \frac{x^4}{b_{tf}^4}) \cdot (1 - \frac{2 \cdot (|y| - 1/2 \cdot L_{lb})}{L_{span} - L_{lb}}) \qquad (|x| \le 1/2 \cdot b_{tf} \cap |y| > 1/2 \cdot L_{lb}) \qquad \text{(C.42b)}$$

$$w_w(x,y) = w_2 \cdot (1 + c_{1;w} \cdot \frac{x^2}{b_w^2} + c_{2;w} \cdot \frac{x^4}{b_w^4}) \qquad (|x| \le 1/2 \cdot b_w \ \cap \ |y| \le 1/2 \cdot L_{lb}) \tag{C.42c}$$

$$w_{tf}(x,y) = w_2 \cdot n \cdot (1 + c_{1;tf} \cdot \frac{x^2}{b_{tf}^2} + c_{2;tf} \cdot \frac{x^4}{b_{tf}^4}) \qquad (|x| \le 1/2 \cdot b_{tf} \ \cap \ |y| \le 1/2 \cdot L_{lb}) \tag{C.42d}$$

in which the coefficients $c_{1;w}$, $c_{2;w}$, $c_{1;tf}$ and $c_{2;tf}$ are given by equations C.33d to C.33g.

After substitution of the equations C.42 into equation C.26 (and taking into account that the effective length equals the span length), the total potential energy can be written as

$$V = \frac{D \cdot \cdot w_2^2 \cdot (L_{span} + 3 \cdot L_{lb}) \cdot (20 \cdot c_{1;w}^2 + 20 \cdot c_{1;w} \cdot c_{2;w} + 9 \cdot c_{2;w}^2)}{15 \cdot b_w^3} + \frac{D \cdot L_{span} \cdot n^2 \cdot w_2^2 \cdot (20 \cdot c_{1;tf}^2 + 20 \cdot c_{1;tf} \cdot c_{2;tf} + 9 \cdot c_{2;tf}^2)}{30 \cdot b_{tf}^3}$$

$$+ \frac{D \cdot L_{lb} \cdot n^2 \cdot w_2^2 \cdot (20 \cdot b_{tf}^4 \cdot c_{1;tf}^2 + 20 \cdot b_{tf}^2 \cdot b_w^2 \cdot c_{1;tf} \cdot c_{2;tf} + 9 \cdot b_w^4 \cdot c_{2;tf}^2)}{10 \cdot b_{tf}^3 \cdot b_w^4}$$

$$- 4 \cdot F \cdot w_2 \cdot n \cdot (1 + \frac{c_{1;tf} \cdot (1/2 \cdot b_{tf} - r_{i;tf} \cdot \sin\theta_w)^2}{b_{tf}^2} + \frac{c_{2;tf} \cdot (1/2 \cdot b_{tf} - r_{i;tf} \cdot \sin\theta_w)^4}{b_{tf}^4}) \tag{C.43}$$

Minimizing the total potential energy with respect to w_2 gives

$$w_2 = \frac{[15 \cdot F \cdot b_w^4 \cdot n \cdot (b_{tf}^4 \cdot (16 + 4 \cdot c_{1;tf} + c_{2;tf}) - 8 \cdot b_{tf}^3 \cdot r_{i;tf} \cdot \sin\theta_w \cdot (2 \cdot c_{1;tf} + c_{2;tf})}{[4 \cdot D \cdot b_{tf} \cdot ((L_{span} + 3 \cdot L_{lb}) \cdot (b_{tf}^3 \cdot b_w \cdot (40 \cdot c_{1;w}^2 + 40 \cdot c_{1;w} \cdot c_{2;w} + 18 \cdot c_{2;w}^2) + 9 \cdot b_w^4 \cdot n^2 \cdot c_{2;tf}^2)$$

$$\frac{+ b_{tf}^2 \cdot r_{i;tf}^2 \cdot \sin^2\theta_w \cdot (16 \cdot c_{1;tf} + 24 \cdot c_{2;tf}) - 32 \cdot b_{tf} \cdot c_{2;tf} \cdot r_{i;tf}^3 \cdot \sin^3\theta_w + 16 \cdot c_{2;tf} \cdot r_{i;tf}^4 \cdot \sin^4\theta_w))]}{+ 20 \cdot b_w^2 \cdot n^2 \cdot c_{1;tf} \cdot c_{2;tf} \cdot (b_w^2 \cdot L_{span} + b_{tf}^2 \cdot L_{lb}) + c_{1;tf}^2 \cdot n^2 \cdot (20 \cdot b_w^4 \cdot L_{span} + 60 \cdot b_{tf}^4 \cdot L_{lb}))] \tag{C.44}$$

Substituting equation C.44 into equation C.42d and using equation C.31, it may be readily verified that

$$k_{\Delta h_w} = \frac{[D \cdot b_{tf}^9 \cdot (b_w^4 \cdot (L_{lb} \cdot (56/5 + 7 \cdot n - 41/4 \cdot n^2) + 41/15 \cdot L_{span}) + b_{tf} \cdot b_w^3 \cdot (L_{lb} \cdot (12/5 + 15 \cdot n + 15/2 \cdot n^2) + 4/5 \cdot L_{span}))}{[b_w^4 \cdot \sin^2\theta_w \cdot r_{i;tf}^2 \cdot (b_{tf} - \sin\theta_w \cdot r_{i;tf})^2 \cdot (b_{tf}^2 \cdot (b_{tf} \cdot (4 \cdot \sin\theta_w \cdot r_{i;tf} - b_{tf}) - b_w \cdot n \cdot (b_w + 5 \cdot \sin\theta_w \cdot r_{i;tf}) - 4 \cdot \sin^2\theta_w \cdot r_{i;tf}^2)}$$

$$\frac{+ D \cdot b_{tf}^8 \cdot (b_{tf}^3 \cdot L_{lb} \cdot (b_w^2 \cdot (25/4 \cdot n^2 - 3 \cdot n - 4) + b_{tf} \cdot (b_{tf} - 5 \cdot b_w \cdot n)) + 10 \cdot b_w^5 \cdot (L_{lb} \cdot (1 - 86/50 \cdot n - n^2) + 1/3 \cdot L_{span}))]}{+ b_w \cdot \sin\theta_w \cdot r_{i;tf} \cdot n \cdot (\sin\theta_w \cdot r_{i;tf} \cdot (b_w + 5 \cdot b_{tf}) - b_w \cdot b_{tf}))^2]}$$

$$+ \frac{[D \cdot b_{tf}^7 \cdot b_w^5 \cdot n \cdot (-12/5 \cdot b_{tf} \cdot L_{span} + b_w \cdot (L_{lb} \cdot (39/4 \cdot n - 98/5) + L_{span} \cdot (5/3 \cdot n - 26/5)))}{[b_w^4 \cdot \sin^2\theta_w \cdot r_{i;tf}^2 \cdot (b_{tf} - \sin\theta_w \cdot r_{i;tf})^2 \cdot (b_{tf}^2 \cdot (b_{tf} \cdot (4 \cdot \sin\theta_w \cdot r_{i;tf} - b_{tf}) - b_w \cdot n \cdot (b_w + 5 \cdot \sin\theta_w \cdot r_{i;tf}) - 4 \cdot \sin^2\theta_w \cdot r_{i;tf}^2)}$$

$$\frac{+ D \cdot b_{tf}^5 \cdot b_w^7 \cdot n^2 \cdot (b_{tf} \cdot (129/10 \cdot L_{lb} + 52/15 \cdot L_{span}) + 2/5 \cdot b_w \cdot L_{span}))}{+ b_w \cdot \sin\theta_w \cdot r_{i;tf} \cdot n \cdot (\sin\theta_w \cdot r_{i;tf} \cdot (b_w + 5 \cdot b_{tf}) - b_w \cdot b_{tf}))^2]} \tag{C.45}$$

C.3.5 *Combination 5: Fourth degree polynomial, hinge compatibility approach & approximate solution*

Combination 5 makes use of the fourth degree polynomial that describes the deformations over the length of the member. It is based upon the hinge compatibility approach and the total potential energy is minimized with respect to L_{ef} and w_2.

The deformation functions $w_w(x,y)$ and $w_{tf}(x,y)$ for combination 5 are given by

$$w_w(x,y) = w_2 \cdot (1 - 24/5 \cdot \frac{x^2}{b_w^2} + 16/5 \cdot \frac{x^4}{b_w^4}) \cdot \frac{16}{L_{ef}^4} \cdot (y^2 - 1/4 \cdot L_{ef}^2)^2 \qquad (|x| \le 1/2 \cdot b_w \cap |y| \le 1/2 \cdot L_{ef}) \qquad \text{(C.46a)}$$

$$w_{tf}(x,y) = w_2 \cdot n \cdot (1 - 24/5 \cdot \frac{x^2}{b_{tf}^2} + 16/5 \cdot \frac{x^4}{b_{tf}^4}) \cdot \frac{16}{L_{ef}^4} \cdot (y^2 - 1/4 \cdot L_{ef}^2)^2 \qquad (|x| \le 1/2 \cdot b_{tf} \cap |y| \le 1/2 \cdot L_{ef}) \qquad \text{(C.46b)}$$

Substituting these deformation functions into the total potential energy (equation C.26) gives

$$V = \frac{131072 \cdot D \cdot w_2^2 \cdot (42 \cdot L_{ef}^4 + 102 \cdot b_w^2 \cdot L_{ef}^2 + 217 \cdot b_w^4)}{275625 \cdot b_w^3 \cdot L_{ef}^3}$$

$$+ \frac{65536 \cdot D \cdot w_2^2 \cdot n^2 \cdot (42 \cdot L_{ef}^4 + 102 \cdot b_{tf}^2 \cdot L_{ef}^2 + 217 \cdot b_{tf}^4)}{275625 \cdot b_{tf}^3 \cdot L_{ef}^3}$$

$$- \frac{64 \cdot F \cdot w_2 \cdot n \cdot r_{i;tf} \cdot \sin\theta_w \cdot (L_{fb}^2 - L_{ef}^2)^2 \cdot (b_{tf}^3 - 2 \cdot b_{tf} \cdot r_{i;tf}^2 \cdot \sin^2\theta_w + r_{i;tf}^3 \cdot \sin^3\theta_w)}{5 \cdot b_{tf}^4 \cdot L_{ef}^4} \qquad \text{(C.47)}$$

Just as in case of the combinations 3 and 4, it is not possible to derive an exact solution for the web crippling stiffness. Therefore, the web crippling stiffness is approximately determined by negelecting some terms out of the total potential energy functional which are thought to have a negligible influence on the web crippling stiffness compared to other terms. It is assumed that the effective length is much larger than the height of the web and the width of the top flange. Moreover, it is assumed that the width of the top flange greatly exceeds the magnitude of the corner radii for every member. For a large series of members the influence of each term of equation C.47 on the total potential energy has been calculated. In these calculations the effective length is taken equal to the eventual effective length for combination 5, which is based upon the neglect of some terms (equation C.50). From these calculations it may be concluded that the total potential energy may be approximated by

$$V = \frac{131072 \cdot D \cdot w_2^2 \cdot (42 \cdot L_{ef}^4 + 102 \cdot b_w^2 \cdot L_{ef}^2)}{275625 \cdot b_w^3 \cdot L_{ef}^3} + \frac{65536 \cdot D \cdot w_2^2 \cdot n^2 \cdot (42 \cdot L_{ef}^4 + 102 \cdot b_{tf}^2 \cdot L_{ef}^2)}{275625 \cdot b_{tf}^3 \cdot L_{ef}^3}$$

$$- \frac{64 \cdot F \cdot w_2 \cdot b_{tf}^3 \cdot n \cdot r_{i;tf} \cdot \sin\theta_w \cdot (L_{fb}^2 - L_{ef}^2)^2}{5 \cdot b_{tf}^4 \cdot L_{ef}^4} \qquad \text{(C.48)}$$

Now, the approximated total potential energy is minimized with respect to the coefficients w_2 and L_{ef}. After proper calculations it may be derived that

$$w_2 = \frac{55125 \cdot F \cdot b_{tf}^2 \cdot b_w^3 \cdot n \cdot r_{i;tf} \cdot \sin\theta_w \cdot (L_{ef}^2 - L_{fb}^2)^2}{2048 \cdot D \cdot L_{ef}^3 \cdot (42 \cdot L_{ef}^2 \cdot (b_w^3 \cdot n^2 + 2 \cdot b_{tf}^3) + 102 \cdot b_{tf}^2 \cdot b_w^2 \cdot (b_w \cdot n^2 + 2 \cdot b_{tf}))} \tag{C.49}$$

and

$$L_{ef} = \sqrt{\frac{b_{tf}^3 \cdot (34 \cdot b_w^2 + 504 \cdot L_{fb}^2) + b_w^3 \cdot n^2 \cdot (17 \cdot b_{tf}^2 + 252 \cdot L_{fb}^2)}{14 \cdot b_{tf}^3 + 7 \cdot b_w^3 \cdot n^2}} \tag{C.50}$$

Substitution of the equations C.49 and C.50 into C.46b and using equation C.31 results in

$$k_{\Delta h_w} = [\frac{512 \cdot D \cdot \sqrt{2 \cdot b_{tf}^3 + b_w^3 \cdot n^2} \cdot (b_{tf}^3 \cdot (34 \cdot b_w^2 + 252 \cdot L_{fb}^2) + b_w^3 \cdot n^2 \cdot (17 \cdot b_{tf}^2 + 126 \cdot L_{fb}^2))}{525 \cdot \sqrt{7} \cdot b_{tf} \cdot \sin^2\theta_w \cdot r_{i;tf}^2 \cdot b_w^3 \cdot n \cdot (b_{tf}^3 \cdot (34 \cdot b_w^2 + 490 \cdot L_{fb}^2) + b_w^3 \cdot n^2 \cdot (17 \cdot b_{tf}^2 + 245 \cdot L_{fb}^2))^4}]$$

$$\cdot [b_{tf}^3 \cdot (34 \cdot b_w^2 + 504 \cdot L_{fb}^2) + b_w^3 \cdot n^2 \cdot (17 \cdot b_{tf}^2 + 252 \cdot L_{fb}^2)]^{7/2} \tag{C.51}$$

C.3.6 Combination 6: Fourth degree polynomial, geometrical compatibility approach & approximate solution

Combination 6 can be thought of as the most complicated and reliable combination. The deformations over the length of the member are described by the fourth degree polynomial and the coupling between the plates is established using the geometrical compatibility approach.

The deformation functions $w_w(x,y)$ and $w_{tf}(x,y)$ for combination 6 are given by

$$w_w(x,y) = w_2 \cdot (1 + c_{1;w} \cdot \frac{x^2}{b_w^2} + c_{2;w} \cdot \frac{x^4}{b_w^4}) \cdot \frac{16}{L_{ef}^4} \cdot (y^2 - 1/4 \cdot L_{ef}^2)^2 \qquad (|x| \le 1/2 \cdot b_w \cap |y| \le 1/2 \cdot L_{ef}) \tag{C.52a}$$

$$w_{tf}(x,y) = w_2 \cdot n \cdot (1 + c_{1;tf} \cdot \frac{x^2}{b_{tf}^2} + c_{2;tf} \cdot \frac{x^4}{b_{tf}^4}) \cdot \frac{16}{L_{ef}^4} \cdot (y^2 - 1/4 \cdot L_{ef}^2)^2 \qquad (|x| \le 1/2 \cdot b_{tf} \cap |y| \le 1/2 \cdot L_{ef}) \tag{C.52b}$$

in which the coefficients $c_{1;w}$, $c_{2;w}$, $c_{1;tf}$ and $c_{2;tf}$ are given by equations C.33d to C.33g.

After substitution of the equations C.52 into equation C.26, the total potential energy can be written as

$$V = \frac{4 \cdot D \cdot w_2^2 \cdot b_w^4 \cdot (564480 + 94080 \cdot c_{1;w} + 7056 \cdot c_{1;w}^2 + 14112 \cdot c_{2;w} + 2520 \cdot c_{1;w} \cdot c_{2;w} + 245 \cdot c_{2;w}^2)}{11025 \cdot b_w^3 \cdot L_{ef}^3}$$

$$- \frac{4 \cdot D \cdot w_2^2 \cdot b_w^2 \cdot L_{ef}^2 \cdot (53760 \cdot c_{1;w} + 4480 \cdot c_{1;w}^2 + 26880 \cdot c_{2;w} + 4704 \cdot c_{1;w} \cdot c_{2;w} + 720 \cdot c_{2;w}^2)}{11025 \cdot b_w^3 \cdot L_{ef}^3}$$

$$+\frac{4\cdot D\cdot w_2^2\cdot L_{ef}^4\cdot(4480\cdot c_{1;w}^2+4480\cdot c_{1;w}\cdot c_{2;w}+2016\cdot c_{2;w}^2)}{11025\cdot b_w^3\cdot L_{ef}^3}$$

$$+\frac{2\cdot D\cdot w_2^2\cdot b_{tf}^4\cdot(564480+94080\cdot c_{1;tf}+7056\cdot c_{1;tf}^2+14112\cdot c_{2;tf}+2520\cdot c_{1;tf}\cdot c_{2;tf}+245\cdot c_{2;tf}^2)}{11025\cdot b_{tf}^3\cdot L_{ef}^3}$$

$$-\frac{2\cdot D\cdot w_2^2\cdot b_{tf}^2\cdot L_{ef}^2\cdot(53760\cdot c_{1;tf}+4480\cdot c_{1;tf}^2+26880\cdot c_{2;tf}+4704\cdot c_{1;tf}\cdot c_{2;tf}+720\cdot c_{2;tf}^2)}{11025\cdot b_{tf}^3\cdot L_{ef}^3}$$

$$+\frac{2\cdot D\cdot w_2^2\cdot L_{ef}^4\cdot(4480\cdot c_{1;tf}^2+4480\cdot c_{1;tf}\cdot c_{2;tf}+2016\cdot c_{2;tf}^2)}{11025\cdot b_{tf}^3\cdot L_{ef}^3}$$

$$-\frac{4\cdot F\cdot w_2\cdot n\cdot(L_{lb}^2-L_{ef}^2)^2\cdot(1+\frac{c_{1;tf}\cdot(1/2\cdot b_{tf}-r_{i;tf}\cdot\sin\theta_w)^2}{b_{tf}^2}+\frac{c_{2;tf}\cdot(1/2\cdot b_{tf}-r_{i;tf}\cdot\sin\theta_w)^4}{b_{tf}^4})}{L_{ef}^4} \qquad \text{(C.53)}$$

Just as in combination 5 it is not possible to derive an exact solution for the web crippling stiffness. Therefore, the web crippling stiffness is approximately determined by negelecting some terms out of the total potential energy functional which are thought to have a negligible influence on the web crippling stiffness compared to other terms. It is assumed that the effective length is much larger than the height of the web and the width of the top flange. Moreover, it is assumed that the width of the top flange greatly exceeds the magnitude of the corner radii for every member. For a large series of members the influence of each term of equation C.53 on the total potential energy has been calculated. In these calculations the effective length is taken equal to the eventual effective length for combination 6, which is based upon the neglect of some terms (equation C.56). From these calculations it may be concluded that the total potential energy may be approximated by

$$V=\frac{4\cdot D\cdot w_2^2\cdot L_{ef}^4\cdot(4480\cdot c_{1;w}^2+4480\cdot c_{1;w}\cdot c_{2;w}+2016\cdot c_{2;w}^2)}{11025\cdot b_w^3\cdot L_{ef}^3}$$

$$-\frac{4\cdot D\cdot w_2^2\cdot b_w^2\cdot L_{ef}^2\cdot(53760\cdot c_{1;w}+4480\cdot c_{1;w}^2+26880\cdot c_{2;w}+4704\cdot c_{1;w}\cdot c_{2;w}+720\cdot c_{2;w}^2)}{11025\cdot b_w^3\cdot L_{ef}^3}$$

$$-\frac{2\cdot D\cdot w_2^2\cdot b_{tf}^2\cdot L_{ef}^2\cdot(53760\cdot c_{1;tf}+4480\cdot c_{1;tf}^2+26880\cdot c_{2;tf}+4704\cdot c_{1;tf}\cdot c_{2;tf}+720\cdot c_{2;tf}^2)}{11025\cdot b_{tf}^3\cdot L_{ef}^3}$$

$$+\frac{2\cdot D\cdot w_2^2\cdot L_{ef}^4\cdot(4480\cdot c_{1;tf}^2+4480\cdot c_{1;tf}\cdot c_{2;tf}+2016\cdot c_{2;tf}^2)}{11025\cdot b_{tf}^3\cdot L_{ef}^3}$$

$$- \frac{4 \cdot F \cdot w_2 \cdot n \cdot (L_{lb}^2 - L_{ef}^2)^2 \cdot (1 + \frac{c_{1;tf} \cdot (1/4 \cdot b_{tf} - r_{i;tf} \cdot \sin\theta_w) + c_{2;tf} \cdot (1/16 \cdot b_{tf} - 1/2 \cdot r_{i;tf} \cdot \sin\theta_w)}{b_{tf}})}{L_{ef}^4} \tag{C.54}$$

The approximated total potential energy (equation C.54) is minimized with respect to the coefficients w_2 and L_{ef}. From here, it may be derived that

$$\frac{1}{w_2} = \frac{16 \cdot D \cdot b_{tf} \cdot L_{ef}^5 \cdot (b_{tf}^3 \cdot (8960 \cdot c_{1;w} \cdot (c_{1;w} + c_{2;w}) + 4032 \cdot c_{2;w}^2) + b_w^3 \cdot (4480 \cdot c_{1;tf} \cdot (c_{1;tf} + c_{2;tf}) + 2016 \cdot c_{2;tf}^2))}{11025 \cdot F \cdot b_w^3 \cdot (b_{tf}^4 \cdot (16 + 4 \cdot c_{1;tf} + c_{2;tf}) - b_{tf}^3 \cdot r_{i;tf} \cdot \sin\theta_w \cdot (16 \cdot c_{1;tf} + 8 \cdot c_{2;tf})}$$

$$- \frac{16 \cdot D \cdot b_{tf}^4 \cdot L_{ef}^3 \cdot b_w^2 \cdot (8960 \cdot c_{1;w}^2 + 107520 \cdot c_{1;w} + 53760 \cdot c_{2;w} + 9408 \cdot c_{1;w} \cdot c_{2;w} + 1440 \cdot c_{2;w}^2)}{11025 \cdot F \cdot b_w^3 \cdot (b_{tf}^4 \cdot (16 + 4 \cdot c_{1;tf} + c_{2;tf}) - b_{tf}^3 \cdot r_{i;tf} \cdot \sin\theta_w \cdot (16 \cdot c_{1;tf} + 8 \cdot c_{2;tf})}$$

$$- \frac{16 \cdot D \cdot b_{tf}^3 \cdot L_{ef}^3 \cdot b_w^3 \cdot n^2 \cdot (4480 \cdot c_{1;tf}^2 + 53760 \cdot c_{1;tf} + 26880 \cdot c_{2;tf} + 4704 \cdot c_{1;tf} \cdot c_{2;tf} + 720 \cdot c_{2;tf}^2)}{11025 \cdot F \cdot b_w^3 \cdot (b_{tf}^4 \cdot (16 + 4 \cdot c_{1;tf} + c_{2;tf}) - b_{tf}^3 \cdot r_{i;tf} \cdot \sin\theta_w \cdot (16 \cdot c_{1;tf} + 8 \cdot c_{2;tf})} \tag{C.55}$$

In the derivation of the effective length (minimizing the total potential energy of equation C.54 with respect to L_{ef}) it turns out to be impossible to determine the effective length analytically. This is because an equation of the effective length in the fifth degree remains to be solved after differentiating the total potential energy with respect to L_{ef}.

Combination 5 consists of a less complicated total potential energy functional, resulting in an equation of the effective length in the second degree, that can be solved analytically, after the neglect of some terms (section C.3.5). The difference in complexity between the combinations 5 and 6 stems from the unknown magnitude of the constants $c_{1;w}$, $c_{2;w}$, $c_{1;f}$ and $c_{2;f}$ in case of combination 6, resulting in an impossibility to ignore certain terms. The kinematical admissible trial function $w(x,y)$ is defined to be the product of two separate functions $w(x)$ and $w(y)$. The deformation over the length of the member for combination 5 and 6 is described by the same fourth degree polynomial $w(y)$. The only difference is formed by the compatibility approach and thus by the descriptions of the deformations over the cross-section of the member $w(x)$. Only $w(y)$ is a function of the effective length. Hereby, $w(x)$ can be thought of as a constant in minimizing the total potential energy with respect to the effective length, resulting in the same kind of equation (with different constants) for combination 5 and 6, from which the effective length can be solved. It is assumed that the difference in the description of $w(x)$ has no significant influence on the resulting effective length. Henceforth, the effective length in combination 6 is taken equal to the effective lenth of combination 5 and given by

$$L_{ef} = \sqrt{\frac{b_{tf}^3 \cdot (34 \cdot b_w^2 + 504 \cdot L_{lb}^2) + b_w^3 \cdot n^2 \cdot (17 \cdot b_{tf}^2 + 252 \cdot L_{lb}^2)}{14 \cdot b_{tf}^3 + 7 \cdot b_w^3 \cdot n^2}} \tag{C.56}$$

Substitution of the equations C.55 and C.56 into C.52b and using equation C.31 results in

$$K_{\Delta b_w} = \frac{D \cdot b_{tf}^2 \cdot L_{ef}^5}{1575 \cdot (L_{lb}^2 - L_{ef}^2)^4 \cdot (b_{tf}^2 + b_w^2 \cdot n)}$$

$$\cdot [\frac{[b_{tf}^4 \cdot (b_w^3 \cdot L_{ef}^2 \cdot (8640 + 2400 \cdot n) + 5248 \cdot L_{ef}^4 \cdot b_w + b_{tf} \cdot (L_{ef}^2 \cdot (1536 \cdot L_{ef}^2 + 3936 \cdot b_w^2 + 2400 \cdot b_w^2 \cdot n))}{[b_w \cdot \sin^2\theta_w \cdot r_{i;tf}^2 \cdot (\sin\theta_w \cdot r_{i;tf} - b_{tf}) \cdot (b_{tf}^2 \cdot (b_{tf} \cdot (4 \cdot \sin\theta_w \cdot r_{i;tf} - b_{tf}) - b_w \cdot n \cdot (b_w + 5 \cdot \sin\theta_w \cdot r_{i;tf}) - 4 \cdot \sin^2\theta_w \cdot r_{i;tf}^2)}$$

$$\frac{+ b_{tf}^5 \cdot b_w^3 \cdot (b_w \cdot (3150 + 15750 \cdot n^2) + 7875 \cdot b_{tf} \cdot n^2) + b_w^4 \cdot (b_{tf}^3 \cdot L_{ef}^2 \cdot (2400 \cdot n^2 - 768 \cdot n + 8800) + 6656 \cdot b_{tf} \cdot L_{ef}^4 \cdot n^2)]}{+ b_w \cdot \sin\theta_w \cdot r_{i;tf} \cdot n \cdot (\sin\theta_w \cdot r_{i;tf} \cdot (b_w + 5 \cdot b_{tf}) - b_w \cdot b_{tf}))]}$$

$$+ \frac{[b_w^5 \cdot (L_{ef}^2 \cdot n^2 \cdot (768 \cdot L_{ef}^2 + 2400 \cdot b_{tf}^2) + b_{tf}^2 \cdot n \cdot (7875 \cdot b_{tf}^2 \cdot n - 8960 \cdot L_{ef}^2) - 2100 \cdot b_{tf}^4 + 4096 \cdot b_w \cdot b_{tf} \cdot L_{ef}^2 \cdot n^2)}{[b_w \cdot \sin^2\theta_w \cdot r_{i;tf}^2 \cdot (\sin\theta_w \cdot r_{i;tf} - b_{tf}) \cdot (b_{tf}^2 \cdot (b_{tf} \cdot (4 \cdot \sin\theta_w \cdot r_{i;tf} - b_{tf}) - b_w \cdot n \cdot (b_w + 5 \cdot \sin\theta_w \cdot r_{i;tf}) - 4 \cdot \sin^2\theta_w \cdot r_{i;tf}^2)}$$

$$\frac{+ b_{tf}^2 \cdot (b_w^6 \cdot (8400 \cdot n \cdot (b_{tf} + b_w) - 5250 \cdot b_{tf}) + L_{ef}^4 \cdot b_w^2 \cdot (b_w \cdot n \cdot (3200 \cdot n - 9984) - b_{tf} \cdot (4608 \cdot n - 6400)))]}{+ b_w \cdot \sin\theta_w \cdot r_{i;tf} \cdot n \cdot (\sin\theta_w \cdot r_{i;tf} \cdot (b_w + 5 \cdot b_{tf}) - b_w \cdot b_{tf}))]}] \qquad \text{(C.57)}$$

Equation C.57 is thought to represent the most accurate approximation of the web crippling stiffness in the energy model.

Appendix D

This appendix gives an overview of the results of the parameter study that is carried out on the finite element model, the energy model and the beam on elastic foundation model, as well as specifications of the batch file that is used within ANSYS to carry out the parameter study.

D.1 Results of the parameter study

The whole parameter study is carried out for three members with small, medium and large corner radii (section 7.2). The geometrical dimensions (in mm) of the general members are:

- General member 1: L_{span}=1560, θ_w=90°, b_{bf}=60, b_w=65, b_{tf}=60, $r_{i;bf}$=1, $r_{i;tf}$=1, t=0.7 and L_{lb}=100;
- General member 2: L_{span}=1560, θ_w=90°, b_{bf}=60, b_w=65, b_{tf}=60, $r_{i;bf}$=5, $r_{i;tf}$=5, t=0.7 and L_{lb}=100;
- General member 3: L_{span}=1560, θ_w=90°, b_{bf}=60, b_w=65, b_{tf}=60, $r_{i;bf}$=10, $r_{i;tf}$=10, t=0.7 and L_{lb}=100.

For each member the parameters (except the corner radii) are varied as follows (in mm):

- L_{span}: 520, 1040, 1560, 2080, 2600;
- θ_w: 50°, 60°, 70°, 80°, 90°;
- b_{bf}: 20, 40, 60, 80, 100, 120;
- b_w: 30, 50, 65, 80, 100;
- b_{tf}: 20, 40, 60, 80, 100, 120;
- t: 0.5, 0.7, 0.9, 1.1, 1.3, 1.5;
- L_{lb}: 25, 50, 100, 150, 200, 250, 300.

Besides, the influence of the corner radii is once more investigated by varying $r_{i;tf}$(and thus $r_{i;bf}$) from 1 to 10 mm (steps of 1 mm) using the geometrical dimensions of the abovementioned general members (except for the corner radii).

The parameter study is carried out on the finite element model (FEM), the energy model and the beam on elastic foundation model. For the energy model, all six combinations are involved. They differ from each other in the deformation variation description over the length of the member and the kind of approach which is applied in describing the connection between the plates (hinge compatibility approach (hca) and geometrical compatibility approach (gca)). The beam on elastic foundation model (boef) is evaluated for four different values of α, namely 0.2, 0.4, 0.6 and 0.8. For sake of clarity the six combinations of the energy model are once more given below.

- Combination 1: Bilinear deformation pattern over the length of the member (bilinear), hca;
- Combination 2: Bilinear deformation pattern over the length of the member (bilinear), gca;
- Combination 3: Trilinear deformation pattern over the length of the member (trilinear), hca;
- Combination 4: Trilinear deformation pattern over the length of the member (trilinear), gca;
- Combination 5: Fourth degree polynomial deformation pattern over the length of the member (fdp), hca;
- Combination 6: Fourth degree polynomial deformation pattern over the length of the member (fdp), gca.

Considering the energy model the emphasis of the discussion of the results will be on the combinations which are based upon the geometrical compatibility approach as the hinge compatibility approach is only a simplified version of the former. The results are grouped per parameter. The web crippling stiffnesses of the general member with varying corner radii are given in table D.1. These results are shown once more in the figures D.1 and D.2.

Table D.1: *Web crippling stiffness against corner radii for the general member*

	Fem	Beam on elastic foundation model				Energy model					
r_i		α=0.2	α=0.4	α=0.6	α=0.8	1	2	3	4	5	6
1	43478	62679	84140	95426	105289	199667	130953	361316	295745	121352	136670
2	20305	22661	28368	32874	37162	48196	31937	85434	73009	29766	33529
3	12384	11509	14498	17173	19714	20795	13819	36134	32027	13006	14643
4	8811	7032	9031	10865	12586	11414	7558	19454	177784	7207	8107
5	6897	4803	6288	7652	8922	7162	4701	11982	11244	4551	5116
6	5706	3530	4699	5768	6757	4897	3174	8050	7722	3123	3510
7	4872	2731	3688	4557	5357	3558	2268	5749	5620	2271	2552
8	4251	2194	3000	3726	4391	2705	1691	4299	4271	1722	1938
9	3756	1815	2507	3128	3693	2130	1303	3333	3357	1350	1522
10	3364	1537	2141	2681	3170	1726	1032	2660	2711	1086	1228

From figure D.1 and table D.1 it becomes clear that the energy model produces poor results for small corner radii (1-2 mm). The combinations 5 and 6 which are based upon the fourth degree polynomial description of the deformations over the length of the member give poor approximations for members with corner radii larger than 5 mm, while the combinations 3 (figure D.2) and 4 are relatively worse for corner radii smaller than 6 mm. The models which are based upon the bilinear description of the deformation variations over the length of the member perform badly for almost all corner radii. It may be concluded that the influence of the corner radii is poorly covered in the energy model. It is striking that the combinations 3 and 4 which are based upon the trilinear deformation description over the length of the member give the best approximations for large corner radii. The results of the beam on elastic foundation model and combination 3 of the energy model for varying corner radii are given in figure D.2.

Combination 6 which is based upon the fourth degree polynomial description of the deformations over the length of the member performs relatively best for small corner radii, while combination 3 which is based upon the trilinear description of the deformations over the length of the member perform relatively best for

large corner radii.

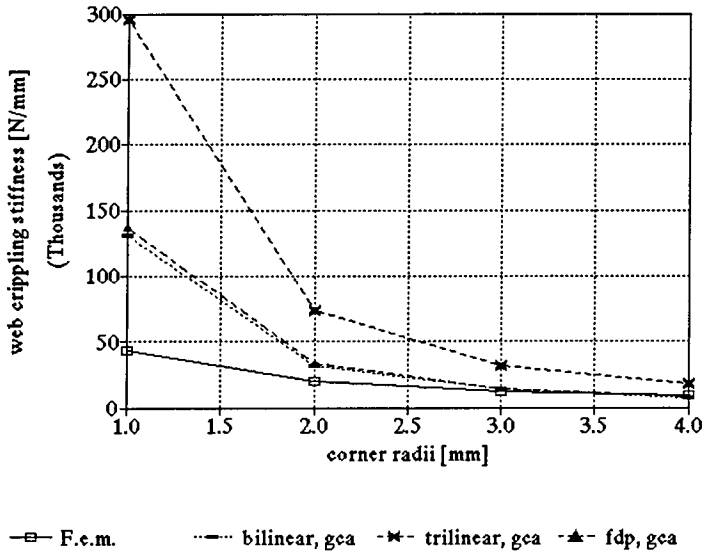

Figure D.1a: Web crippling stiffness for varying corner radii (1-4 mm)

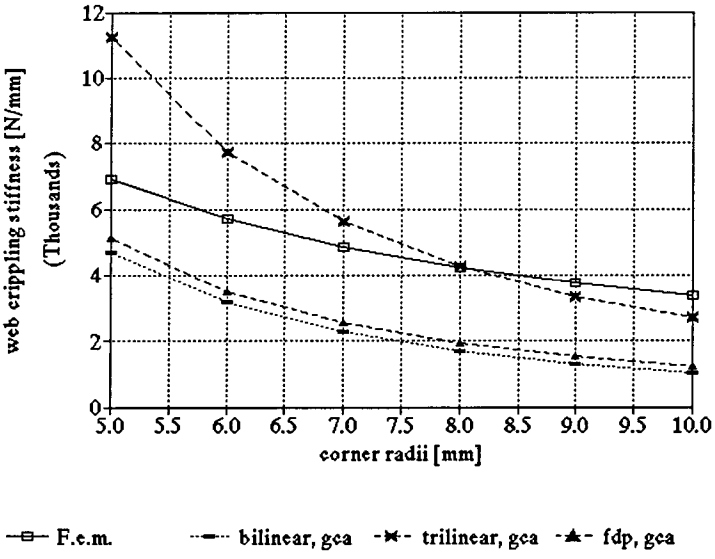

Figure D.1b: Web crippling stiffness for varying corner radii (5-10 mm)

It may be concluded that the corner radii are not very well accounted for throughout the energy model. The energy models result in a web crippling stiffness that is inversely proportional to the square corner radii while

the finite element simulations tend to show a behaviour in which the web crippling stiffness is more or less inversely proportional to the corner radii.

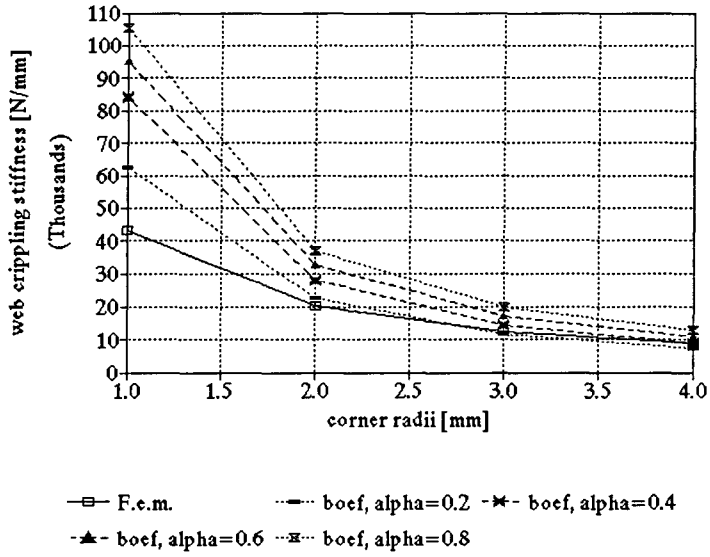

Figure D.2a: Web crippling stiffness for varying corner radii (1-4 mm)

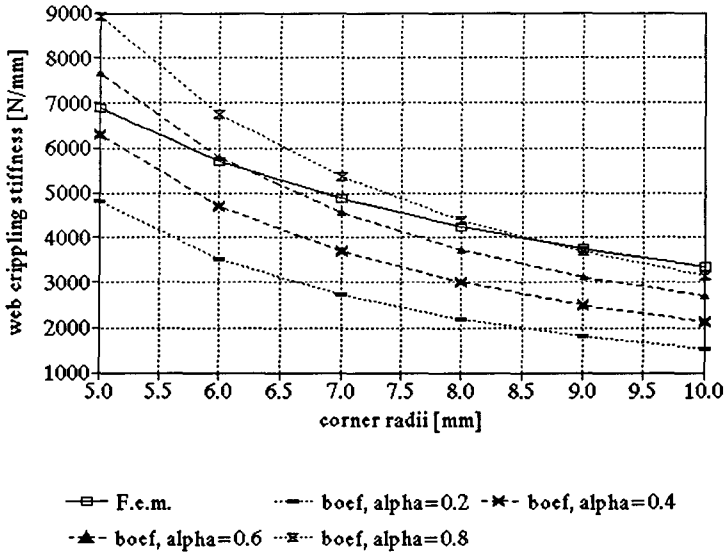

Figure D.2b: Web crippling stiffness for varying corner radii (5-10 mm)

From the figures D.2 and table D.1 it is clear that the beam on elastic foundation model does not perform

very well over the whole range for α having a constant value. However, if α is taken proportional to the magnitude of the corner radii it is possible to produce reliable web crippling stiffness approximations for the general member with varying corner radii.

The other parameters are varied for the three general members. First the results for each parameter are discussed separately for the general member with corner radii of 1 mm, whereafter the results for the members with corner radii of 5 and 10 mm respectively are treated.

General member 1 (r=1):

Influence concerning the bottom flange

The influence of the bottom flange on the web crippling stiffness in case of general member 1, according to the several models is tabulated in table D.2.

Table D.2: *Web crippling stiffness against bottom flange for general member 1*

b_{bf}	Fem	Beam on elastic foundation model				Energy model					
		α=0.2	α=0.4	α=0.6	α=0.8	1	2	3	4	5	6
20	38462	58604	78027	88526	97821	180253	116345	307821	273317	115475	127245
40	41667	61089	81745	92719	102360	192386	125644	341252	287108	119135	133030
60	43478	62679	84140	95425	105289	199667	130953	361316	295745	121352	136671
80	44944	63784	85813	97317	107335	204512	134379	374665	301576	122828	139133
100	45977	64596	87047	98713	108846	207965	136771	384180	305758	123878	140900
120	46512	65219	87995	99787	110007	210549	138535	391302	308897	124663	142228

These results are shown once more in the figures D.3 and D.4.

From figure D.3 it is clear that all combinations overestimate the web crippling stiffness greatly. However, this overestimation is caused by the fact that the corner radii are not covered very well in the energy model. The deviations between the finite element simulations and the energy model combinations are more or less constant over the whole range of the bottom flange. This indicates that the energy model performs reasonably well as far as the influence of the bottom flange is concerned. Hence, it can be concluded that the neglect of the deformation variations over the bottom flange is justified by these results. It is remarkable that combination 4 produces large deviations from the finite element simulations compared to the other combinations of the model in varying the width of the bottom flange.

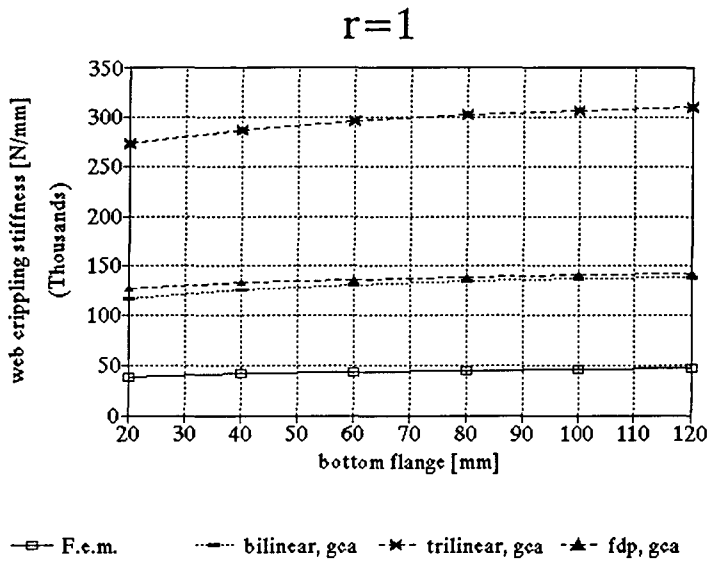

Figure D.3: Web crippling stiffness for varying bottom flanges

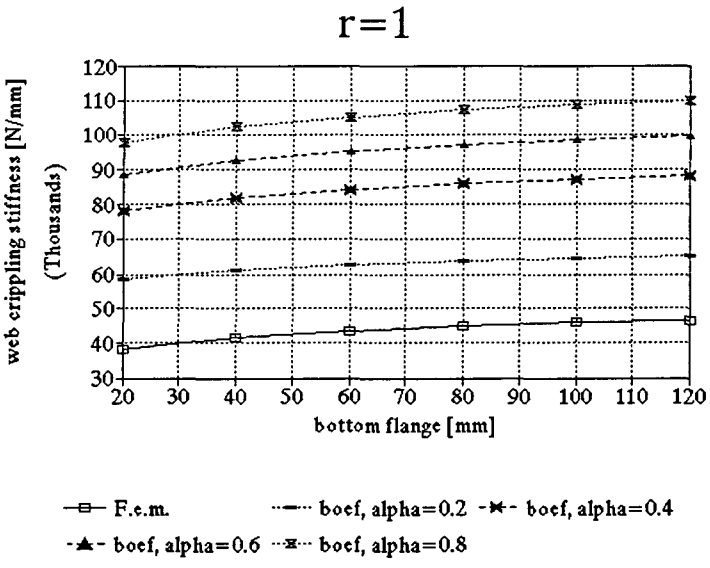

Figure D.4: Web crippling stiffness for varying bottom flanges

In figure D.4 it is shown the beam on elastic foundation model performs not very good for $\alpha>0.2$. It is to be expected that $\alpha=0.1$ produces good results. Note that the deviations between the finite element simulations and the beam on elastic foundation model have a constant value over the whole range of the bottom flange,

implying that the influence of the bottom flange is fairly taken into account.

Influence concerning the top flange

The influence of the top flange on the web crippling stiffness in case of general member 1, according to the several models is tabulated in table D.3. These results are shown once more in the figures D.5 and D.6.

Table D.3: Web crippling stiffness against top flange for general member 1

b_{tf}	Fem	Beam on elastic foundation model				Energy model					
		α=0.2	α=0.4	α=0.6	α=0.8	1	2	3	4	5	6
20	54054	91434	134950	155384	169968	397521	620595	505989	463293	59830	225306
40	47059	71310	98367	111540	122430	248547	220320	390028	335816	90247	160318
60	43478	62679	84140	95426	105289	199667	130953	361316	295745	121352	136671
80	42105	57599	76253	86706	96097	175330	99982	365036	285505	152787	124218
100	40816	54120	71055	81030	90141	160755	86534	394023	294000	184478	116568
120	40404	51510	67256	76907	85824	151049	79760	449525	318378	216400	111459

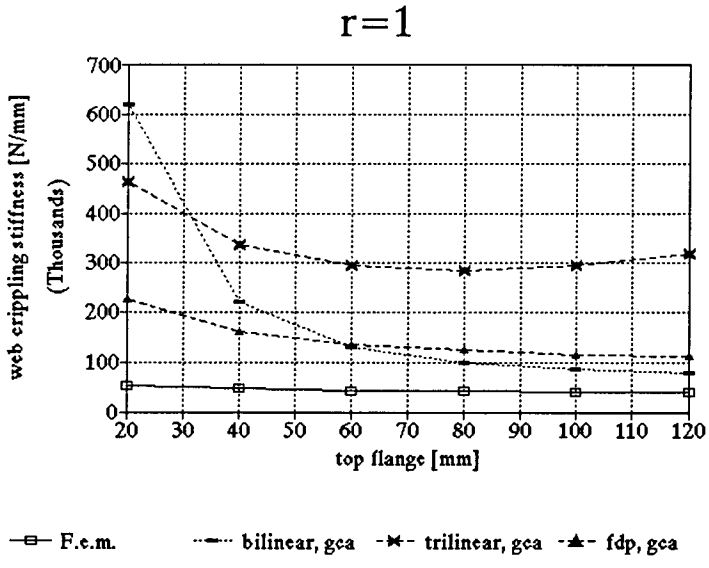

Figure D.5: Web crippling stiffness for varying top flanges

It should be noted that the combination which produces the smallest web crippling stiffness does not automatically represent the most reliable solution (as was the case in comparing the finite element simulations). Due to the different deformation variation descriptions, different solutions for the web crippling stiffness cannot be

compared that way.

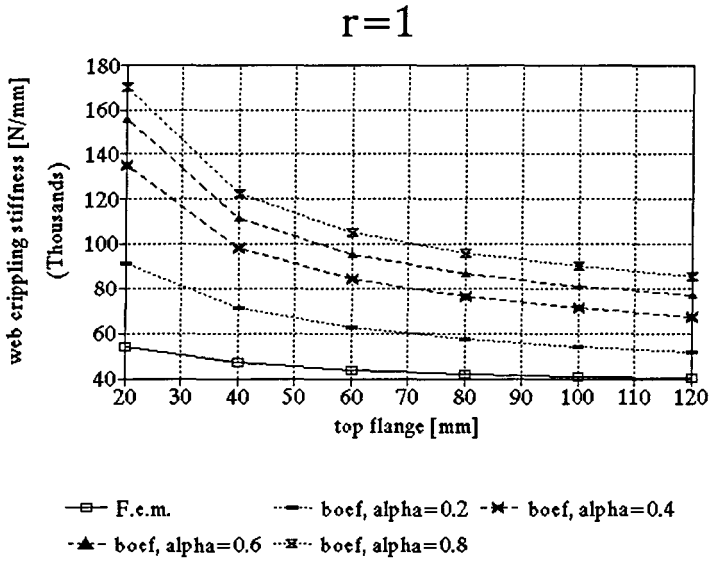

Figure D.6: Web crippling stiffness for varying top flanges

According to figure D.5, only combination 6 produces results that have a rather constant deviation from the finite element simulations. The other combinations do not give reliable results for the influence of the top flange on the web crippling stiffness. It is striking that combination 5 which is based upon the hinge compatibility approach depends differently on the magnitude of the top flange than the combination 6 which is based upon the geometrical compatibility approach. Apparently, the hinge compatibility approach is no longer valid if the magnitude of the top flange is varied strongly. This can be clarified by considering the portal frame of the portal frame model. If the length of the top flange is varied it is clear that the bending moment at the connection between the top flange and the web will vary also. From figure D.6 it becomes clear that the beam on elastic foundation model performs somewhat better than the energy model, as far as the negotiation of the top flange is concerned. However, both the energy model and the beam on elastic foundation model tend to deviate extra from the finite element simulations for small top flanges.

Influence concerning the web

The influence of the web on the web crippling stiffness in case of general member 1, according to the several models is tabulated in table D.4. These results are shown once more in the figures D.7 and D.8.

Table D.4: Web crippling stiffness against web for general member 1

b_w	Fem	Beam on elastic foundation model				Energy model					
		α=0.2	α=0.4	α=0.6	α=0.8	1	2	3	4	5	6
30	54795	53542	89170	114675	130321	328928	174011	1084006	735945	490927	229892
50	47059	59974	89124	102415	111920	233347	134912	480702	375850	192562	161308
65	43478	62679	84140	95426	105289	199667	130953	361316	295745	121352	136671
80	41365	62861	76253	91447	102212	178743	134547	297636	250999	85366	121017
100	39254	61272	71055	88930	100902	160877	143970	246965	214071	59480	107411

Apparently, only the combinations 2 and 6 correspond to the behaviour of the finite element simulations if the magnitude of the web is varied (they have almost constant deviations for webs larger than 40 mm). Due to the fact that the trilinear-hca-approach deviates greatly from the finite element simulations it is difficult to investigate the influence of the webs on the beam on elastic foundation model. However, from table D.4 it is clear that the beam on elastic foundation model shows a significant different behaviour for α=0.2 than for other magnitudes of α. This might be caused by the schematisation of the beam on the elastic foundation, which implies a use of the web in the model that depends on the magnitude of α. A better insight in this problem is established for general member 2.

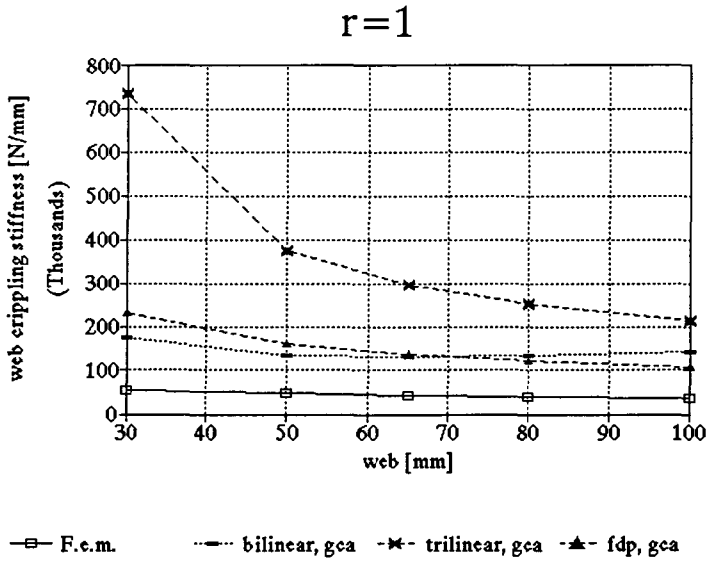

Figure D.7: Web crippling stiffness for varying webs

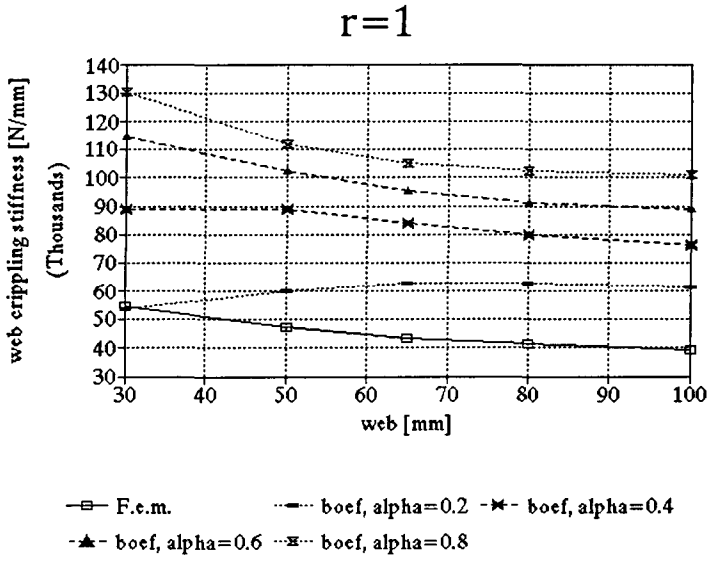

Figure D.8: Web crippling stiffness for varying webs

Influence concerning the web angle

The influence of the web angle on the web crippling stiffness in case of general member 1, according to the several models is tabulated in table D.5.

Table D.5: Web crippling stiffness against web angle for general member 1

θ_w	Fem	Beam on elastic foundation model				Energy model					
		α=0.2	α=0.4	α=0.6	α=0.8	1	2	3	4	5	6
50	66667	85819	120400	136797	150025	343340	224368	624372	505395	207783	207783
60	67797	74702	102674	116471	128048	267594	175150	485603	394966	162243	182706
70	62500	67723	91829	104133	114707	226639	148511	410642	335169	137595	154958
80	52632	63891	85975	97500	107534	205994	135073	372883	304996	125163	140962
90	43478	62679	84140	95426	105289	199667	130953	361316	295745	121352	136671

These results are shown once more in the figures D.9 and D.10. Both the energy model (all six approaches) and the finite element simulations tend to show an increasing web crippling stiffness with a decreasing web angle. This seems quite logical because the smaller the web angle, the smaller the eccentricity of the load which corresponds to an increasing web crippling stiffness. However, the gradients of the combination of the energy model and the finite element simulations differ greatly from each other.

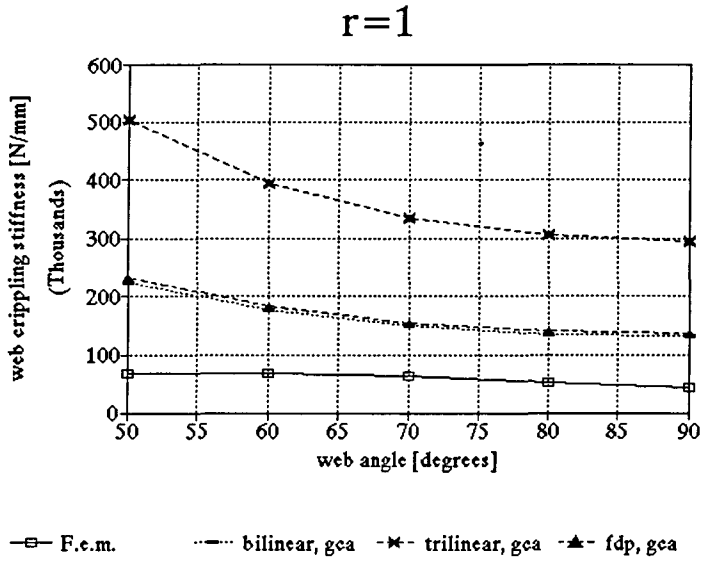

Figure D.9: Web crippling stiffness for varying web angles

The beam on elastic foundation model (figure D.10) performs somewhat better than the energy model: the approximations are reasonably more accurate, but this might also be caused by the different negotiation of the corner radii.

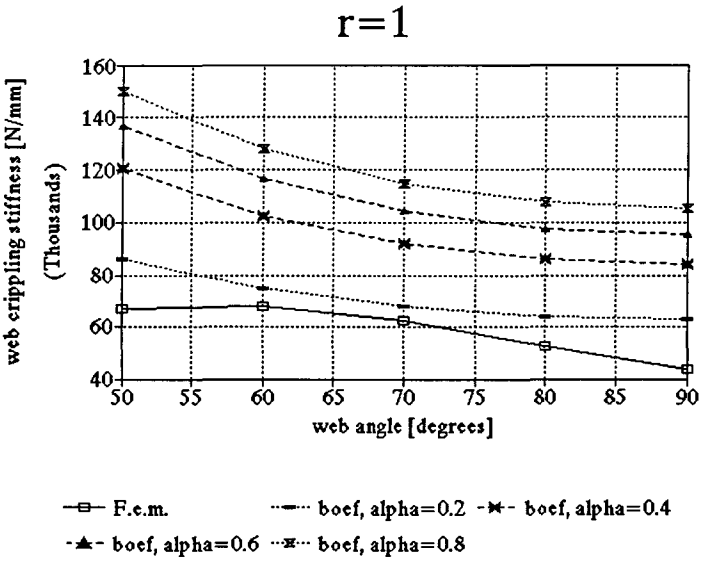

Figure D.10: Web crippling stiffness for varying web angles

Influence concerning the load bearing plate

The influence of the load bearing plate on the web crippling stiffness in case of general member 1, according to the several models is tabulated in table D.5.

Table D.6: *Web crippling stiffness against load bearing plate for general member 1*

L_{lb}	Fem	Beam on elastic foundation model				Energy model					
		α=0.2	α=0.4	α=0.6	α=0.8	1	2	3	4	5	6
25	37383	35450	51832	66052	78889	49917	32738	320677	263312	44218	53054
50	42105	46724	60547	73263	85143	99834	65477	334223	274123	66941	76376
100	43478	62679	84140	95426	105289	199667	130953	361316	295745	121352	136671
150	43956	61823	98943	117974	129503	299501	196430	388408	317367	178391	200464
200	43478	60459	100432	130058	148856	399335	261906	415501	338989	236141	265158
250	43956	60383	98135	131912	158230	499168	327383	442594	360611	294181	330216
300	43478	60460	96678	129824	159675	599002	392860	469687	382232	352366	395455

These results are shown once more in the figures D.11 and D.12.

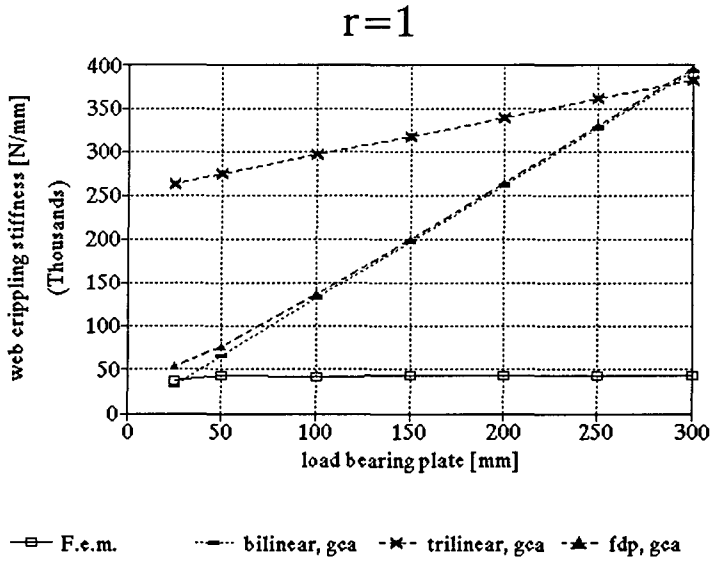

Figure D.11: *Web crippling stiffness for varying load bearing plates*

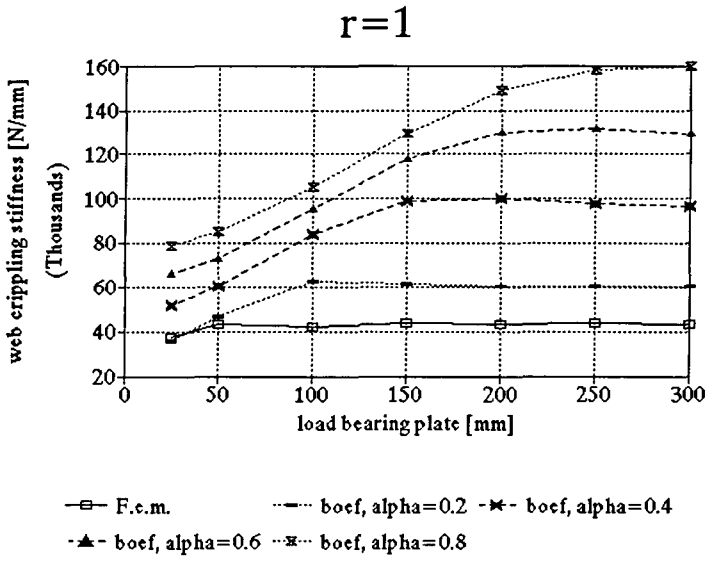

Figure D.12: Web crippling stiffness for varying load bearing plates

It may be concluded that the load bearing plate is poorly covered in the energy model. Probably, this is caused by the chosen deformation descriptions over the length of the member: in these descriptions it is assumed that the deformations continuously increase under the load bearing plate, except by the trilinear description. It is this trilinear description that relatively produces the most constant deviations. In reality the top flange curls downward under the load bearing plate but simultaneously some upward curling occurs under the centre of the load bearing plate (figure 5.3), especially in case of longer load bearing plates. For this decrease in the deformation of the top flange not taking into account, it seems quite logical that the larger the load bearing plate the worse the energy model predicts the web crippling stiffness.
Apparently, the beam on elastic foundation model, in which the deformation variation over the length of the member is described by the deflection curve of the beam on elastic foundation theory, performs slightly better as far as the load bearing plate is concerned. For large load bearing plates the web crippling stiffness is more or less independent of the magnitude of the load bearing plate, just as the finite element simulations tend to point out.

Influence concerning the span length

The influence of the span length on the web crippling stiffness in case of general member 1, according to the several models is tabulated in table D.7.

Table D.7: Web crippling stiffness against span length for general member 1

L_{span}	Fem	Beam on elastic foundation model				Energy model					
		α=0.2	α=0.4	α=0.6	α=0.8	1	2	3	4	5	6
520	43568	62679	84150	95297	104514	199667	130953	156562	127411	121352	136671
1040	43526	62679	84150	95426	105286	199667	130953	258939	211578	121352	136671
1560	43478	62679	84150	95426	105286	199667	130953	361316	295745	121352	136671
2080	43479	62679	84150	95426	105286	199667	130953	463693	379912	121352	136671
2600	43479	62679	84150	95426	105286	199667	130953	566069	464079	121352	136671

These results are shown once more in the figures D.13 and D.14.

The assumption that the web crippling deformations tend to concentrate in a rather small region around the load bearing plate is confirmed by the finite element simulations. The web crippling stiffness appears to be independent of the span length. Hence, the introduction of an effective length is justified by these simulations.

The combinations 1, 2, 5 and 6 have a constant deviation from the finite element simulations and perform well as far as the span length is concerned.

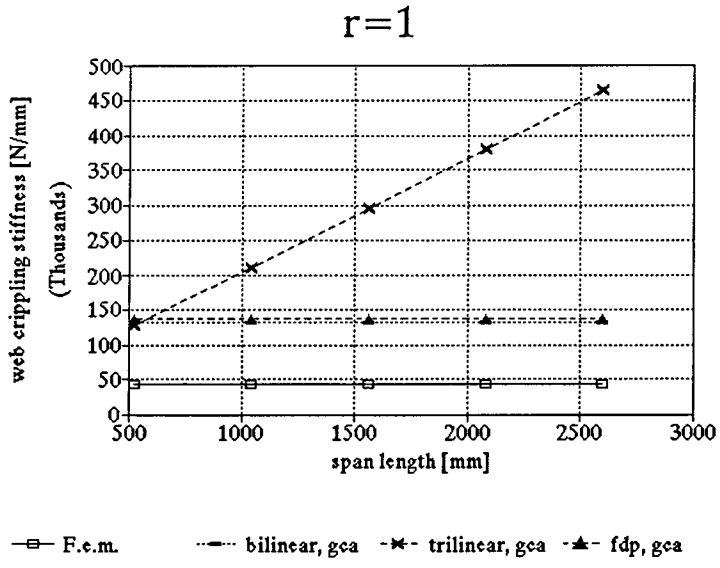

Figure D.13: Web crippling stiffness for varying span lengths

Similarly, the beam on elastic foundation model performs well also as far as the span length is concerned.

Note however, that the web crippling stiffness here is not completely independent of the span length.

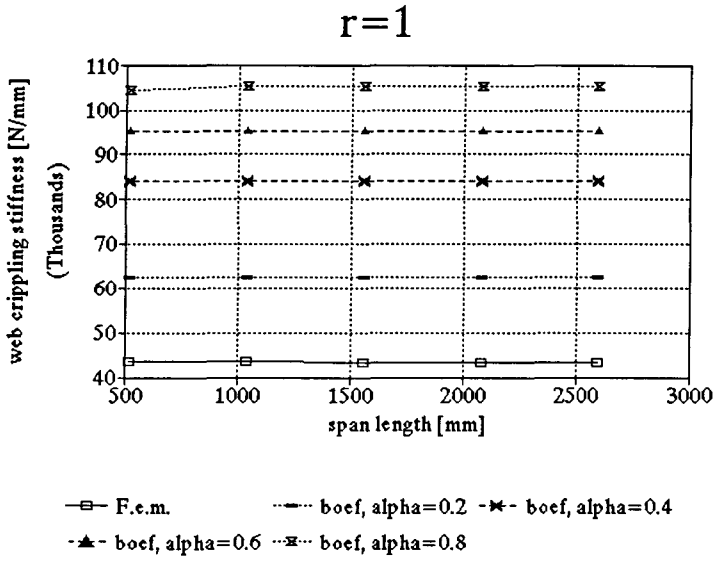

Figure D.14: Web crippling stiffness for varying span lengths

Influence concerning the wall thickness

The influence of the wall thickness on the web crippling stiffness in case of general member 1, according to the several models is tabulated in table D.8.

Table D.8: Web crippling stiffness against wall thickness for general member 1

t	Fem	Beam on elastic foundation model				Energy model					
		α=0.2	α=0.4	α=0.6	α=0.8	1	2	3	4	5	6
0.5	20000	28014	36003	41110	45864	72765	47723	131675	107779	44224	49807
0.7	43478	62679	84140	95426	105289	199667	130953	361316	295745	121352	136671
0.9	74074	109285	152364	172978	189721	424366	278323	767928	628566	257917	290475
1.1	111732	165132	236747	269872	295095	774802	508159	1402074	1147628	470902	530346
1.3	152672	227763	332924	381320	416365	1278918	838788	2314317	1894320	777289	875410
1.5	197044	295212	437153	502945	548855	1964656	1288533	3555221	2910027	1194060	1344792

These results are shown once more in the figures D.15 and D.16.

The energy model treats the wall thickness badly. This might be caused by the neglect of the axial deformations. In the sections A.4 and A.5 it has become clear that the influence of the axial deformations on the web

crippling stiffness might be considerable, especially in case of large wall thicknesses. Throughout the energy model these axial deformations are neglected.

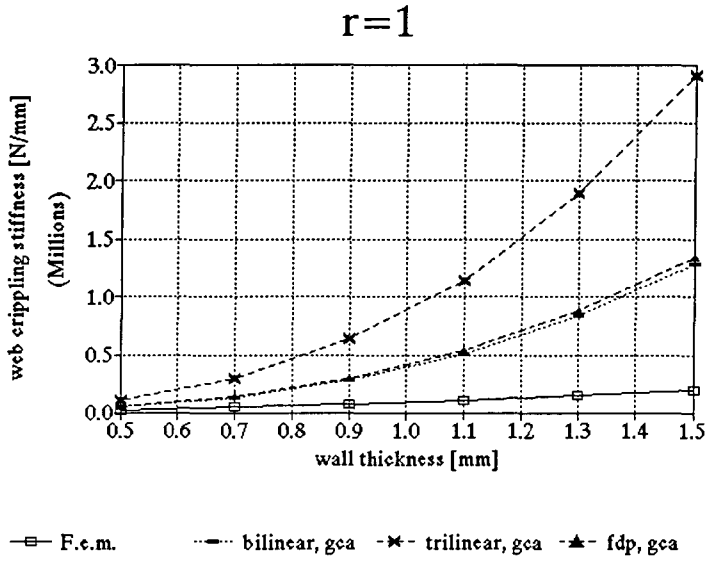

Figure D.15: Web crippling stiffness for varying wall thicknesses

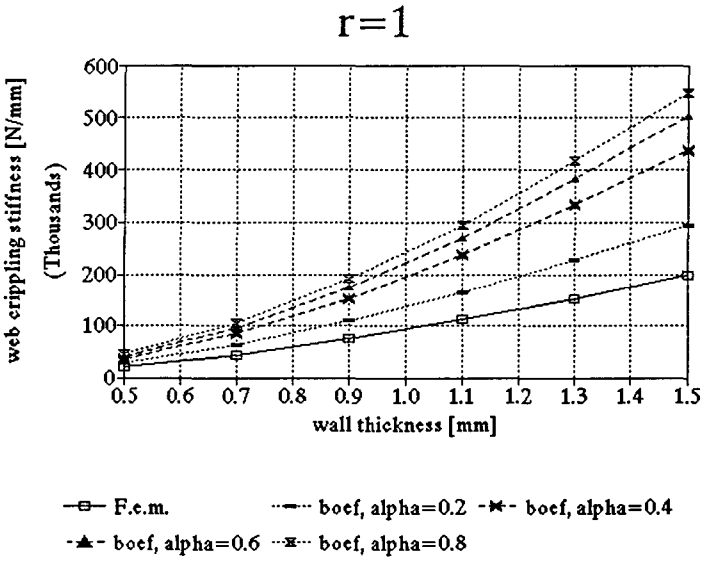

Figure D.16: Web crippling stiffness for varying wall thicknesses

According to figure D.16 and table D.8 it is to be expected that the beam on elastic foundation model produces fairly reliable results for α=0.1.

General member 2 (r=5):

Influence concerning the bottom flange

The influence of the bottom flange on the web crippling stiffness in case of general member 2, according to the several models is tabulated in table D.9. These results are shown once more in the figures D.17 and D.18.

Table D.9: Web crippling stiffness against bottom flange for general member 2

b_{bf}	Fem	Beam on elastic foundation model				Energy model					
		α=0.2	α=0.4	α=0.6	α=0.8	1	2	3	4	5	6
20	6309	4942	6460	7855	9155	6536	4033	10258	10347	4381	4813
40	6689	4854	6351	7726	9007	6925	4453	11332	10886	4484	4993
60	6897	4803	6288	7652	8922	7162	4701	11982	11244	4551	5116
80	7005	4770	6247	7603	8866	7320	4865	12418	11492	4596	5203
100	7080	4747	6218	7569	8827	7433	4981	12729	11673	4629	5266
120	7143	4729	6196	7544	8798	7517	5067	12963	11811	4654	5315

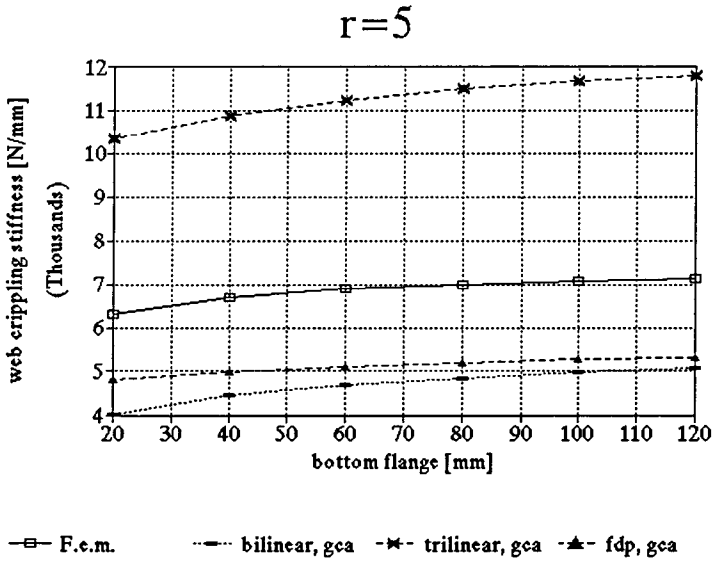

Figure D.17: Web crippling stiffness for varying bottom flanges

The deviations between the finite element simulations and the energy model combinations are more or less constant over the whole range of the bottom flange. This indicates that the energy model performs reasonably well as far as the influence of the bottom flange is concerned, just as was assumed in case of general

member 1. It is striking that the beam on elastic foundation model resulted in constant deviations over the whole range of the bottom flange for each value of α in case of general member 1 but results in slightly increasing deviations with an increasing bottom flange for each value of α in case of general member 2. For α having a magnitude of 0.5 the best approximations of the web crippling stiffness are established.

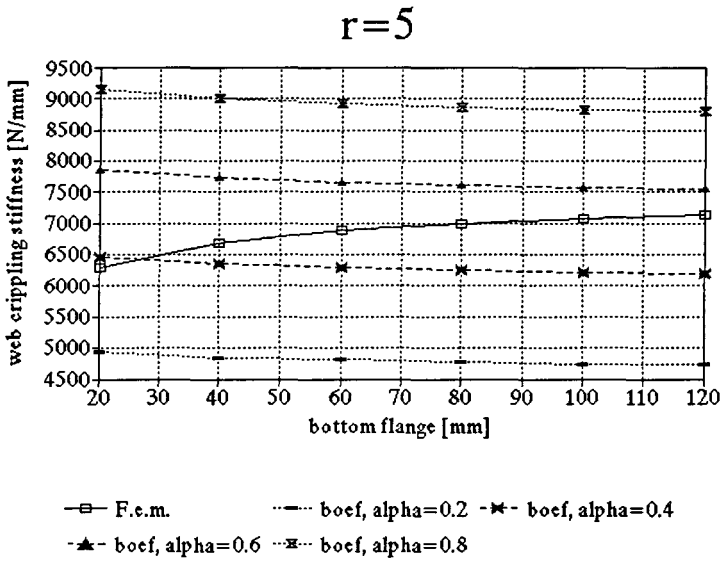

Figure D.18: Web crippling stiffness for varying bottom flanges

Influence concerning the top flange

The influence of the top flange on the web crippling stiffness in case of general member 2, according to the several models is tabulated in table D.10.

Table D.10: Web crippling stiffness against top flange for general member 2

b_{tf}	Fem	Beam on elastic foundation model				Energy model					
		α=0.2	α=0.4	α=0.6	α=0.8	1	2	3	4	5	6
20	9975	9308	11609	13680	15685	18182	25581	20667	20221	2459	8929
40	7576	5805	7454	8972	10402	9343	8068	13258	12759	3458	5960
60	6897	4803	6288	7652	8922	7162	4701	11982	11244	4551	5116
80	6557	4325	5735	7030	8230	6159	3595	12178	11119	5678	4700
100	6349	4044	5411	6668	7831	5579	3144	13406	11873	6824	4451
120	6221	3859	5197	6431	7572	5202	2933	15674	13425	7985	4288

These results are shown once more in the figures D.19 and D.20.

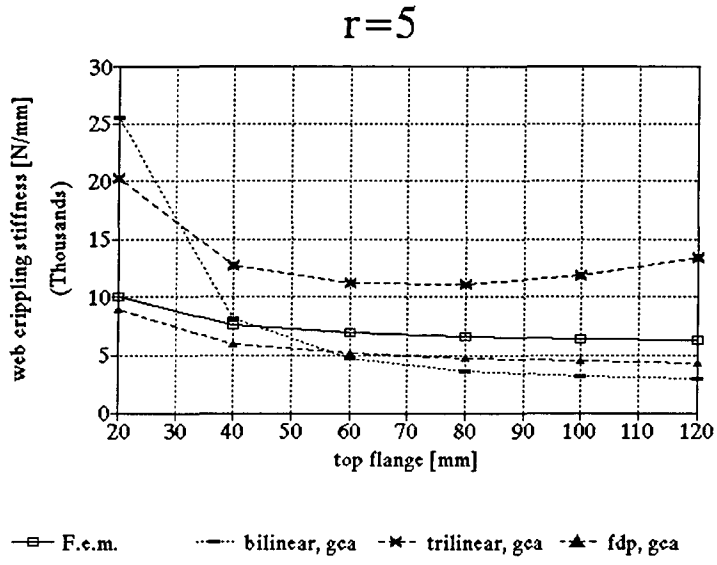

Figure D.19: Web crippling stiffness for varying top flanges

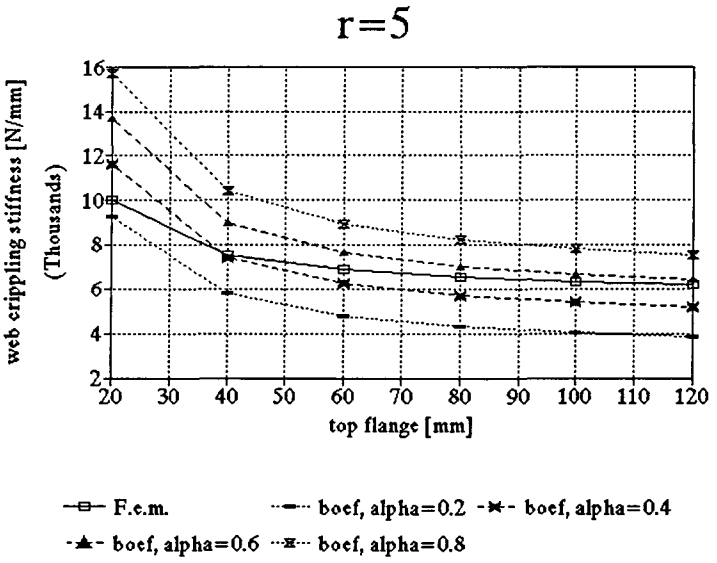

Figure D.20: Web crippling stiffness for varying top flanges

According to figure D.19, only combination 6 produces results that have a rather constant deviation from the finite element simulations. The other combinations do not give reliable results for the influence of the top

flange on the web crippling stiffness, just as for general member 1. It is remarkable that a different description over the length of the member results in strongly different dependencies of a parameter of the cross-section. Again, combination 5 which is based upon the hinge compatibility approach depends differently on the magnitude of the top flange than the combination 6 which is based upon the geometrical compatibility approach. Apparently, the hinge compatibility approach is no longer valid if the magnitude of the top flange is varied strongly.

From figure D.20 it becomes clear that the beam on elastic foundation model performs somewhat better than the energy model, as far as the treatment of the top flange is concerned. However, both the energy model and the beam on elastic foundation model tend to deviate extra from the finite element simulations for small top flanges.

Influence concerning the web

The influence of the web on the web crippling stiffness in case of general member 2, according to the several models is tabulated in table D.11. These results are shown once more in the figures D.21 and D.22. Considering the energy model, only the combinations 2 and 6 correspond to the behaviour of the finite element simulations if the magnitude of the web is varied. This behaviour correspond to the behaviour of general member 1.

Table D.11: Web crippling stiffness against web for general member 2

b_w	Fem	Beam on elastic foundation model				Energy model					
		α=0.2	α=0.4	α=0.6	α=0.8	1	2	3	4	5	6
30	10127	5348	6911	7893	8802	10098	5861	35116	33397	16841	8503
50	7767	5014	6348	7558	8699	8022	4712	15443	14468	7039	6011
65	6897	4803	6288	7652	8922	7162	4701	11982	11244	4551	5116
80	6296	4707	6354	7847	9226	6589	4935	10157	9559	3258	4549
100	5767	4690	6532	8175	9667	6074	5382	8680	8204	2307	4058

From table D.11 and figure D.22 it is clear that the beam on elastic foundation model shows a slightly different behaviour for different values of α. It may be concluded that this is caused by the schematisation of the beam on the elastic foundation, which implies a use of the web in the model that depends on the magnitude of α. The larger α, the bigger the influence the web has on the web crippling stiffness because a large value of α implies a large influence of the second moment of area of the beam on the resulting web crippling stiffness and the magnitude of the second moment of area depends mainly on the web. Besides, the web crippling stiffness is dependent on the two-dimensional web crippling stiffness, that is also a function of the

web. Hence, it is possible that the influence of the web differs with varying magnitudes of α.

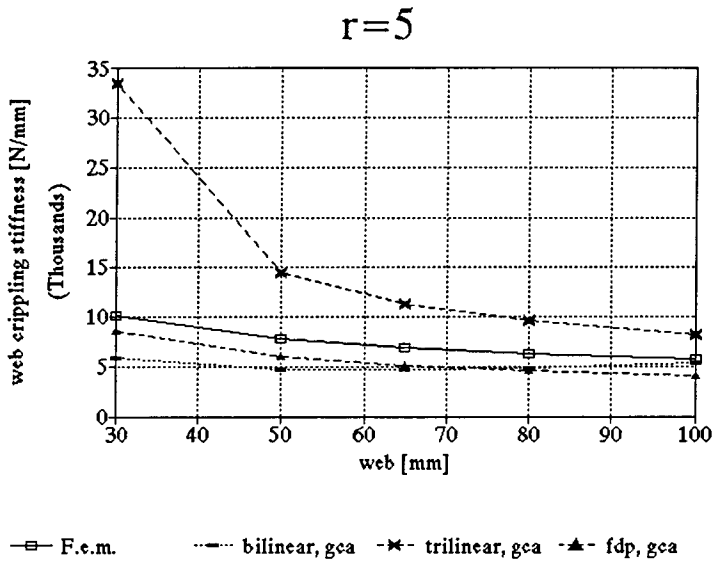

Figure D.21: Web crippling stiffness for varying webs

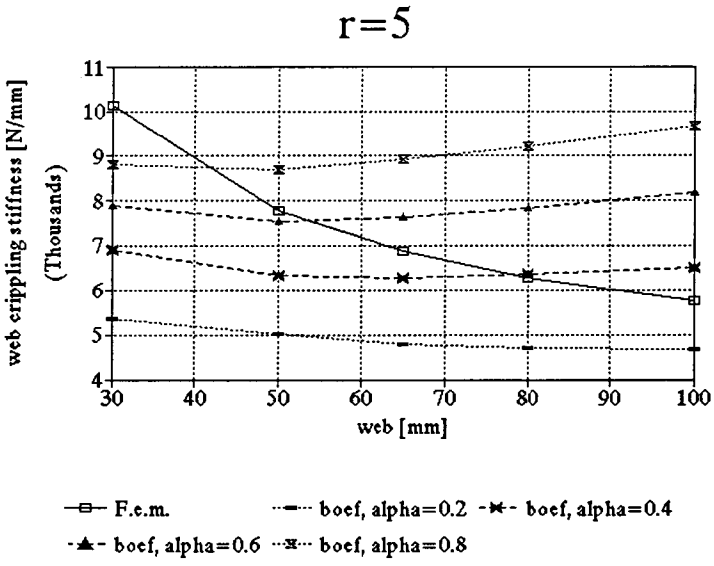

Figure D.22: Web crippling stiffness for varying webs

Influence concerning the web angle

The influence of the web angle on the web crippling stiffness in case of general member 2, according to the several models is tabulated in table D.12.

Table D.12: Web crippling stiffness against web angle for general member 2

θ_w	Fem	Beam on elastic foundation model				Energy model					
		α=0.2	α=0.4	α=0.6	α=0.8	1	2	3	4	5	6
50	16064	7572	9691	11634	13458	12496	8283	21367	19437	7879	8865
60	12539	6138	7934	9585	11130	9671	6389	16382	15113	6889	6889
70	9975	5339	6950	8432	9812	8155	5370	13720	12779	6121	5817
80	8163	4929	6444	7836	9133	7394	4858	12389	11603	5174	5280
90	6897	4803	6288	7652	8922	7162	4701	11982	11244	4697	5116

These results are shown once more in the figures D.23 and D.24. In case of the energy model, all combinations perform reasonably well for general member. It is striking that the general members 1 and 2 tend to show different deviations from the finite element simulations. Here, the energy model seems to treat the web angle reasonably well.

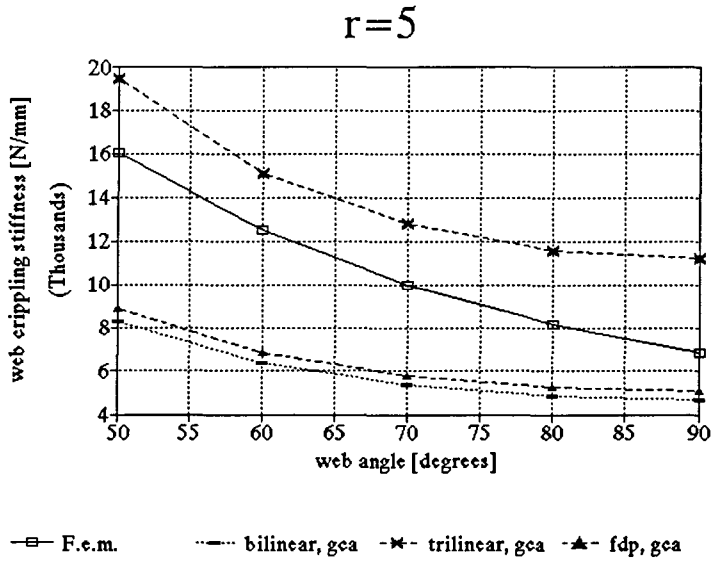

Figure D.23: Web crippling stiffness for varying web angles

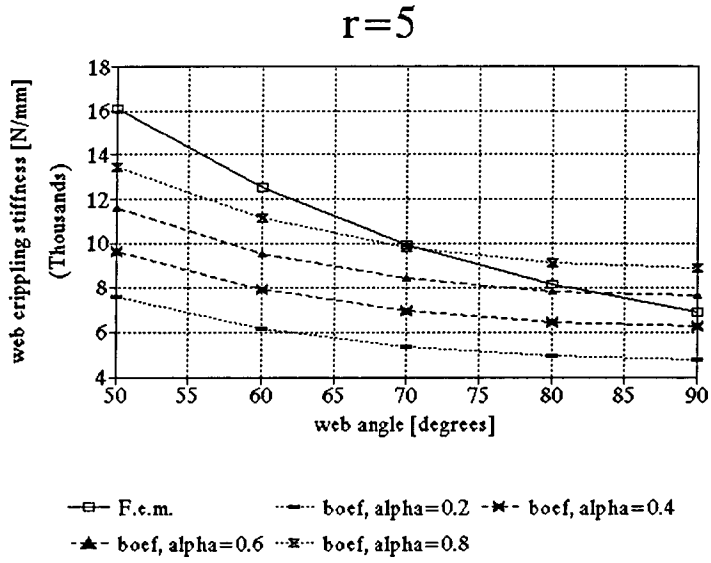

Figure D.24: Web crippling stiffness for varying web angles

The beam on elastic foundation model performs reasonably well also, in predicting the web crippling stiffness for varying web angles, in case of general member 2. It is to be expected that for α=0.7 the best approximations are established. This is contradictory to the rest of the parameters where merely α=0.5 performs best.

Influence concerning the load bearing plate

The influence of the load bearing plate on the web crippling stiffness in case of general member 2, according to the several models is tabulated in table D.13.

Table D.13: Web crippling stiffness against load bearing plate for general member 2

L_{lb}	Fem	Beam on elastic foundation model				Energy model					
		α=0.2	α=0.4	α=0.6	α=0.8	1	2	3	4	5	6
25	4890	3342	5198	6758	8151	1790	1175	10659	10041	1654	2000
50	6033	3699	5448	6959	8322	3581	2351	11100	10442	2508	2860
100	6897	4803	6288	7652	8922	7162	4701	11982	11244	4551	5116
150	6932	5941	7428	8640	9797	10742	7052	12865	12045	6691	7504
200	6908	6571	8643	9816	10875	14323	9402	13747	12846	8858	9926
250	6908	6683	9670	11039	12076	17904	11753	14629	13648	11035	12362
300	6908	6583	10332	12152	13299	21485	14104	15512	14449	13218	14805

These results are shown once more in the figures D.25 and D.26.

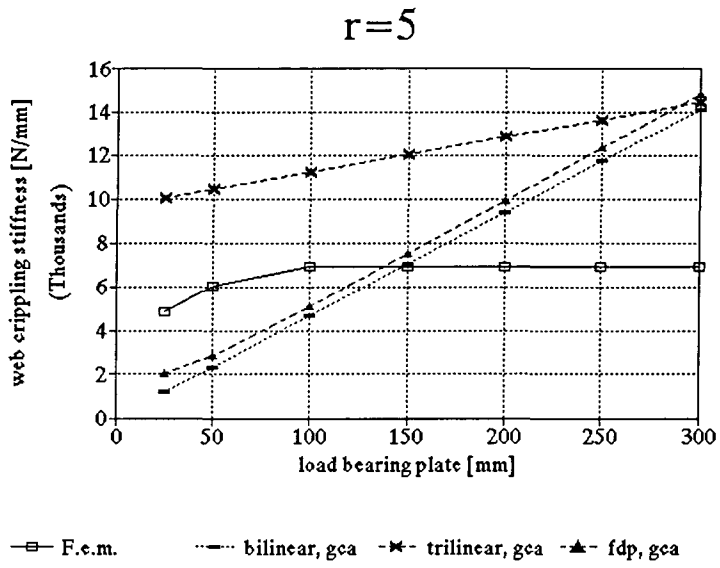

Figure D.25: Web crippling stiffness for varying load bearing plates

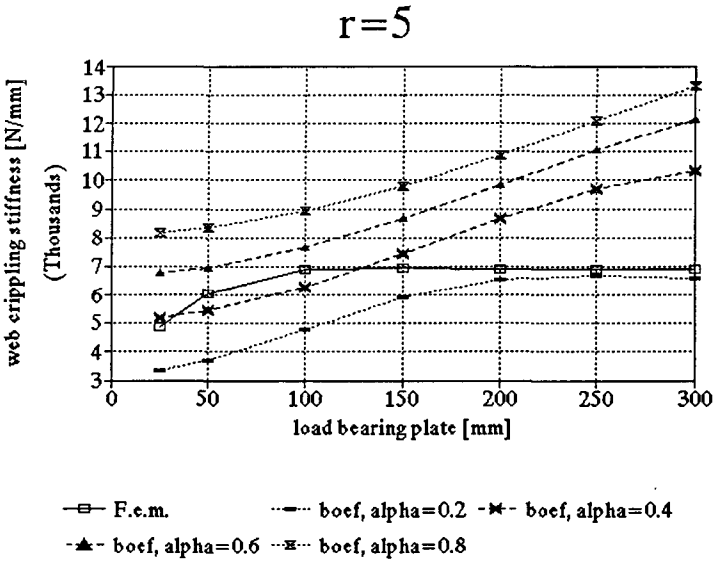

Figure D.26: Web crippling stiffness for varying load bearing plates

Similar to general member 1, it may be concluded that the load bearing plate is poorly covered in the energy model. As mentioned before it is to be expected that this is caused by deformation descriptions over the

length of the member that show increasing deviations from reality with longer load bearing plates.
The beam on elastic foundation model, in which the deformation variation over the length of the member is described by the deflection curve of the beam on elastic foundation theory, performs slightly better as far as the load bearing plate is concerned. For large load bearing plates the web crippling stiffness is more or less independent of the magnitude of the load bearing plate, for small values of α, just as the finite element simulations tend to point out.

Influence concerning the span length

The influence of the span length on the web crippling stiffness in case of general member 2, according to the several models is tabulated in table D.14. These results are shown once more in the figures D.27 and D.28. The assumption that the web crippling deformations tend to concentrate in a rather small region around the load bearing plate is also confirmed by the finite element simulations of general member 2. The web crippling stiffness appears to be independent of the span length. Note that the full length solution which is applied in combination 3 and 4 produces poor results.
The combinations 1, 2, 5 and 6 have a constant deviation from the finite element simulations and perform well as far as the span length is concerned. The deviation is caused by the poor covering of the corner radii.

Table D.14: Web crippling stiffness against span length for general member 2

L_{span}	Fem	Beam on elastic foundation model				Energy model					
		α=0.2	α=0.4	α=0.6	α=0.8	1	2	3	4	5	6
520	6887	4796	6151	7440	8719	7162	4701	5171	4816	4551	5116
1040	6881	4803	6288	7649	8887	7162	4701	8576	8030	4551	5116
1560	6897	4803	6288	7652	8922	7162	4701	11982	11244	4551	5116
2080	6885	4803	6288	7652	8922	7162	4701	15388	14457	4551	5116
2600	6885	4803	6288	7652	8922	7162	4701	18794	17671	4551	5116

Similarly, the beam on elastic foundation model performs well also as far as the span length is concerned. Note however, that the web crippling stiffness here is not completely independent of the span length. The best approximations of the web crippling stiffness are established for α=0.5.

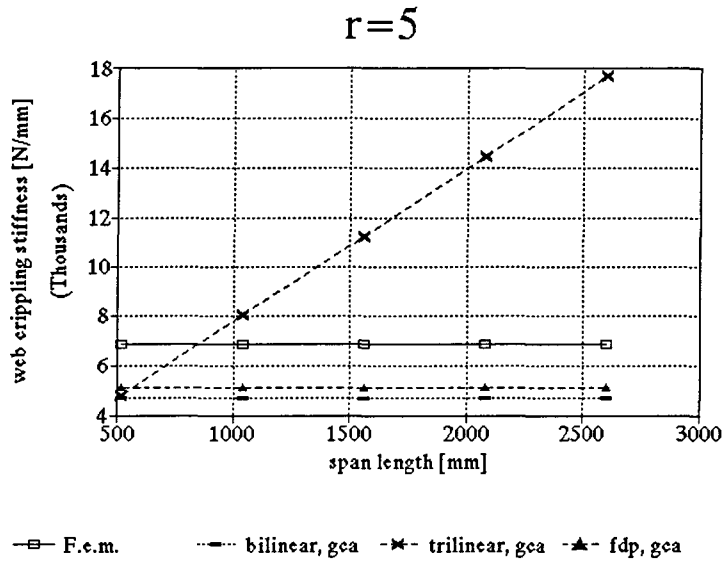

Figure D.27: Web crippling stiffness for varying span lengths

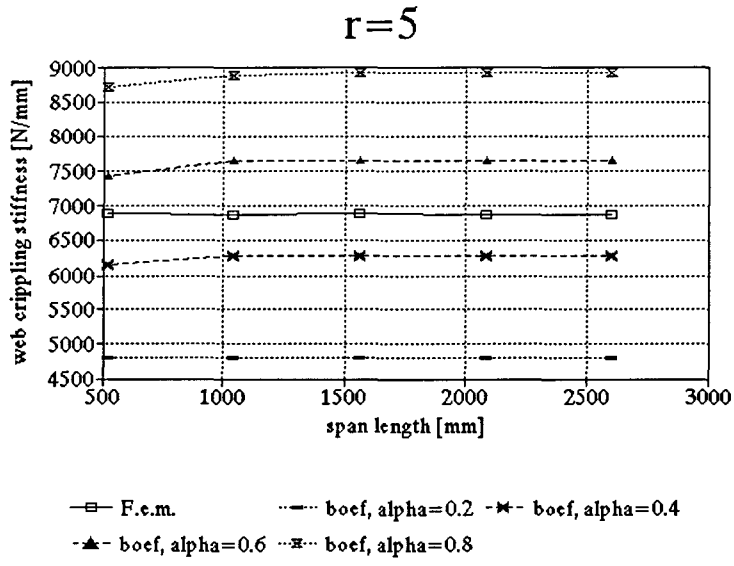

Figure D.14: Web crippling stiffness for varying span lengths

Influence concerning the wall thickness

The influence of the wall thickness on the web crippling stiffness in case of general member 2, according to

the several models is tabulated in table D.15. The results are shown once more in the figures D.29 and D.30.

Table D.15: Web crippling stiffness against wall thickness for general member 2

t	Fem	Beam on elastic foundation model				Energy model					
		α=0.2	α=0.4	α=0.6	α=0.8	1	2	3	4	5	6
0.5	2909	1911	2586	3199	3763	2610	1713	4367	4098	1658	1864
0.7	6897	4803	6288	7652	8922	7162	4701	11982	11244	4551	5116
0.9	13115	9592	12274	14736	17047	15221	9992	25467	23897	9672	10873
1.1	21966	16655	20992	24917	28627	27790	18243	46497	43630	17660	19852
1.3	33642	26302	32847	38613	44092	45871	30112	76750	72018	29149	32769
1.5	48193	38781	48196	56197	63820	70467	46258	117902	110633	44779	50339

It seems that the combinations 2, 5 and 6 are better predictors of the web crippling stiffness than the other combinations: they have a smaller deviation of the finite element simulation. However, the treatment of the wall thickness is equal throughout the energy model. The different performances are caused by the differences between the deviations for general member 2 with a wall thickness of 0.7 mm. These deviations are intensified for members with a larger wall thickness and vice versa, implying a rather poor treatment of the wall thickness that overestimates the influence of the wall thickness.

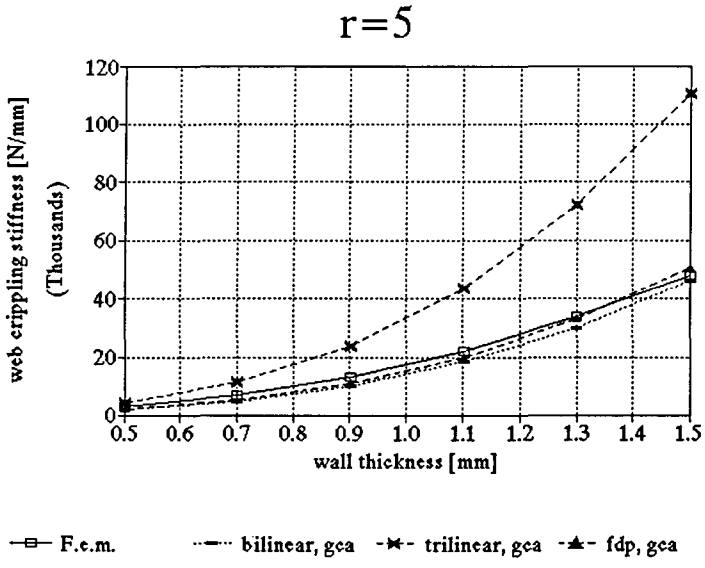

Figure D.29: Web crippling stiffness for varying wall thicknesses

Despite this poor treatment figure D.29 indicates that it is possible to apply the energy model in describing the influence of the wall thickness, but only for members having wall thicknesses smaller than 1 mm. According to figure D.30 and table D.15 it is to be expected that the beam on elastic foundation model produces fairly reliable results for α=0.4 à 0.5.

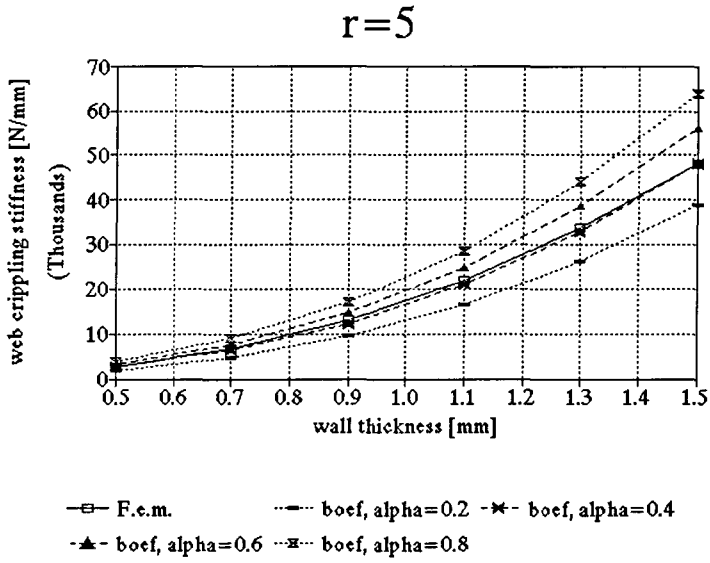

Figure D.30: Web crippling stiffness for varying wall thicknesses

General member 3 (r=10):

Influence concerning the bottom flange

The influence of the bottom flange on the web crippling stiffness in case of general member 2, according to the several models is tabulated in table D.16. The results are shown once more in the figures D.31 and D.32.

Table D.16: *Web crippling stiffness against bottom flange for general member 3*

b_{bf}	Fem	Beam on elastic foundation model				Energy model					
		α=0.2	α=0.4	α=0.6	α=0.8	1	2	3	4	5	6
40	3231	1551	2161	2705	3198	1676	968	2523	2630	1075	1206
60	3364	1537	2141	2681	3170	1726	1032	2660	2711	1086	1228
80	3442	1527	2129	2666	3151	1759	1075	2753	2769	1094	1244
100	3490	1520	2120	2655	3138	1783	1106	2819	2813	1099	1257
120	3524	1515	2113	2647	3129	1801	1130	2869	2846	1104	1266

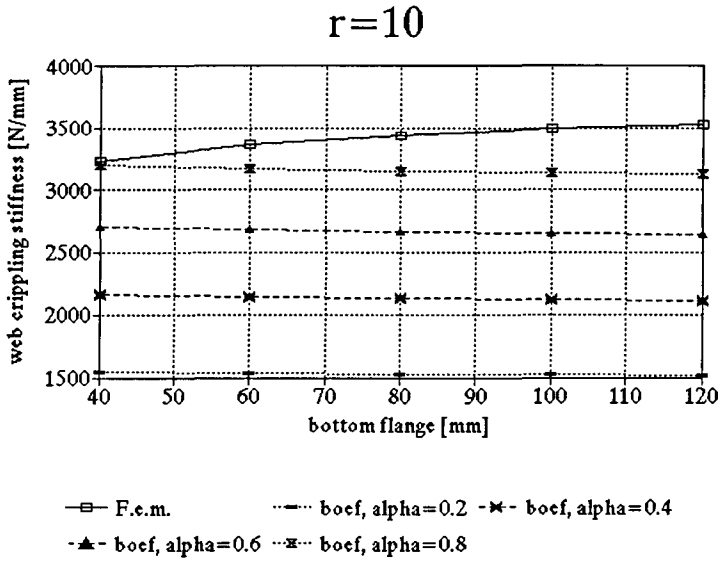

Figure D.32: Web crippling stiffness for varying bottom flanges

The deviations between the finite element simulations and the energy model combinations are more or less constant over the whole range of the bottom flange. This indicates that the energy model performs reasonably well as far as the influence of the bottom flange is concerned, just as was assumed in case of the general member 1 and 2. The neglect of the deformation variations over the bottom flange is justified by these results.

It is striking that the beam on elastic foundation model resulted in constant deviations over the whole range of the bottom flange for each value of α in case of general member 1 but results in slightly increasing deviations with an increasing bottom flange for each value of α in case of general member 3. as well as member 2. For α having a magnitude of ± 0.9, probably the best approximations of the web crippling stiffness are established. Although the deviations between the beam on elastic foundation model and the finite element simulations differ with varying magnitudes of the bottom flange, these deviation variations are relatively small. It is to be expected that it is still possible to establish sufficient accurate results for varying magnitudes of the bottom flange because the deviations only slightly differ.

Influence concerning the top flange

The influence of the top flange on the web crippling stiffness in case of general member 3, according to the several models is tabulated in table D.17.

Table D.17: Web crippling stiffness against top flange for general member 3

b_{tf}	Fem	Beam on elastic foundation model				Energy model					
		α=0.2	α=0.4	α=0.6	α=0.8	1	2	3	4	5	6
40	4044	1954	2660	3297	3884	2538	1942	3286	3351	851	1497
60	3364	1537	2141	2781	3170	1726	1032	2660	2711	1086	1228
80	3065	1356	1917	2415	2862	1412	775	2637	2679	1334	1119
100	2905	1255	1791	2267	2691	1244	682	2922	2954	1589	1061
120	2805	1191	1711	2173	2582	1140	644	3483	3498	1850	1026

These results are shown once more in the figures D.33 and D.34.

According to figure D.33, only the combinations 1, 2 and 6 produce results that have a rather constant deviation from the finite element simulations. The other combinations do not give reliable results for the influence of the top flange on the web crippling stiffness, just as for the general members 1 and 2. Just as in case of the general members 1 and 2, combination 5 (which is based upon the hinge compatibility approach) depends differently on the magnitude of the top flange than the combination 6 which is based upon the geometrical compatibility approach. It may be concluded that the hinge compatibility approach is no longer valid if the magnitude of the top flange is varied strongly.

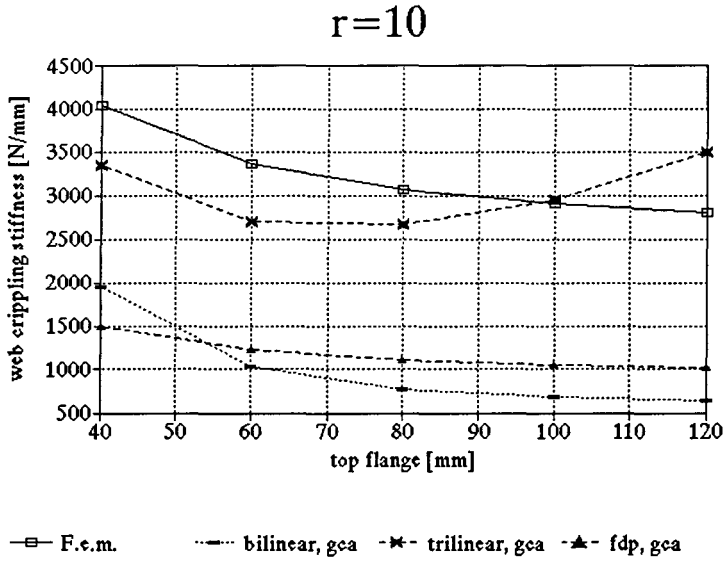

Figure D.33: Web crippling stiffness for varying top flanges

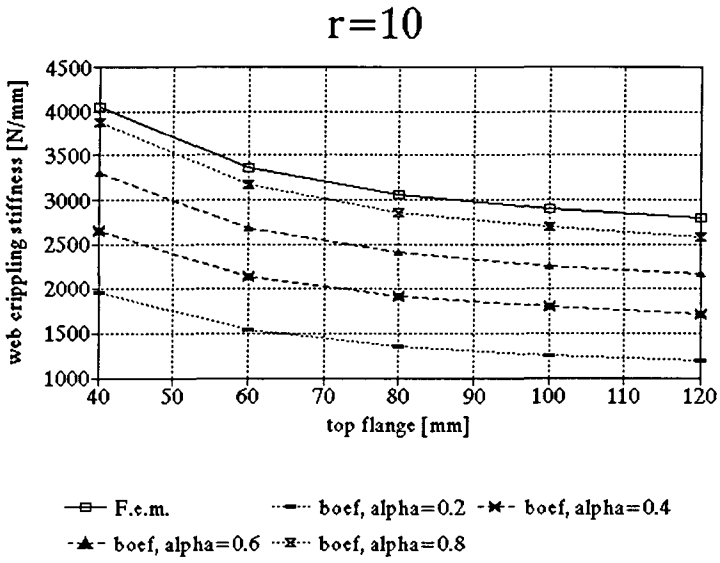

Figure D.34: Web crippling stiffness for varying top flanges

From figure D.34 it becomes clear that the beam on elastic foundation model performs somewhat better than the energy model, as far as the negotiation of the top flange is concerned. The extra deviations that were noticed in case of small top flanges for general member 2 do not appear here.

Influence concerning the web

The influence of the web on the web crippling stiffness in case of general member 3, according to the several models is tabulated in table D.18.

Table D.18: *Web crippling stiffness against web for general member 3*

b_w	Fem	Beam on elastic foundation model				Energy model					
		α=0.2	α=0.4	α=0.6	α=0.8	1	2	3	4	5	6
30	5602	1664	2089	2470	2832	2172	1146	7956	9100	3750	1991
50	3964	1555	2086	2572	3019	1871	989	3355	3481	1644	1431
65	3364	1537	2141	2681	3170	1726	1032	2660	2711	1086	1228
80	2985	1547	2213	2794	3310	1623	1121	2310	2332	789	1099
100	2658	1583	2316	2938	3485	1526	1259	2027	2032	567	987

These results are shown once more in the figures D.35 and D.36.

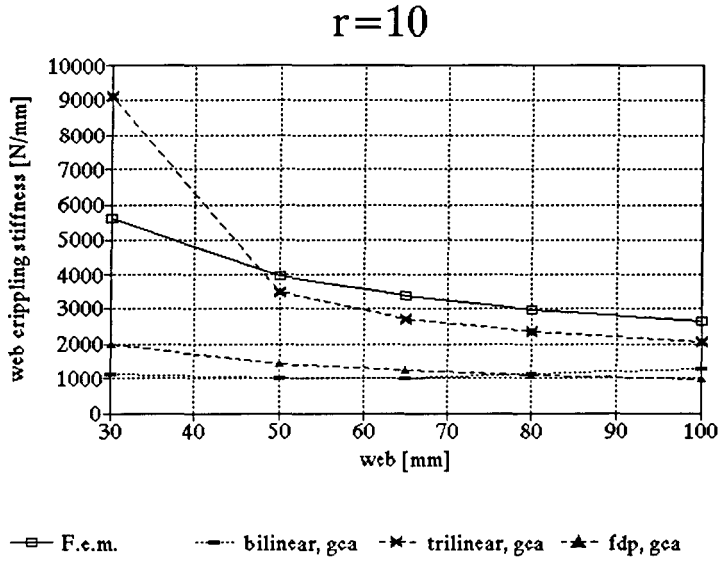

Figure D.35: Web crippling stiffness for varying webs

Only the combinations 5 and 6 correspond to the behaviour of the finite element simulations if the magnitude of the web is varied; note that in case of the general members 1 and 2 this holds true for the combinations 2 and 6.

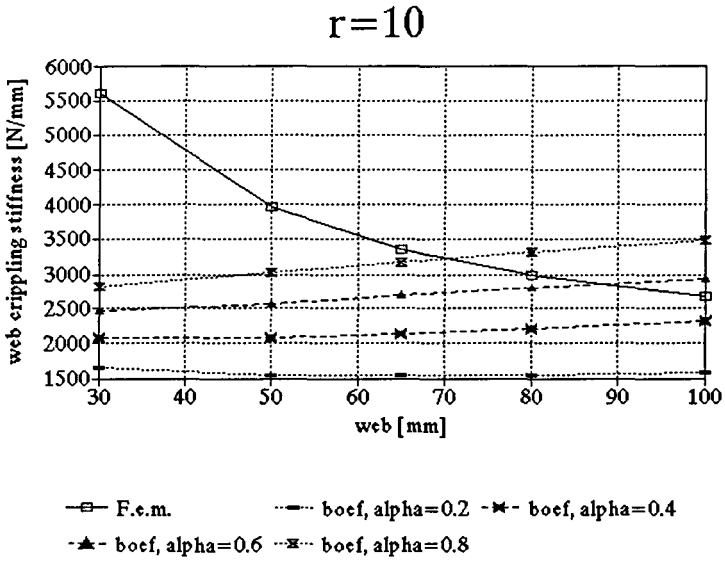

Figure D.36: Web crippling stiffness for varying webs

From figure D.36 it is clear that the beam on elastic foundation model performs poorly in describing the

influence of the web on the web crippling stiffness. Here, the different values of α result web crippling stiffnesses which only slightly different depend on the height of the web.

Influence concerning the web angle

The influence of the web angle on the web crippling stiffness in case of general member 3, according to the several models is tabulated in table D.18. These results are shown once more in the figures D.37 and D.38.

Table D.18: *Web crippling stiffness against web angle for general member 3*

θ_w	Fem	Beam on elastic foundation model				Energy model					
		α=0.2	α=0.4	α=0.6	α=0.8	1	2	3	4	5	6
50	6515	2354	3206	3976	4682	2956	1861	4724	4669	1884	2119
60	5270	1930	2657	3311	3907	2302	1419	3621	3631	1462	1930
70	4995	1695	2349	2936	3468	1953	1185	3038	3075	1394	1695
80	3887	1574	2191	2742	3240	1779	1068	2749	2796	1267	1574
90	3364	1537	2141	2681	3170	1726	1032	2660	2711	1086	1228

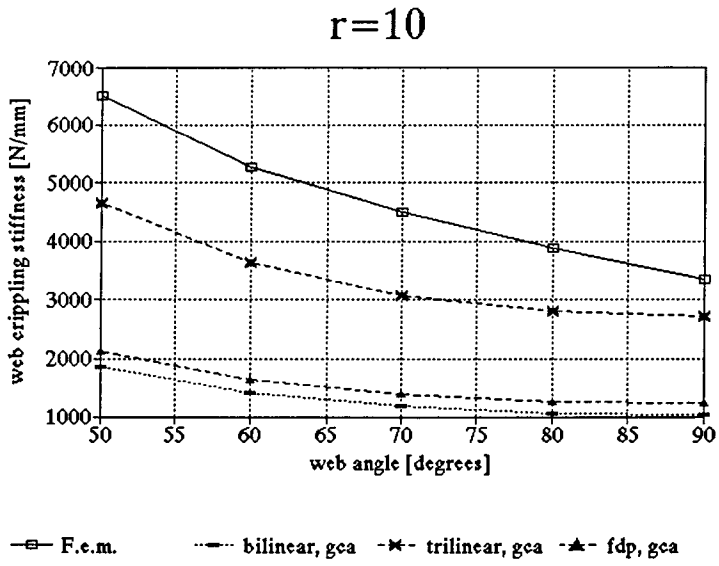

Figure 37: *Web crippling stiffness for varying web angles*

The finite element simulations nearly have constant deviations from each combination of the energy model for the whole range over which the web angle is varied. Reliable results were also established for general member 2 in varying the web angle. Hence it can be concluded that the treatment of the web angle is rather well in case of members having large corner radii.

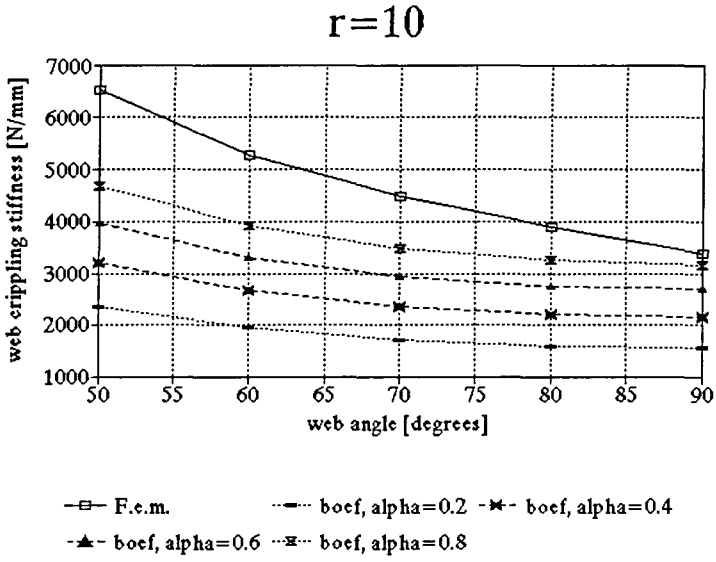

Figure D.38: Web crippling stiffness for varying web angles

The beam on elastic foundation model turns out to perform reasonably also in varying the web angle for both general member 1 and 2. However, for small web angles the results of the beam on elastic foundation model tend to deviate increasingly from the finite element simulations.

Influence concerning the load bearing plate

The influence of the load bearing plate on the web crippling stiffness in case of general member 3, according to the various models is given in table D.20. The results are shown once more in the figures D.39 and D.40.

Table D.20: *Web crippling stiffness against load bearing plate for general member 3*

L_{lb}	Fem	Beam on elastic foundation model				Energy model					
		α=0.2	α=0.4	α=0.6	α=0.8	1	2	3	4	5	6
25	2305	1217	1914	2497	3014	431	258	2373	2428	394	480
50	2701	1291	1964	2538	3048	863	516	2469	2522	598	685
100	3364	1537	2141	2681	3170	1726	1032	2660	2711	1086	1228
150	3670	1855	2396	2893	3351	2588	1548	2852	2900	1597	1802
200	3717	2161	2702	3158	3582	3451	2065	3044	3089	2114	2384
250	3693	2373	3030	3461	3851	4314	2581	3236	3277	2634	2970
300	3673	2469	3341	3785	4147	5177	3097	3428	3466	3155	3557

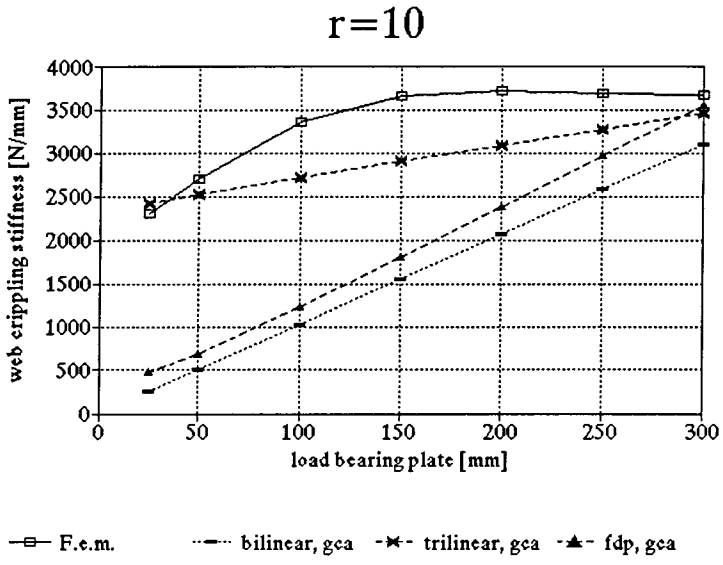

Figure D.39: Web crippling stiffness for varying load bearing plates

Similar to the general members 1 and 2, it may be concluded that the load bearing plate is poorly covered in the energy model. As mentioned before it is to be expected that this is caused by deformation descriptions over the length of the member that show increasing deviations from reality with longer load bearing plates.

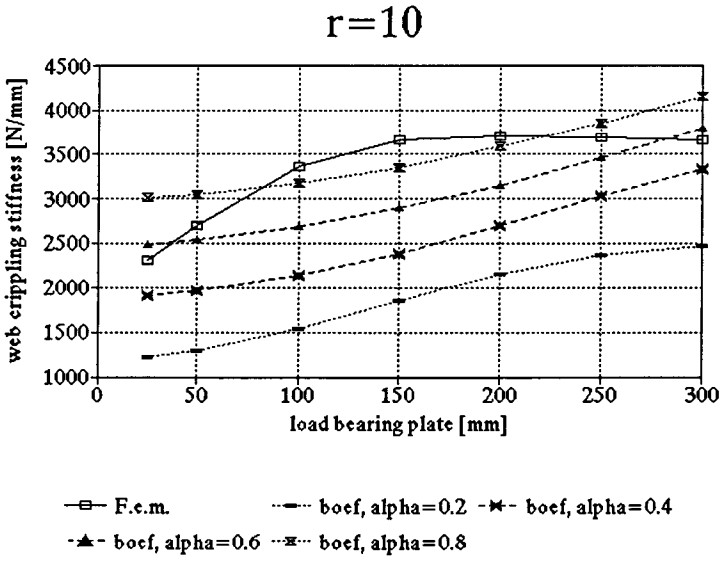

Figure D.40: Web crippling stiffness for varying load bearing plates

According to the finite element simulations the web crippling stiffness is more or less independent of the magnitude of the load bearing plate, for large load bearing plates. In the beam on elastic foundation model this independence holds true for small values of α, in case of general member 3. This is contradictory to the other parameters for which the beam on elastic foundation model corresponds best to the finite element simulations for $\alpha = \pm 0.9$.

Influence concerning the span length

The influence of the span length on the web crippling stiffness in case of general member 2, according to the several models is tabulated in table D.21. These results are shown once more in the figures D.41 and D.42.

Table D.21: Web crippling stiffness against span length for general member 3

L_{span}	Fem	Beam on elastic foundation model				Energy model					
		α=0.2	α=0.4	α=0.6	α=0.8	1	2	3	4	5	6
520	3472	1514	2084	2642	3176	1726	1032	1143	1155	1086	1228
1040	3362	1536	2139	2656	3116	1726	1032	1902	1933	1086	1228
1560	3364	1537	2141	2681	3170	1726	1032	2660	2711	1086	1228
2080	3364	1537	2142	2681	3174	1726	1032	3419	3489	1086	1228
2600	3364	1537	2142	2681	3174	1726	1032	4178	4267	1086	1228

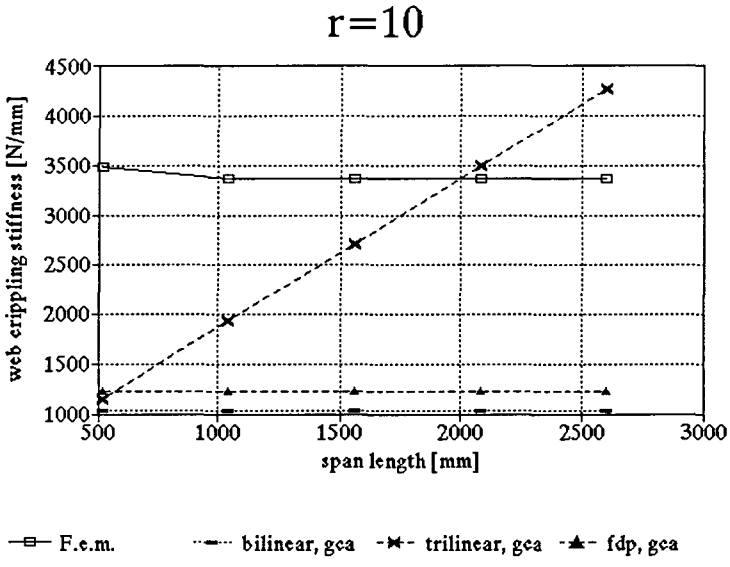

Figure D.41: Web crippling stiffness for varying span lengths

The assumption that the web crippling deformations tend to concentrate in a rather small region around the load bearing plate is also confirmed by the finite element simulations of general member 3. The web crippling stiffness appears to be almost independent of the span length, except for very small span lengths. This may be occasioned by the existence of an effective length in practice, where outside the web crippling deformations are negligibly small (just as in the energy model). If the span length exceeds this effective length the web crippling stiffness is independent of the span length but if the span length is smaller than the effective length the web crippling stiffness may vary with a varying span length.
Note that the full length solution which is applied in combination 3 and 4 produces poor results.
The combinations 1, 2, 5 and 6 have a constant deviation from the finite element simulations and perform well as far as the span length is concerned. The deviation is caused by the poor covering of the corner radii. Similarly, the beam on elastic foundation model performs well also as far as the span length is concerned. Note however, that the web crippling stiffness here is not completely independent of the span length. The best approximations of the web crippling stiffness are established for $\alpha = \pm 0.9$.

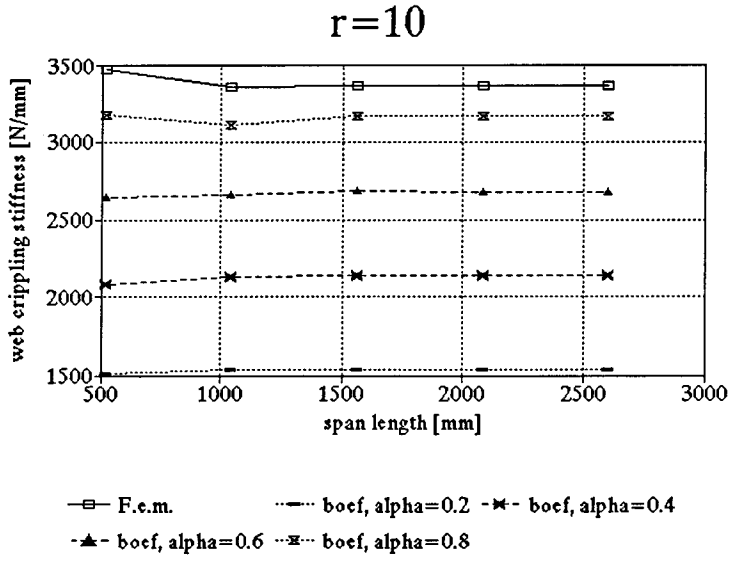

Figure D.42: *Web crippling stiffness for varying span lengths*

Influence concerning the wall thickness

The influence of the wall thickness on the web crippling stiffness in case of general member 3, according to the several models is tabulated in table D.22.

These results are shown once more in the figures D.43 and D.44.

Table D.22: Web crippling stiffness against wall thickness for general member 3

t	Fem	Beam on elastic foundation model				Energy model					
		α=0.2	α=0.4	α=0.6	α=0.8	1	2	3	4	5	6
0.5	1381	623	895	1132	1341	629	376	970	988	396	448
0.7	3364	1537	2141	2681	3170	1726	1032	2660	2711	1086	1228
0.9	6483	3038	4131	5120	6028	3668	2194	5654	5762	2308	2610
1.1	10899	5257	7007	8604	10082	6696	4006	10324	10520	4214	4765
1.3	16736	8320	10903	13277	15487	11053	6612	17041	17365	6956	7865
1.5	24125	12344	15950	19277	22387	16979	10157	26178	26676	10685	12083

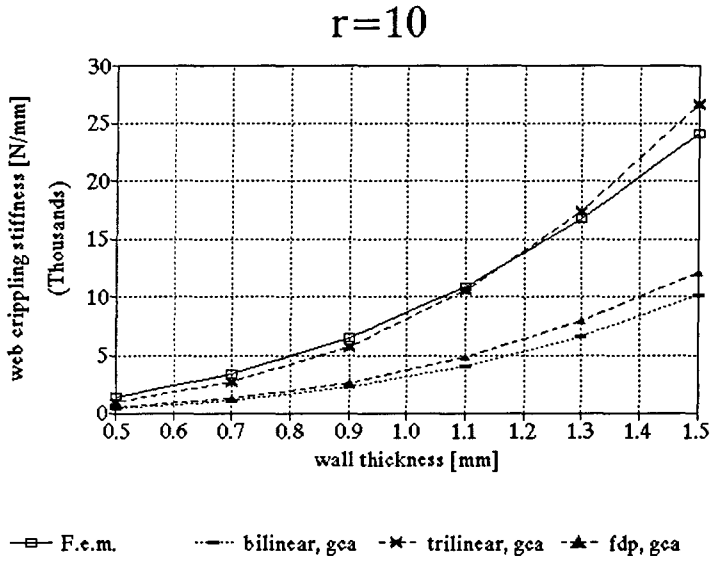

Figure D.43: Web crippling stiffness for varying wall thicknesses

In contradictory to general member 2, combinations 2, 5 and 6 appear to produce poor results in case of general member 3, as far as the wall thickness is concerned. Nevertheless, it was already stated that this change in reliability of the predictions might mainly be caused by the poor covering of the corner radii and a negotiation of the wall thickness that overestimates its influence. However, according to figure D.43 it is possible to use the energy model in describing the influence of the wall thickness on the web crippling stiffness for members having wall thicknesses smaller than 1 mm.

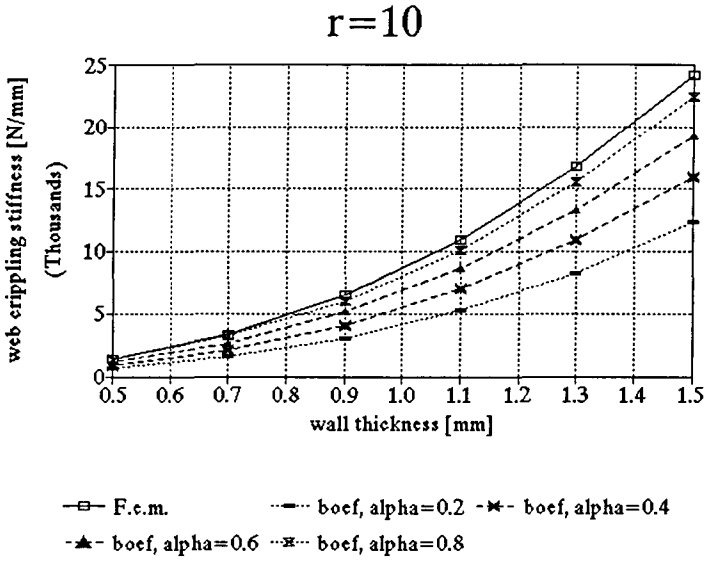

Figure D.44: Web crippling stiffness for varying wall thicknesses

According to figure D.44 and table D.22 it is to be expected that the beam on elastic foundation model produces fairly reliable results for α=0.8 à 0.9.

D.2 Batch file

The parameter study is carried out using a batch file within ANSYS. The format of the batch file is the same throughout the parameter study, only the values which are assigned to the parameters differ from each other for each test. The batch file for the web crippling test of general member 2 is given below.

/BATCH
/UNITS, SI
/PREP7
: the setting of the parameters
*AFUN, DEG
t=0.7
b_w=65
b_{bf}=60
b_{tf}=60
θ_w=90
$r_{i;bf}$=5

$r_{i;tf}$=5

L_{span}=1560

L_{lb}=100

: number of elements over the bottom and top flange rounding of the corners, as well as their element size

numebf=3

numetf=3

esizebf=3.14*rcbf/(2*numebf)

esizetf=3.14*rctf/(2*numetf)

: general element size

esizege=8

: calculation of the midline corner radii out of the inner corner radii

rcbf=$r_{i;bf}$ + 1/2*t + 0.02

rctf=$r_{i;tf}$ + 1/2*t + 0.02

: calculation of width of bottom flange plate and the height of the web plate

hbbffl=b_{bf} - rcbf*(COS(90 - θ_w))

hbtffl=b_{tf} - rctf*(COS(90 - θ_w))

bwrest=b_w - rcbf*(1 - SIN(90 - θ_w))/SIN(θ_w) - rctf*(1 - SIN(90 - θ_w))/SIN(θ_w)

: setting of keypoints that are used in the development of the curved areas at the rounding of the top flange corners

k202x=1/2*b_{bf} + bwrest*COS(θ_w) + rctf*(COS(90 - θ_w))

k202y=b_w*SIN(θ_w) - rctf

: setting of the element parameters

ETYPE

STAT

ET, 1, shell93

R, 1

RMOD, 1, 1, t

MP, EX, 1, 210000

: building up the bottom flange

WPRO, 0, 90, 0

RECTNG, , hbbffl, , 1/2*(L_{span} - L_{lb})

KWPA, P50X

1

4

RECTNG,, hbbffl,, 1/2*L_{lb}

: building up the rounding of the bottom flange corners

K, 104, hbbffl, rcbf

K, 105, hbbffl, rcbf, 100

AROTAT, 2, , , , , , 104, 105, θ_w

AROTAT, 6, , , , , , 104, 105, θ_w

: building up the web

KWPA, P50X

1

9

WPRO, 0, 0, θ_w

RECTNG, , bwrest, , $1/2*(L_{span} - L_{lb})$

KWPA, P50X

1

10

RECTNG, , bwrest, , $1/2*L_{lb}$

: building up the rounding of the top flange corners

K, 102, k202x, k202y

K, 103, k202x, k203y, 100

AROTAT, 16, , , , , , 102, 103, $-\theta_w$

AROTAT, 20, , , , , , 102, 103, $-\theta_w$

: building up the top flange

KWPA, P50X

1

21

WPRO, 0, 0, θ_w

RECTNG, , hbtffl, , $1/2*(L_{span} - L_{lb})$

KWPA, P50X

1

22

RECTNG, , hbtffl, , $1/2*L_{lb}$

: connecting the areas together

AGLUE, ALL

FINISH

: type of analysis

/SOLU

```
ANTYP, 0
STAT
: symmetry conditions
DL, 30, 14, SYMM
DL, 47, 17, SYMM
DL, 48, 17, SYMM
DL, 28, 15, SYMM
DL, 46, 16, SYMM
DL, 14, 13, SYMM
DL, 7, 11, SYMM
DL, 38, 11, SYMM
DL, 4, 1, SYMM
: degrees of freedom constraints of the supports
DK, 1, UX, , , 1, UY, ROTY, ROTZ
DK, 2, UX, , , 1, UY, ROTY, ROTZ
: application of a load F that equals 100 N
FK, 22, FY, -100
FINSH
: establishment of the element shape and size
/PREP7
ESHAPE, 2, 0
EZISE, esizege
: establishment of the element size at the rounding of the corners
LESIZE, 10, esizebf
LESIZE, 11, esizebf
LESIZE, 14, esizebf
LESIZE, 24, esizetf
LESIZE, 25, esizetf
LESIZE, 28, esizetf
: meshing the solid model
MAT, 1
REAL, 1
TYPE, 1
AMESH, ALL
FINISH
```

```
: establishment of the solution
/SOLU
SOLVE
FINISH
: copying of the deformations with which the web crippling stiffness is calculated, to the file 'disp.uit'
KSEL, S, KP, ,          22
KSEL, A, KP, ,          3
nslk, s
/output, disp, uit
PRNSOL, U, Y
/output
FINISH
EXIT
```

Basically, this batch file enables the simulation of any elastic web crippling test. Note that the file is based on an almost constant element size throughout the member. The magnitude of the element size should depend on the dimensions of the member itself and the maximum wavefront of the software in each particular case.

Appendix E

This appendix treats the results of the parameter study if a factor γ is added to the energy model and the results of the beam on elastic foundation model if α is defined to be a function of the corner radii.

E.1 Adjustment of energy model (γ) & Usement of varying α in Boef-model

The energy model and the beam on elastic foundation model (for α having a constant value) perform poorly on several parameters (section 7.3). Some of the parameters can be better accounted for by simple adjustments.

The development of the adjusted energy model is confined to combination 6 because this is the only combination within the energy model that produces reasonable results for most of the parameters. Principally, the derivation of this factor for other combinations is similar. In the energy model the corner radii, the length of the load bearing plate, the wall thickness and the web angle are poorly accounted for.

In section 7.3 and appendix D.1 it has become clear that the poor treatment of the corner radii in the energy and model enlarges the deviations of those models from the finite element simulations in case of several other parameters. In the energy model the covering the of the corner radii is improved by the addition of a correction factor which is empirically determined.

According to section 7.3 the wall thickness is poorly accounted for due to the neglect of axial (web crippling) deformations. Taking these stretching action into account would greatly improve the energy model concerning the wall thickness. However, this also highly complicates the resulting web crippling stiffness. The treatment of the wall thickness can be improved relatively simple by adding an empirical correction factor. In the current situation this means that the web crippling stiffness should be divided by roughly the square root of the wall thickness.

The correction factor on the corner radii and the wall thickness has been established using a trial and error method with the aid of a spreadsheet program that calculates the consequences of the application of the correction factor for each test of the parameter study. Eventually, this resulted in a correction factor γ with which the web crippling stiffness has to be multiplied. For combination 6 γ is given by

$$\gamma = \frac{r_{i;tf}^{0.92}}{4.035 \cdot t^{0.65}} \qquad \text{(E.1)}$$

As mentioned before, the poor covering of the length of the load bearing plate stems from the disregarding of the upward curling underneath it. This a lack of the model that can be solved on physical grounds by adjusting the deformation description of the top flange over the length of the member. The most simple solution is to assume that the deformations have a constant value underneath the load bearing plate, applying the fourth degree polynomial only outside the plate. A more complicated but physically more relevant solution lies in the description of the upward curling of the top flange underneath the load bearing plate. If it

is possible to establish an appropriate deformation description of the upward curling, the influence of the load bearing plate would be covered much better. Finally, a more provisional solution can be applied making use of the fact that the web crippling stiffness is independent of L_{lb}, if L_{lb} >100 mm. Hence, it is possible to replace L_{lb} by a constant value. In the adjusted model the length of the load bearing plate is replaced by a constant value of 100 mm.

No adjustment is made on the covering of the web angle. It is recommended to improve the treatment of the web angle by using a different deformation description (and thus a different value for n) over the cross-section.

In the adjusted energy model (combination 6) the web crippling stiffness is given by

$$k_{\Delta h_w} = \frac{D \cdot b_{tf}^2 \cdot L_{ef}^5 \cdot r_{i;tf}^{0.92}}{6355 \cdot t^{0.65} \cdot (100^2 - L_{ef}^2)^4 \cdot (b_{tf}^2 + b_w^2 \cdot n)}$$

$$\cdot [\frac{[b_{tf}^4 \cdot (b_w^3 \cdot L_{ef}^2 \cdot (8640 + 2400 \cdot n) + 5248 \cdot L_{ef}^4 \cdot b_w + b_{tf} \cdot (L_{ef}^2 \cdot (1536 \cdot L_{ef}^2 + 3936 \cdot b_w^2 + 2400 \cdot b_w^2 \cdot n))}{[b_w \cdot \sin^2\theta_w \cdot r_{i;tf}^2 \cdot (\sin\theta_w \cdot r_{i;tf} - b_{tf}) \cdot (b_{tf}^2 \cdot (b_{tf} \cdot (4 \cdot \sin\theta_w \cdot r_{i;tf} - b_{tf}) - b_w \cdot n \cdot (b_w + 5 \cdot \sin\theta_w \cdot r_{i;tf}) - 4 \cdot \sin^2\theta_w \cdot r_{i;tf}^2)}$$

$$\frac{+ b_{tf}^5 \cdot b_w^3 \cdot (b_w \cdot (3150 + 15750 \cdot n^2) + 7875 \cdot b_{tf} \cdot n^2) + b_w^4 \cdot (b_{tf}^3 \cdot L_{ef}^2 \cdot (2400 \cdot n^2 - 768 \cdot n + 8800) + 6656 \cdot b_{tf} \cdot L_{ef}^4 \cdot n^2)]}{+ b_w \cdot \sin\theta_w \cdot r_{i;tf} \cdot n \cdot (\sin\theta_w \cdot r_{i;tf} \cdot (b_w + 5 \cdot b_{tf}) - b_w \cdot b_{tf}))]}$$

$$+ \frac{[b_w^5 \cdot (L_{ef}^2 \cdot n^2 \cdot (768 \cdot L_{ef}^2 + 2400 \cdot b_{tf}^2) + b_{tf}^2 \cdot n \cdot (7875 \cdot b_{tf}^2 \cdot n - 8960 \cdot L_{ef}^2) - 2100 \cdot b_{tf}^4 + 4096 \cdot b_w \cdot b_{tf} \cdot L_{ef}^2 \cdot n^2)}{[b_w \cdot \sin^2\theta_w \cdot r_{i;tf}^2 \cdot (\sin\theta_w \cdot r_{i;tf} - b_{tf}) \cdot (b_{tf}^2 \cdot (b_{tf} \cdot (4 \cdot \sin\theta_w \cdot r_{i;tf} - b_{tf}) - b_w \cdot n \cdot (b_w + 5 \cdot \sin\theta_w \cdot r_{i;tf}) - 4 \cdot \sin^2\theta_w \cdot r_{i;tf}^2)}$$

$$\frac{+ b_{tf}^2 \cdot (b_w^6 \cdot (8400 \cdot n \cdot (b_{tf} + b_w) - 5250 \cdot b_{tf}) + L_{ef}^4 \cdot b_w^2 \cdot (b_w \cdot n \cdot (3200 \cdot n - 9984) - b_{tf} \cdot (4608 \cdot n - 6400)))]}{+ b_w \cdot \sin\theta_w \cdot r_{i;tf} \cdot n \cdot (\sin\theta_w \cdot r_{i;tf} \cdot (b_w + 5 \cdot b_{tf}) - b_w \cdot b_{tf}))]}] \qquad \text{(D.2)}$$

in which

$$L_{ef} = \sqrt{\frac{b_{tf}^3 \cdot (34 \cdot b_w^2 + 504 \cdot 10^4) + b_w^3 \cdot n^2 \cdot (17 \cdot b_{tf}^2 + 252 \cdot 10^4)}{14 \cdot b_{tf}^3 + 7 \cdot b_w^3 \cdot n^2}} \qquad \text{(D.3)}$$

In the beam on elastic foundation model the corner radii, the web and the web angle are poorly accounted for. For this model including already a correction factor α, it is unnecessary to add an extra factor with which the web crippling stiffness need to be multiplied in order to improve the treatment of the corner radii. It is more obvious to determine α, so, that a better treatment of the corner radii is established. According to the results of the parameter study, the magnitude of α which provides the best approximations is proportional to the magnitude of the corner radii. In deriving a formula for α that provides the best approximations for all parameters, a difficulty is formed by the fact that some parameters are contradictory in their optimum for α. Therefore, the derivation of this formula turns out to be impossible. Within this project, the derivation of α is

limited to optimize the treatment of the corner radii. Several formulae can be applied, providing solutions that differ from each other in the value of the corner radii where they perform best. The chosen solution is directed to the medium and large corner radii as those are thought to be most relevant in practice. The solution for α is given by

$$\alpha = 0.118 \cdot r_{i;tf}^{0.89} \tag{D.4}$$

It is difficult to adjust the model as far as the treatment of the web is concerned. The web has a different function for each value of α, that in the circumstances cannot be changed easily, without affecting the fundamental basis on which the model has been developed. The factor α could be adjusted to the magnitude of the web angle. However, it is recommended to get first clear physical insight in how α depends on this parameter. Hence, no adjustments are made for the treatment of these parameters.
The parameter study is once more carried out for the energy model and the beam on elastic foundation model applying these adjustments.
The influence of the corner radii on the web crippling stiffness is tabulated in table E.1.

Table E.1: *Web crippling stiffness against corner radii for the adjusted models*

r_i	1	2	3	4	5	6	7	8	9	10
Fem	43478	20305	12384	8811	6897	5706	4872	4251	3756	3364
Boef	43465	23398	13286	9080	6944	5672	4831	4234	3784	3432
Energy	42710	19825	12573	9070	7028	5702	4778	4103	3591	3192

These results are shown once more in figure E.1. From table E.1 and figure E.1 it is clear that the treatment of the corner radii in the energy model is very well. Apparently, the web crippling stiffness is more or less inversely proportional to the corner radii, where the original energy model assumes an inverse proportionality to the square corner radii. The corner radii are reasonably well covered within the beam on elastic foundation model but this model still slightly deviates from the finite element simulations for corner radii around 2 mm. The addition of the factor α of equation E.2 in the beam on elastic foundation model implies a different proportionality of the web crippling stiffness to the corner radii also: now. the web crippling stiffness is here more or less inversely proportional to the corner radii too.

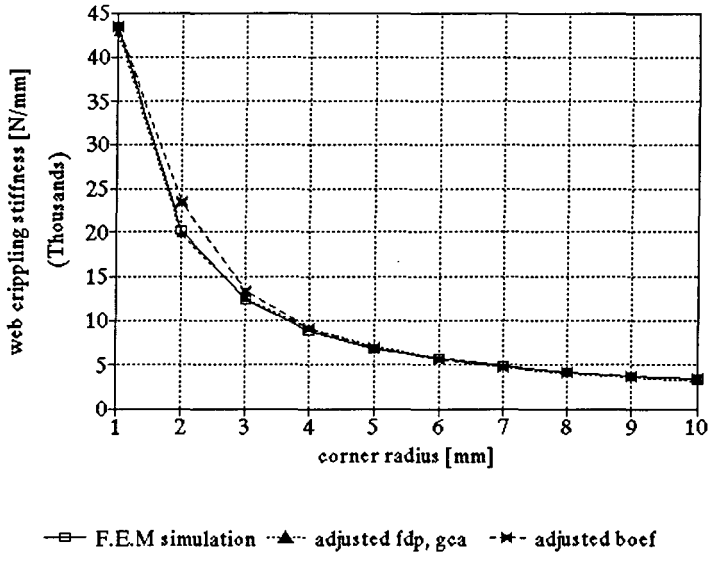

Figure E.1: *Web crippling stiffness for varying corner radii, adjusted models*

The results of the rest of the parameters are described for general member 1, 2 and 3 simultaneously. The influence of the bottom flanges on the web crippling stiffness for the general members 1, 2 and 3 is tabulated in table E.2.

Table E.2: *Web crippling stiffness against bottom flange for the adjusted models*

b_{bf}	Fem			Beam on elastic foundation model			Energy model		
	r_i=1	r_i=5	r_i=10	r_i=1	r_i=5	r_i=10	r_i=1	r_i=5	r_i=10
20	38462	6309	-	40864	7131	-	39764	6612	-
40	41667	6689	3231	42450	7012	3463	41572	6859	3135
60	43478	6897	3364	43465	6944	3432	42710	7028	3192
80	44944	7005	3442	40259	6899	3413	43479	7147	3234
100	45977	7080	3490	38086	6868	3399	44031	7235	3266
120	46512	7143	3524	36462	6845	3388	44446	7301	3292

These results are shown once more in the figures E.2, E.3 and E.4.

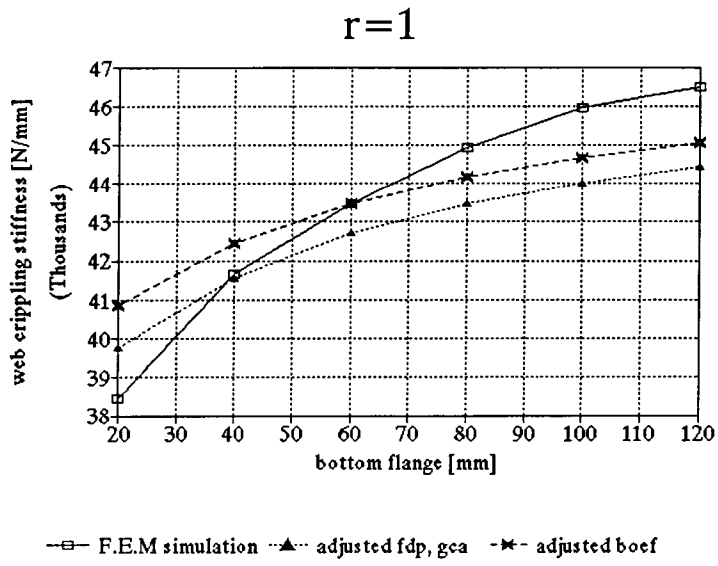

Figure E.2: *Web crippling stiffness for varying bottom flanges*

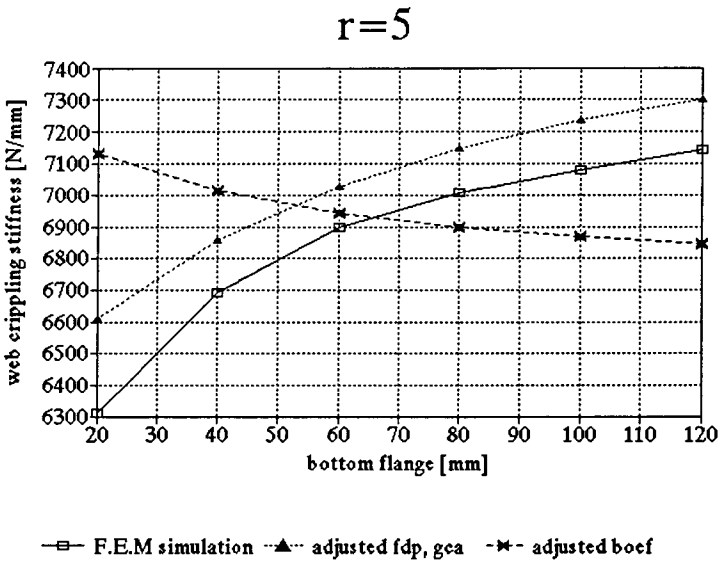

Figure E.3: *Web crippling stiffness for varying bottom flanges*

According to the figures E.2, E.3 and E.4, the energy model performs reasonably well as far as the bottom flange is concerned. Only in case of small corner radii the web crippling stiffness behaviour of the energy model slightly deviates from the finite element simulations. The beam on elastic foundation model on the

other hand, shows greatly varying performances with varying corner radii. Hereby, it may be concluded that the bottom flange is not covered very well in the beam on elastic foundation model.

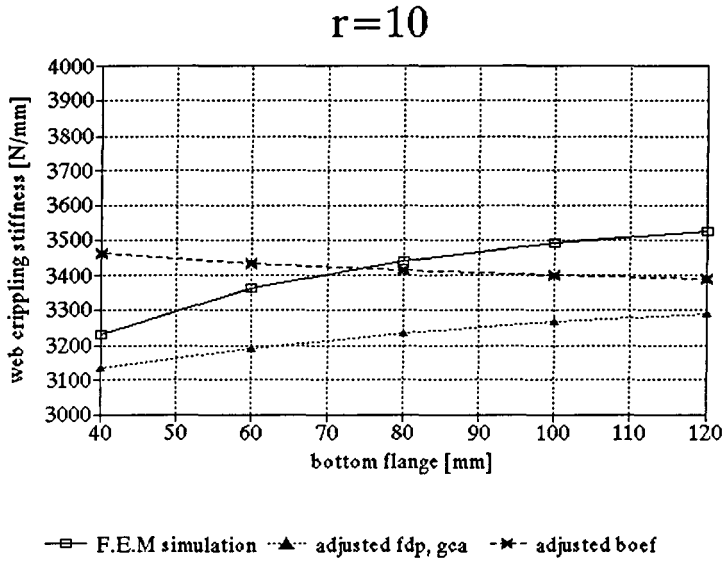

Figure E.4: *Web crippling stiffness for varying bottom flanges*

The influence of the top flange on the web crippling stiffness is tabulated in table E.3.

Table E.3: *Web crippling stiffness against top flange for the adjusted models*

b_{tf}	Fem			Beam on elastic foundation model			Energy model		
	r_i=1	r_i=5	r_i=10	r_i=1	r_i=5	r_i=10	r_i=1	r_i=5	r_i=10
20	54054	9975	-	62740	12594	-	70408	12266	-
40	47059	7576	4044	49032	8182	4205	50099	8187	3892
60	43478	6897	3364	43465	6944	3432	42710	7028	3192
80	42105	6557	3065	40259	6358	3100	38818	6456	2809
100	40816	6349	2905	38086	6017	2916	36427	6115	2758
120	40404	6221	2805	36462	5792	2800	34831	5890	2667

These results are shown once more in the figures E.5, E.6 and E.7.

It is striking that both the energy model and the beam on elastic foundation model perform better for large corner radii than for small corner radii as far as the top flange is concerned. This indicates that the

schematisation of the portal frame model corresponds better to reality in case of larger corner radii. They both perform reasonably well for top flanges larger than 30 mm and smaller than 110 mm.

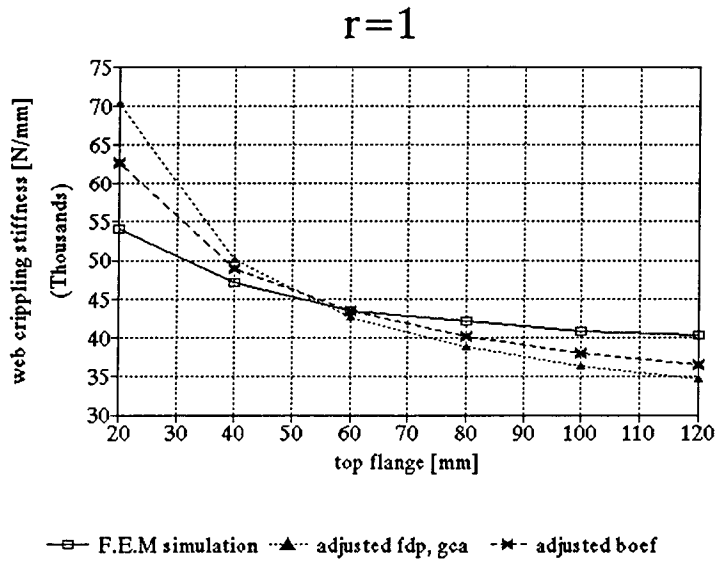

Figure E.5: *Web crippling stiffness for varying top flanges*

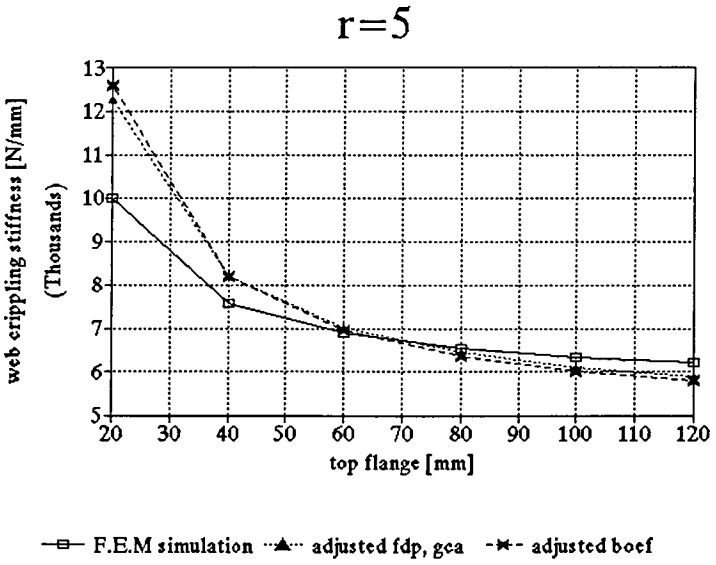

Figure E.6: *Web crippling stiffness for varying top flanges*

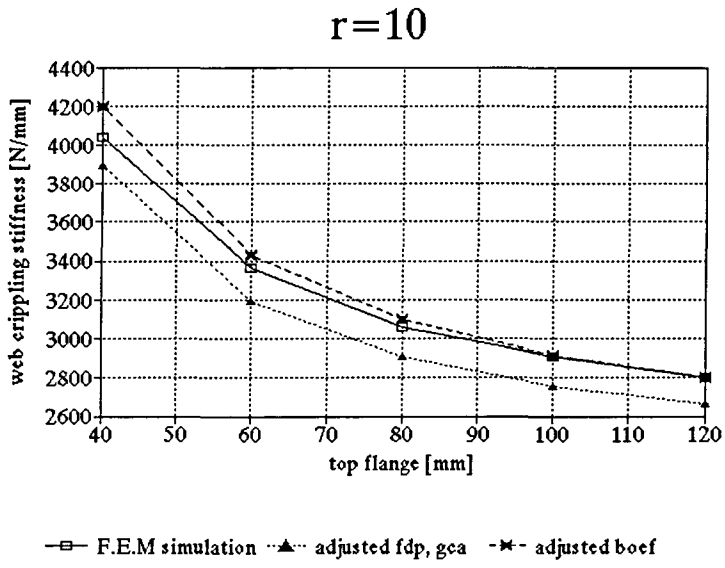

Figure E.7: *Web crippling stiffness for varying top flanges*

The influence of the web on the web crippling stiffness is tabulated in table E.4.

Table E.4: *Web crippling stiffness against web for the adjusted models*

b_{tf}	Fem			Beam on elastic foundation model			Energy model		
	r_i=1	r_i=5	r_i=10	r_i=1	r_i=5	r_i=10	r_i=1	r_i=5	r_i=10
30	54795	10127	5602	37947	7391	3033	71841	11680	5176
50	47059	7767	3964	40559	6927	3264	50409	8258	3720
65	43478	6897	3364	43465	6944	3432	42710	7028	3192
80	41365	6296	2985	46091	7074	3586	37818	6249	2856
100	39254	5767	2658	48188	7327	3780	33566	5575	2565

These results are shown once more in the figures E.8, E.9 and E.10. According to these figures, the negotiation of the web in the beam on elastic foundation model is poorly established. As mentioned in appendix D this may be caused by the definition of the beam and the elastic foundation, because with varying α (and α now varies with varying corner radii and web angles) the influence of the web on the web crippling stiffness varies. This varying influence of the web is confirmed by the figures E.8, E.9 and E.10.

Consequently, the influence of the web on the web crippling stiffness is poorly covered.
The energy model performs much better as far as the influence of the web is concerned. Just as in case of the influence of the top flange, the energy model performs best for large corner radii. It may be concluded that for webs larger than 40 mm reliable approximations are established, especially in case of large corner radii.

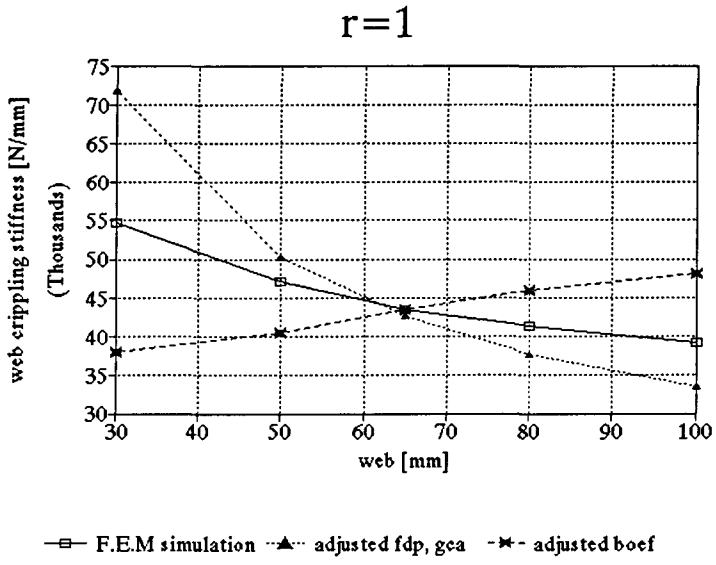

Figure E.8: *Web crippling stiffness for varying webs*

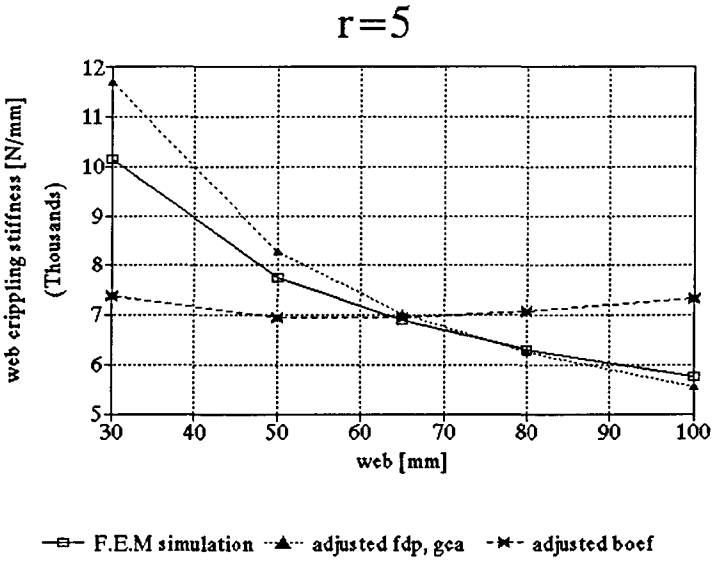

Figure E.9: *Web crippling stiffness for varying webs*

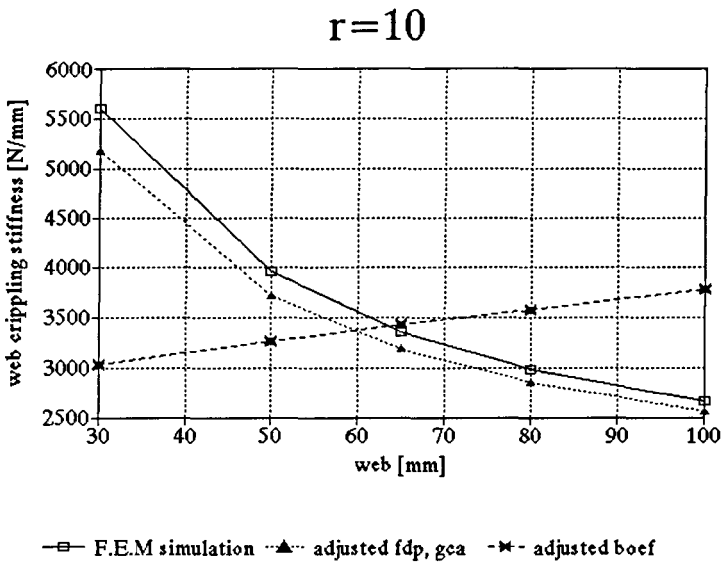

Figure E.10: *Web crippling stiffness for varying webs*

The influence of the web angle on the web crippling stiffness is tabulated in table E.5.

Table E.5: *Web crippling stiffness against web angle for the adjusted models*

θ_w	Fem			Beam on elastic foundation model			Energy model		
	r_i=1	r_i=5	r_i=10	r_i=1	r_i=5	r_i=10	r_i=1	r_i=5	r_i=10
50	66667	16064	6515	49114	9590	4416	57217	9530	4311
60	67797	12539	5270	46518	8230	3924	50019	8285	3750
70	62500	9975	4995	44789	7464	3635	45731	7547	3421
80	52632	8163	3887	43788	7067	3481	43434	7152	3247
90	43478	6897	3364	43465	6944	3432	42710	7028	3192

These results are shown once more in the figures E.11, E.12 and E.13.

It is striking that both the energy model and the beam on elastic foundation model perform better for large corner radii than for small corner radii as far as the influence of the web angle is concerned, mainly because the web crippling stiffness has a rather strange bend at an web angle of 60°. The figures E.11, E.12 and E.13 point out that the finite element simulations depend stronger on the web angle than the energy model and the

beam on elastic foundation model. It may be concluded that the results are only reliable for members which have average or large corner radii and web angles larger than 60°.

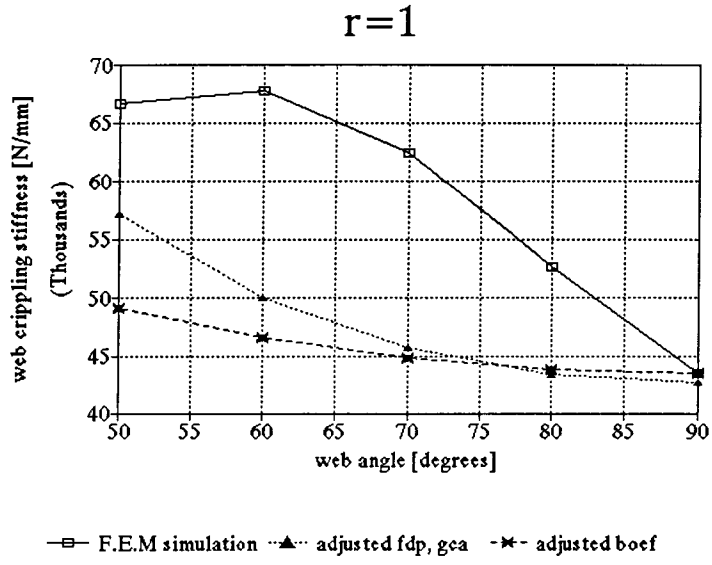

Figure E.11: *Web crippling stiffness for varying web angles*

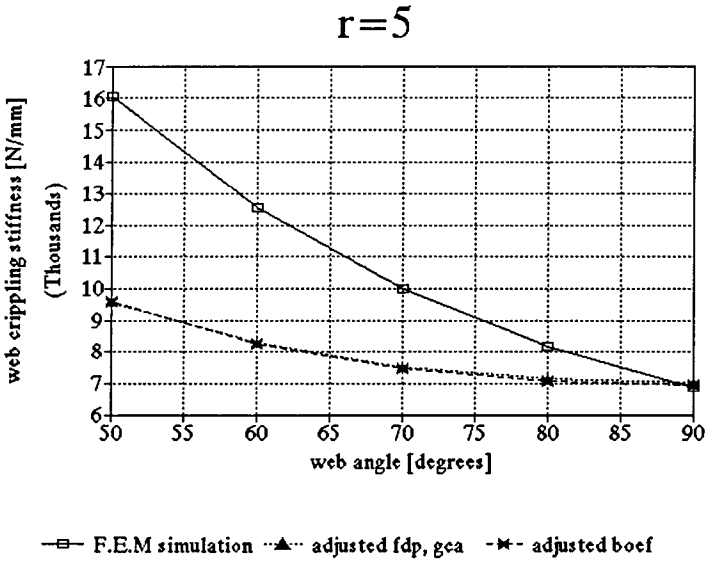

Figure E.12: *Web crippling stiffness for varying web angles*

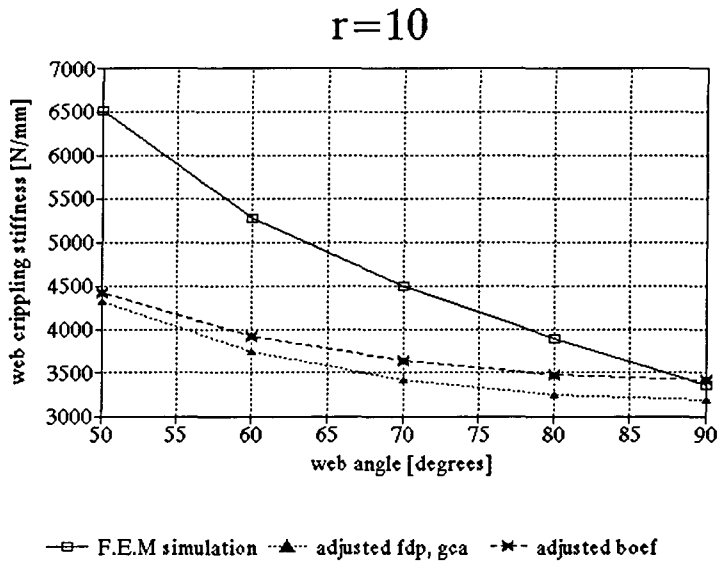

Figure E.13: *Web crippling stiffness for varying web angles*

The influence of the load bearing plate on the web crippling stiffness is tabulated in table E.6.

Table E.6: *Web crippling stiffness against load bearing plate for the adjusted models*

L_{lb}	Fem			Beam on elastic foundation model			Energy model		
	$r_i=1$	$r_i=5$	$r_i=10$	$r_i=1$	$r_i=5$	$r_i=10$	$r_i=1$	$r_i=5$	$r_i=10$
25	37383	4890	2305	27890	5960	3291	42710	7028	3192
50	42105	6033	2701	39407	6183	3321	42710	7028	3192
100	43478	6897	3364	43465	6944	3432	42710	7028	3192
150	43956	6932	3670	42216	8009	3600	42710	7028	3192
200	43478	6908	3717	42267	9224	3813	42710	7028	3192
250	43956	6908	3693	42285	10395	4064	42710	7028	3192
300	43478	6908	3673	42282	11333	4344	42710	7028	3192

These results are shown once more in the figures E.14, E.15 and E.16.

The adjusted energy model treats the load bearing plate reasonably well, except that the model shows

increasing deviations for load bearing plates smaller than 100 mm.

The beam on elastic foundation model uses a different description for the deformation variations over the length of the member and performs somewhat better, considering the load bearing plate. However, in case of members with corner radii of about 5 mm, it is to be expected that the web crippling stiffness approximations of the beam on elastic foundation model satisfy neither in case of load bearing plates longer than 150 mm.

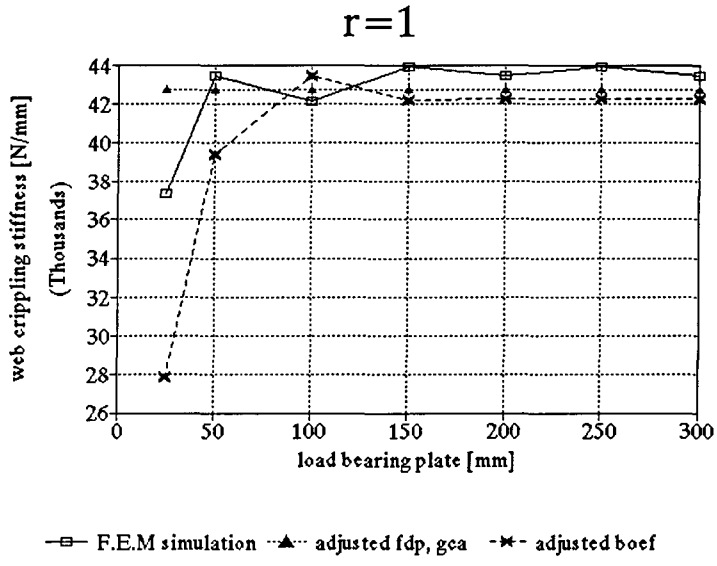

Figure E.14: Web crippling stiffness for varying load bearing plates

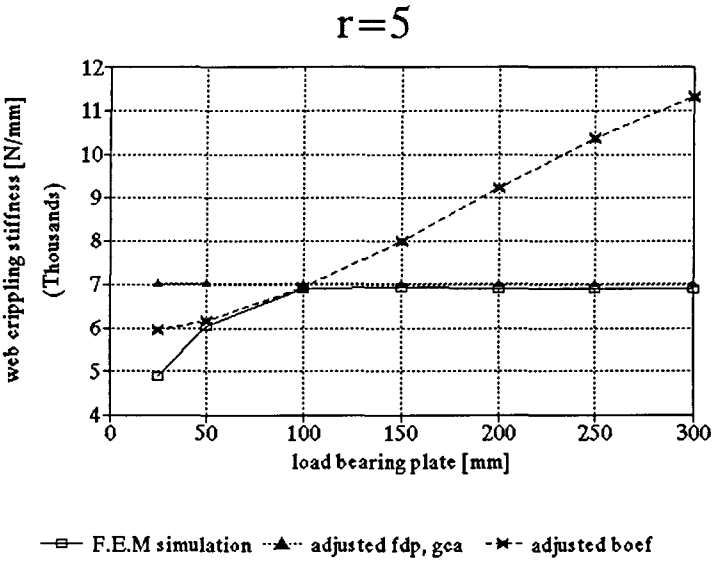

Figure E.15: Web crippling stiffness for varying load bearing plates

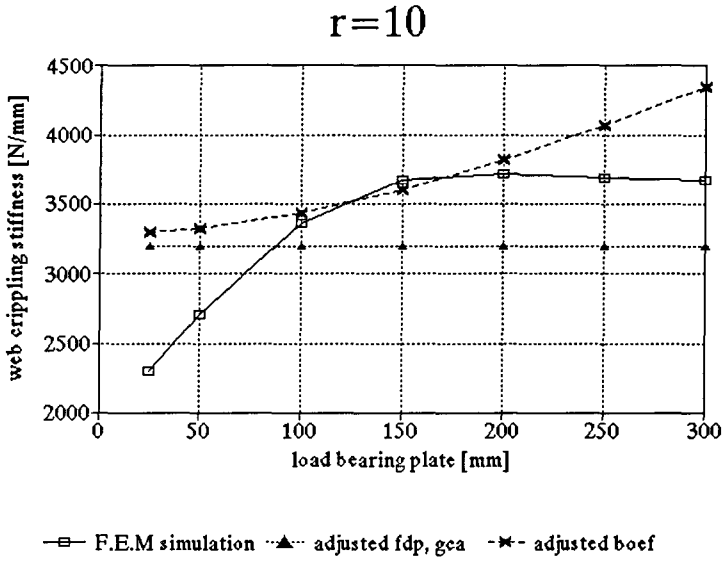

Figure E.16: *Web crippling stiffness for varying load bearing plates*

The influence of the span length on the web crippling stiffness is tabulated in table E.7.

Table E.7: *Web crippling stiffness against span length for the adjusted models*

L_{span}	Fem			Beam on elastic foundation model			Energy model		
	$r_i=1$	$r_i=5$	$r_i=10$	$r_i=1$	$r_i=5$	$r_i=10$	$r_i=1$	$r_i=5$	$r_i=10$
520	43568	6887	3472	43465	6759	3472	42710	7028	3192
1040	43526	6881	3362	43465	6945	3369	42710	7028	3192
1560	43478	6897	3364	43465	6944	3432	42710	7028	3192
2080	43478	6885	3364	43465	6944	3444	42710	7028	3192
2600	43478	6885	3364	43465	6944	3443	42710	7028	3192

These results are shown once more in the figures E.17, E.18 and E.19.

According to the figures E.17, E.18 and E.19 both the energy model and the beam on elastic foundation model perform well, considering the span length of the member. As mentioned in appendix D, the web crippling stiffness appears to be almost independent of the span length of the member. Hereby, the effective length approach in the energy model is justified.

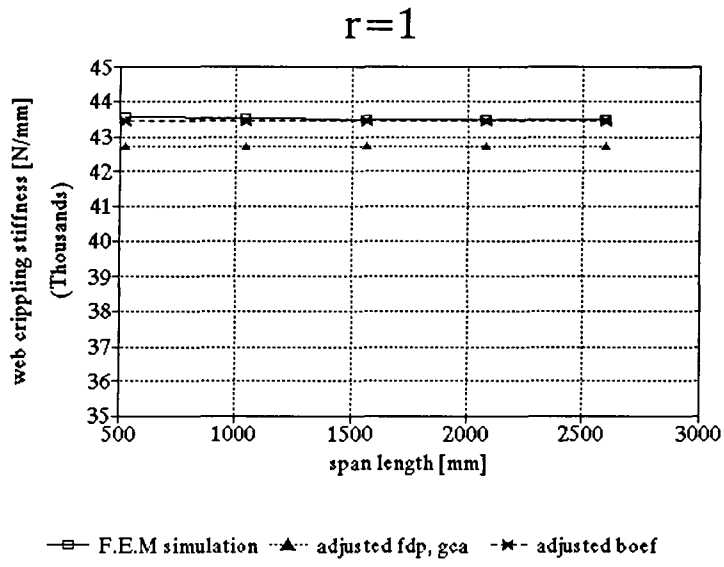

Figure E.17: Web crippling stiffness for varying span lengths

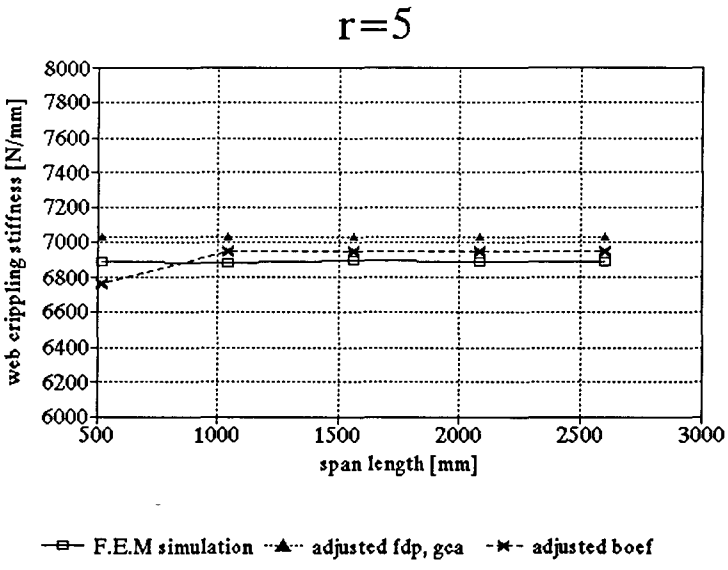

Figure E.18: Web crippling stiffness for varying span lengths

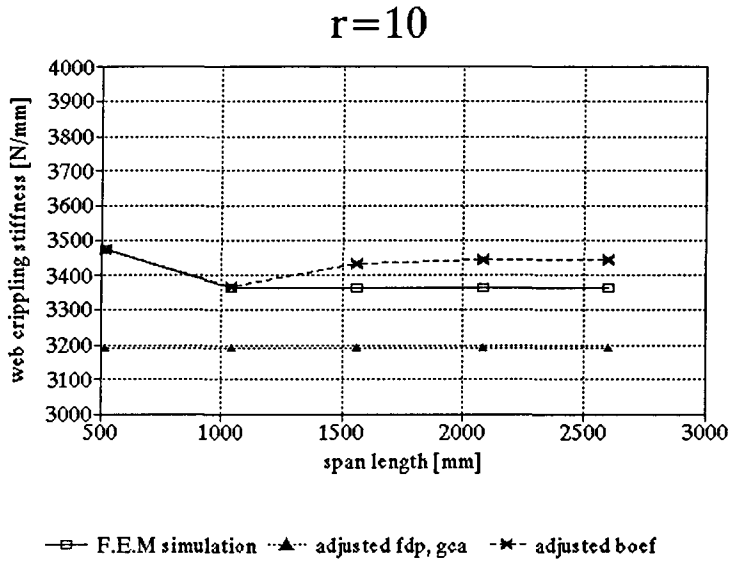

Figure E.19: *Web crippling stiffness for varying span lengths*

The beam on elastic foundation model makes use of the span length in describing the deformation variations over the length of the member, but the web crippling deformations diminish towards the hinge ends, so the span length has no significant influence in the beam on elastic foundation model either.
The influence of the wall thickness on the web crippling stiffness is tabulated in table E.8.

Table E.8: *Web crippling stiffness against wall thicknesses for the adjusted models*

b_{tf}	**Fem**			**Beam on elastic foundation model**			**Energy model**		
	$r_i=1$	$r_i=5$	$r_i=10$	$r_i=1$	$r_i=5$	$r_i=10$	$r_i=1$	$r_i=5$	$r_i=10$
0.5	20000	2909	1381	20187	2882	1453	19369	3187	1448
0.7	43478	6897	3364	43465	6944	3432	42710	7028	3192
0.9	74074	13115	6483	74820	13455	6522	77092	12686	5761
1.1	111732	21966	10899	112874	22871	10894	123541	20329	9232
1.3	152672	33642	16736	156155	35605	16706	182938	30103	13671
1.5	197044	48193	24125	203373	52024	24110	256066	42136	19136

These results are shown once more in the figures E.20, E.21 and E.22.

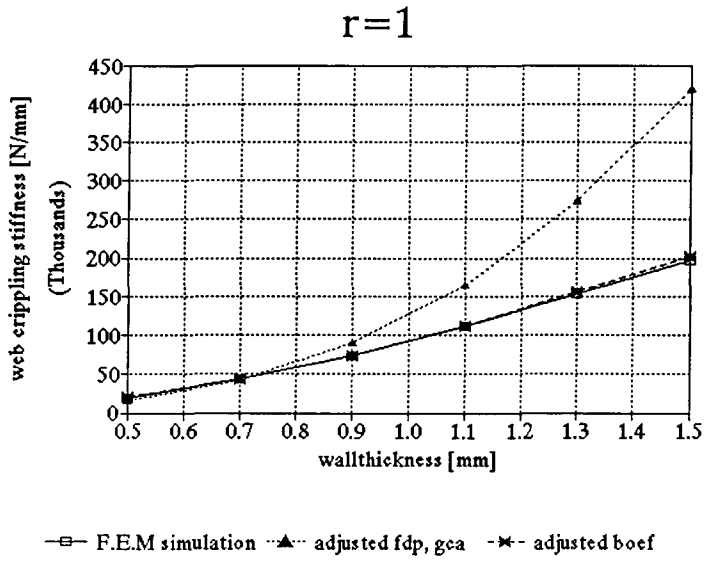

Figure E.20: Web crippling stiffness for varying wall thicknesses

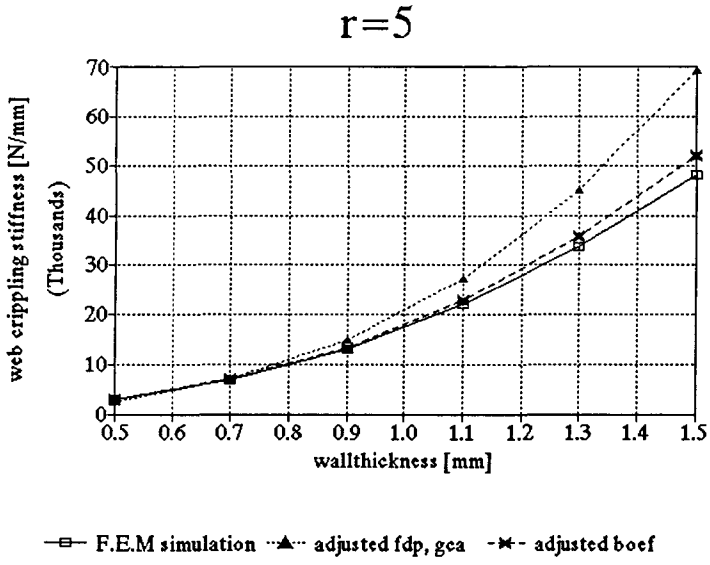

Figure E.21: Web crippling stiffness for varying wall thicknesses

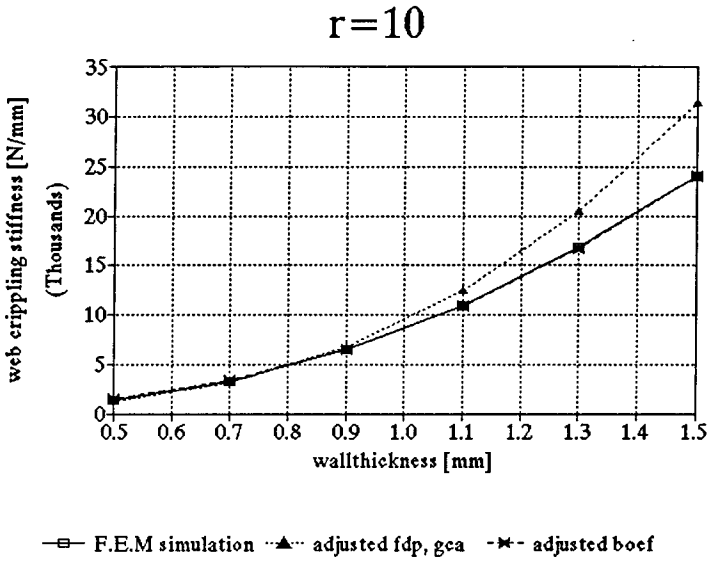

Figure E.22: *Web crippling stiffness for varying wall thicknesses*

The wall thickness is better treated within the beam on elastic foundation model than it is within the energy model. In the beam on elastic foundation model the web crippling stiffness is proportional to the wall thickness raised to the 5/2 power, while in the energy model it is proportional to the wall thickness raised to the third power. The energy model only produces reliable results for wall thicknesses smaller than 1 mm.